FUNCTIONAL CHARACTERIZATION OF ESSENTIAL GENES IN *ACINETOBACTER BAUMANNII*

by

Jennifer Suzanne Tran

A dissertation submitted in partial fulfillment of

the requirements for the degree of

Doctor of Philosophy

(Microbiology)

at the

UNIVERSITY OF WISCONSIN-MADISON

2024

Date of final oral examination: 08/01/2024

The dissertation is approved by the following members of the Final Oral Committee:

Joseph P. Dillard, Professor, Medical Microbiology & Immunology

Tu-Anh Huynh, Assistant Professor, Food Science

Mark J. Mandel, Professor, Medical Microbiology & Immunology

Jason M. Peters, Assistant Professor, Pharmaceutical Sciences

Warren E. Rose, Associate Professor, Pharmacy & Medicine

John-Demian Sauer, Associate Professor, Medical Microbiology & Immunology

ABSTRACT

Acinetobacter baumannii is a clinically important bacterial pathogen known for developing antibiotic resistance, driven in part by its unique biology and physiology. Despite its medical relevance, the essential genes of *A. baumannii* have been largely unexplored. Systems biology, which provides a global and integrated view of biology, offers a comprehensive approach to characterizing the function of these genes. Prior to this thesis work, systems biology studies in *A. baumannii* focused mainly on non-essential genes due to limitations in genetic tools. In this work, I employed an essential gene knockdown library and developed other genetic tools to investigate essential gene vulnerabilities, drug-gene interactions, and gene functions in *A. baumannii*. I supported the construction and validation of an *A. baumannii* essential gene CRISPRi knockdown library, which identified genes sensitive to knockdown (e.g., NADH dehydrogenase I and a phage repressor), modeled fitness by gene knockdown, and uncovered specific drug-gene interactions. I then screened this library with a large chemical set to create a comprehensive database of chemical-gene interactions, showing that most essential genes show additional phenotypes under chemical stress. I identified lipooligosaccharide transport as crucial for generalized antibiotic resistance as its inhibition increased membrane permeability and drug sensitivity. My phenotype-driven essential gene network linked poorly characterized genes to well-conserved pathways such as cell division. Moreover, I developed a method to combine cheminformatics with gene-chemical effects, revealing distinct mechanisms of action for chemical classes. Finally, I describe expression vectors developed for more in-depth study of these genes, then present findings to a general audience as part of a science communication initiative. In summary, this thesis advances our understanding of *A. baumannii* essential genetics, offering biological and computational tools for future studies. The comprehensive datasets generated provide invaluable resources for essential gene characterization and developing effective therapeutic strategies against this pathogen.

ACKNOWLEDGMENTS

I would like to thank my advisor, Jason Peters, for providing a place for me to learn and grow over the past six years and for the folder full of your funny jokes. My thanks also go to Amy Banta for being an endless source of technical guidance and skill, and to all the past and present members of the lab for always being willing to brainstorm, commiserate, or just chat about life.

I am forever grateful to my friends and family who have cheered me on from the beginning. Your support has kept me going. To my parents and sister especially—thank you for the long-distance calls and occasional visits, where you showed me parts of Madison and Wisconsin I didn't know existed, even though I live here.

To the new friends I've made in graduate school and in Madison, thank you for keeping me grounded, giving me excuses to go out and be social, helping me realize I am quite bad at trivia, and for all the laughter.

Thanks to Eddie and Rika for the moral support, for keeping the house crumbless, for protecting me from the garbage truck every week, and for adding fur to everything I own.

And my deepest gratitude to Mason, who followed me to the ends of the earth just to support me every day and in every way.

This PhD would not have happened without you all.

TABLE OF CONTENTS

LIST OF FIGURES

LIST OF TABLES

CHAPTER 1

Introduction

I wrote this chapter to review *Acinetobacter baumannii*, drug resistance mechanisms, and the tools available to study *A. baumannii* genetics and to outline the work presented in the remainder of this thesis.

Acinetobacter baumannii: a clinically relevant pathogen

Acinetobacter baumannii is a Gram-negative, opportunistic bacterial pathogen characterized by its lack of motility, strictly aerobic growth, and unique coccobacillus shape (1). Although *Acinetobacter* species are considered ubiquitous environmental microorganisms commonly found in soil and water samples (2), *A. baumannii* is particularly notorious for its prevalence in hospital environments (3). Community-acquired *Acinetobacter* infections are rare (4), as the vast majority of *A. baumannii* infections are nosocomial or healthcare-associated (5). This is especially true in intensive care units, where immunocompromised and chronically ill patients, often with a history of prolonged hospitalization or antimicrobial therapies, are the most at risk for these types of infections (5). Additionally, *A. baumannii* can colonize surfaces of artificial devices such as catheters, sutures, and ventilators, making patients who require these devices at risk of urinary tract, surgical wound, skin, respiratory tract, and bloodstream infections (6). It has the ability to colonize even healthy individuals and healthcare workers and to survive for extended periods on dry surfaces without nutrients, contributing to its spread and transmission in hospital settings (7–9). However, the biggest threat *A. baumannii* poses is resistance to antibiotics, particularly carbapenems, which typically have the highest *in vitro* activity against Gram-negative bacterial infections (10). As of 2019, *A. baumannii* cases associated with or attributable to antibiotic resistance were responsible for over 400,000 deaths worldwide (11).

Mechanisms of *A. baumannii* drug resistance and persistence

Multidrug resistance in *A. baumannii* is largely driven by its robust defensive barriers and genetic adaptability, allowing it to acquire and/or upregulate various resistance determinants. Of highest concern are carbapenem-resistant *A. baumannii* (CRAB) strains, which exemplify the pathogen's

ability to resist even last-resort antibiotics, posing significant treatment challenges due to intrinsic and acquired resistance mechanisms (12).

Efflux pumps

Efflux pumps play a critical role in resistance by actively expelling antibiotics and other toxic substances from bacterial cells, thereby reducing the intracellular concentration of the drugs and diminishing their efficacy. Based on phylogenetic diversity, size, and energy source, efflux pumps have been classified into six major families: resistance nodulation division (RND), ATP binding cassette (ABC) transporter, multidrug and toxin extrusion (MATE), small multidrug resistance (SMR), and major facilitator superfamily (MFS), and proteobacterial antimicrobial compound efflux (PACE) (13). *A. baumannii* is known to carry genes encoding for any of these efflux pump families (14); the most well-studied and prevalent are RND pumps Ade ABC and AdeIJK, which contribute heavily to drug resistance, including to carbapenems (15–18). These pumps can expel a variety of antibiotics, including aminoglycosides, β-lactams, and tetracyclines, and rely on different energy sources; for example, AdeABC is dependent on the proton motive force (PMF), while others utilize ATP (13). Clinical strains of *A. baumannii* often exhibit upregulated or mutated efflux pumps, enhancing their resistance profiles and complicating treatment efforts (19). Ongoing research is focused on developing efflux pump inhibitors as potential therapeutics, aiming to block these pumps and restore the effectiveness of antibiotics against multidrug-resistant *A. baumannii* (20).

Outer membrane permeability and polymyxin resistance

The cell envelope of Gram-negative organisms, including *A. baumannii*, acts as a robust barrier to environmental stressors and significantly contributes to antibiotic resistance. The standard Gram-negative cell envelope comprises three distinct layers: the cytoplasmic membrane, a peptidoglycan (PG) cell wall, and an asymmetric outer membrane (OM) composed of an inner

leaflet of phospholipids and an outer leaflet of lipopolysaccharides (LPS) (Fig. 1.1) (21). LPS is negatively charged and typically contains a lipid A anchor, glycosylated with a core oligosaccharide and attached O-antigen; however, many bacteria, including *Neisseria* sp., *Bordetella pertussis*, *Haemophilus influenzae, Campylobacter jejuni*, and A. *baumannii* (22), possess a truncated chemotype of LPS, called lipooligosaccharide (LOS) which lacks O-antigen (23). LPS^- and LOS^- containing outer membranes are more rigid than normal phospholipid bilayers with narrow pores, slowing passive diffusion of hydrophobic compounds and limiting entry of larger hydrophilic drugs (24). In conjunction with efflux pumps, this reduced permeability typically prevents the accumulation of harmful compounds within the cell, thereby fortifying the bacteria against a wide range of antimicrobial agents. However, antibiotics like polymyxins have detergent-like properties that aid in disrupting this outer membrane, targeting the lipid A moiety of LPS/LOS to compromise membrane integrity (25, 26). *A. baumannii* clinical strains have been reported to gain resistance to these antibiotics by modifying the target LOS through the addition of phosphoethanolamine (PEtN) (27, 28) or cationic sugars (29) to lipid A moieties. Additionally, while LPS/LOS is essential in most *Gammaproteobacteria*, many *A. baumannii* strains do not require LOS for survival (30). Outside of the genus *Spirochetes* which have a heavily differentiated outer membrane (31), only three Gram-negative species have been shown to survive without lipid A: *Neisseria meningiditis* (32), *Moraxella catarrhalis* (33), and *A. baumannii* (34). Yet, *A. baumannii* is the only organism to date which has been shown to readily accumulate LOS biosynthesis mutations in response to polymyxin exposure (35–37).

Unique coordination of the outer membrane with the cell wall contributes to the loss of LOS in *A. baumannii*. Enzymes involved in cell wall synthesis and outer membrane assembly have been shown to be coordinated in other Gram-negative pathogens like *Pseudomonas aeruginosa* (38). However, *A. baumannii* is distinct in that PG synthesis by the elongasome, which allows for cell

Figure 1.1. The *A. baumannii* cell envelope. Cell wall and outer membrane components (peptidoglycan and lipooligosaccharide shown here) are synthesized within the cell. Other proteins are required to transport and incorporate the components into the right subcellular location.

Figure 1.1

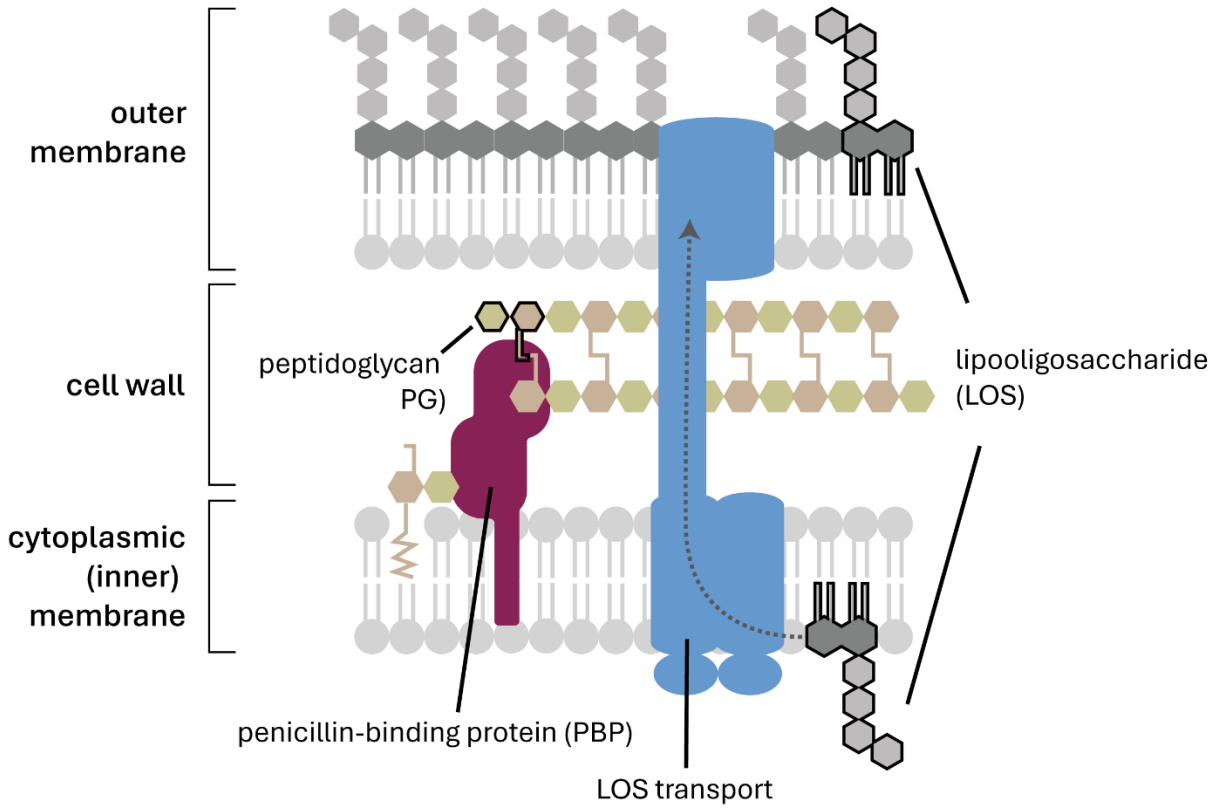
outer membrane
cell wall
cytoplasmic (inner) membrane
peptidoglycan PG)
lipooligosaccharide (LOS)
penicillin-binding protein (PBP)
LOS transport

elongation, is sufficient to structurally support an LOS-deficient outer membrane (34). Indeed, high levels of penicillin-binding protein PBP1A are toxic to LOS-deficient *A. baumannii* (30)—likely due to the negative impact on elongasome activity (34)—and PG-recycling enzymes directly promote outer membrane integrity and lower permeability (39). Furthermore, disruptions in core oligosaccharide synthesis in *A. baumannii* directly lead to PG synthesis defects (40). Although exact mechanisms of coordination are not yet clarified, the intricate interplay between these two layers of the cell envelope is crucial for antibiotic resistance.

Cell wall and cell division drug targets

Beyond its impact on outer membrane synthesis and LOS deficiencies in *A. baumannii*, PG is a critical structural component of the periplasm. Proper synthesis of PG, which is composed of glycan chains cross-linked by peptides, is crucial for cell growth and division (41). Many major enzymes involved in PG synthesis and cell division that have been extensively studied in model organisms like *E. coli* are present and play essential roles in *A. baumannii* (42, 43). Well-conserved cell wall proteins have the potential to be novel broad-spectrum drug targets; for example, inhibitors of the enzyme FtsZ have been proposed as antibiotics against *A. baumannii* and other pathogens (44, 45). However, the aforementioned outer membrane barrier poses challenges to these newer inhibitors and *A. baumannii* has already demonstrated a capacity to rapidly develop resistance to commonly used β-lactam antibiotics, which also inhibit cell wall synthesis.

The primary targets for β-lactam antibiotics are penicillin-binding proteins (PBPs), essential for the synthesis and remodeling of the PG cell wall (Fig 1.1). These proteins catalyze the final stages of PG assembly, including the polymerization of glycan strands and the cross-linking of peptide chains (46). However, *A. baumannii* carries various β-lactamases that hydrolyze β-lactam antibiotics, rendering many of these therapeutics ineffective. It is reported that up to 98.5% of clinically

recovered isolates of *A. baumannii* contain at least one highly expressed native β-lactamase, such *bla*$_{ADC}$ (AmpC, ADC-type cephalosporinase) and *bla*$_{OXA-51}$ (OXA-51) (47). Due to their ability to somewhat withstand modifications by these naturally produced β-lactamases, carbapenems, like imipenem and meropenem, were initially the most effective therapeutic options available to treat *A. baumannii* infections (48). Yet, many strains have now gained carbapenem resistance through reduced outer membrane permeability (49), upregulation of the OXA-51 gene (50, 51), horizontal acquisition of carbapenem-hydrolyzing β-lactamases (52, 53), and production of extended-spectrum AmpC β-lactamases active against carbapenems (54).

Understanding unique aspects of the *A. baumannii* cell division machinery may uncover potential targets for novel antibacterial therapies. For example, a recently identified protein, AdvA, which lacks close orthologs outside of *Acinetobacter* species, was found to have essential function in *A. baumannii* cell division (43, 55) and interacts with key cell division machinery (56). Another gene unique to *Acinetobacter*, *blhA*, was also linked to cell division, and a mutation in this gene conferred β-lactam sensitivity (57). In addition to *Acinetobacter*-specific cell division proteins, structural features of the *A. baumannii* cell wall promote bacterial persistence and other clinical challenges. Some strains of *A. baumannii* modify peptidoglycan with noncanonical d-amino acids, which increase the ability to outcompete bacterial competitors (58) and could strengthen resistance against environmental stressors, like osmotic stress (59). *A. baumannii* is also notorious for variable morphology, forming rods during rapid growth but rounded coccobacilli during stationary phase; this directly contributes to differential uptake of Gram stain and misclassification in clinical phenotypic tests (60). Additionally, some strains of *A. baumannii* display colony phase variants that affect virulence and biofilm formation, with one of these variants having abnormally elongated cell morphologies at early stationary phase (61). While the cell wall orchestrates much of

cell length and shape, the cause of variable morphology remains unclear and may be due to unique players in the cell wall synthesis and division.

Adaptive stress response and metabolic remodeling

Adaptability to environmental stressors and unique metabolic characteristics significantly promote *A. baumannii* persistence and virulence. While knowledge of protective stress responses in *A. baumannii* is lacking compared to better-characterized pathogens such as *P. aeruginosa* (62), *A. baumannii* is known to have noncanonical response systems. For example, unlike other members of the *Gammaproteobacteria*, *A. baumannii* does not encode the canonical RpoS sigma factor to coordinate its general stress response; rather, transcriptional regulator DksA acts as a regulator for broad stress protection (63). Additionally, two component systems have been shown to control multiple major pathways, including BfmRS, which regulates multiple stress pathways such as oxidative stress, osmotic stress, protein folding, fimbriae and pili synthesis, capsule production, and siderophore biosynthesis (64), and AmsSR, which is responsible for major reordering of metabolism circuits (65). These major transcriptional changes are linked to environmental persistence such as desiccation tolerance (66), motility (67), and biofilm formation (68).

A. baumannii showcases unique metabolic traits as well, utilizing unusual and variable carbon sources (69) as a non-fermenter, unable to catabolize glucose (2). The ability to alter metabolic flux and amino acid metabolism has been shown to bolster its virulence in nutrient-poor host environments (70). As an obligate aerobe, *A. baumannii* relies heavily on cellular respiration, highlighting the possibility for drugs to target ATP synthase (71) and other oxidative phosphorylation complexes (72), though limited information exists on the intricacies of flux through this pathway. Importantly, cellular respiration has been linked directly to antibiotic efficacy (73). Yet, *A. baumannii* can survive for extended periods, up to 28 days, without oxygen, demonstrating its

robust stress response pathways and ability to persist in anaerobic environments (74). The complex interplay between stress response mechanisms and metabolic pathways enhances the ability of *A. baumannii* to adapt and survive in hostile environments, directly impacting its success as an infectious agent. This adaptability underscores the pathogen's resilience and highlights the challenges in developing effective treatments against A. baumannii infections.

Mobile genetic elements and antibiotic resistance

Mobile genetic elements (MGEs), including transposons, integrons, plasmids, insertion sequences, and prophages, are another significant source of antibiotic resistance in *A. baumannii* (Fig 1.2) (75). As the name suggests, MGEs are segments of DNA that mediate movement of genetic material within genomes, allowing for the acquisition and dissemination of resistance genes across strains and even species (76). MGEs are widespread and diverse across *A. baumannii* species and represent a major source of genetic differences between closely related strains (77, 78). Many MGEs in *A. baumannii* carry genes directly encoding for resistance to carbapenems, tetracyclines, macrolides, and aminoglycosides. Notably, insertion sequences are known to confer and promote antibiotic resistance through strong promoters that upregulate native or already acquired β-lactamases (75) or through gene disruption affecting the drug target (36), permeability (79), or stress response mechanisms (80, 81).

Prophages are MGEs from lysogenic bacteriophages, which integrate into the genome of their host and are a large source of new genes in *A. baumannii*, with an average sequence length of ~25-30 kb (82). They contribute to virulence and pathogenicity, as they can carry antibiotic resistance genes, toxin-antitoxin systems, anti-phage defense islands, and efflux pumps (83). Yet, under specific conditions, intact prophages can excise from the host chromosome, and enter the lytic cycle, replicating, producing progeny virions, and lysing the cell. Proteins produced by *A. baumannii*

Figure 1.2. Mobile genetic elements contribute to antibiotic resistance. (A) Insertion elements can upregulate antibiotic resistance genes. (B) Disruption of drug targets, permeases, or regulators can lead to resistance. (C) Mobile genetic elements often carry antibiotic resistance genes, or other virulence and pathogenicity factors. (D) Lysogenic phages can integrate into the genome, bringing antibiotic resistance genes and other virulence factors. Adapted from Noel et al. (75)

Figure 1.2

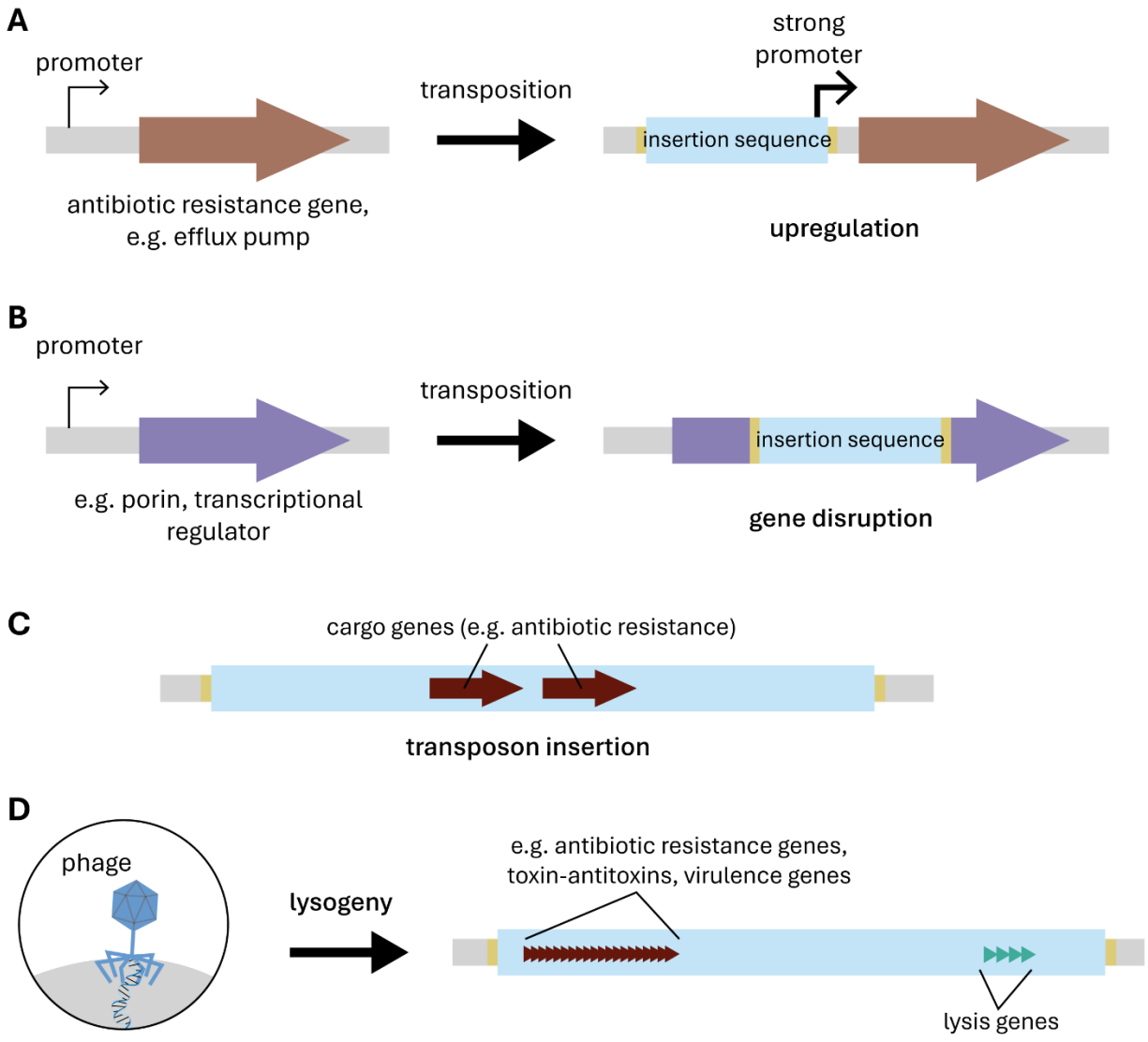
A
promoter
transposition
strong
promoter
insertion sequence
antibiotic resistance gene,
e.g. efflux pump
upregulation
B
promoter
transposition
insertion sequence
e.g. porin, transcriptional
regulator
gene disruption
C
cargo genes (e.g. antibiotic resistance)
transposon insertion
D
phage
lysogeny
e.g. antibiotic resistance genes,
toxin-antitoxins, virulence genes
lysis genes

phages that cause cell lysis, endolysins, have been proposed as a possible therapeutic due to their antibacterial activity and have been shown to enhance antibiotic effectiveness (84–86).

Genetic tools in *A. baumannii*

Many traits of *A. baumannii* that contribute to drug resistance are distinct from model Gram-negative organisms such as *E. coli* K-12. However, bacterial genetics research historically centered on model organisms due to a lack of techniques, tools, reagents, genome sequences, and general knowledge about non-model bacteria (87, 88). However, recent advancements in DNA sequencing, DNA synthesis, and other tools have made genetic analyses across species more accessible, lessening the knowledge and technique gaps between model organisms and clinically relevant pathogens like *A. baumannii*. A select number of approaches are currently used to interrogate *A. baumannii* genetics (Fig 1.3).

Expression vectors are one crucial tool for studying *A. baumannii* genetics. While several vectors for *A. baumannii* have been previously described and are available for cloning (89), they also have limitations. Replicative shuttle vectors in *A. baumannii* typically use a high-copy origin of replication (90, 91), which can pose challenges when expressing toxic gene products. In contrast, integrative vectors, based on the site-specific transposon Tn7, insert DNA cargo into the genome downstream of the *glmS* gene with only a single copy—these vectors have been used extensively in *A. baumannii* (89, 92, 93). Many of these vectors were not designed to contain easily swappable modules (e.g. different antibiotic markers) outside of standard multiple cloning sites. Additionally, existing vectors typically employ inducible promoters that are either native to or designed for use in *E. coli* (94, 95) and can pose challenges for precise control of expression. Despite these limitations, these vectors have been successfully used to express genes *in trans* (89–93).

Figure 1.3. Genetic tools in *A. baumannii.* These include expression vectors, transposon mutagenesis, targeted knockouts, and more recently, CRISPR interference or CRISPRi.

Figure 1.3

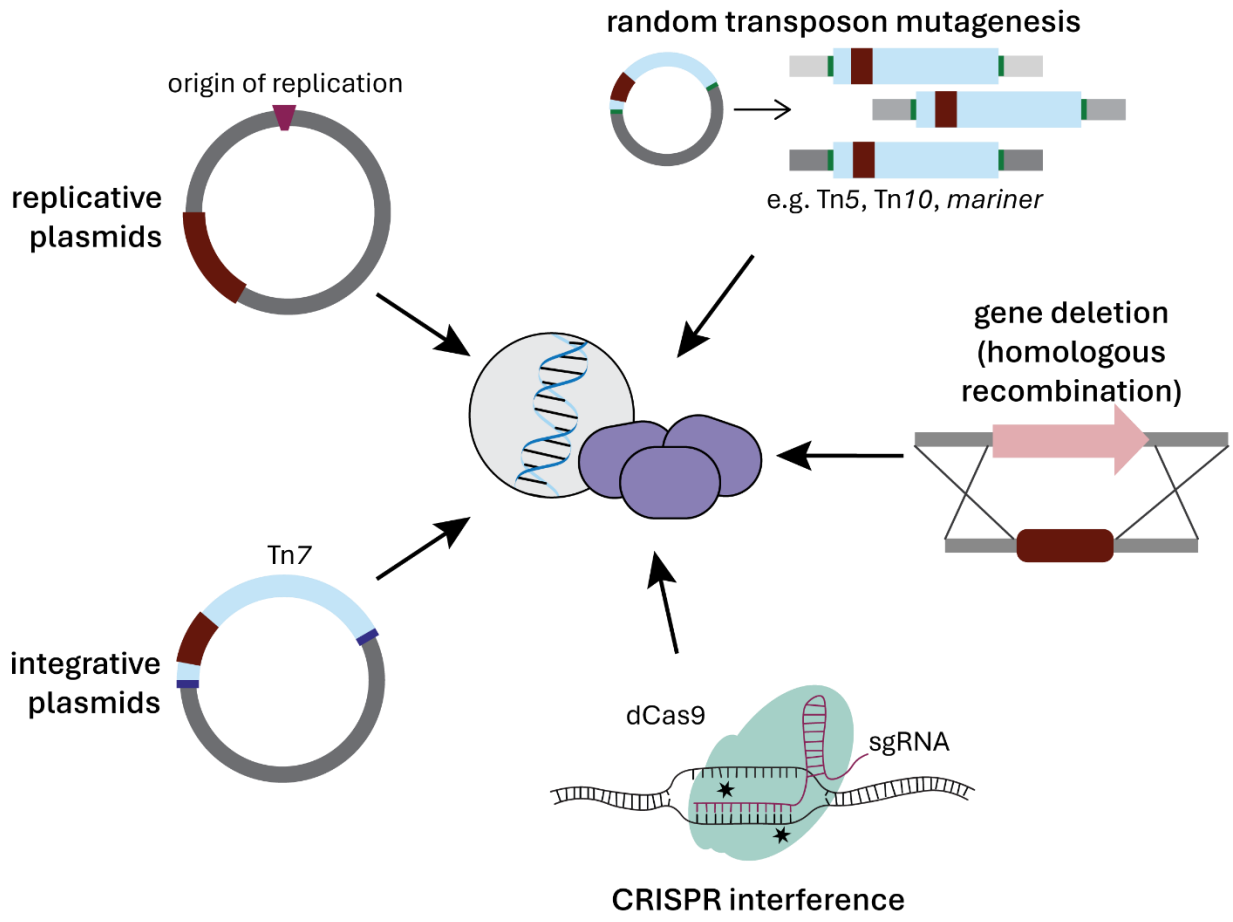
random transposon mutagenesis
origin of replication
replicative plasmids
e.g. Tn5, Tn10, mariner
gene deletion (homologous recombination)
Tn7
integrative plasmids
dCas9
sgRNA
CRISPR interference

Most gene deletion strategies in *A. baumannii* involve homologous recombination and employ a knockout cassette, consisting of an antibiotic resistance marker flanked by homologous regions of the target region (89). Knockout cassettes incorporated into suicide plasmids (96, 97), or linear DNA cassettes combined with the native RecET recombinase system (98) have been successfully utilized in *A. baumannii.* Both methods often use a FLP recombinase system, to remove the antibiotic resistance cassettes after integration, achieving scarless deletions (99).

Knockout mutants can also be created using random transposon mutagenesis. The integration of transposon mutagenesis with high-throughput sequencing has allowed for precise mapping of insertion sites and quantification of transposon mutant fitness (i.e., Tn-seq) (100–102). In *A. baumannii*, these tools have been used successfully with three different random transposon vectors: *mariner* (43), Tn*5* (42, 103), and Tn*10* (43, 104). In both gene deletion and transposon mutagenesis strategies, further investigation of essential genes is challenging due to the lethality associated with their disruption.

More recently, CRISPR tools have been used to study *A. baumannii* genetics. A Cas9 nuclease-mediated genome cleavage system coupled with RecAb recombination was developed for genome editing in *A. baumannii* (105) and more recently, a similar Cas12a system was described for large-fragment deletion and multiplex gene editing (106). CRISPR interference (CRISPRi) - which uses single guide RNAs (sgRNAs) to direct a deactivated Cas9 (dCas9) to genetic regions of interest for targeted transcriptional repression – has successfully been used in *A. baumannii* as well (55, 107). Briefly, the first 20 nucleotides of the sgRNA, or spacer, are designed to match a complementary sequence in the target gene (protospacer) with an adjacent PAM (protospacer adjacent motif) for dCas9 binding to DNA. The sgRNA spacer guides dCas9 to the target, where it blocks transcription (108). CRISPRi systems used in *A. baumannii* use either a Tn*7*-expressed dCas9 and plasmid-expressed sgRNA (55) or a fully Tn*7*-based system (107).

Functional genomics and systems biology

Functional genomics uses high-throughput, systematic approaches to uncover gene phenotypes and to better understand gene function. Improved genetic tools and sequencing have allowed for scalable and multiplexable characterization of microbial gene function (109), and these approaches could be applied to *A. baumannii* to better understand its genetics. Crucial to high-throughput approaches, which allow large numbers of experiments to be conducted simultaneously, are genetic libraries, containing multiple strains or mutants in an arrayed (e.g., one mutant per well) or pooled fashion. With modern advances in sequencing, pooled libraries have become more feasible and cost-effective due to barcoding, which allows for the simultaneous tracking and identification of individual genetic elements within a mixed population (110). While some gain-of-function libraries do exist in microbes (111–115) and more tools are being developed to enable overexpression or transcriptional activation libraries, a majority of microbial genetic libraries consist of loss-of-function mutants (116, 117).

Knockout libraries

Traditionally, microbial deletion libraries were constructed using recombination strategies and consisted of collections of individual isolates. These libraries, often arrayed, serve as gold-standard resources for non-essential gene phenotyping (112, 118–122). However, due to the labor-intensive and resource-intensive nature of creating these libraries, they are typically only available for model organisms. These deletion mutants can be screened for phenotypes, allowing individual isolates to be selected for further study. Despite their value, these libraries inherently exclude essential genes. In order to expand these genetic libraries, individual strains containing suppressors or mutations that bypass specific essential gene deletions are often necessary (123).

Nevertheless, these libraries provide valuable information on essentiality and growth defects. They have been successfully used for comprehensive gene phenotyping, for example, in high-throughput microscopy studies for cellular morphogenesis and cell cycle phenotyping (124, 125) or under various stress treatments to assess gene function in stress response (126, 127).

Transposon sequencing (Tn-seq) is particularly powerful technique used to create gene knockout libraries without the time and resources of individual gene deletions in a diverse range of microorganisms (100). High-throughput sequencing technology allows for comprehensive characterization of transposon knockout libraries, enabling systematic investigation of gene essentiality and functional phenotyping in clinically relevant ESKAPE pathogens (128): *Enterococcus faecium* (129), *Staphylococcus aureus* (130, 131), *Klebsiella pneumoniae* (132, 133), *A. baumannii* (42, 103, 104, 134), *P. aeruginosa* (135, 136), and *Enterobacter* species (137, 138). Importantly, beyond identifying genes required for survival, many of these studies combine with infection models or antibiotic treatment to better understand genes contributing to these pathogens' ability to escape treatment clinically.

Additionally, integrating these knockout libraries with other omics approaches, such as transcriptomics and metabolomics, can significantly enhance our understanding of gene function and interactions in complex biological systems. For instance, transcriptomics allows for the examination of gene expression changes in response to gene knockouts, providing insights into regulatory networks and compensatory mechanisms (139). Metabolomics, on the other hand, can reveal alterations in metabolic pathways and fluxes, offering a deeper understanding of the physiological impact of gene disruptions (140). By combining data from these omics approaches with knockout libraries, researchers can construct comprehensive models of gene function and identify key nodes and interactions within biological pathways (141).

Furthermore, the multiplexing of deletion and Tn-seq libraries offers a powerful strategy for exploring synthetic lethality and creating detailed microbial interaction networks. Novel gene functions have been identified by creating transposon libraries in deletion mutants, systematically screening for synthetic lethal interactions and identifying novel gene functions (e.g., chromosomal segregation and related protein complexes in yeast (142, 143) and extensively, cell division genes in *E. coli* (144–147)). In yeasts, pioneering work utilized multiplexed knockout libraries to extensively map genetic interactions, providing crucial insights into cellular processes and the interconnected nature of genetic pathways (148–150). In bacterial species, double deletion mutant libraries have been used to create similar genetic networks, from targeted double deletions for small noncoding RNA regulatory networks (151) to genome-wide interaction networks of nutrient stress (152).

CRISPR-based libraries

CRISPR-based libraries provide another approach to functional genomics. In bacteria, the creation of double-strand breaks by CRISPR-Cas9 cleavage is generally lethal, which necessitates the use of alternative CRISPR tools, namely CRISPRi, for library-scale experiments (153). These CRISPRi libraries typically require purposeful design of pooled sgRNA libraries and transfer of the CRISPRi machinery *en masse*—either pooled or arrayed—into the microbe of interest for systematic, targeted transcriptional knockdown (109). CRISPRi libraries have considerable advantages over deletion and Tn-seq libraries in that essential genes can be targeted. Notably, knockdowns levels can be titrated in multiple ways, allowing for further study even in cases where full knockdown of essential genes would result in lethality. By controlling CRISPRi machinery expression with inducible promoters, titrating inducer concentrations allows for partial knockdowns (154) although this method has been shown to be noisy or inconsistent at the single-cell level in *E. coli* (108, 155, 156). Alternatively, modifying the sgRNA with mismatches (157, 158) or truncations (156) can effectively titrate levels of knockdown. Machine learning models trained on mismatched sgRNA

libraries targeting reporter genes can predict the knockdown efficacy of individual mismatched spacers with ~50% accuracy, enabling programmable knockdown gradients of essential genes (157).

Limitations of CRISPRi include toxicity of dCas9 (159, 160) or 'bad seed' off-targeting sgRNAs (161, 162), requirement of PAM sequences ("NGG" for the well-characterized dCas9 protein derived from *Streptococcus pyogenes* (163)), and transcriptional polarity. Because CRISPRi represses transcription, polar effects cause genes downstream in the same transcriptional unit as the target to also be knocked down (108). Reverse polarity, where targeting genes downstream in a transcription unit will knockdown upstream genes, have also been reported at variable levels in some organisms or CRISPRi systems although the mechanism is unknown (155, 161, 164).

Importantly, CRISPRi can be successfully delivered to diverse bacterial species, like *A. baumannii*, using broad-host range plasmids or through integration into the genome. While plasmids can be easily transferred via transformation or conjugation, the need for selective pressure can introduce extra variables in downstream experiments and high-copy plasmids could face toxicity issues mentioned above (109). Mobile-CRISPRi, a suite of integrating vectors, can transfer CRISPRi systems into Gram-positive bacterial species from *Bacillus subtilis* through the ICEBs1 conjugatable element and into Gram-negative recipients from *E. coli* donors using the RP4 mating machinery and Tn*7* transposase (107).

CRISPRi libraries are instrumental in connecting gene vulnerabilities, which relate the magnitude of gene inhibition with the corresponding decrease in bacterial fitness (165), to gene function . By generating knockdown gradients, researchers can investigate dose-response relationships and model gene function (165, 166). As with knockout libraries, CRISPRi knockdown libraries can also be grown in an antibiotic or other stress conditions to phenotype genes and determine specific

chemical-gene interactions (109). For example, a study screening an antibiotic with unknown mechanism of action against a *B. subtilis* CRISPRi library led to the identification of the drug target, UppS, due to hypersensitivity phenotypes (167).

Large-scale chemical genomics

Chemical genetics describes assessments of a drug or chemical activity against genetic libraries, identifying specific gene-drug interactions and gene phenotypes in particular conditions. Expanding on this, chemical genomics conducts large-scale screenings of chemical compound libraries to perturb biological processes and observe the resulting phenotypic changes. By leveraging a wide range of chemical compounds in conjunction with gene perturbation libraries, it is possible to generate extensive drug-gene interaction datasets, predict drug behaviors and drug-drug interactions, and propel drug discovery (168).

Chemical genomics studies across yeast species, using genome-scale collections of yeast gene deletions either arrayed or barcoded, have highlighted significant drug-gene interactions identified from larger datasets, serving as valuable resources (169, 170). Beyond drug-gene interactions and drug target identification, the scale of these chemical genomics approaches facilitates the identification of general drug resistance mechanisms and the mapping of functional connections between these elements. For example, using the gold-standard Keio deletion library in *E. coli* (119), Nichols et al. identified a gene involved in multiple antibiotic resistance and created a drug-gene network that connected drugs with sensitive – and likely directly targeted or related – biological processes. This network also revealed synergistic drug combinations target distinct spaces in the network and provided additional clues for the mode of action of poorly described drugs (171).

Genes with related functions exhibit similar fitness patterns across multiple conditions in chemical genomics, a phenomenon sometimes referred to as cofitness (172). This cofitness property has

been utilized to generate informative genetic networks and identify functional pathways. For instance, a *B. subtilis* CRISPRi library was screened under a variety of conditions to create a functional map of gene interactions, identifying novel connections between core processes such as cell wall biosynthesis and cell division (155). Similar chemical genomics approaches with CRISPRi libraries of non-model organisms like *Corynebacterium glutamicum* (173) and *Mycobacterium tuberculosis* (174) have identified pathways contributing to drug resistance and novel gene functions based on clustering of phenotypic profiles. Another screen in *M. tuberculosis* employed a hypomorph library, consisting of mutants with depleted essential targets, and screened thousands of small molecules, using the resulting chemical-genetic interactions to identify compounds against targets that would have eluded conventional drug discovery (175).

Genetic libraries and chemical genomics thus provide a significant opportunity to better understand *A. baumannii* genetics, its drug resistance, and potential druggable targets. One previous chemical genomics screen, conducted with an *A. baumannii* transposon library, used phenotypic clustering to identify the novel cell division gene AdvA and functionally phenotype other poorly characterized genes (43). However, as a deletion library, this screen lacked essential gene phenotypes, highlighting a gap in the study *A. baumannii* essential genes – typically targets for antibiotics – using these approaches.

Summary and thesis outline

Acinetobacter baumannii is a Gram-negative, opportunistic pathogen notorious for its antibiotic resistance mechanisms. Understanding its genetics in a systematic way, especially its essential genes not been previously examined, is important for developing new therapeutic strategies. Approaches utilizing genetic libraries and chemical screens have been instrumental across microorganisms in identifying chemical-gene interactions, gene functions, and novel drug targets.

The goal of this work is to leverage these systems-level approaches to study and characterize essential genes in *A. baumannii*.

In Chapter 2, we establish an essential gene knockdown library in *A. baumannii*, characterize gene vulnerabilities, and explore chemical-gene interactions with four clinically relevant antibiotics. Chapter 3 significantly expands on this by screening the library across 45 chemical conditions, generating a much larger set of chemical-gene phenotypes and enabling systems-level insights into inhibitor and gene function. Chapter 4 introduces improved expression vectors that can be used in *A. baumannii* and *E. coli*, providing an orthogonal approach for studying these genes. As part of the Wisconsin Initiative for Science Literacy, Chapter 5 explains the basis of this work and highlights important findings for a general, non-science audience. In Chapter 6, I summarize the previous chapters and describe future directions from this work. I close with three appendices, which discuss additional areas of study during my thesis, including strain-to-strain differences, characterization of growth conditions, and investigation into aerobic respiration in *A. baumannii*.

References

1. Peleg AY, Seifert H, Paterson DL. 2008. Acinetobacter baumannii: Emergence of a Successful Pathogen. Clin Microbiol Rev 21:538–582.

2. Baumann P, Doudoroff M, Stanier RY. 1968. A Study of the Moraxella Group II. Oxidative-negative Species (Genus Acinetobacter)1. J Bacteriol 95:1520–1541.

3. Howard A, O'Donoghue M, Feeney A, Sleator RD. 2012. Acinetobacter baumannii. Virulence 3:243–250.

4. Dijkshoorn L, Nemec A, Seifert H. 2007. An increasing threat in hospitals: multidrug-resistant Acinetobacter baumannii. Nat Rev Microbiol 5:939–951.

5. Montefour K, Frieden J, Hurst S, Helmich C, Headley D, Martin M, Boyle DA. 2008. Acinetobacter baumannii: An Emerging Multidrug-Resistant Pathogen in Critical Care. Critical Care Nurse 28:15–25.

6. Fournier PE, Richet H, Weinstein RA. 2006. The Epidemiology and Control of Acinetobacter baumannii in Health Care Facilities. Clinical Infectious Diseases 42:692–699.

7. Thom KA, Rock C, Jackson SS, Johnson JK, Srinivasan A, Magder L, Roghmann M-C, Bonomo RA, Harris AD. 2017. Factors leading to transmission risk of Acinetobacter baumannii. Crit Care Med 45:e633–e639.

8. 2019. Acinetobacter in Healthcare Settings | HAI | CDC. https://www.cdc.gov/hai/organisms/acinetobacter.html. Retrieved 11 July 2023.

9. Wendt C, Dietze B, Dietz E, Rüden H. 1997. Survival of Acinetobacter baumannii on dry surfaces. Journal of Clinical Microbiology 35:1394–1397.

10. Castanheira M, Mendes RE, Gales AC. 2023. Global Epidemiology and Mechanisms of Resistance of Acinetobacter baumannii-calcoaceticus Complex. Clin Infect Dis 76:S166–S178.

11. Antimicrobial Resistance Collaborators. 2022. Global burden of bacterial antimicrobial resistance in 2019: a systematic analysis. Lancet 399:629–655.

12. World Health Organization. 2024. WHO bacterial priority pathogens list, 2024: bacterial pathogens of public health importance, to guide research, development, and strategies to prevent and control antimicrobial resistance. World Health Organization, Genève, Switzerland.

13. Verma P, Tiwari M, Tiwari V. 2021. Efflux pumps in multidrug-resistant *Acinetobacter baumannii*: Current status and challenges in the discovery of efflux pumps inhibitors. Microbial Pathogenesis 152:104766.

14. Zack KM, Sorenson T, Joshi SG. 2024. Types and Mechanisms of Efflux Pump Systems and the Potential of Efflux Pump Inhibitors in the Restoration of Antimicrobial Susceptibility, with a Special Reference to Acinetobacter baumannii. 3. Pathogens 13:197.

15. Coyne S, Courvalin P, Périchon B. 2011. Efflux-mediated antibiotic resistance in Acinetobacter spp. Antimicrob Agents Chemother 55:947–953.

16. Yoon E-J, Chabane YN, Goussard S, Snesrud E, Courvalin P, Dé E, Grillot-Courvalin C. 2015. Contribution of resistance-nodulation-cell division efflux systems to antibiotic resistance and biofilm formation in Acinetobacter baumannii. mBio 6:e00309-15.

17. Raible KM, Sen B, Law N, Bias TE, Emery CL, Ehrlich GD, Joshi SG. 2017. Molecular characterization of β-lactamase genes in clinical isolates of carbapenem-resistant Acinetobacter baumannii. Ann Clin Microbiol Antimicrob 16:75.

18. Sen B, Joshi SG. 2016. Studies on Acinetobacter baumannii involving multiple mechanisms of carbapenem resistance. J Appl Microbiol 120:619–629.

19. Abdi SN, Ghotaslou R, Ganbarov K, Mobed A, Tanomand A, Yousefi M, Asgharzadeh M, Kafil HS. 2020. Acinetobacter baumannii Efflux Pumps and Antibiotic Resistance. Infect Drug Resist 13:423–434.

20. Sharma A, Gupta VK, Pathania R. 2019. Efflux pump inhibitors for bacterial pathogens: From bench to bedside. Indian J Med Res 149:129–145.

21. Silhavy TJ, Kahne D, Walker S. 2010. The Bacterial Cell Envelope. Cold Spring Harb Perspect Biol 2:a000414.

22. Dardelle F, Phelip C, Darabi M, Kondakova T, Warnet X, Combret E, Juranville E, Novikov A, Kerzerho J, Caroff M. 2024. Diversity, Complexity, and Specificity of Bacterial Lipopolysaccharide (LPS) Structures Impacting Their Detection and Quantification. Int J Mol Sci 25:3927.

23. Whitfield C, Trent MS. 2014. Biosynthesis and export of bacterial lipopolysaccharides. Annu Rev Biochem 83:99–128.

24. Zgurskaya HI, Löpez CA, Gnanakaran S. 2015. Permeability Barrier of Gram-Negative Cell Envelopes and Approaches To Bypass It. ACS Infect Dis 1:512–522.

25. Sabnis A, Hagart KL, Klöckner A, Becce M, Evans LE, Furniss RCD, Mavridou DA, Murphy R, Stevens MM, Davies JC, Larrouy-Maumus GJ, Clarke TB, Edwards AM. 2021. Colistin kills bacteria by targeting lipopolysaccharide in the cytoplasmic membrane. eLife 10:e65836.

26. Bhattacharjee MK. 2016. Antibiotics That Affect the Membrane and Other Structural Targets, p. 153–173. *In* Chemistry of Antibiotics and Related Drugs. Springer International Publishing, Cham.

27. Adams MD, Nickel GC, Bajaksouzian S, Lavender H, Murthy AR, Jacobs MR, Bonomo RA. 2009. Resistance to Colistin in Acinetobacter baumannii Associated with Mutations in the PmrAB Two-Component System. Antimicrob Agents Chemother 53:3628–3634.

28. Chin C-Y, Gregg KA, Napier BA, Ernst RK, Weiss DS. 2015. A PmrB-Regulated Deacetylase Required for Lipid A Modification and Polymyxin Resistance in Acinetobacter baumannii. Antimicrob Agents Chemother 59:7911–7914.

29. Pelletier MR, Casella LG, Jones JW, Adams MD, Zurawski DV, Hazlett KRO, Doi Y, Ernst RK. 2013. Unique structural modifications are present in the lipopolysaccharide from colistin-resistant strains of Acinetobacter baumannii. Antimicrob Agents Chemother 57:4831–4840.

30. Boll JM, Crofts AA, Peters K, Cattoir V, Vollmer W, Davies BW, Trent MS. 2016. A penicillin-binding protein inhibits selection of colistin-resistant, lipooligosaccharide-deficient Acinetobacter baumannii. Proc Natl Acad Sci U S A 113:E6228–E6237.

31. Haake DA, Zückert WR. 2015. The Leptospiral Outer Membrane. Curr Top Microbiol Immunol 387:187–221.

32. Steeghs L, den Hartog R, den Boer A, Zomer B, Roholl P, van der Ley P. 1998. Meningitis bacterium is viable without endotoxin. Nature 392:449–450.

33. Peng D, Hong W, Choudhury BP, Carlson RW, Gu X-X. 2005. Moraxella catarrhalis Bacterium without Endotoxin, a Potential Vaccine Candidate. Infect Immun 73:7569–7577.

34. Simpson BW, Nieckarz M, Pinedo V, McLean AB, Cava F, Trent MS. 2021. Acinetobacter baumannii Can Survive with an Outer Membrane Lacking Lipooligosaccharide Due to Structural Support from Elongasome Peptidoglycan Synthesis. mBio 12:e03099-21.

35. Powers MJ, Trent MS. 2018. Expanding the Paradigm for the Outer Membrane: Acinetobacter baumannii in the Absence of Endotoxin. Mol Microbiol 107:47–56.

36. Moffatt JH, Harper M, Harrison P, Hale JDF, Vinogradov E, Seemann T, Henry R, Crane B, St. Michael F, Cox AD, Adler B, Nation RL, Li J, Boyce JD. 2010. Colistin Resistance in Acinetobacter baumannii Is Mediated by Complete Loss of Lipopolysaccharide Production. Antimicrobial Agents and Chemotherapy 54:4971–4977.

37. Novović K, Jovčić B. 2023. Colistin Resistance in Acinetobacter baumannii: Molecular Mechanisms and Epidemiology. Antibiotics (Basel) 12:516.

38. Hummels KR, Berry SP, Li Z, Taguchi A, Min JK, Walker S, Marks DS, Bernhardt TG. 2023. Coordination of bacterial cell wall and outer membrane biosynthesis. Nature 615:300–304.

39. Islam N, Kazi MI, Kang KN, Biboy J, Gray J, Ahmed F, Schargel RD, Boutte CC, Dörr T, Vollmer W, Boll JM. 2022. Peptidoglycan Recycling Promotes Outer Membrane Integrity and Carbapenem Tolerance in Acinetobacter baumannii. mBio 13:e0100122.

40. VanOtterloo LM, Macias LA, Powers MJ, Brodbelt JS, Trent MS. 2024. Characterization of Acinetobacter baumannii core oligosaccharide synthesis reveals novel aspects of lipooligosaccharide assembly. mBio 15:e03013-23.

41. Garde S, Chodisetti PK, Reddy M. 2021. Peptidoglycan: Structure, Synthesis, and Regulation. EcoSal Plus 9.

42. Gallagher LA, Ramage E, Weiss EJ, Radey M, Hayden HS, Held KG, Huse HK, Zurawski DV, Brittnacher MJ, Manoil C. 2015. Resources for Genetic and Genomic Analysis of Emerging Pathogen Acinetobacter baumannii. J Bacteriol 197:2027–2035.

43. Geisinger E, Mortman NJ, Dai Y, Cokol M, Syal S, Farinha A, Fisher DG, Tang AY, Lazinski DW, Wood S, Anthony J, van Opijnen T, Isberg RR. 2020. Antibiotic susceptibility signatures identify potential antimicrobial targets in the Acinetobacter baumannii cell envelope. 1. Nat Commun 11:4522.

44. Scoffone VC, Irudal S, AbuAlshaar A, Piazza A, Trespidi G, Barbieri G, Makarov V, Migliavacca R, De Rossi E, Buroni S. 2022. Bactericidal and Anti-Biofilm Activity of the FtsZ Inhibitor C109 against Acinetobacter baumannii. 11. Antibiotics 11:1571.

45. Roy Chowdhury S, Saha R, Koley T, Naz F, Sharma S, Khan MI, Kumar M, Kaur P, Ethayathulla AS. 2024. Structure-based identification of potential natural compound inhibitors targeting bacterial cytoskeleton protein FtsZ from Acinetobacter baumannii by computational studies. J Biomol Struct Dyn 1–13.

46. Zapun A, Contreras-Martel C, Vernet T. 2008. Penicillin-binding proteins and beta-lactam resistance. FEMS Microbiol Rev 32:361–385.

47. Colquhoun JM, Farokhyfar M, Hutcheson AR, Anderson A, Bethel CR, Bonomo RA, Clarke AJ, Rather PN. 2021. OXA-23 β-Lactamase Overexpression in Acinetobacter baumannii Drives Physiological Changes Resulting in New Genetic Vulnerabilities. mBio 12:e0313721.

48. Doi Y, Murray GL, Peleg AY. 2015. Acinetobacter baumannii: Evolution of Antimicrobial Resistance—Treatment Options. Semin Respir Crit Care Med 36:85–98.

49. Lasarte-Monterrubio C, Vázquez-Ucha JC, Maneiro M, Arca-Suárez J, Alonso I, Guijarro-Sánchez P, Buynak JD, Bou G, González-Bello C, Beceiro A. 2021. Activity of Imipenem, Meropenem, Cefepime, and Sulbactam in Combination with the β-Lactamase Inhibitor LN-1-255 against Acinetobacter spp. Antibiotics (Basel) 10:210.

50. Turton JF, Ward ME, Woodford N, Kaufmann ME, Pike R, Livermore DM, Pitt TL. 2006. The role of ISAba1 in expression of OXA carbapenemase genes in Acinetobacter baumannii. FEMS Microbiol Lett 258:72–77.

51. Figueiredo S, Poirel L, Papa A, Koulourida V, Nordmann P. 2009. Overexpression of the naturally occurring blaOXA-51 gene in Acinetobacter baumannii mediated by novel insertion sequence ISAba9. Antimicrob Agents Chemother 53:4045–4047.

52. Higgins PG, Pérez-Llarena FJ, Zander E, Fernández A, Bou G, Seifert H. 2013. OXA-235, a novel class D β-lactamase involved in resistance to carbapenems in Acinetobacter baumannii. Antimicrob Agents Chemother 57:2121–2126.

53. Mugnier PD, Poirel L, Naas T, Nordmann P. 2010. Worldwide dissemination of the blaOXA-23 carbapenemase gene of Acinetobacter baumannii. Emerg Infect Dis 16:35–40.

54. Tian G-B, Adams-Haduch JM, Taracila M, Bonomo RA, Wang H-N, Doi Y. 2011. Extended-Spectrum AmpC Cephalosporinase in Acinetobacter baumannii: ADC-56 Confers Resistance to Cefepime ▿ . Antimicrob Agents Chemother 55:4922–4925.

55. Bai J, Dai Y, Farinha A, Tang AY, Syal S, Vargas-Cuebas G, van Opijnen T, Isberg RR, Geisinger E. Essential Gene Analysis in Acinetobacter baumannii by High-Density Transposon Mutagenesis and CRISPR Interference. J Bacteriol 203:e00565-20.

56. Chu X, Wang L, Zhu Y, Feng Z, Guan Q, Song L, Luo Z. 2023. A unique cell division protein critical for the assembly of the bacterial divisome https://doi.org/10.7554/eLife.87922.2.

57. Knight Daniel, Dimitrova Daniela D., Rudin Susan D., Bonomo Robert A., Rather Philip N. 2016. Mutations Decreasing Intrinsic β-Lactam Resistance Are Linked to Cell Division in the Nosocomial Pathogen Acinetobacter baumannii. Antimicrobial Agents and Chemotherapy 60:3751–3758.

58. Le N-H, Peters K, Espaillat A, Sheldon JR, Gray J, Di Venanzio G, Lopez J, Djahanschiri B, Mueller EA, Hennon SW, Levin PA, Ebersberger I, Skaar EP, Cava F, Vollmer W, Feldman MF. 2020. Peptidoglycan editing provides immunity to Acinetobacter baumannii during bacterial warfare. Science Advances 6:eabb5614.

59. Lam H, Oh D-C, Cava F, Takacs CN, Clardy J, de Pedro MA, Waldor MK. 2009. D-amino acids govern stationary phase cell wall remodeling in bacteria. Science 325:1552–1555.

60. Alsan M, Klompas M. 2010. Acinetobacter baumannii: An Emerging and Important Pathogen. J Clin Outcomes Manag 17:363–369.

61. Tipton KA, Dimitrova D, Rather PN. 2015. Phase-Variable Control of Multiple Phenotypes in Acinetobacter baumannii Strain AB5075. J Bacteriol 197:2593–2599.

62. Fiester SE, Actis LA. 2013. Stress responses in the opportunistic pathogen Acinetobacter baumannii. Future Microbiol 8:353–365.

63. Maharjan RP, Sullivan GJ, Adams FG, Shah BS, Hawkey J, Delgado N, Semenec L, Dinh H, Li L, Short FL, Parkhill J, Paulsen IT, Barquist L, Eijkelkamp BA, Cain AK. 2023. DksA is a conserved master regulator of stress response in Acinetobacter baumannii. Nucleic Acids Res 51:6101–6119.

64. Palethorpe S, Farrow JM, Wells G, Milton ME, Actis LA, Cavanagh J, Pesci EC. 2022. Acinetobacter baumannii Regulates Its Stress Responses via the BfmRS Two-Component Regulatory System. J Bacteriol 204:e0049421.

65. Casella LG, Torres NJ, Tomlinson BR, Shepherd M, Shaw LN. 2023. The novel two-component system AmsSR governs alternative metabolic pathway usage in Acinetobacter baumannii. Frontiers in Microbiology 14.

66. Green ER, Fakhoury JN, Monteith AJ, Pi H, Giedroc DP, Skaar EP. 2022. Bacterial hydrophilins promote pathogen desiccation tolerance. Cell Host Microbe 30:975-987.e7.

67. Perez Mora B, Giordano R, Permingeat V, Calderone M, Arana N, Müller G, Rodríguez RE, Krasauskas R, Mussi MA. 2023. BfmRS encodes a regulatory system involved in light signal transduction modulating motility and desiccation tolerance in the human pathogen Acinetobacter baumannii. Sci Rep 13:175.

68. Gaddy JA, Actis LA. 2009. Regulation of Acinetobacter baumannii biofilm formation. Future Microbiol 4:273–278.

69. Ren X, Palmer LD. 2023. Acinetobacter Metabolism in Infection and Antimicrobial Resistance. Infection and Immunity 91:e00433-22.

70. Zhao J, Zhu Y, Han J, Lin Y-W, Aichem M, Wang J, Chen K, Velkov T, Schreiber F, Li J. 2020. Genome-Scale Metabolic Modeling Reveals Metabolic Alterations of Multidrug-Resistant Acinetobacter baumannii in a Murine Bloodstream Infection Model. Microorganisms 8:1793.

71. Vestergaard M, Bald D, Ingmer H. 2022. Targeting the ATP synthase in bacterial and fungal pathogens: beyond *Mycobacterium tuberculosis*. Journal of Global Antimicrobial Resistance 29:29–41.

72. Rubin H, Selwood T, Yano T, Weaver DG, Loughran HM, Costanzo MJ, Scott RW, Wrobel JE, Freeman KB, Reitz AB. 2015. Acinetobacter baumannii OxPhos inhibitors as selective anti-infective agents. Bioorg Med Chem Lett 25:378–383.

73. Lobritz MA, Belenky P, Porter CBM, Gutierrez A, Yang JH, Schwarz EG, Dwyer DJ, Khalil AS, Collins JJ. 2015. Antibiotic efficacy is linked to bacterial cellular respiration. Proceedings of the National Academy of Sciences 112:8173–8180.

74. Dekic S, Hrenovic J, van Wilpe E, Venter C, Goic-Barisic I. 2019. Survival of emerging pathogen Acinetobacter baumannii in water environment exposed to different oxygen conditions. Water Sci Technol 80:1581–1590.

75. Noel HR, Petrey JR, Palmer LD. 2022. Mobile genetic elements in Acinetobacter antibiotic-resistance acquisition and dissemination. Ann N Y Acad Sci 1518:166–182.

76. Frost LS, Leplae R, Summers AO, Toussaint A. 2005. Mobile genetic elements: the agents of open source evolution. Nat Rev Microbiol 3:722–732.

77. Wijers CDM, Pham L, Menon S, Boyd KL, Noel HR, Skaar EP, Gaddy JA, Palmer LD, Noto MJ. 2021. Identification of Two Variants of Acinetobacter baumannii Strain ATCC 17978 with Distinct Genotypes and Phenotypes. Infect Immun 89:e0045421.

78. Whiteway C, Valcek A, Philippe C, Strazisar M, De Pooter T, Mateus I, Breine A, Van der Henst C. 2022. Scarless excision of an insertion sequence restores capsule production and virulence in Acinetobacter baumannii. ISME J 16:1473–1477.

79. Lee Y, Kim C-K, Lee H, Jeong SH, Yong D, Lee K. 2011. A novel insertion sequence, ISAba10, inserted into ISAba1 adjacent to the bla(OXA-23) gene and disrupting the outer membrane protein gene carO in Acinetobacter baumannii. Antimicrob Agents Chemother 55:361–363.

80. Gerson S, Nowak J, Zander E, Ertel J, Wen Y, Krut O, Seifert H, Higgins PG. 2018. Diversity of mutations in regulatory genes of resistance-nodulation-cell division efflux pumps in association with tigecycline resistance in Acinetobacter baumannii. J Antimicrob Chemother 73:1501–1508.

81. Geisinger E, Mortman NJ, Vargas-Cuebas G, Tai AK, Isberg RR. 2018. A global regulatory system links virulence and antibiotic resistance to envelope homeostasis in Acinetobacter baumannii. PLoS Pathog 14:e1007030.

82. Loh B, Chen J, Manohar P, Yu Y, Hua X, Leptihn S. 2020. A Biological Inventory of Prophages in A. baumannii Genomes Reveal Distinct Distributions in Classes, Length, and Genomic Positions. Front Microbiol 11:579802.

83. Kondo K, Kawano M, Sugai M. 2021. Distribution of Antimicrobial Resistance and Virulence Genes within the Prophage-Associated Regions in Nosocomial Pathogens. mSphere 6:10.1128/msphere.00452-21.

84. Soontarach R, Srimanote P, Arechanajan B, Nakkaew A, Voravuthikunchai SP, Chusri S. 2024. Characterization of a novel bacteriophage endolysin (LysAB1245) with extended lytic activity

against distinct capsular types associated with Acinetobacter baumannii resistance. PLOS ONE 19:e0296453.

85. Sitthisak S, Manrueang S, Khongfak S, Leungtongkam U, Thummeepak R, Thanwisai A, Burton N, Dhanoa GK, Tsapras P, Sagona AP. 2023. Antibacterial activity of vB_AbaM_PhT2 phage hydrophobic amino acid fusion endolysin, combined with colistin against Acinetobacter baumannii. Sci Rep 13:7470.

86. Khan FM, Rasheed F, Yang Y, Liu B, Zhang R. 2024. Endolysins: a new antimicrobial agent against antimicrobial resistance. Strategies and opportunities in overcoming the challenges of endolysins against Gram-negative bacteria. Front Pharmacol 15:1385261.

87. Blount ZD. 2015. The unexhausted potential of E. coli. Elife 4:e05826.

88. Nora LC, Westmann CA, Guazzaroni M-E, Siddaiah C, Gupta VK, Silva-Rocha R. 2019. Recent advances in plasmid-based tools for establishing novel microbial chassis. Biotechnol Adv 37:107433.

89. Sykes EME, Deo S, Kumar A. 2020. Recent Advances in Genetic Tools for Acinetobacter baumannii. Front Genet 11:601380.

90. Lucidi M, Runci F, Rampioni G, Frangipani E, Leoni L, Visca P. 2018. New Shuttle Vectors for Gene Cloning and Expression in Multidrug-Resistant Acinetobacter Species. Antimicrob Agents Chemother 62:e02480-17.

91. Jie J, Chu X, Li D, Luo Z. 2021. A set of shuttle plasmids for gene expression in Acinetobacter baumannii. PLoS One 16:e0246918.

92. Pérez-Varela M, Tierney ARP, Kim J-S, Vázquez-Torres A, Rather P. 2020. Characterization of RelA in Acinetobacter baumannii. J Bacteriol 202:e00045-20.

93. Williams CL, Neu HM, Alamneh YA, Reddinger RM, Jacobs AC, Singh S, Abu-Taleb R, Michel SLJ, Zurawski DV, Merrell DS. 2020. Characterization of Acinetobacter baumannii Copper Resistance Reveals a Role in Virulence. Front Microbiol 11:16.

94. Terpe K. 2006. Overview of bacterial expression systems for heterologous protein production: from molecular and biochemical fundamentals to commercial systems. Appl Microbiol Biotechnol 72:211–222.

95. Lozano Terol G, Gallego-Jara J, Sola Martínez RA, Martínez Vivancos A, Cánovas Díaz M, de Diego Puente T. 2021. Impact of the Expression System on Recombinant Protein Production in Escherichia coli BL21. Front Microbiol 12:682001.

96. De Silva PM, Kumar A. 2018. Effect of Sodium Chloride on Surface-Associated Motility of Acinetobacter baumannii and the Role of AdeRS Two-Component System. J Membrane Biol 251:5–13.

97. Trebosc V, Gartenmann S, Tötzl M, Lucchini V, Schellhorn B, Pieren M, Lociuro S, Gitzinger M, Tigges M, Bumann D, Kemmer C. 2019. Dissecting Colistin Resistance Mechanisms in Extensively Drug-Resistant Acinetobacter baumannii Clinical Isolates. mBio 10:e01083-19.

98. Tucker AT, Nowicki EM, Boll JM, Knauf GA, Burdis NC, Trent MS, Davies BW. 2014. Defining Gene-Phenotype Relationships in Acinetobacter baumannii through One-Step Chromosomal Gene Inactivation. mBio 5:e01313-14.

99. Hoang TT, Karkhoff-Schweizer RR, Kutchma AJ, Schweizer HP. 1998. A broad-host-range Flp-FRT recombination system for site-specific excision of chromosomally-located DNA sequences: application for isolation of unmarked Pseudomonas aeruginosa mutants. Gene 212:77–86.

100. van Opijnen T, Bodi KL, Camilli A. 2009. Tn-seq: high-throughput parallel sequencing for fitness and genetic interaction studies in microorganisms. Nat Methods 6:767–772.

101. Goodman AL, McNulty NP, Zhao Y, Leip D, Mitra RD, Lozupone CA, Knight R, Gordon JI. 2009. Identifying genetic determinants needed to establish a human gut symbiont in its habitat. Cell Host Microbe 6:279–289.

102. Langridge GC, Phan M-D, Turner DJ, Perkins TT, Parts L, Haase J, Charles I, Maskell DJ, Peters SE, Dougan G, Wain J, Parkhill J, Turner AK. 2009. Simultaneous assay of every Salmonella Typhi gene using one million transposon mutants. Genome Res 19:2308–2316.

103. Subashchandrabose S, Smith S, DeOrnellas V, Crepin S, Kole M, Zahdeh C, Mobley HLT. 2015. Acinetobacter baumannii Genes Required for Bacterial Survival during Bloodstream Infection. mSphere 1:10.1128/msphere.00013-15.

104. Wang N, Ozer EA, Mandel MJ, Hauser AR. 2014. Genome-Wide Identification of Acinetobacter baumannii Genes Necessary for Persistence in the Lung. mBio 5:e01163-14.

105. Wang Y, Wang Z, Chen Y, Hua X, Yu Y, Ji Q. 2019. A Highly Efficient CRISPR-Cas9-Based Genome Engineering Platform in Acinetobacter baumannii to Understand the H2O2-Sensing Mechanism of OxyR. Cell Chem Biol 26:1732-1742.e5.

106. Wang S, Ding Y, Rong H, Wang Y. 2024. The Development of a CRISPR-FnCpf1 System for Large-Fragment Deletion and Multiplex Gene Editing in Acinetobacter baumannii. Curr Issues Mol Biol 46:570–584.

107. Peters JM, Koo B-M, Patino R, Heussler GE, Hearne CC, Qu J, Inclan YF, Hawkins JS, Lu CHS, Silvis MR, Harden MM, Osadnik H, Peters JE, Engel JN, Dutton RJ, Grossman AD, Gross CA, Rosenberg OS. 2019. Enabling genetic analysis of diverse bacteria with Mobile-CRISPRi. Nat Microbiol 4:244–250.

108. Qi LS, Larson MH, Gilbert LA, Doudna JA, Weissman JS, Arkin AP, Lim WA. 2013. Repurposing CRISPR as an RNA-Guided Platform for Sequence-Specific Control of Gene Expression. Cell 152:1173–1183.

109. Enright AL, Heelan WJ, Ward RD, Peters JM. 2024. CRISPRi functional genomics in bacteria and its application to medical and industrial research. Microbiol Mol Biol Rev 88:e0017022.

110. Voogdt CGP, Tripathi S, Bassler SO, McKeithen-Mead SA, Guiberson ER, Koumoutsi A, Bravo AM, Buie C, Zimmermann M, Sonnenburg JL, Typas A, Deutschbauer AM, Shiver AL, Huang KC. 2024. Randomly barcoded transposon mutant libraries for gut commensals II: Applying libraries for functional genetics. Cell Rep 43:113519.

111. Lian J, Schultz C, Cao M, HamediRad M, Zhao H. 2019. Multi-functional genome-wide CRISPR system for high throughput genotype-phenotype mapping. Nat Commun 10:5794.

112. Mutalik VK, Novichkov PS, Price MN, Owens TK, Callaghan M, Carim S, Deutschbauer AM, Arkin AP. 2019. Dual-barcoded shotgun expression library sequencing for high-throughput characterization of functional traits in bacteria. Nat Commun 10:308.

113. Huang YY, Price MN, Hung A, Gal-Oz O, Ho D, Carion H, Deutschbauer AM, Arkin AP. 2023. Barcoded overexpression screens in gut Bacteroidales identify genes with new roles in carbon utilization and stress resistance. bioRxiv https://doi.org/10.1101/2022.10.10.511384.

114. Melief E, Kokoczka R, Files M, Bailey MA, Alling T, Li H, Ahn J, Misquith A, Korkegian A, Roberts D, Sacchettini J, Parish T. 2018. Construction of an overexpression library for Mycobacterium tuberculosis. Biol Methods Protoc 3:bpy009.

115. Banta AB, Myers KS, Ward RD, Cuellar RA, Place M, Freeh CC, Bacon EE, Peters JM. 2024. A Targeted Genome-scale Overexpression Platform for Proteobacteria. bioRxiv 2024.03.01.582922.

116. Brochado AR, Typas A. 2013. High-throughput approaches to understanding gene function and mapping network architecture in bacteria. Curr Opin Microbiol 16:199–206.

117. Todor H, Silvis MR, Osadnik H, Gross CA. 2021. Bacterial CRISPR screens for gene function. Curr Opin Microbiol 59:102–109.

118. Winzeler EA, Shoemaker DD, Astromoff A, Liang H, Anderson K, Andre B, Bangham R, Benito R, Boeke JD, Bussey H, Chu AM, Connelly C, Davis K, Dietrich F, Dow SW, El Bakkoury M, Foury F, Friend SH, Gentalen E, Giaever G, Hegemann JH, Jones T, Laub M, Liao H, Liebundguth N, Lockhart DJ, Lucau-Danila A, Lussier M, M'Rabet N, Menard P, Mittmann M, Pai C, Rebischung C, Revuelta JL, Riles L, Roberts CJ, Ross-MacDonald P, Scherens B, Snyder M, Sookhai-Mahadeo S, Storms RK, Véronneau S, Voet M, Volckaert G, Ward TR, Wysocki R, Yen GS, Yu K, Zimmermann K, Philippsen P, Johnston M, Davis RW. 1999. Functional Characterization of the S. cerevisiae Genome by Gene Deletion and Parallel Analysis. Science 285:901–906.

119. Baba T, Ara T, Hasegawa M, Takai Y, Okumura Y, Baba M, Datsenko KA, Tomita M, Wanner BL, Mori H. 2006. Construction of Escherichia coli K-12 in-frame, single-gene knockout mutants: the Keio collection. Molecular Systems Biology 2:2006.0008.

120. Koo B-M, Kritikos G, Farelli JD, Todor H, Tong K, Kimsey H, Wapinski I, Galardini M, Cabal A, Peters JM, Hachmann A-B, Rudner DZ, Allen KN, Typas A, Gross CA. 2017. Construction and Analysis of Two Genome-Scale Deletion Libraries for Bacillus subtilis. cels 4:291-305.e7.

121. Porwollik S, Santiviago CA, Cheng P, Long F, Desai P, Fredlund J, Srikumar S, Silva CA, Chu W, Chen X, Canals R, Reynolds MM, Bogomolnaya L, Shields C, Cui P, Guo J, Zheng Y, Endicott-Yazdani T, Yang H-J, Maple A, Ragoza Y, Blondel CJ, Valenzuela C, Andrews-Polymenis H, McClelland M. 2014. Defined Single-Gene and Multi-Gene Deletion Mutant Collections in Salmonella enterica sv Typhimurium. PLOS ONE 9:e99820.

122. de Berardinis V, Vallenet D, Castelli V, Besnard M, Pinet A, Cruaud C, Samair S, Lechaplais C, Gyapay G, Richez C, Durot M, Kreimeyer A, Le Fèvre F, Schächter V, Pezo V, Döring V, Scarpelli C, Médigue C, Cohen GN, Marlière P, Salanoubat M, Weissenbach J. 2008. A complete collection of single-gene deletion mutants of Acinetobacter baylyi ADP1. Molecular Systems Biology 4:174.

123. van Leeuwen J, Pons C, Tan G, Wang JZ, Hou J, Weile J, Gebbia M, Liang W, Shuteriqi E, Li Z, Lopes M, Ušaj M, Dos Santos Lopes A, van Lieshout N, Myers CL, Roth FP, Aloy P, Andrews BJ, Boone C. 2020. Systematic analysis of bypass suppression of essential genes. Molecular Systems Biology 16:e9828.

124. Ohya Y, Sese J, Yukawa M, Sano F, Nakatani Y, Saito TL, Saka A, Fukuda T, Ishihara S, Oka S, Suzuki G, Watanabe M, Hirata A, Ohtani M, Sawai H, Fraysse N, Latgé J-P, François JM, Aebi M, Tanaka S, Muramatsu S, Araki H, Sonoike K, Nogami S, Morishita S. 2005. High-dimensional and large-scale phenotyping of yeast mutants. Proc Natl Acad Sci U S A 102:19015–19020.

125. Campos M, Govers SK, Irnov I, Dobihal GS, Cornet F, Jacobs-Wagner C. 2018. Genomewide phenotypic analysis of growth, cell morphogenesis, and cell cycle events in Escherichia coli. Mol Syst Biol 14:e7573.

126. Berry DB, Guan Q, Hose J, Haroon S, Gebbia M, Heisler LE, Nislow C, Giaever G, Gasch AP. 2011. Multiple means to the same end: the genetic basis of acquired stress resistance in yeast. PLoS Genet 7:e1002353.

127. Sargentini NJ, Gularte NP, Hudman DA. 2016. Screen for genes involved in radiation survival of *Escherichia coli* and construction of a reference database. Mutation Research/Fundamental and Molecular Mechanisms of Mutagenesis 793–794:1–14.

128. De Oliveira DMP, Forde BM, Kidd TJ, Harris PNA, Schembri MA, Beatson SA, Paterson DL, Walker MJ. 2020. Antimicrobial Resistance in ESKAPE Pathogens. Clin Microbiol Rev 33:e00181-19.

129. Zhang X, de Maat V, Guzmán Prieto AM, Prajsnar TK, Bayjanov JR, de Been M, Rogers MRC, Bonten MJM, Mesnage S, Willems RJL, van Schaik W. 2017. RNA-seq and Tn-seq reveal fitness determinants of vancomycin-resistant Enterococcus faecium during growth in human serum. BMC Genomics 18:893.

130. Coe KA, Lee W, Stone MC, Komazin-Meredith G, Meredith TC, Grad YH, Walker S. 2019. Multi-strain Tn-Seq reveals common daptomycin resistance determinants in Staphylococcus aureus. PLoS Pathog 15:e1007862.

131. Lo H-Y, Long DR, Holmes EA, Penewit K, Hodgson T, Lewis JD, Waalkes A, Salipante SJ. 2023. Transposon sequencing identifies genes impacting Staphylococcus aureus invasion in a human macrophage model. Infect Immun 91:e0022823.

132. Paczosa MK, Silver RJ, McCabe AL, Tai AK, McLeish CH, Lazinski DW, Mecsas J. 2020. Transposon Mutagenesis Screen of Klebsiella pneumoniae Identifies Multiple Genes Important for Resisting Antimicrobial Activities of Neutrophils in Mice. Infect Immun 88:e00034-20.

133. Bachman MA, Breen P, Deornellas V, Mu Q, Zhao L, Wu W, Cavalcoli JD, Mobley HLT. 2015. Genome-Wide Identification of Klebsiella pneumoniae Fitness Genes during Lung Infection. mBio 6:e00775.

134. Boinett CJ, Cain AK, Hawkey J, Do Hoang NT, Khanh NNT, Thanh DP, Dordel J, Campbell JI, Lan NPH, Mayho M, Langridge GC, Hadfield J, Chau NVV, Thwaites GE, Parkhill J, Thomson NR, Holt KE, Baker S. 2019. Clinical and laboratory-induced colistin-resistance mechanisms in Acinetobacter baumannii. Microb Genom 5:e000246.

135. Turner KH, Wessel AK, Palmer GC, Murray JL, Whiteley M. 2015. Essential genome of Pseudomonas aeruginosa in cystic fibrosis sputum. Proceedings of the National Academy of Sciences 112:4110–4115.

136. Poulsen BE, Yang R, Clatworthy AE, White T, Osmulski SJ, Li L, Penaranda C, Lander ES, Shoresh N, Hung DT. 2019. Defining the core essential genome of Pseudomonas aeruginosa. Proc Natl Acad Sci U S A 116:10072–10080.

137. Guérin F, Lallement C, Goudergues B, Isnard C, Sanguinetti M, Cacaci M, Torelli R, Cattoir V, Giard J-C. 2020. Landscape of in vivo Fitness-Associated Genes of Enterobacter cloacae Complex. Front Microbiol 11:1609.

138. Cain AK, Barquist L, Goodman AL, Paulsen IT, Parkhill J, van Opijnen T. 2020. A decade of advances in transposon-insertion sequencing. Nat Rev Genet 21:526–540.

139. Wang Z, Gerstein M, Snyder M. 2009. RNA-Seq: a revolutionary tool for transcriptomics. Nat Rev Genet 10:57–63.

140. Tang J. 2011. Microbial Metabolomics. Curr Genomics 12:391–403.

141. Stephanopoulos G, Alper H, Moxley J. 2004. Exploiting biological complexity for strain improvement through systems biology. Nat Biotechnol 22:1261–1267.

142. Measday V, Baetz K, Guzzo J, Yuen K, Kwok T, Sheikh B, Ding H, Ueta R, Hoac T, Cheng B, Pot I, Tong A, Yamaguchi-Iwai Y, Boone C, Hieter P, Andrews B. 2005. Systematic yeast synthetic lethal and synthetic dosage lethal screens identify genes required for chromosome segregation. Proc Natl Acad Sci U S A 102:13956–13961.

143. Collins SR, Miller KM, Maas NL, Roguev A, Fillingham J, Chu CS, Schuldiner M, Gebbia M, Recht J, Shales M, Ding H, Xu H, Han J, Ingvarsdottir K, Cheng B, Andrews B, Boone C, Berger SL, Hieter P, Zhang Z, Brown GW, Ingles CJ, Emili A, Allis CD, Toczyski DP, Weissman JS,

Greenblatt JF, Krogan NJ. 2007. Functional dissection of protein complexes involved in yeast chromosome biology using a genetic interaction map. Nature 446:806–810.

144. Bernhardt TG, de Boer PAJ. 2004. Screening for synthetic lethal mutants in Escherichia coli and identification of EnvC (YibP) as a periplasmic septal ring factor with murein hydrolase activity. Mol Microbiol 52:1255–1269.

145. Bernhardt TG, de Boer PAJ. 2005. SlmA, a Nucleoid-Associated, FtsZ Binding Protein Required for Blocking Septal Ring Assembly over Chromosomes in E. coli. Mol Cell 18:555–564.

146. Paradis-Bleau C, Markovski M, Uehara T, Lupoli TJ, Walker S, Kahne DE, Bernhardt TG. 2010. Lipoprotein cofactors located in the outer membrane activate bacterial cell wall polymerases. Cell 143:1110–1120.

147. Paradis-Bleau C, Kritikos G, Orlova K, Typas A, Bernhardt TG. 2014. A genome-wide screen for bacterial envelope biogenesis mutants identifies a novel factor involved in cell wall precursor metabolism. PLoS Genet 10:e1004056.

148. Boone C, Bussey H, Andrews BJ. 2007. Exploring genetic interactions and networks with yeast. Nat Rev Genet 8:437–449.

149. Tong AHY, Lesage G, Bader GD, Ding H, Xu H, Xin X, Young J, Berriz GF, Brost RL, Chang M, Chen Y, Cheng X, Chua G, Friesen H, Goldberg DS, Haynes J, Humphries C, He G, Hussein S, Ke L, Krogan N, Li Z, Levinson JN, Lu H, Ménard P, Munyana C, Parsons AB, Ryan O, Tonikian R, Roberts T, Sdicu A-M, Shapiro J, Sheikh B, Suter B, Wong SL, Zhang LV, Zhu H, Burd CG, Munro S, Sander C, Rine J, Greenblatt J, Peter M, Bretscher A, Bell G, Roth FP, Brown GW, Andrews B, Bussey H, Boone C. 2004. Global Mapping of the Yeast Genetic Interaction Network. Science 303:808–813.

150. Beltrao P, Cagney G, Krogan NJ. 2010. Quantitative genetic interactions reveal biological modularity. Cell 141:739–745.

151. Rachwalski K, Ellis MJ, Tong M, Brown ED. 2022. Synthetic Genetic Interactions Reveal a Dense and Cryptic Regulatory Network of Small Noncoding RNAs in Escherichia coli. mBio 13:e01225-22.

152. Côté J-P, French S, Gehrke SS, MacNair CR, Mangat CS, Bharat A, Brown ED. 2016. The Genome-Wide Interaction Network of Nutrient Stress Genes in Escherichia coli. mBio 7:10.1128/mbio.01714-16.

153. Arroyo-Olarte RD, Bravo Rodríguez R, Morales-Ríos E. 2021. Genome Editing in Bacteria: CRISPR-Cas and Beyond. Microorganisms 9:844.

154. Li S, Jendresen CB, Landberg J, Pedersen LE, Sonnenschein N, Jensen SI, Nielsen AT. 2020. Genome-Wide CRISPRi-Based Identification of Targets for Decoupling Growth from Production. ACS Synth Biol 9:1030–1040.

155. Peters JM, Colavin A, Shi H, Czarny TL, Larson MH, Wong S, Hawkins JS, Lu CHS, Koo B-M, Marta E, Shiver AL, Whitehead EH, Weissman JS, Brown ED, Qi LS, Huang KC, Gross CA. 2016.

A Comprehensive, CRISPR-based Functional Analysis of Essential Genes in Bacteria. Cell 165:1493–1506.

156. Vigouroux A, Oldewurtel E, Cui L, Bikard D, van Teeffelen S. 2018. Tuning dCas9's ability to block transcription enables robust, noiseless knockdown of bacterial genes. Molecular Systems Biology 14:e7899.

157. Hawkins JS, Silvis MR, Koo B-M, Peters JM, Osadnik H, Jost M, Hearne CC, Weissman JS, Todor H, Gross CA. 2020. Mismatch-CRISPRi Reveals the Co-varying Expression-Fitness Relationships of Essential Genes in Escherichia coli and Bacillus subtilis. Cell Systems 11:523-535.e9.

158. Mathis AD, Otto RM, Reynolds KA. 2021. A simplified strategy for titrating gene expression reveals new relationships between genotype, environment, and bacterial growth. Nucleic Acids Res 49:e6.

159. Cho S, Choe D, Lee E, Kim SC, Palsson B, Cho B-K. 2018. High-Level dCas9 Expression Induces Abnormal Cell Morphology in *Escherichia coli*. ACS Synth Biol 7:1085–1094.

160. Zhang S, Voigt CA. 2018. Engineered dCas9 with reduced toxicity in bacteria: implications for genetic circuit design. Nucleic Acids Research https://doi.org/10.1093/nar/gky884.

161. Cui L, Vigouroux A, Rousset F, Varet H, Khanna V, Bikard D. 2018. A CRISPRi screen in E. coli reveals sequence-specific toxicity of dCas9. Nat Commun 9:1912.

162. Rostain W, Grebert T, Vyhovskyi D, Pizarro PT, Tshinsele-Van Bellingen G, Cui L, Bikard D. 2023. Cas9 off-target binding to the promoter of bacterial genes leads to silencing and toxicity. Nucleic Acids Research 51:3485–3496.

163. Marraffini LA. 2016. The CRISPR-Cas system of Streptococcus pyogenes: function and applications, p. . *In* Ferretti, JJ, Stevens, DL, Fischetti, VA (eds.), Streptococcus pyogenes: Basic Biology to Clinical Manifestations. University of Oklahoma Health Sciences Center, Oklahoma City (OK).

164. Enright AL, Banta AB, Ward RD, Rivera Vazquez J, Felczak MM, Wolfe MB, TerAvest MA, Amador-Noguez D, Peters JM. 2023. The genetics of aerotolerant growth in an alphaproteobacterium with a naturally reduced genome. mBio 14:e0148723.

165. Bosch B, DeJesus MA, Poulton NC, Zhang W, Engelhart CA, Zaveri A, Lavalette S, Ruecker N, Trujillo C, Wallach JB, Li S, Ehrt S, Chait BT, Schnappinger D, Rock JM. 2021. Genome-wide gene expression tuning reveals diverse vulnerabilities of M. tuberculosis. Cell 184:4579-4592.e24.

166. Otto RM, Turska-Nowak A, Brown PM, Reynolds KA. 2024. A continuous epistasis model for predicting growth rate given combinatorial variation in gene expression and environment. cels 15:134-148.e7.

167. Martin JK, Sheehan JP, Bratton BP, Moore GM, Mateus A, Li SH-J, Kim H, Rabinowitz JD, Typas A, Savitski MM, Wilson MZ, Gitai Z. 2020. A Dual-Mechanism Antibiotic Kills Gram-Negative Bacteria and Avoids Drug Resistance. Cell 181:1518-1532.e14.

168. Cacace E, Kritikos G, Typas A. 2017. Chemical genetics in drug discovery. Curr Opin Syst Biol 4:35–42.

169. Andrusiak K, Piotrowski JS, Boone C. 2012. Chemical-genomic profiling: systematic analysis of the cellular targets of bioactive molecules. Bioorg Med Chem 20:1952–1960.

170. Brenner C. 2004. Chemical genomics in yeast. Genome Biol 5:240.

171. Nichols RJ, Sen S, Choo YJ, Beltrao P, Zietek M, Chaba R, Lee S, Kazmierczak KM, Lee KJ, Wong A, Shales M, Lovett S, Winkler ME, Krogan NJ, Typas A, Gross CA. 2011. Phenotypic landscape of a bacterial cell. Cell 144:143–156.

172. Price MN, Wetmore KM, Waters RJ, Callaghan M, Ray J, Liu H, Kuehl JV, Melnyk RA, Lamson JS, Suh Y, Carlson HK, Esquivel Z, Sadeeshkumar H, Chakraborty R, Zane GM, Rubin BE, Wall JD, Visel A, Bristow J, Blow MJ, Arkin AP, Deutschbauer AM. 2018. Mutant phenotypes for thousands of bacterial genes of unknown function. Nature 557:503–509.

173. Sher JW, Lim HC, Bernhardt TG. 2020. Global phenotypic profiling identifies a conserved actinobacterial cofactor for a bifunctional PBP-type cell wall synthase. eLife 9:e54761.

174. Li S, Poulton NC, Chang JS, Azadian ZA, DeJesus MA, Ruecker N, Zimmerman MD, Eckartt KA, Bosch B, Engelhart CA, Sullivan DF, Gengenbacher M, Dartois VA, Schnappinger D, Rock JM. 2022. CRISPRi chemical genetics and comparative genomics identify genes mediating drug potency in Mycobacterium tuberculosis. 6. Nat Microbiol 7:766–779.

175. Johnson EO, LaVerriere E, Office E, Stanley M, Meyer E, Kawate T, Gomez JE, Audette RE, Bandyopadhyay N, Betancourt N, Delano K, Da Silva I, Davis J, Gallo C, Gardner M, Golas AJ, Guinn KM, Kennedy S, Korn R, McConnell JA, Moss CE, Murphy KC, Nietupski RM, Papavinasasundaram KG, Pinkham JT, Pino PA, Proulx MK, Ruecker N, Song N, Thompson M, Trujillo C, Wakabayashi S, Wallach JB, Watson C, Ioerger TR, Lander ES, Hubbard BK, Serrano-Wu MH, Ehrt S, Fitzgerald M, Rubin EJ, Sassetti CM, Schnappinger D, Hung DT. 2019. Large-scale chemical-genetics yields new M. tuberculosis inhibitor classes. Nature 571:72–78.

CHAPTER 2

Essential Gene Knockdowns Reveal Genetic Vulnerabilities and Antibiotic Sensitivities in *Acinetobacter baumannii*

A version of this chapter has been published:

Ryan D. Ward, Jennifer S. Tran, Amy B. Banta, Emily E. Bacon, Warren E. Rose, Jason M. Peters. 2024. Essential gene knockdowns reveal genetic vulnerabilities and antibiotic sensitivities in *Acinetobacter baumannii*. *mBio* 15:e02051-23.

I performed initial optimization of Mobile-CRISPRi transfer and expression in *A. baumannii*, characterized the prophage repressor, performed growth curves and NAD+/NADH experiments, and created and compiled figures. RDW designed computational tools, analyzed data, and performed synergy/ antagonism assays. ABB created the library and performed competition fitness and MIC assays. JMP sequenced the novel dCas9 promoter, performed membrane potential experiments, and wrote the paper. Supplementary figures can be found at the end of the chapter. Other supplementary material is available for download at https://doi.org/10.1128/mbio.02051-23.

Abstract

The emergence of multidrug-resistant Gram-negative bacteria underscores the need to define genetic vulnerabilities that can be therapeutically exploited. The Gram-negative pathogen, *Acinetobacter baumannii*, is considered an urgent threat due to its propensity to evade antibiotic treatments. Essential cellular processes are the target of existing antibiotics and a likely source of new vulnerabilities. Although *A. baumannii* essential genes have been identified by transposon sequencing (Tn-seq), they have not been prioritized by sensitivity to knockdown or antibiotics. Here, we take a systems biology approach to comprehensively characterize *A. baumannii* essential genes using CRISPR interference (CRISPRi). We show that certain essential genes and pathways are acutely sensitive to knockdown, providing a set of vulnerable targets for future therapeutic investigation. Screening our CRISPRi library against last-resort antibiotics uncovered genes and pathways that modulate beta-lactam sensitivity, an unexpected link between NADH dehydrogenase activity and growth inhibition by polymyxins, and anticorrelated phenotypes that may explain synergy between polymyxins and rifamycins. Our study demonstrates the power of systematic genetic approaches to identify vulnerabilities in Gram-negative pathogens and uncovers antibiotic-essential gene interactions that better inform combination therapies.

Importance

Acinetobacter baumannii is a hospital-acquired pathogen that is resistant to many common antibiotic treatments. To combat resistant *A. baumannii* infections, we need to identify promising therapeutic targets and effective antibiotic combinations. In this study, we comprehensively characterize the genes and pathways that are critical for *A. baumannii* viability. We show that genes involved in aerobic metabolism are central to *A. baumannii* physiology and may represent appealing drug targets. We also find antibiotic-gene interactions that may impact the efficacy of carbapenems, rifamycins, and polymyxins, providing a new window into how these antibiotics function in mono- and combination therapies. Our studies offer a useful approach for characterizing interactions between drugs and essential genes in pathogens to inform future therapies.

Introduction

The rise of antibiotic resistance in Gram-negative pathogens, including *Acinetobacter baumannii*, is a pressing healthcare concern, as many infections become untreatable amid a stalled pipeline for novel therapies (1). *A. baumannii* causes serious infections in hospitalized patients and is considered an urgent threat for its ability to evade killing by last-resort antibiotics (2). It has numerous defenses against antibiotics including a propensity to acquire resistance genes through horizontal transfer (3, 4), low membrane permeability coupled with robust efflux to prevent antibiotics from reaching their cytoplasmic targets (5), and rapid accumulation of resistance mutations (6). Although its unique strengths in resisting antibiotics are well documented, less is known about whether *A. baumannii* carries any unique vulnerabilities that could be therapeutically exploited.

The distinct physiology of *A. baumannii* sets it apart from well-studied, Gram-negative bacteria. Among the Gram-negative ESKAPE pathogens (*i.e.*, *Klebsiella*, *Acinetobacter*, *Pseudomonas*, and *Enterobacter*), *A. baumannii* is the only obligate aerobe, requiring oxidative phosphorylation to generate ATP (7). Further, the outer membrane of *A. baumannii* contains lipooligosaccharide (LOS) rather than lipopolysaccharide (LPS) found in most Gram-negative bacteria (8). LOS and LPS both contain a core lipid A moiety, but LOS lacks the repeating units of O-polysaccharide found in LPS (8). Although LPS is essential for viability in other Gram-negative ESKAPE pathogens, a recent study showed that LOS was dispensable in ~60% of *A. baumannii* strains tested, including contemporary clinical isolates (9). LOS^- strains cannot be targeted by lipid A-binding antibiotics, such as polymyxins, increasing the antibiotic resistance threat posed by *A. baumannii* (10). Finally, *A. baumannii* has numerous genes of unknown function, including essential genes that are not present in model Gram-negatives or other ESKAPE pathogens (11). These distinctions underscore

the importance of examining essential gene phenotypes and antibiotic interactions directly in *A. baumannii*.

Systematic genetic studies of *Acinetobacter* species have provided valuable physiological insights, although *A. baumannii* essential genes have not been comprehensively characterized. Tn-seq studies in *A. baumannii* identified putative essential genes (11, 12), defined phenotypes for previously uncharacterized genes (13), and uncovered the mechanism for strain-specific essentiality of LOS biosynthesis (9). An elegant Tn-seq study of non-pathogenic *Acinetobacter baylyi* monitored depletion of strains with disrupted essential genes following natural transformation (14), but it remains unclear whether those findings are directly applicable to *A. baumannii*.

CRISPR interference (CRISPRi) is the premier genetic tool to define essential gene function and antibiotic-gene interactions in bacteria. This gene knockdown technology uses a programmable, single guide RNA (sgRNA) to direct a catalytically inactive Cas effector protein (typically dCas9) to a target gene for silencing (15, 16). CRISPRi partial knockdowns enable phenotyping of essential genes either by titrating the levels of CRISPRi components using inducible or weak promoters (15, 17, 18), or by modifying the sgRNA to weaken its interaction with target DNA (19–21) or dCas9 (22). Due to its portability, CRISPRi has proven valuable for phenotyping essential genes in diverse bacteria, including ESKAPE and other pathogens (11, 23, 24). Antibiotic-gene interaction screens using CRISPRi often recover the direct antibiotic target or related pathways among the largest outliers (17, 25). For instance, we previously identified the direct targets of two uncharacterized antibiotics using a *Bacillus subtilis* essential gene CRISPRi library, followed by genetic and biochemical validation of top hits (17). Although CRISPRi has been previously developed in *A. baumannii* by us and others (11, 23), only a handful of essential genes have been phenotyped to date.

To systematically probe for genetic vulnerabilities in *A. baumannii*, we generated and screened a pooled CRISPRi library targeting all putative essential genes (Fig 2.1A). We identified essential genes and pathways that are most sensitive to knockdown, thereby prioritizing targets for future drug screens. We further used CRISPRi to define genetic interactions with last-resort antibiotics, finding antibiotic target pathways, obstacles to drug efficacy, and antibiotic-gene phenotypes that that inform synergistic drug combinations.

Results

Construction and validation of an A. baumannii essential gene CRISPRi library

We constructed a CRISPRi library targeting all putative essential genes in *A. baumannii* 19606, a strain extensively used to characterize the fundamental biology of *A. baumannii* that is also the type strain for antibiotic susceptibility testing (26). Notably, this strain is viable without LOS (9), allowing us to examine the phenotypic consequences of LOS loss. Developing our library in a susceptible strain made it straightforward to use antibiotics as probes for gene function.

To systematically investigate essential genes, we first optimized CRISPRi in *A. baumannii*, finding that reduced expression of *dcas9* lowered toxicity and still achieved ~20-fold knockdown (Fig 2.S1A-E, Supplementary Methods, and Tables 2.1-2.3). We next designed and constructed a CRISPRi library targeting all putative essential genes in *A. baumannii*. As the goal of our study was to characterize rather than define essential genes, we used existing Tn-seq data (12) to generate a list of CRISPRi targets we call the "*Ab* essentials" (406 orthologous essential genes total in 19606). We designed a computationally optimized CRISPRi library targeting the *Ab* essentials that consisted of three types of sgRNAs: 1) perfect match sgRNAs (15) to maximize knockdown (~4/gene), 2) single-base mismatch sgRNAs (19) to create a gradient of partial gene knockdowns (~10/gene), and 3) control sgRNAs that are non-targeting (1000 total). This library was cloned and site-specifically

Figure 2.1. CRISPRi screening overview. (A) Design and construction of a Mobile-CRISPRi library targeting all putative essential genes in *A. baumannii* 19606. The library was screened with CRISPRi inducer (1 mM IPTG (Isopropyl ß-D-1-thiogalactopyranoside) to identify genes that are vulnerable to knockdown or with inducer and a sub-minimal inhibitory concentration of antibiotic to identify antibiotic-gene interactions. (B and C) Density plot showing depletion of essential gene targeting sgRNA spacers (perfect match or mismatch) from the library but not depletion of non-targeting control sgRNAs during growth over two time points (T1 and T2). (D) The population diversity (N_b) of essential gene targeting sgRNAs is reduced relative to controls, indicating that those sgRNAs are depleted during growth. The white horizontal line through the bars indicates a break in the data.

Figure 2.1

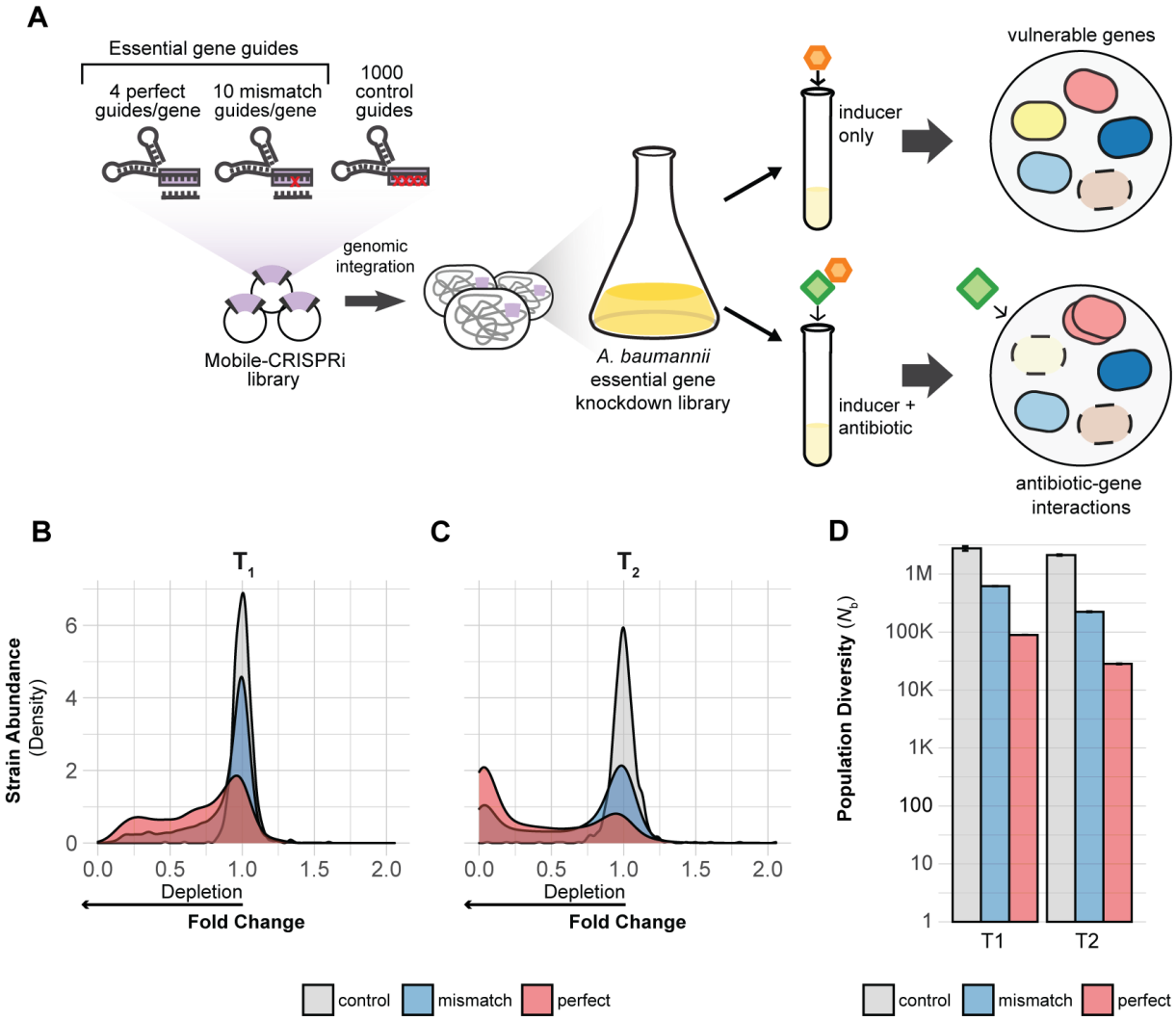
A
Essential gene guides
4 perfect guides/gene
10 mismatch guides/gene
1000 control guides
genomic integration
Mobile-CRISPRi library
A. baumannii essential gene knockdown library
inducer only
inducer + antibiotic
vulnerable genes
antibiotic-gene interactions
B
T1
Strain Abundance (Density)
Depletion
Fold Change
C
T2
Depletion
Fold Change
D
Population Diversity (N_b)
1M
100K
10K
1K
100
10
1
T1
T2
control
mismatch
perfect

integrated into the 19606 genome using Mobile-CRISPRi (Fig 2.1A) (23). Illumina sequencing of integrated sgRNA spacers confirmed that our CRISPRi library successfully targeted all the *Ab* essentials (median = 14 guides/gene; (Fig 2.S2A)). Our approach, which includes using multiple sgRNAs per gene and robust statistics, mitigates potential issues with toxic or inactive guides.

To validate our *A. baumannii* CRISPRi library, we measured the depletion of essential-gene-targeting sgRNAs during pooled growth. We grew the library to exponential phase in rich medium (LB) without induction (T0), diluted back into fresh medium with saturating IPTG to induce CRISPRi and grew cells for ~7 doublings (T1), then diluted back a second time in IPTG-containing medium and grew cells for an additional ~7 doublings (T2). Quantifying strain depletion using $\log_2$ fold change ($\log_2$FC) and population diversity (N_b; (27)) between T0, T1, and T2 (Fig 2.1B-D, 2.S2B) revealed noticeable depletion of essential-gene-targeting sgRNAs by T1 and substantial depletion by T2, while control sgRNAs were unaffected. The lack of an induction effect on control strain abundance suggests that toxic guide RNAs such as “bad seeds” (28) are largely absent from our library. Taken together, our CRISPRi library effectively and comprehensively perturbs essential gene functions in *A. baumannii*.

Identification of A. baumannii essential genes and pathways that are sensitive to knockdown

Essential genes with a strong, negative impact on fitness when knocked down, *i.e.*, “vulnerable" genes, are potential high-value targets for antibiotic development. CRISPRi enables the identification of vulnerable genes by controlling the duration and extent of knockdown (19, 20, 29). To define a set of vulnerable genes, we first quantified depletion of strains containing perfect match guides from the CRISPRi library during growth in rich medium (LB) (Fig 2.S3A). At T1, 88 genes showed significant depletion ($\log_2$FC<-1 and Stouffer's p<0.05), and by T2 an additional 192 genes were depleted (280/406 total or 69%). Screening our library in antibiotics at sub-MIC (minimal

inhibitory concentration) levels recovered phenotypes for 74 for the 126 genes that were non-responsive in rich medium (see below), suggesting that these genes could be involved in antibiotic mode of action (Fig 2.S3B). The remaining 52 genes that were non-responsive in all our conditions may require additional depletion (19), are false positives from the Tn-seq analysis used to define the *Ab* essentials (12), or are not essential in 19606. Overall, most *Ab* essentials (354/406 or 87%) showed significant phenotypes in our CRISPRi screens.

We sought to prioritize target genes and pathways by sensitivity to knockdown. Because CRISPRi knockdown affects transcription units (TUs) that can encode multiple gene products, we assigned essential genes to TUs and then organized the TUs into two groups: those containing only one essential gene and those containing multiple essential genes. We observed that most essential genes fall into one of two groups with respect to TUs: 1) TUs containing only one essential gene, or 2) TUs containing multiple essential genes that participate in the same cellular process; thus, most CRISPRi knockdowns affected single genes or single processes. Next, we ranked TU sensitivity to knockdown by the median $\log_2$FC of perfect match guides targeting essential genes present in the TU. Our measurements of $\log_2$FC are robust; however, we caution that small quantitative differences in gene/TU ranks may not always indicate meaningful variations in vulnerability.

Knockdowns of *murA*, *rpmB*, *aroC* and the poorly characterized gene, GO593_00515 were among the most depleted strains in our CRISPRi library (Fig 2.2A-B). These genes represent established as well as underexplored therapeutic targets, and are in TUs containing only one essential gene, allowing straightforward interpretation of phenotypes. The *murA* gene, which encodes the target of fosfomycin (30), is vulnerable to knockdown despite fosfomycin's inefficacy against *A. baumannii* due to efflux by the AbaF pump (31). L28, encoded by *rpmB*, is a bacterium-specific ribosomal protein that is required for assembly of the 70S ribosome in *Escherichia coli* (32, 33), but has no characterized inhibitors to our knowledge. Interestingly, *E. coli* cells with reduced L28 levels

Figure 2.2. *A. baumannii* genes and pathways that are vulnerable to knockdown. (A-B) Depletion of sgRNAs targeting transcription units (TUs) from the CRISPRi library during growth in inducer over two time points (T_1 and T_2). Vertical dashed lines indicate a two-fold change in relative fitness score, and horizontal dashed lines indicate a Stouffer's *p* value of ≤ 0.05. Stouffer's *p* values were calculated at the TU level by combining the false discovery rates (FDRs) of all individual sgRNAs targeting the TU. TUs related to pathways discussed in the text are colored according to the legend and the number of essential genes in a TU is indicated by point size.

Figure 2.2

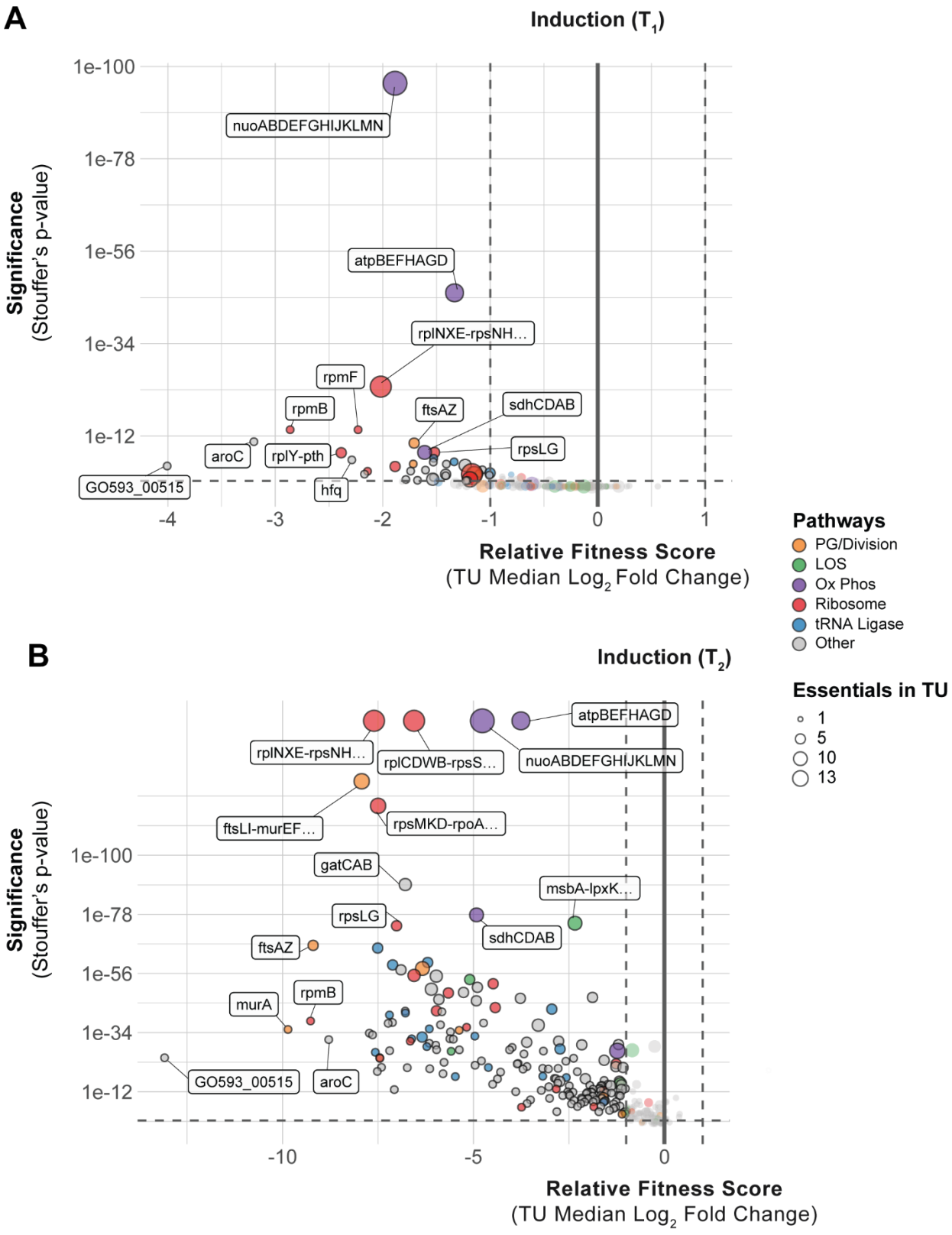
A
Induction (T_1)
Significance
(Stouffer's p-value)
1e-100
1e-78
1e-56
1e-34
1e-12
nuoABDEFGHIJKLMN
atpBEFHAGD
rplNXE-rpsNH…
rpmF
rpmB
ftsAZ
sdhCDAB
rpsLG
aroC
rplY-pth
hfq
GO593_00515
-4
-3
-2
-1
0
1
Relative Fitness Score
(TU Median Log$_2$ Fold Change)
Pathways
PG/Division
LOS
Ox Phos
Ribosome
tRNA Ligase
Other
Essentials in TU
1
5
10
13
B
Induction (T_2)
Significance
(Stouffer's p-value)
atpBEFHAGD
rplNXE-rpsNH…
rplCDWB-rpsS…
nuoABDEFGHIJKLMN
ftsLI-murEF…
rpsMKD-rpoA…
gatCAB
msbA-lpxK…
rpsLG
sdhCDAB
ftsAZ
rpmB
murA
GO593_00515
aroC
1e-100
1e-78
1e-56
1e-34
1e-12
-10
-5
0
Relative Fitness Score
(TU Median Log$_2$ Fold Change)

accumulate ribosome fragments that can be assembled into translation-competent ribosomes by expressing additional L28 (33), suggesting that L28 could play a role in regulation of ribosome assembly. The *aroC* gene encodes chorismate synthase, a metabolic enzyme genetically upstream of aromatic amino acid and folate biosynthesis. The abundance of aromatic amino acids in LB medium used in our screen suggests that the essential role of *aroC* is likely in folate biosynthesis. Chorismate synthase is essential in several bacterial species including Gram-positives, such as *B. subtilis* (34), and is vulnerable to knockdown in *Mycobacterium tuberculosis* (29), raising the possibility that *aroC* could be a general, high-value target.

Surprisingly, the most depleted knockdown strain in our library targeted an uncharacterized gene: GO593_00515 (Fig 2.2A-B). GO593_00515 is predicted to encode an Arc family transcriptional repressor; Arc repressors have been extensively studied for their role in the Phage P22 life cycle (35). Accordingly, GO593_00515 is located within a predicted prophage in the 19606 genome; this locus is occupied by a similar but distinct prophage in the model resistant strain AB5075 (Fig 2.S4A). Synteny between the 19606 prophage and P22 suggested a role for GO593_00515 in lysogeny maintenance. Consistent with this hypothesis, we found that GO593_00515 knockdown cells showed little growth 10 hours after dilution into IPTG-containing medium (Fig 2.S4C), and inducing knockdown in growing GO593_00515 CRISPRi cells caused complete lysis occurred within 7 hours (Fig 2.S4B). We reasoned that if the essential function of GO593_00515 is to repress expression of toxic prophage genes, we could suppress its essentiality by deleting the surrounding prophage genes entirely. Indeed, we recovered prophage deletion strains lacking GO593_00515 after inducing GO593_00515 in the presence of an integrated knockout plasmid (Fig 2.S4C). Thus, repression of toxic prophage genes is a critical but conditionally essential function in *A. baumannii*. Given the ubiquity of prophages harboring toxic lysis genes (36), we suggest that knockdown of phage repressors could aid in identifying proteins that are exceptional at lysing *A. baumannii*.

Sensitivity to knockdown among groups of genes with related functions provided further insight into *A. baumannii* vulnerabilities. Strong depletion of knockdowns targeting components of the ribosome, peptidoglycan (PG) synthesis, and cell division validated our CRISPRi screen by identifying pathways targeted by clinically relevant antibiotics (Fig 2.2A-B). Genes encoding aminoacyl-tRNA synthetases (aaRSs) were functionally enriched among strains with reduced abundance at T2. Mupirocin, which targets IleRS, is the only inhibitor of a bacterial aaRS used clinically, although other aaRS inhibitors are used to treat infections caused by eukaryotic microbes (37). aaRSs are currently prioritized as targets for tuberculosis treatment as *M. tuberculosis* aaRS genes are vulnerable to knockdown (29) and a LeuRS/MetRS dual inhibitor is currently undergoing clinical trials (38). Our data demonstrate the vulnerability of aaRS genes in *A. baumannii* and suggest that aaRSs could serve as effective targets. Oxidative phosphorylation (oxphos) genes also stood out by degree of functional depletion in our library as early as T1 (Fig 2.2A). Among the oxphos outliers, genes encoding the NADH dehydrogenase complex I (NDH-1; *nuo* genes) were particularly sensitive to knockdown. This finding highlights the distinct importance of aerobic metabolism in *A. baumannii* compared to other Gram-negative pathogens, such as *E. coli*, where NDH-1 is not essential for viability in aerobic conditions (39).

Ideal antibiotic targets have a tight relationship between target function and fitness such that small perturbations result in a substantial loss of viability. Recent work in model bacteria (19, 20) and *M. tuberculosis* (29) has found that the relationship between knockdown and fitness for essential genes is non-linear and varies by gene or pathway. To examine this phenomenon for *A. baumannii* vulnerable genes, we fit the relationship between gene knockdown (predicted by machine learning (19)) and fitness (log_2FC of mismatch guides) to generate "knockdown-response" curves (Fig 2.3A-B). We found that vulnerable genes and pathways were highly sensitive to even low levels of knockdown. Knockdown-response curves allowed us to determine the amount of knockdown

Figure 2.3. Knockdown-response curves describe gene and pathway vulnerability. (A-B) Knockdown-response curves of the LOS gene *lpxA* and the PG/division gene *murA*. Points are individual mismatch sgRNAs; mismatch sgRNA knockdown was predicted as previously described (19). Colored lines are a 4-parameter logistic fit describing the relationship between relative fitness score and knockdown. The effective knockdown 50 (EK_{50}) is the amount of predicted knockdown needed to achieve a half-maximal effect on relative fitness score. EK_{50}s are depicted as crosshairs. (C-D) Knockdown response curves for genes in LOS synthesis or PG/division pathways. Points indicate the EK_{50} for individual pathway genes. Boxplots on the y-axis show the distribution of relative fitness scores at EK_{50} for genes in the pathway and boxplots on the x-axis show the distribution of EK_{50} values for genes in the pathway. Statistical significance was assessed using Wilcoxon Rank Sum Test; asterisks indicate $p \leq 0.05$ and ns for not significant.

Figure 2.3

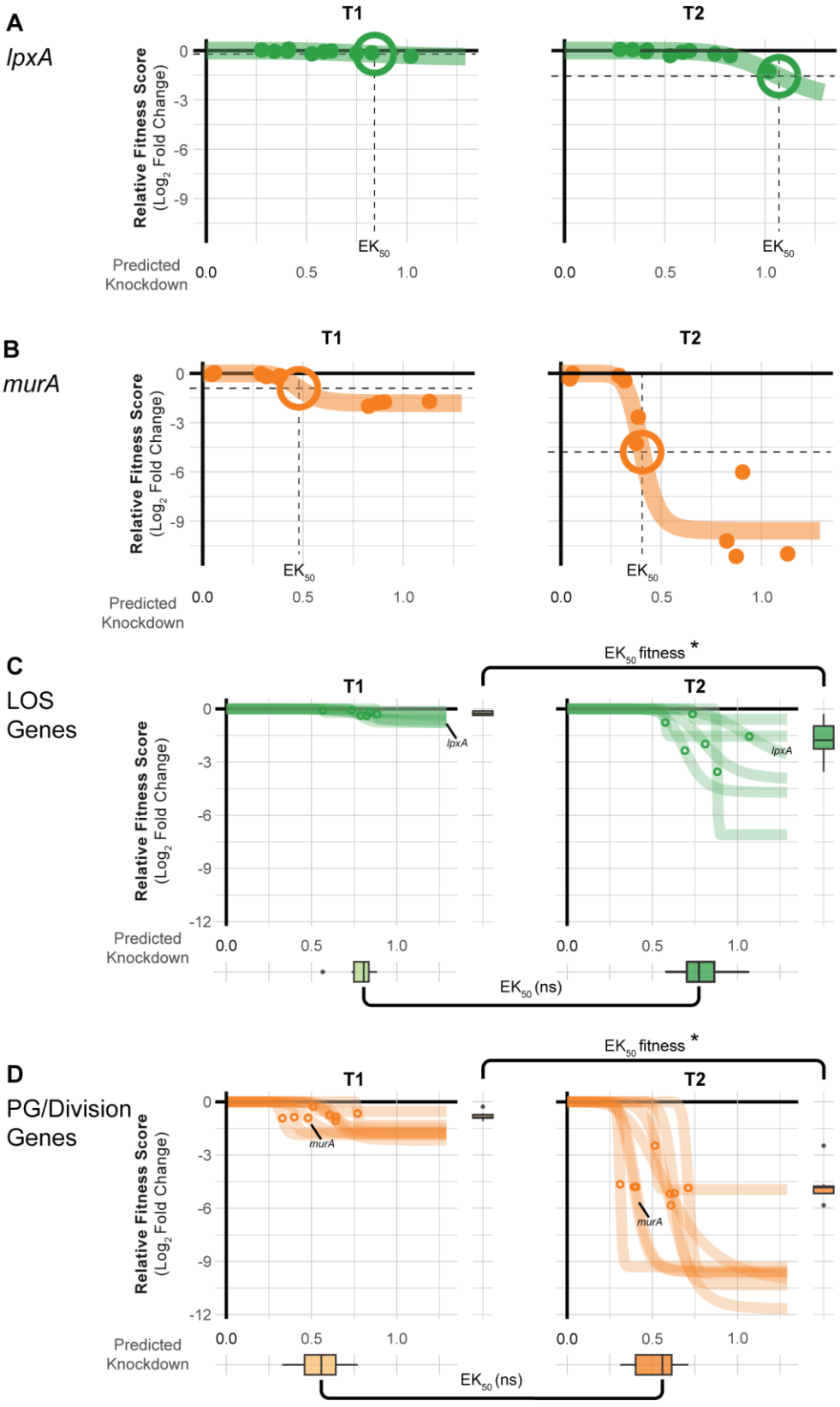
A
lpxA
T1
T2
Relative Fitness Score
(Log2 Fold Change)
0
-3
-6
-9
EK50
Predicted
Knockdown
0.0
0.5
1.0
B
murA
C
LOS
Genes
EK50 fitness *
lpxA
EK50 (ns)
D
PG/Division
Genes
murA
-12

required to elicit a half-maximal reduction in fitness (effective knockdown, or EK_{50}) at the gene level. Vulnerable essential genes, such as *murA*, showed a substantial fitness defect at less than half of the maximal knockdown, whereas non-essential genes, such as *lpxA*, showed little fitness defects even at higher levels of knockdown. Other vulnerable genes (e.g., *rpmB*, *aroC*, and GO593_00515) also showed heightened sensitivity to knockdown (Fig 2.S5). We extended our knockdown-response analysis to the pathway level, finding that pathways with many vulnerable genes (PG/division) required less knockdown, on average, than pathways with few vulnerable genes (LOS) (Fig 2.3C-D). Interestingly, although fitness at T2 was generally lower than T1 for vulnerable genes, EK_{50} values at both time points were statistically indistinguishable. This demonstrates that even guides with weak knockdown contribute to vulnerability phenotypes and suggests that gene phenotypes occur when a threshold of knockdown is crossed and that threshold is pathway dependent in *A. baumannii*.

Essential gene knockdowns that potentiate or mitigate carbapenem sensitivity in A. baumannii

Antibiotic-gene interaction screens have the potential to identify targets that synergize with or antagonize existing therapies. Carbapenems, a class of beta-lactam antibiotics, are first-line treatments for *A. baumannii* that block PG synthesis by inhibiting penicillin binding proteins (PBPs) (40). To uncover antibiotic-essential gene interactions that impact sensitivity to carbapenems, we screened our CRISPRi library against sub-MIC concentrations of imipenem (IMI) and meropenem (MER) (Fig 2.4A, 2.S6A-B). We found that knockdown of genes involved in cell wall synthesis, including the direct target (*ftsI*, TU: *ftsLI-murEF-mraY*), increased carbapenem sensitivity. Knockdowns of genes required for PG precursor synthesis (*murA*, *dapA*) and translocation (*murJ*) were strongly depleted in both IMI and MER. MurA catalyzes the first committed step of PG synthesis, DapA is part of a pathway that converts L-aspartate to meso-diaminopimelate which is incorporated into PG precursors by MurE, and MurJ, the lipid II flippase, translocates PG precursors from the inside to the outside of the cytoplasmic membrane (41). To validate screen hits, we

Figure 2.4. Essential gene interactions with carbapenem antibiotics in *A. baumannii*. (A) Boxplots showing the relative fitness scores of selected TUs that interact with imipenem (IMI, 0.09 μg/mL) across the genome at T_1. Points are individual guides in the TU. Boxplots are colored by relevant pathways; light-blue boxplots indicate TUs where tRNA synthetase genes are present with genes in other pathways. (B-C) CoMBaT-seq data from a growth competition between either a *murA* or *glnS* knockdown strain and a non-targeting control strain in the presence or absence of IMI (0.09 μg/mL). Only data from the gene targeting strain is depicted as the non-targeting control is the remaining proportion of the population. Points are data from individual experiments (N = 2).

Figure 2.4

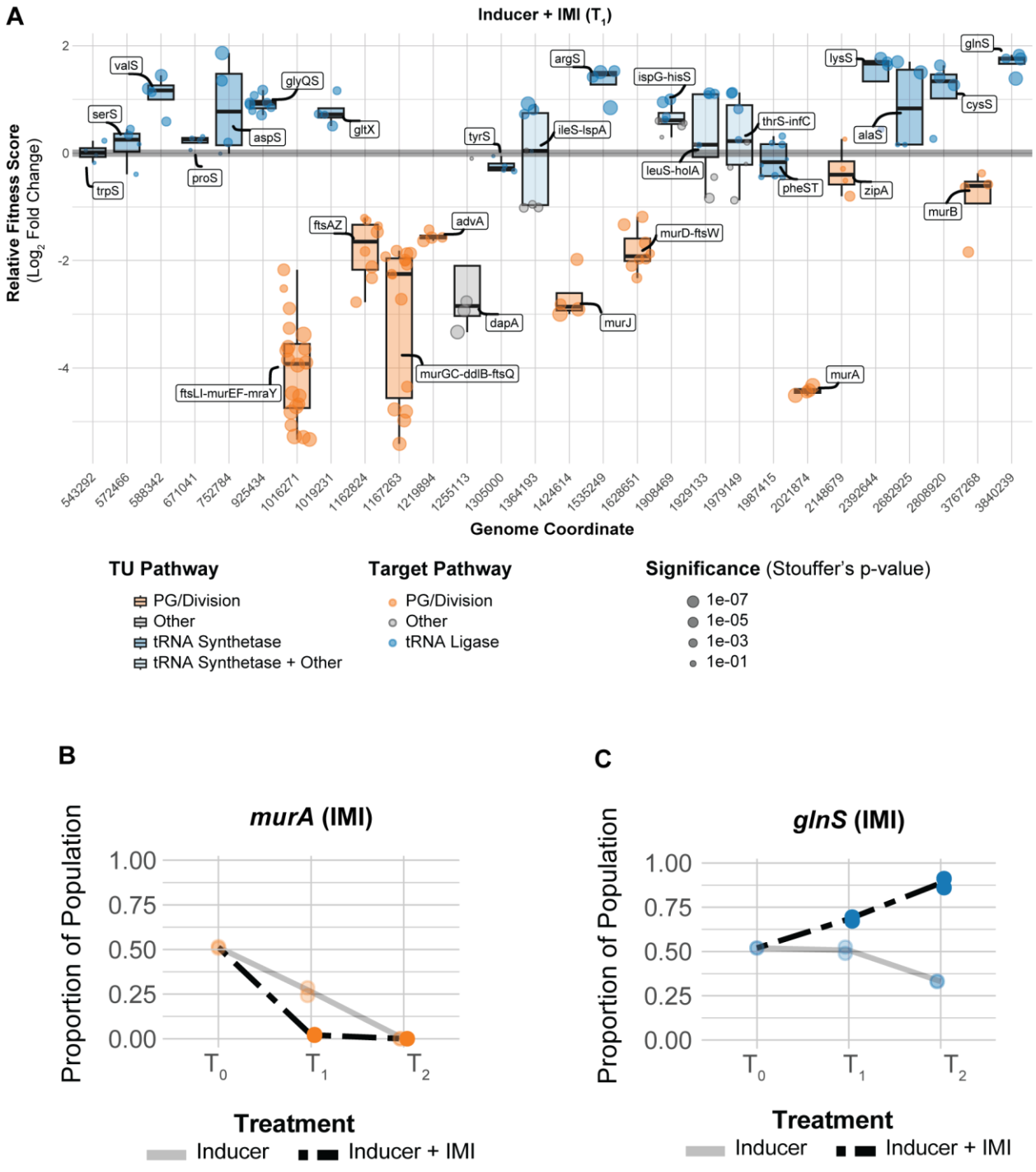
A
Inducer + IMI (T1)
Relative Fitness Score (Log2 Fold Change)
Genome Coordinate
valS
serS
trpS
proS
aspS
glyQS
gltX
tyrS
argS
ileS-lspA
ispG-hisS
leuS-holA
thrS-infC
pheST
lysS
alaS
zipA
glnS
cysS
murB
ftsAZ
advA
murD-ftsW
murJ
dapA
murGC-ddlB-ftsQ
ftsLI-murEF-mraY
murA
TU Pathway
PG/Division
Other
tRNA Synthetase
tRNA Synthetase + Other
Target Pathway
PG/Division
Other
tRNA Ligase
Significance (Stouffer's p-value)
1e-07
1e-05
1e-03
1e-01
B
murA (IMI)
Proportion of Population
Treatment
Inducer
Inducer + IMI
C
glnS (IMI)
Proportion of Population
Treatment
Inducer
Inducer + IMI

developed a small-scale version of our initial screen that retains its high sensitivity while reducing pool complexity; this assay uses Next Generation Sequencing to measure competitive fitness between a non-targeting and CRISPRi knockdown strain (*i.e.*, "CoMBaT-seq" or Competition of Multiplexed Barcodes over Time). We validated CoMBaT-seq by recapitulating *murA* vulnerability to knockdown and further sensitivity to IMI (Fig 2.4B). Because IMI targets cell wall synthesis, reduced growth of gene knockdowns in the same pathway could be considered a “dosing effect” rather than a true synergy. To test for synergy, we performed a checkerboard assay between IMI and fosfomycin. Consistent with our *murA*-IMI interaction, we found that fosfomycin and IMI synergize in *A. baumannii* (FIC<0.5) (Fig 2.S7A), as is the case in other Gram-negative pathogens (e.g., *Pseudomonas aeruginosa* (42)). Although no clinically relevant inhibitors of DapA and MurJ exist, to our knowledge, we speculate that such inhibitors would have the potential to synergize with carbapenems. Intriguingly, knockdowns of *advA*—an Acinetobacter-specific division gene (13)—were also sensitized to carbapenems, raising the possibility of *A. baumannii* targeting combination therapies should inhibitors of AdvA be identified.

Gene knockdowns that mitigate antibiotic function can reveal routes to resistance or target combinations that result in antagonism and should be avoided therapeutically. Given that increasing carbapenem resistance is an urgent clinical concern for *A. baumannii*, we sought to identify genes and pathways that mitigate the efficacy of IMI and MER. Although previous work suggested that growth rate and beta-lactam resistance are linearly related (43, 44), we found only a modest linear relationship growth and IMI/MER resistance across knockdown strains in our library (R^2 = 0.005, and 0.007, respectively (Fig 2.S8A-B)). This indicates that slow growing strains of *A. baumannii* are not necessarily more resistant to beta-lactam treatment. Instead, we found that specific genetic pathways govern carbapenem resistance. Using gene set enrichment analysis, we identified ribosomal protein genes as a pathway that increases resistance to IMI/MER when

perturbed [IMI: enrichment score = 4.65, FDR (afc) = 2.12e-06; MER: enrichment score = 2.43, FDR (afc) = 0.002], consistent with antagonism between beta-lactams and ribosome inhibitors described for other bacteria (45).

aaRS genes also emerged from our enrichment analysis [IMI: enrichment score = 4.93, FDR (afc) = 1.04e-06; MER: enrichment score = 5.04, FDR (afc) = 1.16e-06], uncovering a connection between tRNA charging and carbapenem resistance, as well as a surprising relationship between knockdown and fitness unique to antagonistic interactions. A subset of aaRS gene knockdowns including *argS*, *lysS*, *valS*, *cysS* and *glnS* showed increased relative fitness in our IMI pooled screen (Fig 2.4A, 2.S8C). Although *glnS* resistance to IMI in MIC test strip and growth curve assays was modest (Fig 2.S9), our more sensitive CoMBaT-seq assay showed a clear growth advantage for the *glnS* knockdown when competed against a non-targeting control (in contrast to sensitive knockdowns such as *murA*) (Fig 2.4B-C). Our observations that the *glnS* knockdown is depleted during growth in rich medium and enriched during growth in IMI implied that the relationship between knockdown and fitness changed across the two conditions. Indeed, a 4-parameter knockdown-response curve fit well to mismatch guides targeting *glnS* without treatment, but poorly to the same guides in IMI treatment (Fig 2.5A-D, 2.S10A-B). Remarkably, IMI treated *glnS* knockdown strains showed increased relative fitness as knockdown increased up until a point at the strains lost viability, presumably due to a lack of glutamine tRNA charging. This pattern is reminiscent of a hormetic response in dose-response curves (46) where a low amount of drug produces a positive response that eventually becomes negative at higher doses (Fig 2.5A-B). Accordingly, a 5-parameter logistic curve typically used in the context of hormetic responses improved the fit to IMI treated *glnS* mismatch strains but did not improve the fit of untreated strains (Fig 2.5C-D, 2.S10B). To test if the hormetic effect we observed between IMI and *glnS* in an antibiotic-gene interaction was relevant to antibiotic-antibiotic interactions, we measured the

Figure 2.5. Knockdown extent affects the sign of antibiotic-gene interactions. (A-B) Schematics of idealized dose-response curves showing monotonic or hormetic relationships between dose and response; hormetic responses change the sign of the response depending on dose. (C-D) Knockdown-response curves of *glnS* show a nearly monotonic response in the absence of IMI, but a hormetic response in the presence of IMI. (E) The interaction between the IleRS tRNA synthetase inhibitor mupirocin (MUP) and IMI shows a hormetic response at intermediate concentrations of IMI.

Figure 2.5

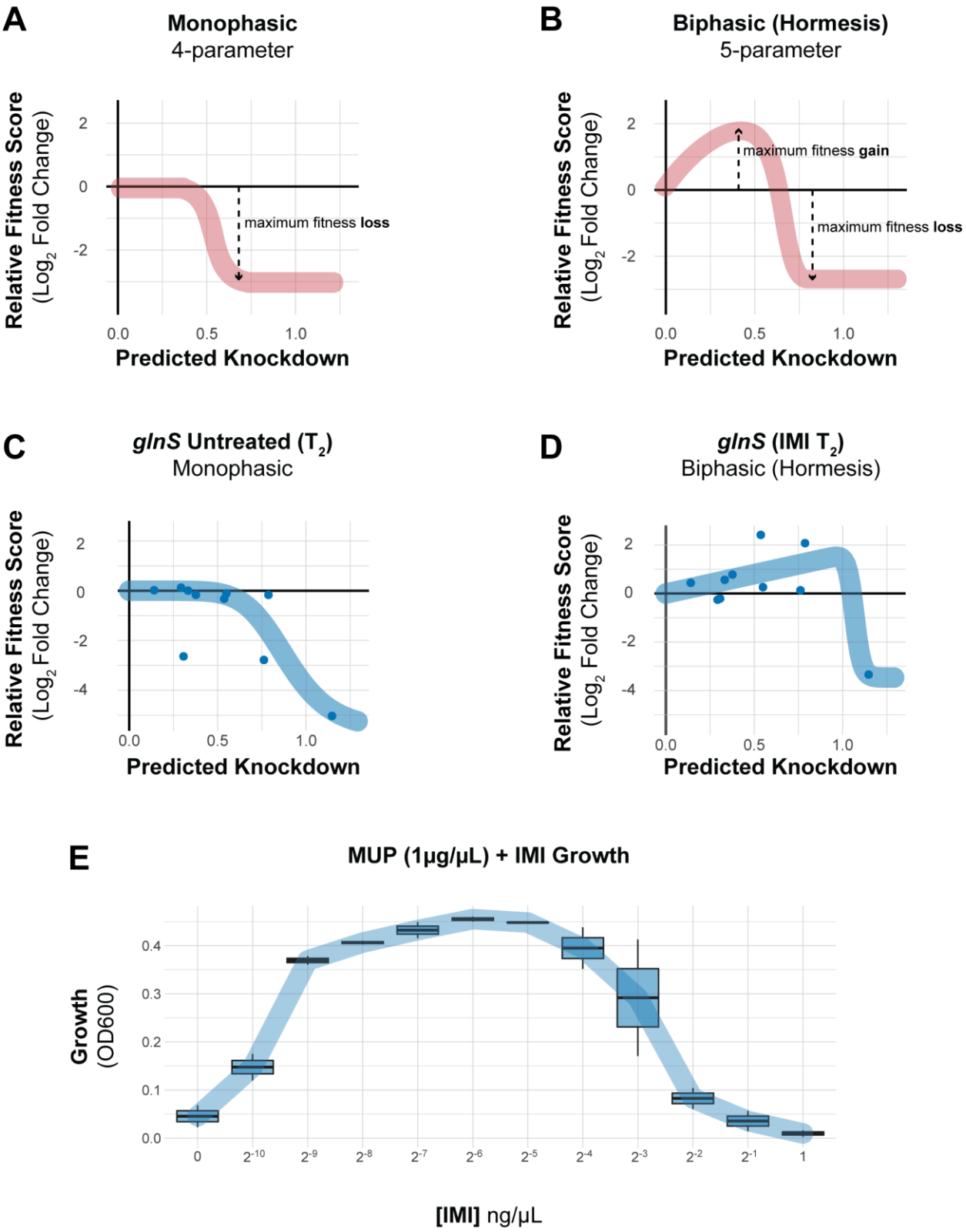
A
Monophasic
4-parameter
Relative Fitness Score
(Log2 Fold Change)
maximum fitness loss
Predicted Knockdown
B
Biphasic (Hormesis)
5-parameter
maximum fitness gain
maximum fitness loss
C
glnS Untreated (T2)
Monophasic
D
glnS (IMI T2)
Biphasic (Hormesis)
E
MUP (1µg/µL) + IMI Growth
Growth
(OD600)
[IMI] ng/µL

growth of wild-type *A. baumannii* treated with IMI and the aaRS inhibitor, mupirocin. Consistent with hormesis, IMI antagonized the effect of mupirocin at low concentrations, but had no positive impact on growth at higher concentrations (Fig 2.5E). Although mupirocin treatment is not clinically relevant for *A. baumannii* due to high-level resistance, our work provides proof of principle that hormetic effects can be predicted by genetic approaches and influence antibiotic susceptibility.

The synergistic antibiotic pair, colistin and rifampicin, show anticorrelated phenotypes

Antibiotic-gene interaction screens can identify genes and pathways that contribute to drug synergy. Colistin (COL) and rifampicin (RIF) synergistically inhibit *A. baumannii* growth (Fig 2.S11) (47), in part due to permeabilization of the outer membrane by COL (48). To define antibiotic-gene interactions that may inform COL-RIF synergy, we screened our CRISPRi library against COL and RIF individually. We found strong, opposing phenotypes in COL and RIF for genes encoding NDH-1 and LOS biosynthesis genes. COL, a polymyxin class antibiotic, is a last-resort treatment for carbapenem-resistant *A. baumannii* (49). COL binds to the lipid A moiety of LOS and is thought to kill cells by membrane disruption (50); complete loss of LOS results in a >500-fold increase in COL resistance (9). As expected, screening our library against a sub-MIC dose of COL identified LOS synthesis genes as resistant outliers (Fig 2.6A, 2.S12). Among the most resistant outliers were *lpxC* (TU: *lpxC*) and *lpxA* (TU: *lpxD-fabZ-lpxA*), which encode enzymes that catalyze the first two committed steps in LOS synthesis and are commonly found in selections for COL resistant mutants (9). Genes involved in fatty acid biosynthesis (TU: *fabDG*, TU: *aroQ-accBC*) also showed increased resistance to COL, possibly by limiting the pool of fatty acids available for LOS synthesis (Fig 2.6A). Surprisingly, knockdown of genes encoding NDH-1 (TU: *nuoABDEFGHIJKLMN*) caused heightened sensitivity to COL in the context of our pooled screen (Fig 2.6A, 2.S12). We robustly confirmed the COL sensitivity of a *nuoB* knockdown using our CoMBaT-seq assay (Fig 2.7A), although MIC test strips showed a more muted effect (Fig 2.S13). NDH-1 couples conversion

Figure 2.6. Essential gene knockdown phenotypes in colistin or rifampicin. Volcano plots for (A) colistin (COL) or (B) rifampicin (RIF). Depletion of sgRNA spacers from the CRISPRi library (relative fitness score) during growth in antibiotic and IPTG compared to IPTG alone at the level of transcription units (TUs). Dashed lines indicate a two-fold change in relative fitness score and a *p* value of ≤ 0.05. Stouffer's *p* values were calculated at the TU level by aggregating false discovery rates (FDRs) of individual sgRNAs targeting the TU. TUs related to pathways discussed in the text are colored as described in the legend and the number of essential genes in the TU is indicated by point size.

Figure 2.6

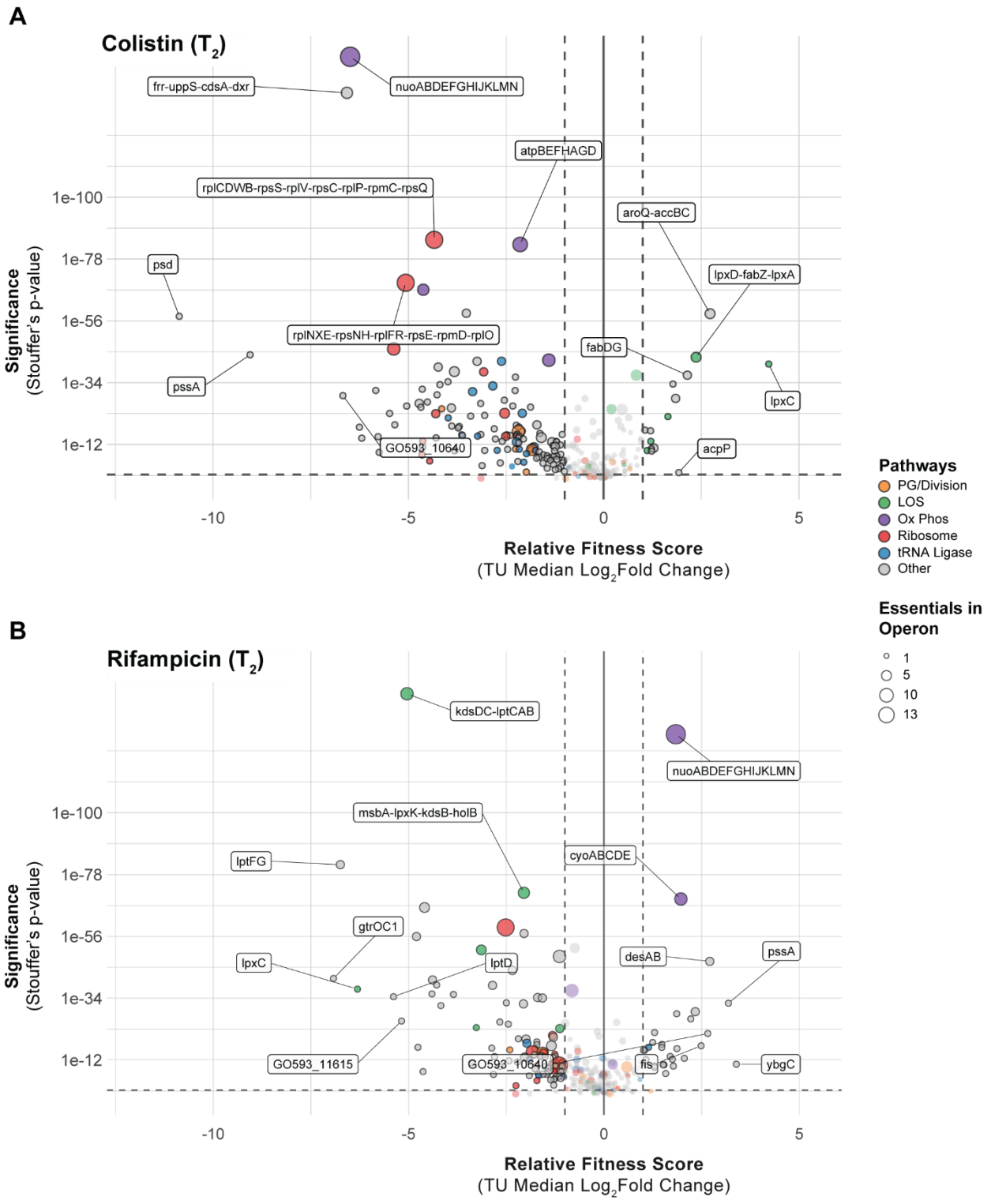
A
Colistin (T_2)
frr-uppS-cdsA-dxr
nuoABDEFGHIJKLMN
atpBEFHAGD
rplCDWB-rpsS-rplV-rpsC-rplP-rpmC-rpsQ
aroQ-accBC
psd
lpxD-fabZ-lpxA
rplNXE-rpsNH-rplFR-rpsE-rpmD-rplO
fabDG
pssA
lpxC
GO593_10640
acpP
1e-100
1e-78
1e-56
1e-34
1e-12
Significance
(Stouffer's p-value)
-10
-5
0
5
Relative Fitness Score
(TU Median Log2Fold Change)
Pathways
PG/Division
LOS
Ox Phos
Ribosome
tRNA Ligase
Other
Essentials in Operon
1
5
10
13
B
Rifampicin (T_2)
kdsDC-lptCAB
nuoABDEFGHIJKLMN
msbA-lpxK-kdsB-holB
lptFG
cyoABCDE
gtrOC1
lpxC
lptD
desAB
pssA
GO593_11615
GO593_10640
fis
ybgC
1e-100
1e-78
1e-56
1e-34
1e-12
Significance
(Stouffer's p-value)
-10
-5
0
5
Relative Fitness Score
(TU Median Log2Fold Change)

Figure 2.7. COL/RIF interaction with and physiological characterization of NDH-1 knockdown. (A) CoMBaT-seq data from a growth competition between a *nuoB* knockdown strain and a non-targeting control strain in the presence or absence of COL. Only data from the gene targeting strain is depicted as the non-targeting control is the remaining proportion of the population. Points are data from individual experiments (N = 2). (B) Measurement of the NAD+/NADH ratio in *nuoB* knockdown and non-targeting cells using the NAD/NADH-Glo assay. An unequal variance t-test was performed, and the asterisk indicates that the *p* value ≤ 0.05. (C-D) Knockdown-response curves of *nuoB* show a nearly monotonic response in the absence of RIF, but a hormetic response in the presence of RIF. (E) CoMBaT-seq data from a growth competition between a *nuoB* knockdown strain and a non-targeting control strain in the presence or absence of RIF. (F) EtBr permeability assay of non-targeting and *nuoB* knockdown strains; *nuoB* knockdowns show decreased access of EtBr to DNA in the cytoplasm.

Figure 2.7

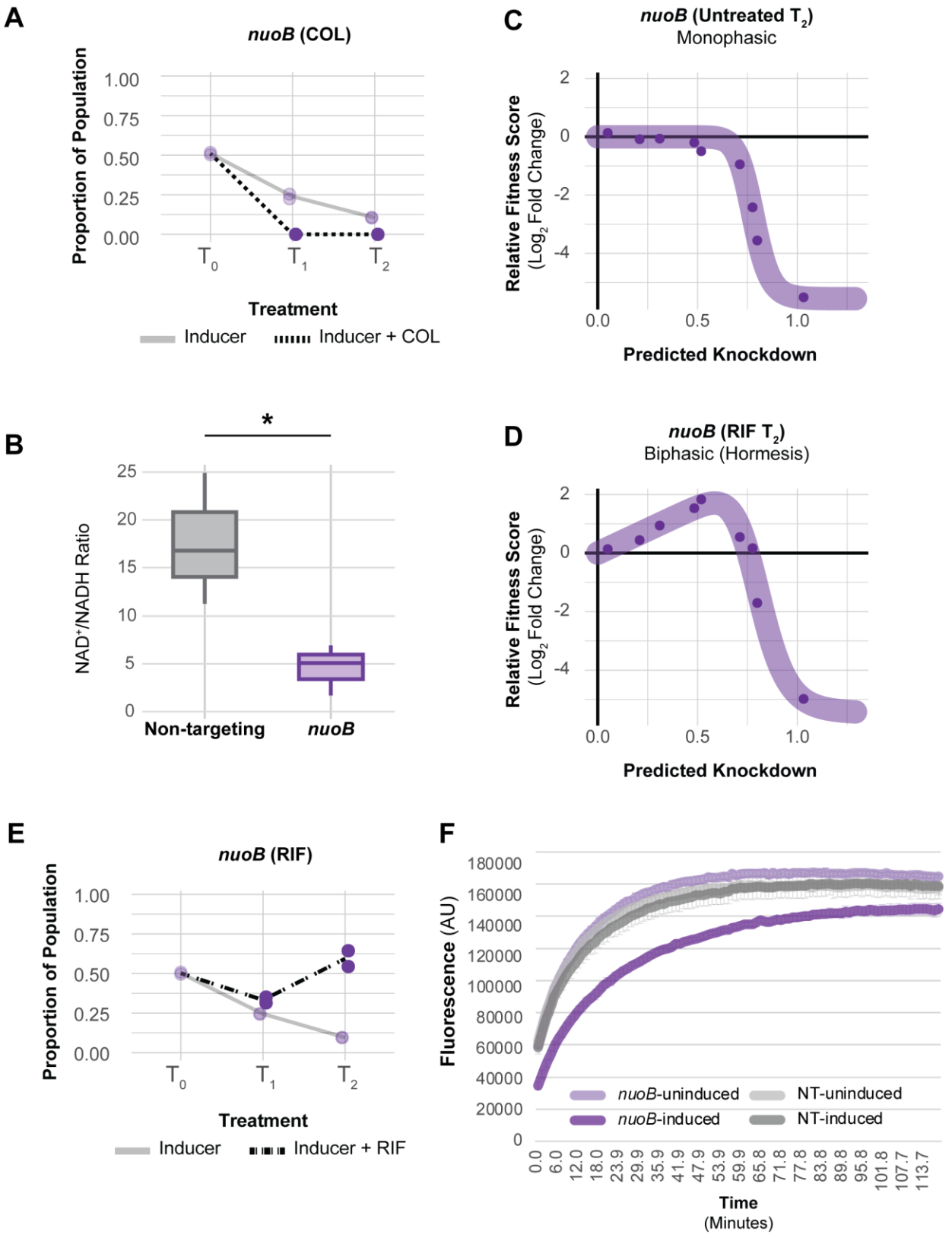
A
nuoB (COL)
Proportion of Population
1.00
0.75
0.50
0.25
0.00
T0
T1
T2
Treatment
Inducer
Inducer + COL
B
*
NAD+/NADH Ratio
25
20
15
10
5
0
Non-targeting
nuoB
C
nuoB (Untreated T2)
Monophasic
Relative Fitness Score
(Log2 Fold Change)
2
0
-2
-4
0.0
0.5
1.0
Predicted Knockdown
D
nuoB (RIF T2)
Biphasic (Hormesis)
Relative Fitness Score
(Log2 Fold Change)
2
0
-2
-4
0.0
0.5
1.0
Predicted Knockdown
E
nuoB (RIF)
Proportion of Population
1.00
0.75
0.50
0.25
0.00
T0
T1
T2
Treatment
Inducer
Inducer + RIF
F
Fluorescence (AU)
180000
160000
140000
120000
100000
80000
60000
40000
20000
0
nuoB-uninduced
nuoB-induced
NT-uninduced
NT-induced
0.0
6.0
12.0
18.0
23.9
29.9
35.9
41.9
47.9
53.9
59.9
65.8
71.8
77.8
83.8
89.8
95.8
101.8
107.7
113.7
Time
(Minutes)

of NADH to NAD+ to proton translocation across the inner membrane, but whether the key role for NDH-1 in *A. baumannii* physiology is NAD+ recycling or contributing to membrane potential (Δψ) is unknown. To address this issue, we measured the NAD+/NADH ratio and Δψ using an enzyme-coupled luminescence assay (NAD/NADH-Glo) and the membrane potential-sensitive dye Thioflavin T (ThT), respectively (Fig 2.7B, 2.S14A). Knockdown of *nuoB* lowered the NAD+/NADH ratio, consistent with reduced conversion of NADH to NAD+ by NDH-1 (Fig 2.7B). Unexpectedly, *nuoB* knockdown did not impact Δψ, although reduced Δψ in cells treated with the ionophore CCCP was readily apparent in our ThT assay (Fig 2.S14B). Thus, recycling of NADH to NAD+ for use in the TCA cycle, rather than maintenance of membrane potential, may be the critical cellular role of NDH-1. *A. baumannii* also encodes a non-essential, non-proton pumping NDH-2 enzyme that can be inhibited by COL *in vitro* (51). We speculate that NDH-2 inhibition by COL combined with knockdown of NDH-1 critically reduces cellular NAD+ levels, leading to enhanced sensitivity.

Rifampicin is a relatively large antibiotic (822.9 Da) that targets RNA polymerase (RNAP) in the cytoplasm but is typically avoided for treating Gram-negative infections due to low permeability (52). Consistent with a permeability barrier to rifampicin function (53), we found that knockdown of LOS synthesis and transport genes strongly sensitized cells to rifampicin [enrichment score = 8.83, FDR (afc) = 3.97e-05]. Again, knockdown of genes encoding NDH-1 produced an unexpected phenotype, this time increasing RIF resistance by an unknown mechanism (Fig 2.6B, 2.S12). To further characterize the NDH-1 RIF resistance phenotype, we examined the knockdown-response curve of *nuoB* with and without RIF treatment. As seen previously with *glnS*, *nuoB* knockdown showed a hormetic response: increasing knockdown of *nuoB* increased relative fitness in RIF until the highest levels of *nuoB* knockdown where growth decreased (Fig 2.7C-D, 2.S10C-D). Although MIC changes were modest Fig(2.S15), our CoMBaT-seq assay showed a clear fitness benefit for *nuoB* knockdown in RIF relative to a non-targeting control (Fig 2.7E). We considered that NDH-1

knockdown cells may have reduced permeability, limiting RIF entry into the cytoplasm. To test permeability, we measured uptake of ethidium bromide (EtBr) which fluoresces when bound to DNA in the cytoplasm (Fig 2.7F). We found that *nuoB* knockdown cells had a reduced rate of EtBr uptake, demonstrating that cells with reduced NDH-1 activity are less permeable and suggesting a possible mechanism for increased RIF resistance.

COL and RIF showed the strongest anticorrelated phenotypes in our CRISPRi screen (linear regression, $p<0.001$), with LOS related knockdowns causing resistance to COL and sensitivity to RIF and NDH-1 knockdowns resulting in sensitivity to COL and resistance to RIF (Fig 2.8). These anticorrelated phenotypes are consistent with a model in which COL increases the permeability of the outer membrane to RIF (48), but also suggest additional complexities due to *nuo* interactions with COL and RIF. The extent to which NADH-1 modulates COL-RIF synergy will be explored in future studies.

Figure 2.8. Anticorrelated gene-antibiotic interactions for colistin and rifampicin. Relative fitness score changes for genes encoding NDH-1 or involved in LOS biosynthesis in COL or RIF treated conditions relative to untreated.

Figure 2.8

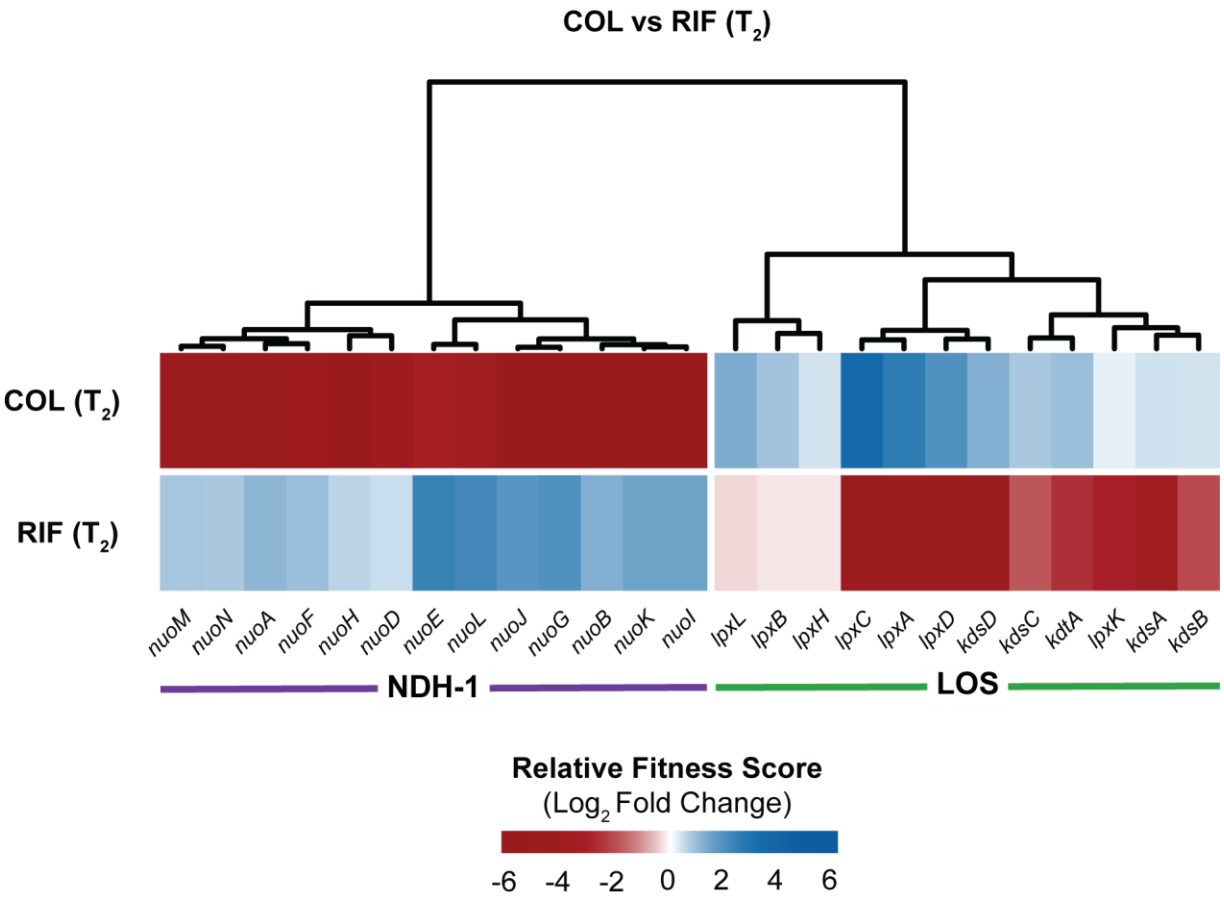
COL vs RIF (T2)
COL (T2)
RIF (T2)
nuoM nuoN nuoA nuoF nuoH nuoD nuoE nuoL nuoJ nuoG nuoB nuoK nuoI
lpxL lpxB lpxH lpxC lpxA lpxD kdsD kdsC kdtA lpxK kdsA kdsB
NDH-1
LOS
Relative Fitness Score
(Log2 Fold Change)
-6 -4 -2 0 2 4 6

Discussion

Bacterial susceptibility to antibiotics is underpinned by species- and condition-specific gene essentiality. The recent lack of innovative treatments for *A. baumannii* and other Gram-negative pathogens can be attributed to our limited knowledge of genetic weaknesses in these bacteria. This work advances our understanding of genetic vulnerabilities in *A. baumannii* by systematically perturbing and phenotyping essential genes. Using CRISPRi to knock down essential gene products, we identified genes that are sensitive to knockdown as well as genes that potentiate or mitigate antibiotic action. Together, these studies define potential targets for antibiotic discovery and provide a genetic approach for understanding synergistic therapies that is broadly applicable.

Our study of essential gene knockdown phenotypes in *A. baumannii* points to both unique and shared genetic vulnerabilities with other bacterial species. Our finding that *A. baumannii* is highly sensitive to depletion of genes encoding NDH-1 highlights a unique weakness in pathogens that are obligate aerobes and a possible therapeutic target. Among the Gram-negative ESKAPE pathogens, only *A. baumannii* is known to require *nuo* genes for aerobic growth in rich medium (54). Recent work from Manoil and colleagues in the non-pathogenic model strain, *Acinetobacter baylyi*, found that genes involved in oxidative phosphorylation were among the first to be depleted from a pool of transposon mutants (14); combining these observations with our CRISPRi results suggests that oxygen-dependent energy production is a physiological linchpin across the *Acinetobacter* genus. Our finding that *A. baumannii* genes involved in PG synthesis and translation are vulnerable to depletion underscores the conserved importance of these pathways across bacterial species (19, 29) and their foundational role as antibiotic targets.

Our finding that knockdown gradients of essential genes treated with antibiotics can mimic hormetic effects seen in dose-response curves (46) has implications for modeling conditional

phenotypes of essential genes and dosing of combination therapies. For most essential genes, complete loss of gene function results in lethality under the majority of conditions. However, our mismatch guide strategy allowed us to examine intermediate levels of essential gene function that may be analogous to partial loss of function alleles found in resistant clinical isolates or adaptive evolution experiments. Partial loss of function mutants can exhibit striking differences in phenotype over a narrow range of function, as we observed with *glnS* and *nuoB* resistance during IMI and RIF treatment, respectively. These hormetic resistance phenotypes fit poorly to established 4-parameter logistic models, emphasizing the importance of considering alternative model parameters and comprehensive statistical approaches when quantifying intricate biological processes. Given our limited set of screening conditions, it is currently unclear how widespread the phenomenon of hormesis is for antibiotic-gene interactions, although we note that clear instances of hormesis were rare in our data. Hormesis in antibiotic interactions may have clinical relevance as well, as doses of combination therapies falling within the concentration window of a hormetic/antagonistic response would be ineffective. Although we could not find further evidence in the *Acinetobacter* literature, certain mutations aaRS genes result in beta-lactam resistance in *E. coli* (55), supporting our results. Our ability to predict antagonism between an aaRS inhibitor and carbapenems based on genetic data suggests that screening for antibiotic-gene interactions will have as much value in avoiding antagonisms as it does in identifying potential synergies.

Our data show an unexpected link between NADH dehydrogenase activity and growth inhibition by COL. NDH-1 knockdown strains were highly sensitized to COL in competitive growth assays, but the precise mechanism behind this sensitivity is unclear. Based on our measurements, NDH-1 knockdown primarily affects the ratio of NADH to NAD+ in cells, rather than membrane potential. COL inhibits conversion of NADH to NAD+ by the type II NADH dehydrogenase (NDH-2) in a purified system (51), although at much higher concentrations than used in our experiments. We speculate

that the sensitivity of NDH-1 knockdowns to COL is due insufficient recycling of NAD+, which would be expected to reduce flux through the TCA cycle. In this scenario, CRISPRi knockdown reduces NDH-1 activity while COL inhibits NDH-2 activity, resulting in further skewing of the NADH/NAD+ ratio toward NADH and away from NAD+. Flux through the TCA cycle would be expected to decrease as multiple steps in the cycle require available NAD+ (56, 57). In general, identifying targets that potentiate COL activity may be clinically relevant in the context of combination therapy because toxicity is a major dose-limiting concern of polymyxin antibiotics (58). Employing effective combination treatments using colistin concentrations below toxicity thresholds would greatly improve its clinical utility and safety against *A. baumannii*. Our CRISPRi approach could inform not only combinations with polymyxins, but also other antibiotics which have dose-limiting toxicity concerns that prevent more widespread use.

COL and RIF have been shown to synergistically kill *A. baumannii* and other Gram-negatives (58) in part due to COL disruption of the outer membrane (48). The anticorrelated phenotypes we observed in COL and RIF treatment may be relevant to the spectrum of available mutations that allow for the emergence of resistance. For instance, treatment with COL selects for mutations in LOS biosynthesis genes (10), while the loss of LOS promotes permeability to RIF (and other antibiotics (58)). Accordingly, the presence of RIF has been shown to reduce recovery of inactivated *lpx* genes in selections for COL resistance (59). Mutations in *nuo* genes are commonly obtained in screens for tobramycin resistance in *P. aeruginosa* (60, 61), supporting a model in which reduced NDH-1 function decreases permeability of the inner membrane to antibiotics. Consistent with this model, we found that EtBr fluorescence, which is often used as a proxy for measuring permeability of small molecules, was decreased in NDH-1 knockdown strains. Mutations in *nuo* can negatively impact other Gram-negative ESKAPE pathogens but are particularly relevant in *A. baumannii* because NDH-1 is uniquely required for viability. We speculate that anticorrelated phenotypic

signatures are predictive of antibiotic synergy in cases where permeability of one antibiotic is enhanced by the second, particularly in the context of bacteria with low permeability such as *A. baumannii* and *P. aeruginosa*. Interrogating a larger chemical genomics dataset with a greater diversity of antibiotics for these organisms will shed light on general rules for antibiotic-gene interactions and their implications for discovering synergy.

Our approach is not without limitations. The high sensitivity of our pooled CRISPRi screens enables us to detect even subtle phenotypes, but these phenotypes may not exceed clinically relevant thresholds. For instance, we detected several gene-antibiotic interactions with significant pooled phenotypes that resulted in modest MIC changes when assayed in isolation. One challenge with studying essential genes is that excessive knockdown will not only reduce cellular viability but will also select for preexisting suppressors of CRISPRi (often found in the *dcas9* gene (62)). Thus, knockdown levels that enable stable interrogation of essential genes may not be sufficient to push MICs past clinical breakpoints. Nonetheless, our recovery of direct antibiotic targets among the strongest outliers in most CRISPRi screens strongly supports the utility of CRISPRi in elucidating antibiotic function (17, 63). Future work combining CRISPRi with orthogonal essential gene perturbations, such as CRISPR base editing (64), may reveal allele-specific changes in resistance that are often larger in magnitude and more closely reflect resistance mutations found in the clinic. Our work recovered phenotypes for most, but not all the *Ab* essentials. Although we expect some of the non-responsive genes to be false positives from Tn-seq (14), other genes may be non-responsive due to limitations of CRISPRi. For instance, we estimate that our system produces roughly 20-fold knockdown, but variations in guide activity could affect phenotype calls at the margin. Further, TU-level knockdowns could mask phenotypes for some genes, such as eliminating the phenotype of an antitoxin gene in a co-transcribed toxin/antitoxin system.

Materials and Methods

Strains and growth conditions

Strains are listed in Table 2.1. Details of strain growth conditions are described in the Supporting Information.

General molecular biology techniques and plasmid construction

Plasmids and construction details are listed in Table 2.2. Oligonucleotides are listed in Table 2.3. Details of molecular biology techniques are described in the Supporting Information.

A. baumannii Mobile-CRISPRi system construction

An *A. baumannii* strain with the Mobile-CRISPRi (MCi) system from pJMP1183 (23) inserted into the att_{Tn7} site (Fig. 2.S1A), which constitutively expresses mRFP and has an mRFP-targeting sgRNA, has a growth defect when induced with 1mM IPTG (Fig 2.S1B; "parent"). Strains with suppressors of the growth defect that still maintained a functional CRISPRi system were identified by plating on LB supplemented with 1mM IPTG and selecting white colonies (red colonies would indicate a no longer functional MCi system; Fig 2.S1B and 2.S1C). gDNA was extracted and mutations in the dCas9 promoter were identified by Sanger sequencing (Fig 2.S1D). The Mobile-CRISPRi plasmid pJMP2748 is a variant of pJMP2754 (Addgene 160666) with the sgRNA promoter derived from pJMP2367 (Addgene 160076) and the dCas9 promoter region amplified from the *A. baumannii* suppressor strain gDNA with oJMP635 and oJMP636. Plasmid pJMP2776, which was used to construct the *A. baumannii* essential gene library and individual sgRNA constructs, was created by removal of the GFP expression cassette from pJMP2748 by digestion with PmeI and re-ligation. This system shows ~20-fold knockdown when targeting the *GFP* gene (Fig 2.S1E). Plasmids were submitted to Addgene.

A. baumannii Mobile-CRISPRi individual gene and gene library construction

sgRNAs were designed to knockdown essential genes in *A. baumannii* 19606 using a custom python script and Genbank accession numbers CP046654.1 and CP046655.1 as detailed in reference (65). Mismatch guides were designed and predicted knockdown was assigned as previously described (19). sgRNA-encoding sequences were cloned between the BsaI sites of Mobile-CRISPRi (MCi) plasmid pJMP2776. Methodology for cloning individual guides was described previously in detail (65). Briefly, two 24-nucleotide (nt) oligonucleotides encoding an sgRNA were designed to overlap such that when annealed, their ends would be complementary to the BsaI-cut ends on the vector.

The pooled essential gene CRISPRi library was constructed by amplification of sgRNA-encoding spacer sequences from a pooled oligonucleotide library followed by ligation into the BsaI-digested MCi plasmid. Specifically, a pool of sgRNA-encoding inserts was generated by PCR amplification with primers oJMP697 and oJMP698 from a 78-nt custom oligonucleotide library (2020-OL-J, Agilent) with the following conditions per 500 µl reaction: 100 µl Q5 buffer, 15 µl GC enhancer, 10 µl 10mM each dNTPs, 25 µl each 10 µM primers oJMP897 and oJMP898, 10 µl 10 nM oligonucleotide library, 5 µl Q5 DNA polymerase, and 310 µl H2O with the following thermocycling parameters: 98°C, 30s; 15 cycles of: 98°C, 15s; 56°C, 15s; 72°C, 15s; 72°C, 10 min; 10°C, hold. Spin-purified PCR products were digested with BsaI-HF-v2 (R3733; NEB) and the size and integrity of full length and digested PCR products were confirmed on a 4% agarose e-gel (Thermo). The BsaI-digested PCR product (without further purification) was ligated into a BsaI-digested MCi plasmid as detailed in (65). The ligation was purified by spot dialysis on a nitrocellulose filter (Millipore VSWP02500) against 0.1 mM Tris, pH 8 buffer for 20 min prior to transformation by electroporation into *E. coli* strain BW25141 (sJMP3053). Cells were plated at a density of ~50,000 cells/plate on 150mm LB-2% agar plates supplemented with carbenicillin. After incubation for 14 h at 37°C, colonies (~900,000

total) were scraped from the agar plates into LB, pooled, and the plasmid DNA was extracted from ~1x10^{11} cells using a midiprep kit. This pooled Mobile-CRISPRi library was transformed by electroporation into *E. coli* mating strain sJMP3049, plated at a density of ~50,000 cells/plate on 150mm LB-2% agar plates supplemented with carbenicillin and DAP. After incubation for 14 h at 37°C, colonies (~1,000,000 total) were scraped from the agar plates and pooled, the OD_{600} was normalized to 27 in LB with DAP and 15% glycerol and aliquots of the pooled CRISPRi library were stored as strain sJMP2942 at -80°C.

Transfer of the Mobile-CRISPRi system to the A. baumannii chromosome

The MCi system was transferred to the att_{Tn7} site on the chromosome of *A. baumannii* by quad-parental conjugation of three donor strains—one with a mobilizable plasmid (pTn*7*C1) encoding Tn*7* transposase, another with a conjugal helper plasmid (pEVS74), and a third with a mobilizable plasmid containing a Tn7 transposon encoding the CRISPRi system—and the recipient strain *A. baumannii* 19606. A detailed mating protocol for strains with individual sgRNAs was described previously (65). Briefly, 100 µl of culture of donor and recipient strains were added to 600 µl LB, pelleted at ~8000 x g, washed twice with LB prior to depositing cells on a nitrocellulose filter (Millipore HAWP02500) on an LB plate, and incubated at 37°C, ~5 hr. Cells were removed from the filter by vortexing in 200 µl LB, serially diluted, and grown with selection on LB-gent plates at 37°C.

For pooled library construction, Tn*7* transposase donor (sJMP2644), conjugation helper strain (sJMP2935), and recipient strain (sJMP490) were scraped from LB plates with appropriate selective additives into LB and the OD_{600} was normalized to ~9. An aliquot of sJMP2942 pooled library strain was thawed and diluted to OD_{600} of ~9. Eight ml of each strain was mixed and centrifuged at 8000xg, 10 min. Pelleted cells were resuspended in 4 ml LB, spread on two LB agar plates, and incubated for 5hr at 37°C prior to resuspension in LB + 15% glycerol and storage at -80°C. Aliquots were thawed

and serial dilutions were plated on LB supplemented with gent (150) and LB. Efficiency of trans-conjugation (colony forming units on LB-gent vs. LB) was ~1 in 10^7. The remaining frozen stocks were plated on 150 mm LB plates solidified with 2% agar and supplemented with gent (150) and incubated for 16 h at 37°C. Cells were scraped from plates and resuspended in EZRDM (Teknova) + 25mM succinate + 15% glycerol at OD_{600} = 15 and aliquots were stored at -80°C as strain sJMP2949.

Library growth experiment

The *A. baumannii* essential gene CRISPRi library (sJMP2949) was revived by dilution of 50 µl frozen stock (OD_{600} = 15) in 50 ml LB (starting OD_{600} = 0.015) and incubation in 250 ml flasks shaking at 37°C until OD_{600} = 0.2 (~2.5 h) (timepoint = T0). This culture was diluted to OD_{600} = 0.02 in 4 ml LB with 1mM IPTG and antibiotics (colistin, imipenem, meropenem, rifampicin, and no antibiotic control) in 14 ml snap cap culture tubes (Corning 352059) in duplicate and incubated with shaking for 18 h at 37°C (T1). These cultures were serially diluted back to OD_{600} = 0.01 into fresh tubes containing the same media and incubated with shaking for 18 h at 37°C again (T2) for a total of ~10-15 doublings. Cells were pelleted from 1 ml of culture in duplicate at each time point (T0, T1, T2) and stored at -20°C. Final antibiotic concentrations were (in µg/ml): colistin (Sigma C4461): 0.44 and 0.67, imipenem (Sigma I0160): 0.06 and 0.09, meropenem (Sigma 1392454): 0.11 and 0.17, and rifampicin (Sigma R3501): 0.34.

Sequencing library samples

DNA was extracted from cell pellets with the DNeasy gDNA extraction kit (Qiagen) according to the manufacturer's protocol, resuspending in a final volume of 100 µl with an average yield of ~50 ng/µl. The sgRNA-encoding region was amplified using Q5 DNA polymerase (NEB) in a 100 µl reaction with 2 µl gDNA (~100 ng) and primers oJMP697 and oJMP698 (nested primers with adapters for index PCR with Illumina TruSeq adapter) according to the manufacturer's protocol using a BioRad C1000

thermocycler with the following program: 98°C, 30s then 16 cycles of: 98°C, 15s; 65°C, 15s; 72°C, 15s. PCR products were purified using the Monarch PCR and DNA Cleanup and eluted in a final volume of 20 µl for a final concentration of ~20 ng/µl).

Samples were sequenced by the UW-Madison Biotech Center Next Generation Sequencing Core facility. Briefly, PCR products were amplified with nested primers containing i5 and i7 indexes and Illumina TruSeq adapters followed by bead cleanup, quantification, pooling and running on a Novaseq 6000 (150bp paired end reads).

Library data analysis

For more information on digital resources and links to custom scripts, see Table 2.4.

Counting sgRNA Sequences

Guides were counted using *seal.sh* script from the *bbtools* package (Release: March 28, 2018). Briefly, paired FASTQ files from amplicon sequencing were aligned in parallel to a reference file corresponding to the guides cloned into the library. Alignment was performed using *k*-mers of 20 nucleotide length—equal to the length of the guide sequence.

Condition Comparisons – Quantification and Confidence

Relative fitness scores ($\log_2$ fold change) and confidence intervals were computed using *edgeR*. Briefly, trended dispersion of guides was estimated and imputed into a quasi-likelihood negative binomial log-linear model. Changes in abundance and the corresponding false discovery rates were identified for each guide in each condition individually. Finally, $\log_2$ fold abundance changes were calculated by taking the median guide-level $\log_2$ fold change for perfect match guides; confidence was calculated by computing the Stouffer's *p*-value (*poolr R* package) using FDR for individual guides across genes. Gene functional enrichment was determined using the STRING database (66).

CoMBaT-seq

CoMBaT-seq experiments consisted of two competing strains, one containing a non-targeting guide and a second containing a guide targeting a gene of interest. CoMBaT-seq strains were added 1:1 in the presence or absence of the indicated antibiotic and grown as described in "library growth experiment" above. Strain abundance at the end of the experiment was quantified using Nanopore sequencing (performed by Plasmidsaurus or Azenta).

Knockdown-Response Curves

Fitting of knockdown response curves is described in detail in the supplemental methods. Briefly, code was adapted from the *drc* (*DoseResponse*) *R* package to generate 4-parameter logistic curves describing the relationship between predicted knockdown (independent) and the $\log_2$ fold change in strain representation (dependent) for all (~10) mismatch guides per gene.

Table 2.1. Strains used in this study.

Strain name	Description[1]	Source
sJMP6	*Escherichia coli* BW25113 F-, Δ(*araD-araB*)567, Δ*lacZ*4787(::*rrnB*-3), λ-, *rph*-1, Δ(*rhaD-rhaB*)568, *hsdR514* (Keio collection WT)	Baba et al. (39)
sJMP32	*Escherichia coli* DH10B F-, *endA1*, *recA1*, *galE15*, *galK16*, *nupG*, *rpsL*, Δ*lacX74*, f80[*lacZ*ΔM15], *araD139*, Δ(*ara-leu*)*7697*, *mcrA*, Δ(*mrr-hsdRMS-mcrBC*) (cloning strain)	Invitrogen
sJMP146	*Escherichia coli* BW25141 Δ(*araD-araB*)567, Δ*lacZ4787*(::*rrnB-3*), Δ(*phoB-phoR*)580, λ-, *galU95*, Δ*uidA3*::*pir+*, *recA1*, *endA9*(D-ins)::FRT, *rph-1*, Δ(*rhaD-rhaB*)*568*, *hsdR514* (*pir+* cloning strain)	Datsenko et al. (67)
sJMP245	*A. baumannii* 19606 with MCi system from pJMP1183 inserted into the Tn*7 att* site, gmR (mRFP, *mrfp* targeting sgRNA, $P_{LlacO-1}$ dCas9 promoter)	Peters et al. (23)
sJMP345	*Escherichia coli* strain sJMP146 with pJP121 (pJMP323), ampR	This study
sJMP424	*Escherichia coli* WM6026 lacI^q, *rrnB3*, DE*lacZ4787*, *hsdR514*, DE(*araBAD*)*567*, DE(*rhaBAD*)568, *rph-1 att*-lambda::pAE12-del (oriR6K/*cat*::FRT5), del 4229(*dapA*)::FRT(DAP-), del(*endA*)::FRT, *uidA*(del*MluI*)::*pir*(wt), *attHK*::pJK1006::del1/2(D*oriR6K-cat*::FRT5, D*trfA*::FRT) (*pir+* mating strain)	Blodgett et al. (68)
sJMP490	*Acinetobacter baumannii* ATCC19606 WT	ATCC
sJMP601	*Escherichia coli* (derived from BW25141, sJMP146) with FRT-*cat*-FRT(cm^r) inserted between *mltB* and *srlA* (closely linked to *recA*)	This study
sJMP604	*Escherichia coli* (derived from WM6026, sJMP424) with FRT-*cat*-FRT(cm^r) inserted between *mltB* and *srlA*, *recA1*	This study
sJMP624	*Escherichia coli* (derived from WM6026, sJMP604) with FRT inserted between *mltB* and *srlA*, *recA1* (*cat* removed) (cmS)	This study
sJMP2644	*Escherichia coli* mating strain sJMP3049 with pJMP1039 (Tn*7* transposase expression strain)	This study
sJMP2935	Escherichia coli mating strain sJMP3049 with pEVS104 (helper strain)	This study
sJMP2942	Escherichia coli mating strain sJMP3049 with *A. baumannii* essential gene MCi pooled plasmid library, ampR, gmR	This study
sJMP2949	*A. baumannii* 19606 (sJMP490) with MCi library from pJMP2942 pooled library inserted into the Tn*7 att* site, gmR (*A. baumannii* essential gene Mobile-CRISPRi pooled library)	This study

sJMP3030	*Escherichia coli* (derived from BW25113, sJMP6) F-, Δ(*araD-araB*)*567*, Δ*lacZ4787*(::*rrnB-3*), λ-, *rph-1*, Δ(*rhaD-rhaB*)*568*, *hsdR514*, *att*Tn*7*::*acrIIA4* FRT-*cat*-FRT (cmR)	This study
sJMP3034	*Escherichia coli* (derived from BW25141, sJMP146) Δ(*araD-araB*)*567*, Δ*lacZ4787*(::*rrnB-3*), Δ(*phoB-phoR*)*580*, λ-, *galU95*, Δ*uidA3*::*pir+*, *recA1*, *endA9*(D-ins)::FRT, *rph-1*, Δ(*rhaD-rhaB*)*568*, *hsdR514*, *att*Tn*7*::*acrIIA4* FRT-*cat*-FRT (cmR)	This study
sJMP3040	*Escherichia coli* strain sJMP624 with pJP121, ampR	This study
sJMP3043	*Escherichia coli* (derived from WM6026, sJMP3040) with FRT inserted between *mltB* and *srlA*, *recA1* (*cat* removed), *att*Tn*7*::*acrIIA4* FRT-*cat*-FRT(cmR)	This study
sJMP3049	*Escherichia coli* (derived from WM6026, sJMP3043) *lacI*^{q}, *rrnB3*, DE*lacZ4787*, *hsdR514*, DE*(araBAD)567*, DE(*rhaBAD*)*568*, *rph-1 att*-lambda::pAE12-del (oriR6K/*cat*::frt5), del 4229(*dapA*)::FRT (DAP-), del(*endA*)::FRT, *uidA*(D*MluI*)::*pir*(wt), *att*HK::pJK1006::del1/2(del oriR6K-*cat*::FRT5, del *trfA*::FRT), FRT inserted between *mltB* and *srlA*, *recA1*, *att*Tn*7*::*acrIIA4* (cmS) (*pir+*, *recAI* mating strain with anti-CRISPR)	This study
sJMP3053	*Escherichia coli* (derived from BW25141, sJMP3034) Δ*(araD-araB*)567, Δ*lacZ4787*(::*rrnB-3*), Δ(*phoB-phoR*)580, l-, *galU95*, Δ*uidA3*::pir+, recA1, endA9(del-ins)::FRT, *rph-1*, Δ(*rhaD-rhaB*)*568*, *hsdR514*, *att*Tn*7*::*acrIIA4* (*pir+*, *recAI* cloning strain with anti-CRISPR)	This study
sJMP4324	*A. baumannii* ATCC 19606 with CRISPRi system from pJMP4189 inserted into the Tn*7 att* site, gmR (non-targeting control 4 sgRNA)	This study
sJMP4341	*A. baumannii* ATCC 19606 with CRISPRi system from pJMP4335 inserted into the Tn*7 att* site, gmR (GO593_00515-targeting sgRNA)	This study
sJMP4353	sJMP4341 with pJMP4345 recombined into genome (single-crossover), kanR	This study
sJMP4358	sJMP4353 with prophage deletion (second-crossover), isolate 1	This study
sJMP4360	sJMP4353 with prophage deletion (second-crossover), isolate 2	This study
sJMP4361	sJMP4353 with prophage deletion (second-crossover), isolate 3	This study
sJMP4362	sJMP4353 with prophage deletion (second-crossover), isolate 4	This study
sJMP4363	sJMP4353 with prophage deletion (second-crossover), isolate 5	This study
sJMP4364	sJMP4353 with prophage deletion (second-crossover), isolate 6	This study
sJMP4365	sJMP4353 with prophage deletion (second-crossover), isolate 7	This study

sJMP4366	sJMP4353 with prophage deletion (second-crossover), isolate 8	This study
sJMP6333	*A. baumannii* 19606 (sJMP490) with MCi system from pJMP2748 inserted into the Tn*7 att* site, gmR (GFP, non-targeting sgRNA)	This study
sJMP6334	*A. baumannii* 19606 (sJMP490) with MCi system from pJMP2768 inserted into the Tn*7 att* site, gmR (GFP, *gfp* sgRNA)	This study
sJMP6335	*A. baumannii* 19606 (sJMP490) with MCi system from pJMP2776 inserted into the Tn*7 att* site, gmR (non-targeting sgRNA)	This study
sJMP10072	*A. baumannii* 19606 (sJMP490) with MCi system from pJMP10046 inserted into the Tn*7 att* site, gmR (*murA* sgRNA)	This study
sJMP10073	*A. baumannii* 19606 (sJMP490) with MCi system from pJMP10052 inserted into the Tn*7 att* site, gmR (*nuoH* sgRNA)	This study
sJMP10074	*A. baumannii* 19606 (sJMP490) with MCi system from pJMP10054 inserted into the Tn*7 att* site, gmR (*nuoB* sgRNA)	This study
sJMP10076	*A. baumannii* 19606 (sJMP490) with MCi system from pJMP10058 inserted into the Tn*7 att* site, gmR (*lpxC* sgRNA)	This study
sJMP10079	*A. baumannii* 19606 (sJMP490) with MCi system from pJMP10050 inserted into the Tn*7 att* site, gmR (*glnS* sgRNA)	This study
sJMP10080	*A. baumannii* 19606 (sJMP490) with MCi system from pJMP10062 inserted into the Tn*7 att* site, gmR (non-targeting-control 1 sgRNA)	This study
sJMP10081	*A. baumannii* 19606 (sJMP490) with MCi system from pJMP10064 inserted into the Tn*7 att* site, gmR (non-targeting control 2 sgRNA)	This study

[1] gmR, gentamicin resistant; kanR, kanamycin resistant; ampR, ampicillin resistant; cmR, chloramphenicol resistant; cmS, chloramphenicol sensitive; MCi, Mobile-CRISPRi

Table 2.2. Plasmids used in this study.

Plasmid	Description	Construction/notes[1]	Source
pJMP38	pSIM19	pSC101 *repA*(ts) for lambda Red recombineering; specR	
pJMP323	pJP121 (pRL2613)	pRC*7*-recA (mini-F vector, unstable without selection); ampR	Robert Landick pRC7 (69)
pJMP1039	pTn*7*C1	Tn*7* transposase expression; ampR	Peters et al. (23), Addgene: 119239
pJMP1183	pTn*7*C89.1	MCi test plasmid. $P_{LlacO\text{-}1}$ dCas9 promoter, Spy dcas9::3Xmyc, $P_{LlacO\text{-}1}$ sgRNA promoter (*mrfp* targeting spacer), GFP expression; ampR, kanR	Peters et al. (23), Addgene: 119254
pJMP1356	pTn*7*C183.1	MCi plasmid; ampR, cmR	Peters et al. (23), Addgene: 119276
pJMP2367	pMCi-vC-GFP_BsaI	MCi test plasmid. *Zymo* dCas9 promoter, Spy dcas9::3Xmyc, vC sgRNA promoter (BsaI site), GFP expression; ampR, cmR	Banta et al. (70), Addgene: 160076
pJMP2748	pAbaMCi-GFP-BsaI	MCi test plasmid. Aba suppressor dCas9 promoter, Spy dcas9::3Xmyc, vC sgRNA promoter (BsaI site), GFP expression; ampR, gmR	This study, Addgene: 208888
pJMP2754	pMCi-v4-GFP_BsaI	MCi test plasmid. pLlacO-1 dCas9 promoter, Spy dcas9::3Xmyc, pLlacO-1 sgRNA promoter (BsaI site), GFP expression; ampR, gmR	Banta et al. (65), Addgene: 160666
pJMP2768	pAbaMCi-GFP-*gfp*	MCi test plasmid. Aba suppressor dCas9 promoter, Spy dcas9::3Xmyc, vC sgRNA promoter (*gfp* targeting spacer), GFP expression. Derivative of pJMP2748; ampR, gmR	This study, Addgene: 208889
pJMP2776	pAbaMCi-BsaI	MCi plasmid. Aba suppressor dCas9 promoter, Spy dcas9::3Xmyc, vC sgRNA promoter (BsaI site). For cloning new guides. Derivative of pJMP2748; ampR (backbone), gmR(transposon)	This study, Addgene: 208890
pJMP2942	pAbaMCi-OL-J	A. baumannii 19606 MCi pooled plasmid library. 6679 guides: 4 perfect match/essential gene, 10 mismatch/essential gene, 1000 nontargeting controls. Constructed by amplification of pooled oligonucleotide library	This study

		2020-OL-J with oJMP897 and oJMP898, followed by BsaI digestion, and ligation into BsaI-digested pJMP2776; ampR, gmR	
pJMP3008	pCP20	pL-FLP (encodes yeast FLP recombinase), (ts, incubate at 30°C); ampR, cmR	Cherepanov and Wackernagel (71)
pJMP3018	pTn*7-acrIIA4*	Contains a Tn7 transposon encoding the *acrIIA4* gene from a *Listeria monocytogenes* prophage under the control of a strong constitutive synthetic promoter and FRT-*cat*-FRT. Cloned by assembly of the MCi backbone (amplified from pJMP1356 with oJMP297/298) and synthetic DNA fragment oJMP299; ampR, cmR	This study
pJMP4003	pEVS104	R6K *ori* helper plasmid for conjugation into *A. baumannii*; kanR	Stabb and Ruby (72)
pJMP4189	p2776-control 4	MCi plasmid. non-targeting control spacer 4. Annealed oligonucleotides oJMP834/835 ligated into pJMP2776 BsaI site; ampR, gmR	This study
pJMP4335	p2776-GO593_00515	MCi plasmid. GO593_00515-targeting spacer. Annealed oJMP1211/1212 ligated into pJMP2776 BsaI site; ampR, gmR	This study
pJMP4345	prophage deletion plasmid	Assemble (1.071 kb) region upstream (oJMP1568/1569 PCR) and (1.093 kb) region downstream (oJMP1570/1571 PCR) of prophage (GenBank accession number: CP046654.1; 84,589-131,888) into pJMP1183 between AscI and EcoRI sites; ampR, kanR	This study
pJMP10042	pAbaMCi-*mraY*	MCi plasmid. *mraY*-targeting spacer. Annealed oligonucleotides oJMP1623/1635 ligated into pJMP2776 BsaI site; ampR, gmR	This study
pJMP10044	pAbaMCi-*ftsI*	MCi plasmid. *ftsI*-targeting spacer. Annealed oligonucleotides oJMP1624/1636 ligated into pJMP2776 BsaI site; ampR, gmR	This study
pJMP10046	pAbaMCi-*murA*	MCi plasmid. *murA*-targeting spacer. Annealed oligonucleotides oJMP1625/1637 ligated into pJMP2776 BsaI site; ampR, gmR	This study
pJMP10048	pAbaMCi-*nuoH*	MCi plasmid. *nuoH*-targeting spacer. Annealed oligonucleotides oJMP1626/1638 ligated into pJMP2776 BsaI site; ampR, gmR	This study

pJMP10050	pAbaMCi-*nuoB*	MCi plasmid. *nuoB*-targeting spacer. Annealed oligonucleotides oJMP1627/1639 ligated into pJMP2776 BsaI site; ampR, gmR	This study
pJMP10052	pAbaMCi-*nuoF*	MCi plasmid. *nuoF*-targeting spacer. Annealed oligonucleotides oJMP1628/1640 ligated into pJMP2776 BsaI site; ampR, gmR	This study
pJMP10054	pAbaMCi-*lpxC*	MCi plasmid. *lpxC*-targeting spacer. Annealed oligonucleotides oJMP1629/1641 ligated into pJMP2776 BsaI site; ampR, gmR	This study
pJMP10056	pAbaMCi-*lpxA*	MCi plasmid. *lpxA*-targeting spacer. Annealed oligonucleotides oJMP1630/1642 ligated into pJMP2776 BsaI site; ampR, gmR	This study
pJMP10058	pAbaMCi-*ileS*	MCi plasmid. *ileS*-targeting spacer. Annealed oligonucleotides oJMP1631/1643 ligated into pJMP2776 BsaI site; ampR, gmR	This study
pJMP10060	pAbaMCi-*glnS*	MCi plasmid. *glnS*-targeting spacer. Annealed oligonucleotides oJMP1632/1644 ligated into pJMP2776 BsaI site; ampR, gmR	This study

[1] MCi, Mobile-CRISPRi; ts, temperature sensitive, gmR, gentamicin resistance; ampR, ampicillin resistance; kanR, kanamycin resistance; cmR, chloramphenicol resistance

Table 2.3. Oligos used in this study.

Oligo	Sequence (5' to 3')	Description
2020-OL-J	CTTCTACCGAACATACAGGGTCTCTTAGT XXXXXXXXXXXXXXXXXXXXGTTTAGAGA CCTCGCGTTATGCTGTATGT	Pooled oligo library (4 perfect match/essential gene, 10 mismatch/essential gene, 1000 controls), (20 X's represent pool of 6679 oligos encoding 4 guides/essential gene, 10 mismatch/essential gene, and 1000 non-targeting controls). Agilent SurePrint. Usage: pooled CRISPRi library amplification template
oJMP60	CGCCCCTCTTTAATACGACG	R primer for Tn*7* right end (Tn*7*R) Usage: verify Tn*7* insertion
oJMP201	ACACTTGATACTGTATGAGC	recA_A Usage: amplify *recA* locus
oJMP202	CTTAAAAAAGCAAAAGGGCC	recA_B Usage: amplify *recA* locus
oJMP211	CCTCGCTATCCTTTTATTCAAACTTTCAAA TTAAAATATCGGCGGTTTTCTTTTCTCTTC	F primer to amplify FRT-*cat*-FRT (chloramphenicol resistance) from pJMP1356 with 40nt homology region for insertion between *mltB* and *srlA* of strain BW25141 Usage: lambda Red recombineering
oJMP212	GATTTAAAAGTGTTATTTTGATCGCAAAATG AAAGATAAGATGAGCTCGAATTGGGGATC	R primer to amplify FRT-*cat*-FRT (chloramphenicol resistance) from pJMP1356 with 40nt homology region for insertion between *mltB* and *srlA* of strain BW25141 Usage: lambda Red recombineering
oJMP297	TAAAAAGTGAGTTGAACTAACGGCGCGC CTCCTTAATG	F primer to amplify pJMP1356 vector backbone Usage: construct pJMP3018
oJMP298	TTCTCTAATTAAGTCATTAATATTCATCCTG GTATTTCCTGTGTGAAAACATAG	F primer to amplify pJMP1356 vector backbone Usage: construct pJMP3018
oJMP299	TTAATGACTTAATTAGAGAAATCAAAAACA AAGATTACACAGTGAAATTGAGTGGTACG GATAGCAATAGTATCACACAGCTAATTATT CGCGTTAATAATGATGGCAACGAGTATGT AATTTCTGAAAGTGAAAATGAATCAATCGT TGAAAAATTCATCTCTGCATTCAAAAACG GTTGGAATCAAGAATACGAGGATGAAGAA GAATTTTATAATGACATGCAAACAATCACC TTAAAAAGTGAGTT	synthetic DNA encoding *acrIIA4* Usage: construct pJMP3018
oJMP398	GGCACACACTATCCAATCGC	F primer, 3' end of *glmS* Usage: verify Tn*7* insertion
oJMP399	GACCAGTTCAGACCCGTTG	R primer downstream of Tn*7* insertion (in murI) Usage: verify Tn*7* insertion
oJMP410	TAGTCATCTAATTCAACAAGAATT	*gfp1*_top Usage: anneal oligos to clone individual guides

oJMP411	AAACAATTCTTGTTGAATTAGATG	*gfp1*_bottom Usage: anneal oligos to clone individual guides
oJMP566	CTGAGGAAGATCTGTAATAAGGCGCG	F primer for Tn*7* left end (Tn*7*L) Usage: verify Tn*7* insertion
oJMP635	TACGTCTGCAGACTAGTGCGAATTGATCT GGTTTGACAGC	Aba_dCas9 promoter F Usage: construction of plasmid pJMP2748
oJMP636	TTGATACTGTGGCGGTCTGTATTTCC	Aba_dCas9 promoter R Usage: construction of plasmid pJMP2748
oJMP697	ACACTCTTTCCCTACACGACGCTCTTCC GATCTCGACTCGGTGCCACTTTTTC	F nested primer with adapter for index PCR with Illumina TruSeq adapter Usage: amplify sample for NGS
oJMP698	GTGACTGGAGTTCAGACGTGTGCTCTTC CGATCTACTACTCTTGCCTACTACCTATC GAC	R nested primer with adapter for index PCR with Illumina TruSeq adapter Usage: amplify sample for NGS
oJMP834	TAGTGGGTCATAACATACTTCGTC	nontargeting control 4_top Usage: nontargeting sgRNA
oJMP835	AAACGACGAAGTATGTTATGACCC	nontargeting control 4_bottom Usage: nontargeting sgRNA
oJMP897	CTTCTACCGAACATACAG	OL-J-F Usage: amplify pooled library
oJMP898	ACATACAGCATAACGCGA	OL-J-R Usage: amplify pooled library
oJMP1211	TAGTAATAATTCTTTGAGCTTGCT	GO593_00515 _top Usage: anneal oligos to clone individual guides
oJMP1212	AAACAGCAAGCTCAAAGAATTATT	GO593_00515_bottom Usage: anneal oligos to clone individual guides
oJMP1241	TGTCAATTTGCGGTATATGGTCC	F primer for *mnt* PCR Usage: to confirm prophage deletion
oJMP1242	ACCTTACTCATGCAGAACCCT	R primer for *mnt* PCR Usage: to confirm prophage deletion
oJMP1381	TGTTGCCTGCACTTCTTGTC	F PCR primer upstream of prophage Usage: to confirm prophage deletion
oJMP1382	TCGAGGAGCTTGGCGTAAAA	R PCR primer downstream of prophage Usage: to confirm prophage deletion
oJMP1568	AACAGAACGGTCAGCCACATGAATTCTG GCAAGCATAAAGGTACAGC	F primer for region upstream of prophage Usage: prophage deletion plasmid construction
oJMP1569	GGGATCGAACCCACGACC	R primer for region upstream of prophage Usage: prophage deletion plasmid construction
oJMP1570	GGTCGTGGGTTCGATCCCCGCCGAGCG CACCATTTTATATATAA	F primer for region downstream of prophage Usage: prophage deletion plasmid construction
oJMP1571	GCTGCAAGTCCCATTAAGGAGGCGCGC CTTATCGAACTAGAGTCCAGAGGGC	R primer for region downstream of prophage Usage: prophage deletion plasmid construction
oJMP1623	TAGTATTTTCTTAGCATGATTTTC	*mraY*_top Usage: anneal oligos to clone individual guides
oJMP1624	TAGTTCAATCACAATTTTCATGAT	*ftsI*_top Usage: anneal oligos to clone individual guides

oJMP1625	TAGTAGAATCATTGCCGCAAGTAA	*murA*_top Usage: anneal oligos to clone individual guides
oJMP1626	TAGTCAACACGGTTTGGACCATAA	*nuoH*_top Usage: anneal oligos to clone individual guides
oJMP1627	TAGTACAATTTGACGATCTTGCAA	*nuoB*_topUsage: anneal oligos to clone individual guides
oJMP1628	TAGTACCTAATGCTTTTTTAAAGC	*nuoF*_top Usage: anneal oligos to clone individual guides
oJMP1629	TAGTCCAGCACTACCATCCATAAT	*lpxC*_top Usage: anneal oligos to clone individual guides
oJMP1630	TAGTTACCAGCACCAATAGTCACT	*lpxA*_top Usage: anneal oligos to clone individual guides
oJMP1631	TAGTAATCTGCTGATAAATGTTGT	*ileS*_top Usage: anneal oligos to clone individual guides
oJMP1632	TAGTTTGCTGCGCAGAATCGACAG	*glnS*_top Usage: anneal oligos to clone individual guides
oJMP1633	TAGTAATATCCTTAAAAAACCAGA	nontargeting control1_top Usage: anneal oligos to clone individual guides
oJMP1634	TAGTCTACCTGTATAACAATTTGA	nontargeting control2_top Usage: anneal oligos to clone individual guides
oJMP1635	AAACGAAAATCATGCTAAGAAAAT	*mraY*_bottom Usage: anneal oligos to clone individual guides
oJMP1636	AAACATCATGAAAATTGTGATTGA	*ftsI*_bottom Usage: anneal oligos to clone individual guides
oJMP1637	AAACTTACTTGCGGCAATGATTCT	*murA*_bottom Usage: anneal oligos to clone individual guides
oJMP1638	AAACTTATGGTCCAAACCGTGTTG	*nuoH*_bottom Usage: anneal oligos to clone individual guides
oJMP1639	AAACTTGCAAGATCGTCAAATTGT	*nuoB*_bottom Usage: anneal oligos to clone individual guides
oJMP1640	AAACGCTTTAAAAAAGCATTAGGT	*nuoF*_bottom Usage: anneal oligos to clone individual guides
oJMP1641	AAACATTATGGATGGTAGTGCTGG	*lpxC*_bottom Usage: anneal oligos to clone individual guides
oJMP1642	AAACAGTGACTATTGGTGCTGGTA	*lpxA*_bottom Usage: anneal oligos to clone individual guides
oJMP1643	AAACACAACATTTATCAGCAGATT	*ileS*_bottom Usage: anneal oligos to clone individual guides
oJMP1644	AAACCTGTCGATTCTGCGCAGCAA	*glnS*_bottom Usage: anneal oligos to clone individual guides
oJMP1645	AAACTCTGGTTTTTTAAGGATATT	nontargeting control1_bottom Usage: anneal oligos to clone individual guides
oJMP1646	AAACTCAAATTGTTATACAGGTAG	nontargeting control2_bottom Usage: anneal oligos to clone individual guides

Table 2.4. Digital resources.

Software, package, or resource	Description	Reference/website
NCBI nucleotide database		https://www.ncbi.nlm.nih.gov/nucleotide/
custom sgRNA design (Python)	sgRNA design	Banta et al. (65)
population diversity metric (Nb)	calculating bottleneck metric	https://rb.gy/zy65jb
seal.sh	counting sgRNA sequences	https://sourceforge.net/projects/bbmap/
edgeR	condition comparisons – quantification and confidence	Robinson et al. (73)
poolr R package	confidence calculation	Cinar and Viechtbauer (74)
drc (DoseResponse) R package (adapted)	knockdown-response curves	Ritz et al. (75)
drc (DoseResponse) R package (adapted)	knockdown-response curves	Ritz et al. (75)
drc (DoseResponse) R package (adapted)	knockdown-response curves	Ritz et al. (75)
tidyverse collection of R packages	data science package collection	https://www.tidyverse.org/
ggplot2	declarative graphic generation platform	ggplot2: Elegant Graphics for Data Analysis (76)
pheatmap R package	clustered heatmap generation platform	https://CRAN.R-project.org/package=pheatmap
growthcurver	bacterial growth analytical platform	Sprouffske and Wagner (77)
Mauve	multiple sequence alignment platform	https://darlinglab.org/mauve/mauve.html
Orthofinder	comparative genomics platform	https://github.com/davidemms/OrthoFinder
STRING-db	predicted protein-protein interacTtion database	https://string-db.org/

Figure 2.S1. Optimization and characterization of an *A. baumannii* Mobile-CRISPRi system. (A) PCR confirmation that Mobile-CRISPRi (MCi) inserted downstream of the *glmS* gene as expected in *A. baumannii*. (B) Expression of dCas9 from the $P_{LlacO-1}$ promoter is toxic in A. baumannii 19606 (Parent (+*mrfp* guide)), but suppressors can readily be obtained that reduce toxicity (Suppressor (red) and Suppressor (white)). White colony suppressors have reduced toxicity of dCas9 expression but are still capable of targeting a chromosomal copy of the gene encoding Red Fluorescent Protein (*mrfp*). (C) RFP fluorescence of parent (P_{LlacO}-1-*dcas9*) and suppressor colonies. Each point is a distinct, single colony. Parent strains likely show intermediate levels of RFP due to the toxic effects of dCas9 expression from $P_{LlacO-1}$. (D) White colony suppressors contain a mutation in $P_{LlacO-1}$ that likely reduces its activity; this mutation likely arose from collapse of identical lac operator sequences. (E) Knockdown quantification of a CRISPRi system that expresses dCas9 from the white suppressor promoter at varying concentrations of inducer (IPTG).

Figure 2.S1

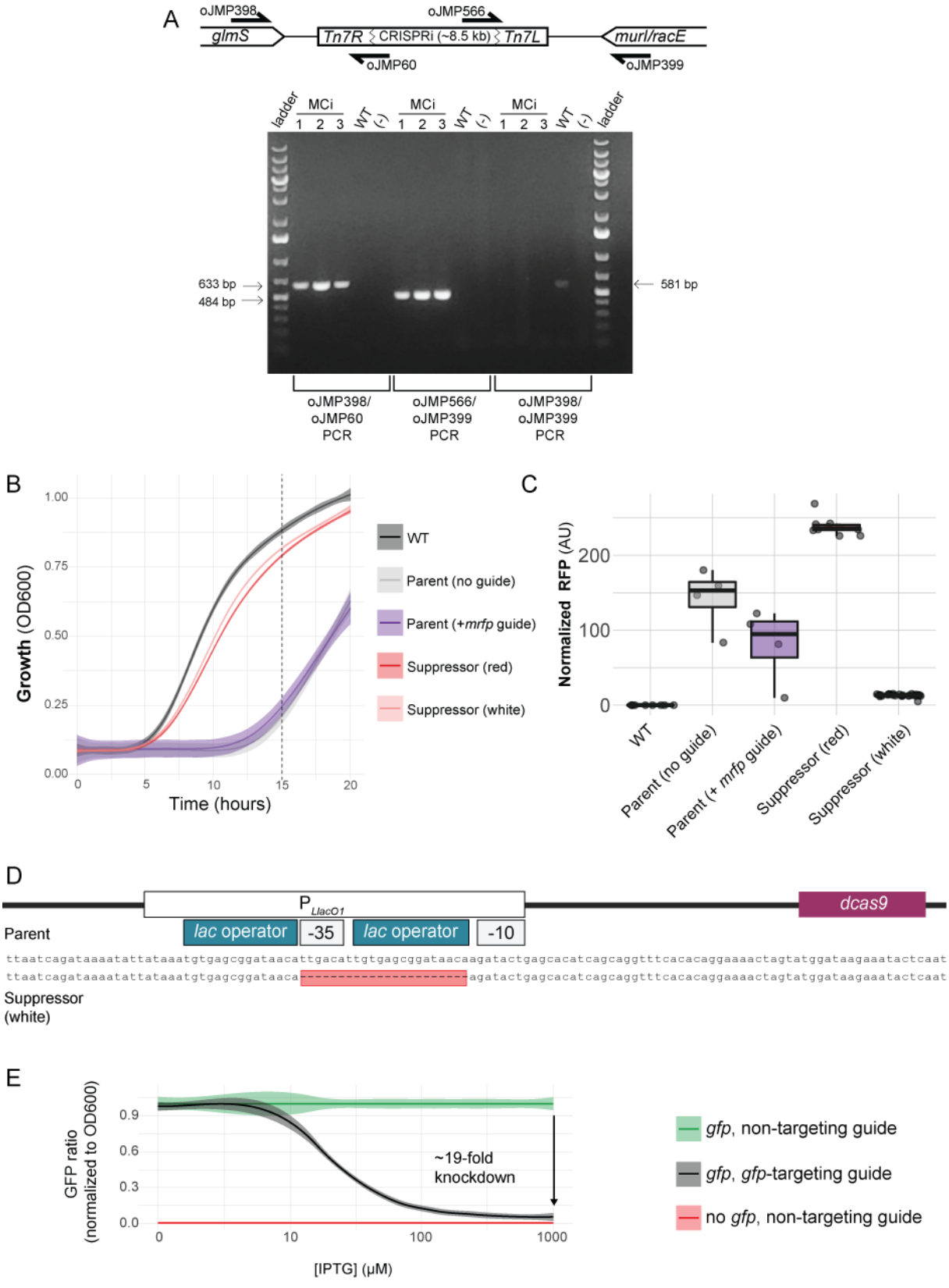
A
oJMP398
oJMP566
glmS
Tn7R
CRISPRi (~8.5 kb)
Tn7L
murI/racE
oJMP60
oJMP399
ladder
MCi
1 2 3
WT
(-)
633 bp
484 bp
581 bp
oJMP398/ oJMP60 PCR
oJMP566/ oJMP399 PCR
oJMP398/ oJMP399 PCR
B
Growth (OD600)
Time (hours)
WT
Parent (no guide)
Parent (+mrfp guide)
Suppressor (red)
Suppressor (white)
C
Normalized RFP (AU)
Parent (+ mrfp guide)
D
P LlacO1
dcas9
Parent
lac operator
-35
-10
ttaatcagataaaatattataaatgtgagcggataacattgacattgtgagcggataacaagatactgagcacatcagcaggtttcacacaggaaaactagtatggataagaaatactcaat
Suppressor (white)
E
GFP ratio (normalized to OD600)
~19-fold knockdown
[IPTG] (μM)
gfp, non-targeting guide
gfp, gfp-targeting guide
no gfp, non-targeting guide

Figure 2.S2. Quality control for the *A. baumannii* essential gene CRISPRi library. (A) Histogram of guides/gene in the library. The vast majority of genes had 14 guides and the smallest number of guides/gene was 11. Libraries shown here were grown with IPTG to two separate time points (see Methods) and sgRNA spacer depletion was quantified at each time point. Of the 7 genes with less than 14 recovered guides, 4 genes had only 13 (N=3) or 12 (N=1) guides in our initial library design. The other 3 genes likely lost a targeting guide during the library cloning or mating procedures. (B) Biological replicates of CRISPRi library experiments showed excellent reproducibility.

Figure 2.S2

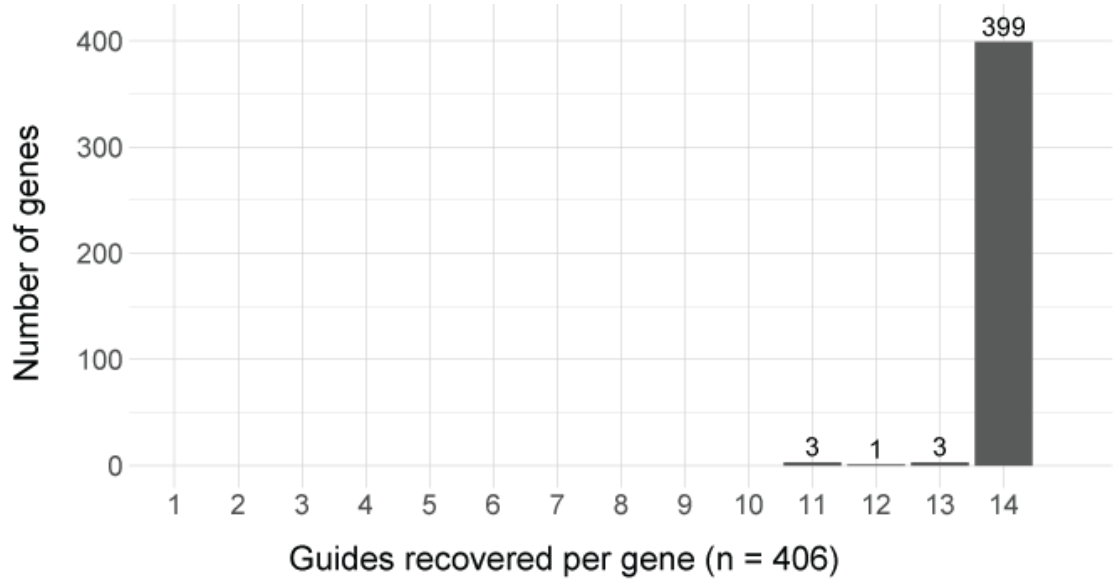
Number of genes
400
300
200
100
0
399
3
1
3
1 2 3 4 5 6 7 8 9 10 11 12 13 14
Guides recovered per gene (n = 406)


B
T1 R2= 0.987
T2 R2= 0.993
Rep 2 - Relative Fitness Score
(Log2 Fold Change)
0
-5
-10
-10 -5 0
Rep 1 - Relative Fitness Score
(Log2 Fold Change)
control
mismatch
perfect

Figure 2.S3. Gene level depletion from the CRISPRi library under different growth conditions. (A) Sankey plot of gene depletion at two time points. Genes are considered vulnerable to knockdown if they were depleted by 2-fold with a Stouffer's *p* value of 0.05 at the time point indicated relative to T0. (B) Sankey plot of gene depletion across any of the conditions assayed in our experiments (IPTG alone, IMI, MER, COL, RIF). Genes are considered responsive if they were depleted by 2-fold with a Stouffer's p value of 0.05 at the time point indicated relative to T0. (C) Growth, measured by OD600, over 18 hours for a non-targeting control strain, *lpxC* knockdown strain, and *nuoH* knockdown strain in LB (uninduced, left) or LB with inducer (1 mM IPTG, right).

Figure 2.S3

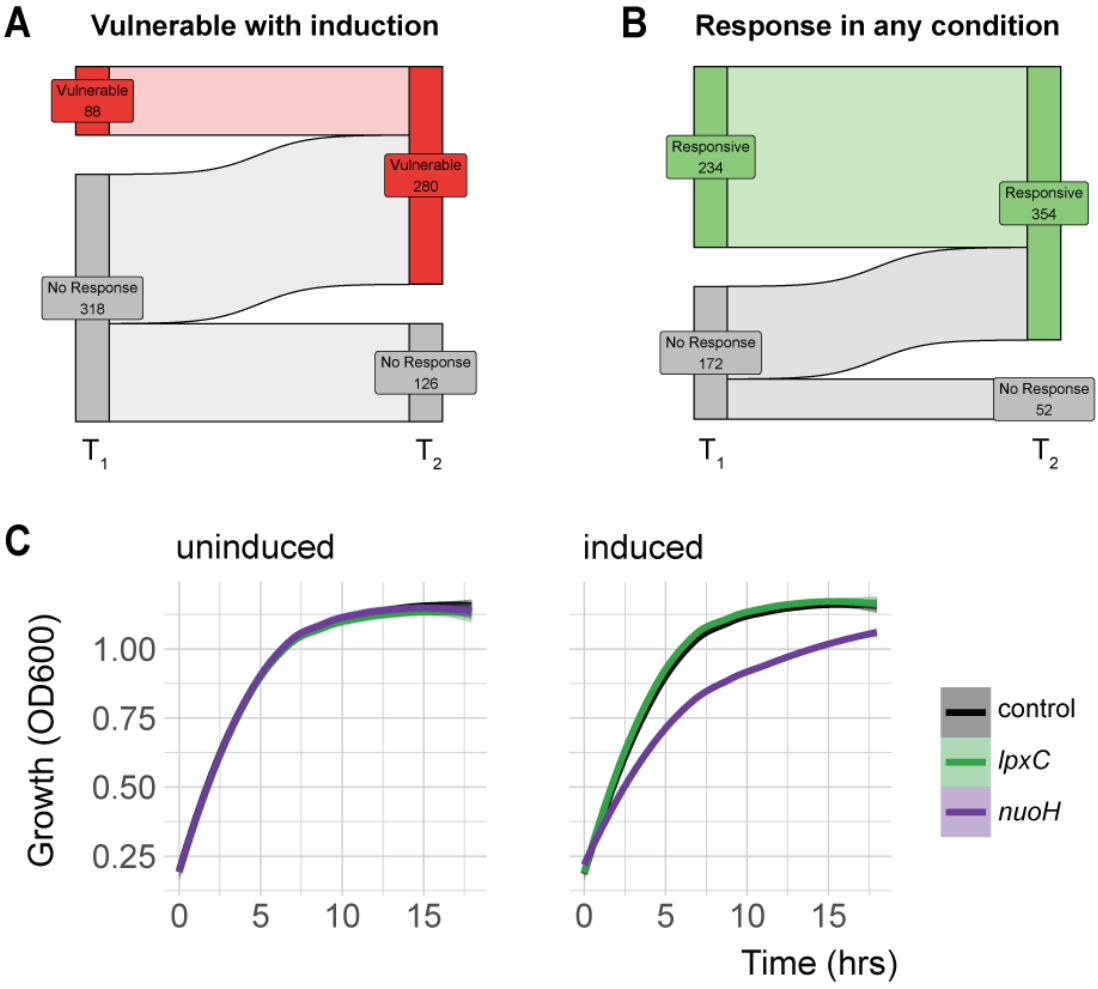
A
Vulnerable with induction
Vulnerable
88
Vulnerable
280
No Response
318
No Response
126
T1
T2
B
Response in any condition
Responsive
234
Responsive
354
No Response
172
No Response
52
T1
T2
C
uninduced
induced
Growth (OD600)
1.00
0.75
0.50
0.25
0
5
10
15
Time (hrs)
control
lpxC
nuoH

Figure 2.S4. The GO593_00515 gene is conditionally essential. (A) Mauve alignment (see Table 2.4) of A. baumannii 19606 genomic locus containing GO593_00515 (pink) and surrounding prophage (yellow) to 17978 and AB5075. Regions of same color represent alignment between genomes. (B) Cultures seven hours after addition of P1 phage lysate to E. coli MG1655 (left) and addition of inducer (1 mM IPTG) to A. baumannii non-targeting control strain (middle) or GO593_00515 knockdown strain (right). (C) Growth, measured by OD600, over 18 hours for a non-targeting control strain, GO593_00515 knockdown strain, GO593_00515 knockdown strain with single-crossover of prophage deletion plasmid (intermediate in construction), and multiple strains of GO593_00515 knockdown with deleted prophage in LB (uninduced, top) or LB with inducer (1 mM IPTG, bottom). (D) Agarose gel electrophoresis of PCR products to confirm prophage deletion using specified primer sets. GeneRuler 1 kb Plus ladder or template genomic DNA are denoted below each lane. PCR products with oJMP1381/1382 for strains with prophage still present suggests prophage excision happens at some frequency in WT.

Figure 2.S4

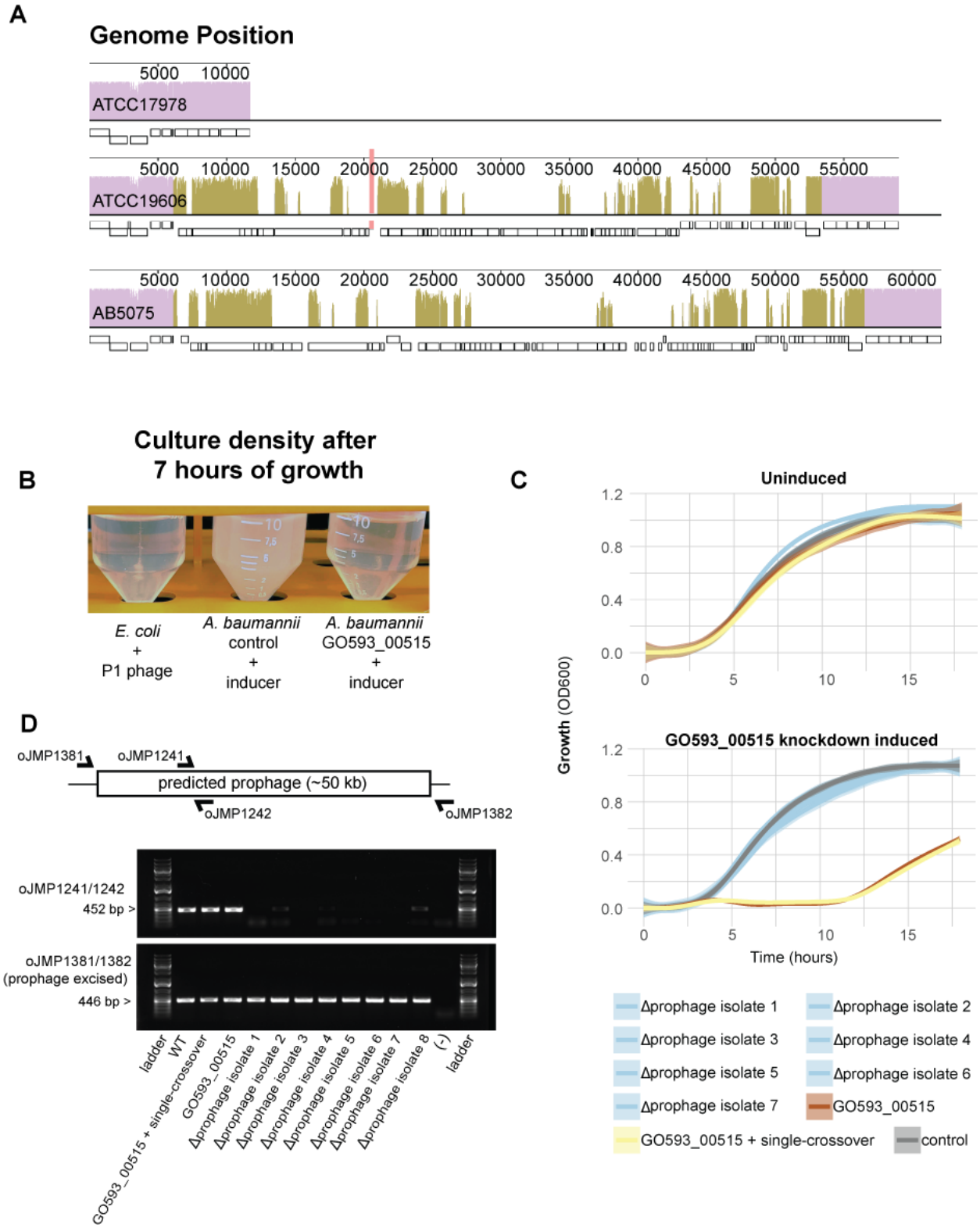
A
Genome Position
ATCC17978
ATCC19606
AB5075
B
Culture density after
7 hours of growth
E. coli
+
P1 phage
A. baumannii
control
+
inducer
A. baumannii
GO593_00515
+
inducer
C
Uninduced
GO593_00515 knockdown induced
Growth (OD600)
Time (hours)
Δprophage isolate 1
Δprophage isolate 2
Δprophage isolate 3
Δprophage isolate 4
Δprophage isolate 5
Δprophage isolate 6
Δprophage isolate 7
GO593_00515
GO593_00515 + single-crossover
control
D
oJMP1381
oJMP1241
predicted prophage (~50 kb)
oJMP1242
oJMP1382
oJMP1241/1242
452 bp >
oJMP1381/1382
(prophage excised)
446 bp >
ladder
WT
GO593_00515 + single-crossover
GO593_00515
Δprophage isolate 1
Δprophage isolate 2
Δprophage isolate 3
Δprophage isolate 4
Δprophage isolate 5
Δprophage isolate 6
Δprophage isolate 7
Δprophage isolate 8
(-)
ladder

Figure 2.S5. Examples of 4-parameter knockdown-response curves at T1 and T2. Examples from genes highlighted in the text. Effective knockdown 50 (EK50) parameters are displayed as crosshairs where the parameter fit resulted in a p value ≤ 0.05. Points are individual sgRNAs.

Figure 2.S5

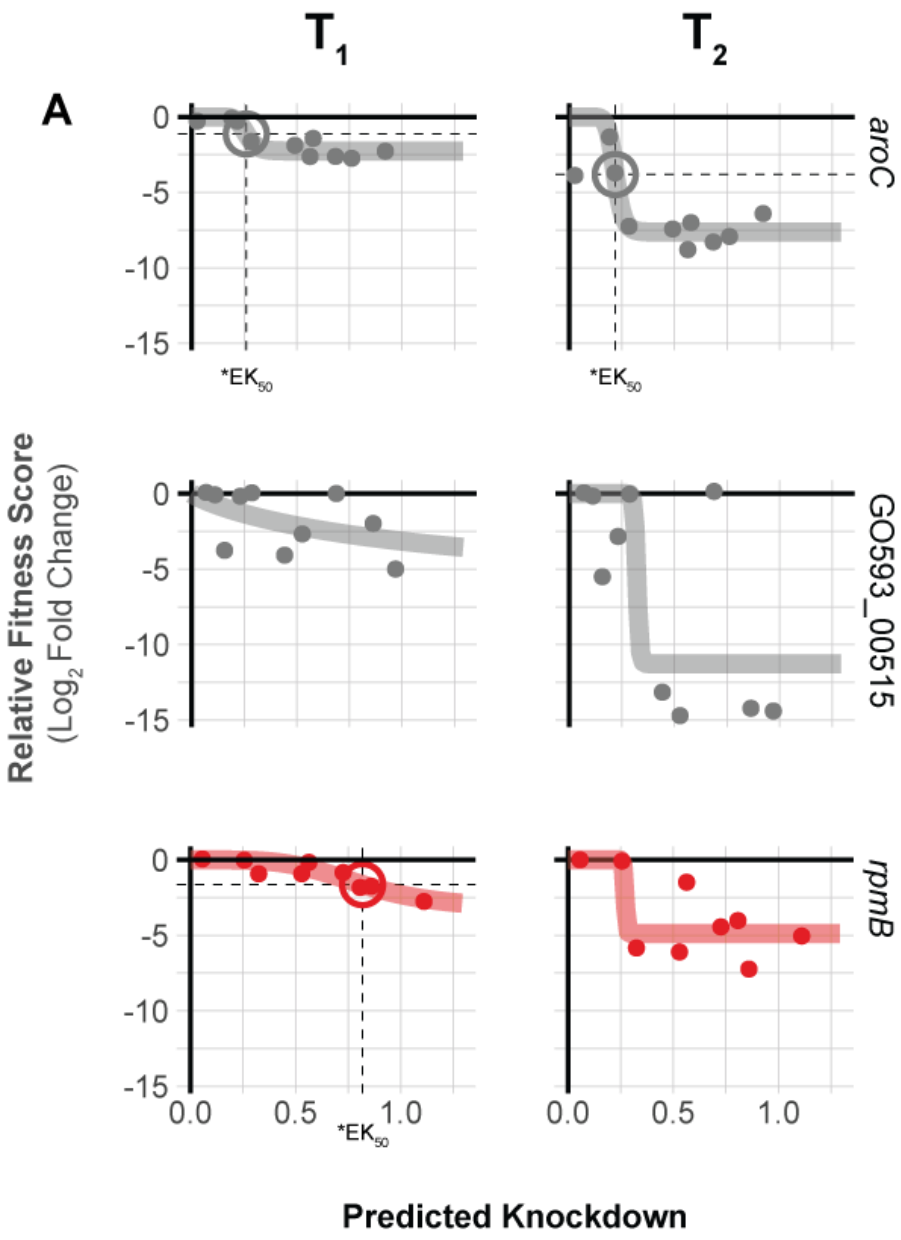
A
T1
T2
aroC
GO593_00515
rpmB
Relative Fitness Score
(Log2 Fold Change)
0
-5
-10
-15
*EK50
0.0
0.5
1.0
Predicted Knockdown

Figure 2.S6. Essential gene knockdown phenotypes in imipenem and meropenem. Volcano plots in (A) imipenem (IMI) and (B) meropenem (MER). Depletion of sgRNA spacers from the CRISPRi library (relative fitness score) during growth in IPTG at the level of transcription units (TUs). Dashed lines indicate a two-fold loss in relative fitness score and a *p* value of ≤ 0.05. Stouffer's *p* values were calculated at the TU level by aggregating false discovery rates (FDRs) of individual sgRNAs targeting the TU. TUs related to pathways discussed in the text are colored as described in the legend and the number of essential genes in the TU is indicated by point size.

Figure 2.S6

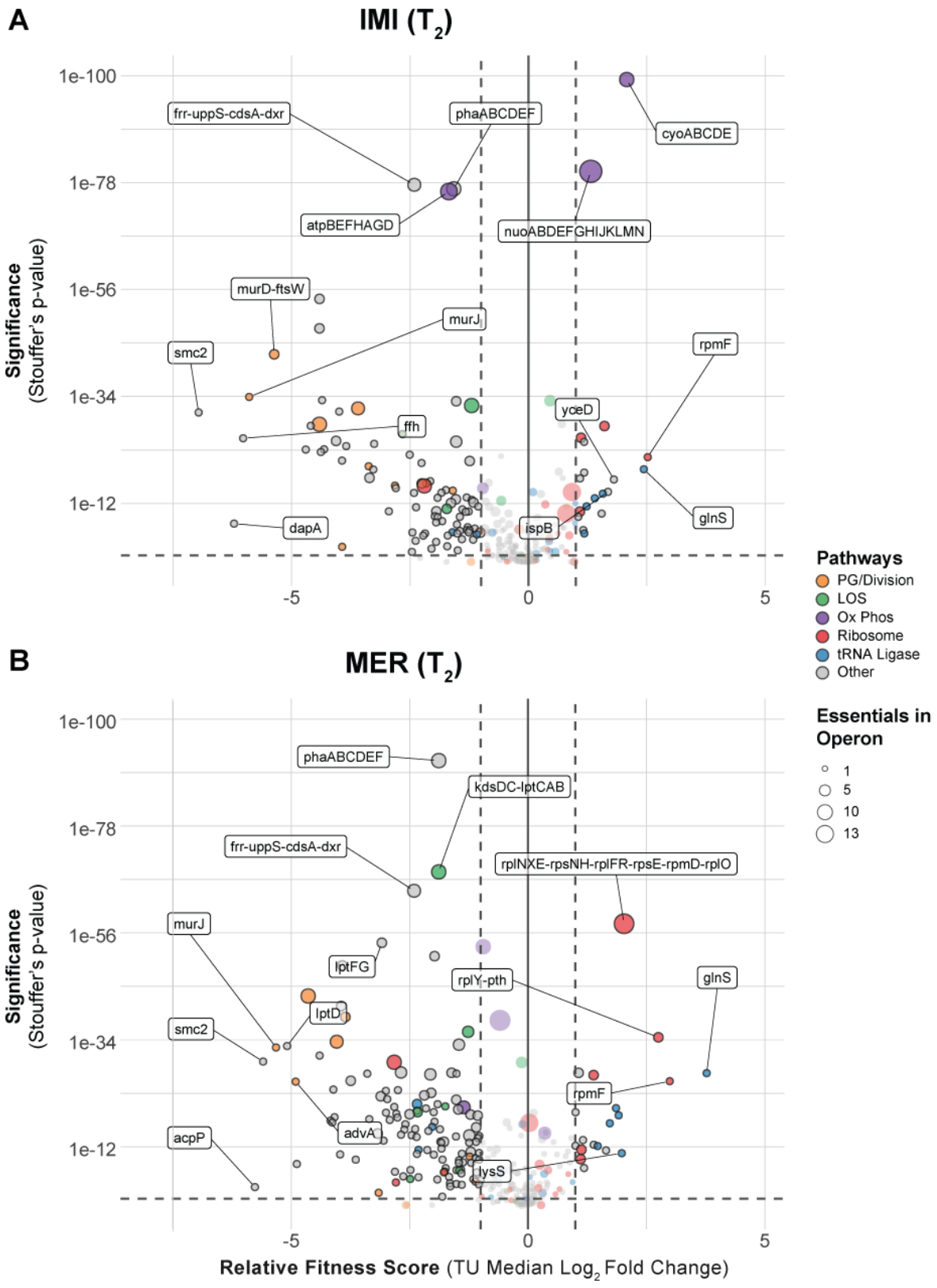
A
IMI (T_2)
1e-100
1e-78
1e-56
1e-34
1e-12
Significance (Stouffer's p-value)
frr-uppS-cdsA-dxr
phaABCDEF
cyoABCDE
atpBEFHAGD
nuoABDEFGHIJKLMN
murD-ftsW
murJ
smc2
rpmF
yceD
ffh
glnS
dapA
ispB
-5
0
5
B
MER (T_2)
phaABCDEF
kdsDC-lptCAB
frr-uppS-cdsA-dxr
rplNXE-rpsNH-rplFR-rpsE-rpmD-rplO
murJ
lptFG
rplY-pth
glnS
lptD
smc2
rpmF
advA
acpP
lysS
Relative Fitness Score (TU Median Log_2 Fold Change)
Pathways
PG/Division
LOS
Ox Phos
Ribosome
tRNA Ligase
Other
Essentials in Operon
1
5
10
13

Figure 2.S7. Carbapenems are synergistic with fosfomycin in *A. baumannii*. 2-fold serial dilutions of drugs from minimum inhibitory concentrations (MICs) represented by gray wedges. Wells with red borders show synergy (i.e., no growth & FIC index <0.5).

Figure 2.S7

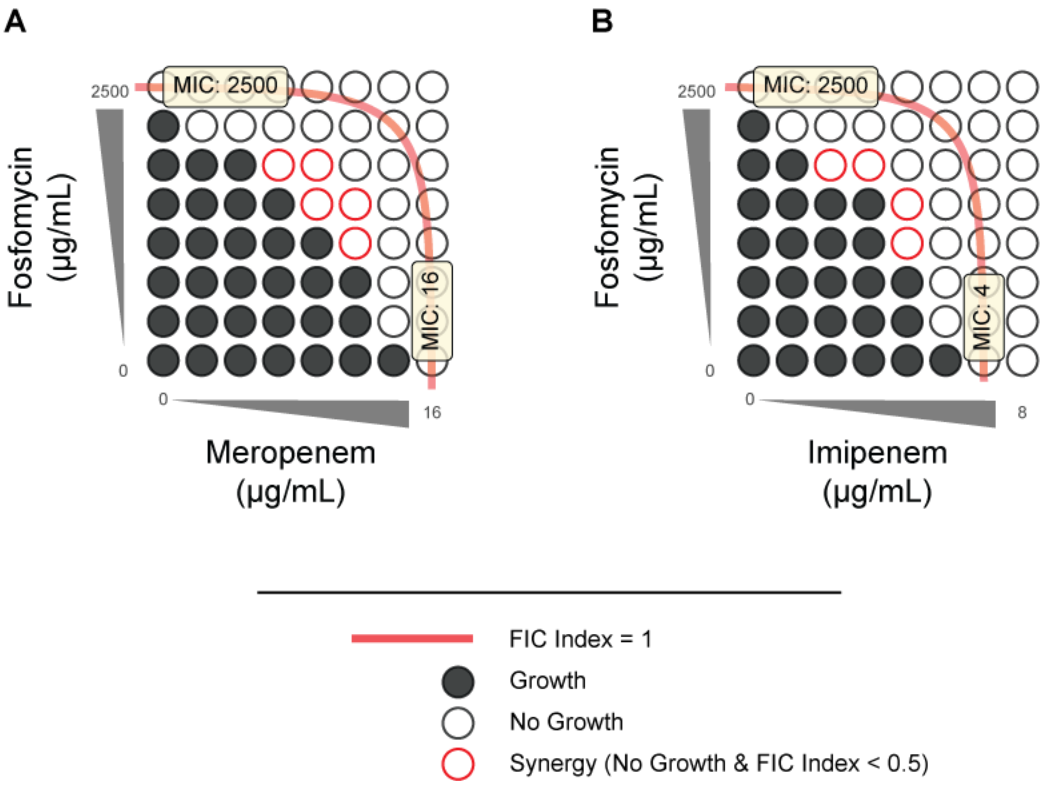
A
B
MIC: 2500
MIC: 16
MIC: 4
2500
0
16
8
Fosfomycin (µg/mL)
Meropenem (µg/mL)
Imipenem (µg/mL)
FIC Index = 1
Growth
No Growth
Synergy (No Growth & FIC Index < 0.5)

Figure 2.S8. Essential gene knockdown interactions with carbapenems. (A-B) Scatterplot of mismatch guide fitness (log_2-fold change) in inducer only compared to relative fitness in imipenem at T1. Lines represent linear model fits with 95% confidence interval. Guides for genes in PG/division or tRNA ligase pathways are divided into groups using hierarchical clustering based on response to imipenem. Left-hand figures in grayscale indicate trend for all guides; right-hand figures indicate trends for guides for specific pathways. High-response indicates most responsive cluster (greatest absolute log_2-fold changes), low-response indicates other clusters (k=3) in C. (C) Hierarchical clustering of tRNA synthetase and PG/division gene knockdowns in response to imipenem (IMI) and meropenem (MER).

Figure 2.S8

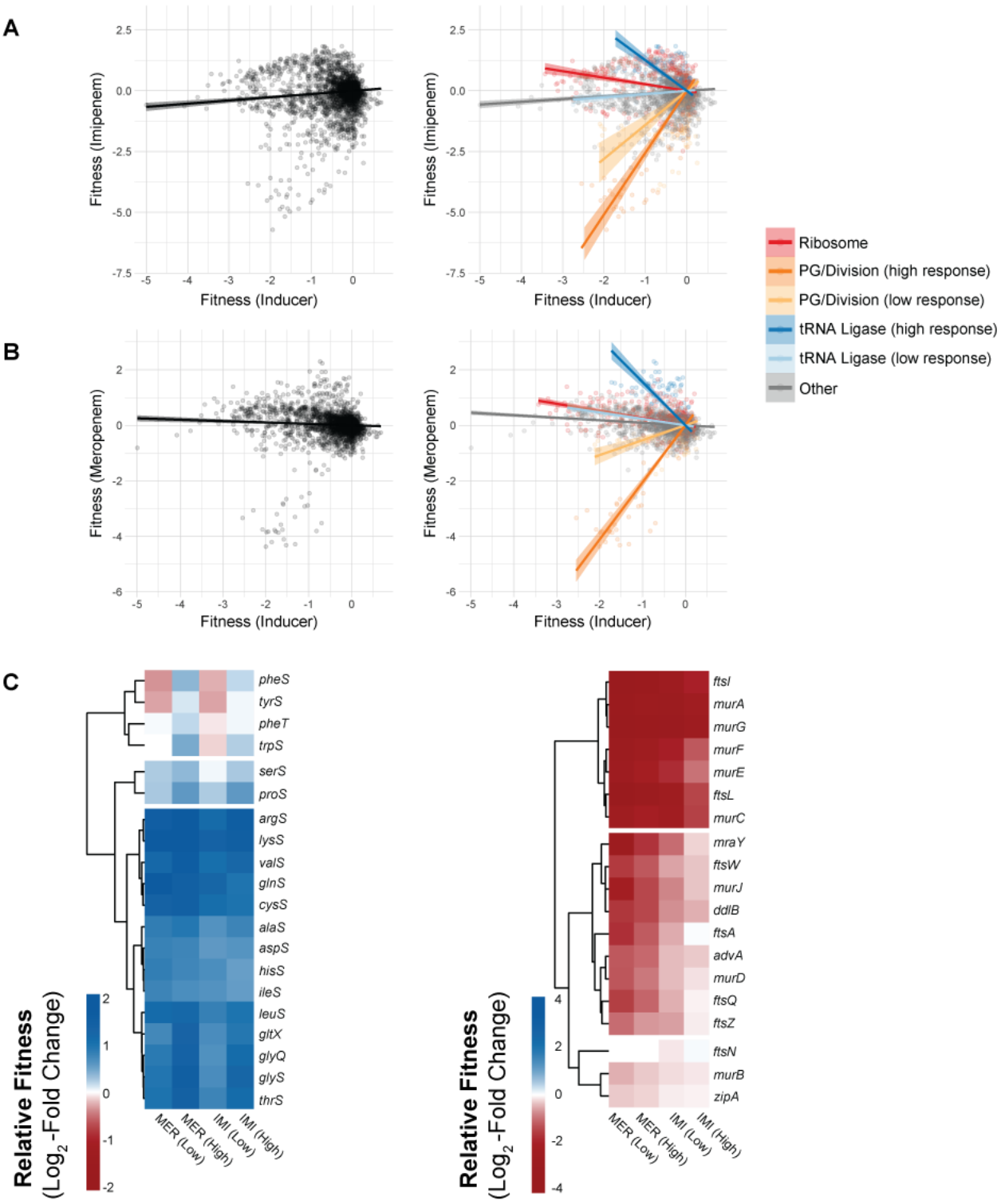
A
B
C
Fitness (Imipenem)
Fitness (Meropenem)
Fitness (Inducer)
Ribosome
PG/Division (high response)
PG/Division (low response)
tRNA Ligase (high response)
tRNA Ligase (low response)
Other
pheS
tyrS
pheT
trpS
serS
proS
argS
lysS
valS
glnS
cysS
alaS
aspS
hisS
ileS
leuS
gltX
glyQ
glyS
thrS
ftsI
murA
murG
murF
murE
ftsL
murC
mraY
ftsW
murJ
ddlB
ftsA
advA
murD
ftsQ
ftsZ
ftsN
murB
zipA
MER (Low)
MER (High)
IMI (Low)
IMI (High)
Relative Fitness
(Log2-Fold Change)

Figure 2.S9. glnS knockdown causes a subtle change in imipenem MIC. Four independently constructed non-targeting (NT) or *glnS* knockdown strains were plated as a lawn on LB + 1mM IPTG and grown in the presence of an IMI MIC test strip. MIC values were read as the concentration line above the intersection between confluent growth and the test strip. The average MICs for NT and *glnS* were 0.6 and 0.9 ng/µL, respectively (p = 0.02, 2 tailed t-test with equal variance).

Figure 2.S9

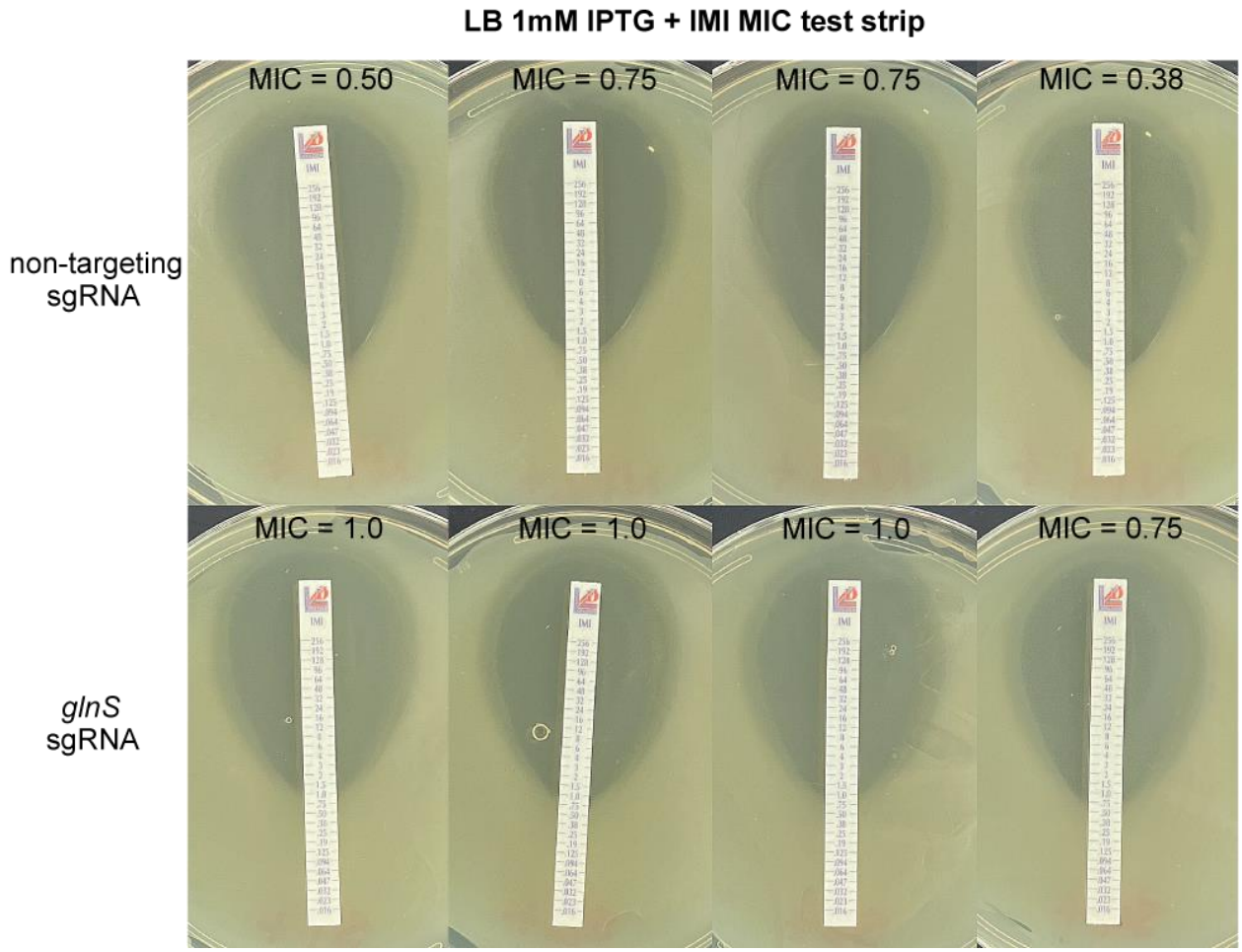
LB 1mM IPTG + IMI MIC test strip
MIC = 0.50
MIC = 0.75
MIC = 0.75
MIC = 0.38
non-targeting sgRNA
MIC = 1.0
MIC = 1.0
MIC = 1.0
MIC = 0.75
glnS sgRNA

Figure 2.S10. Dose-response curves modeling the fits for *glnS* in imipenem (IMI) (A-B) and *nuoB* in rifampicin (RIF) (C-D). Asterisks indicate improvement of the empirical fit from 4-paremeter to 5-parameter, such that the likelihood-ratio test *p* value ≤ 0.05.

Figure 2.S10

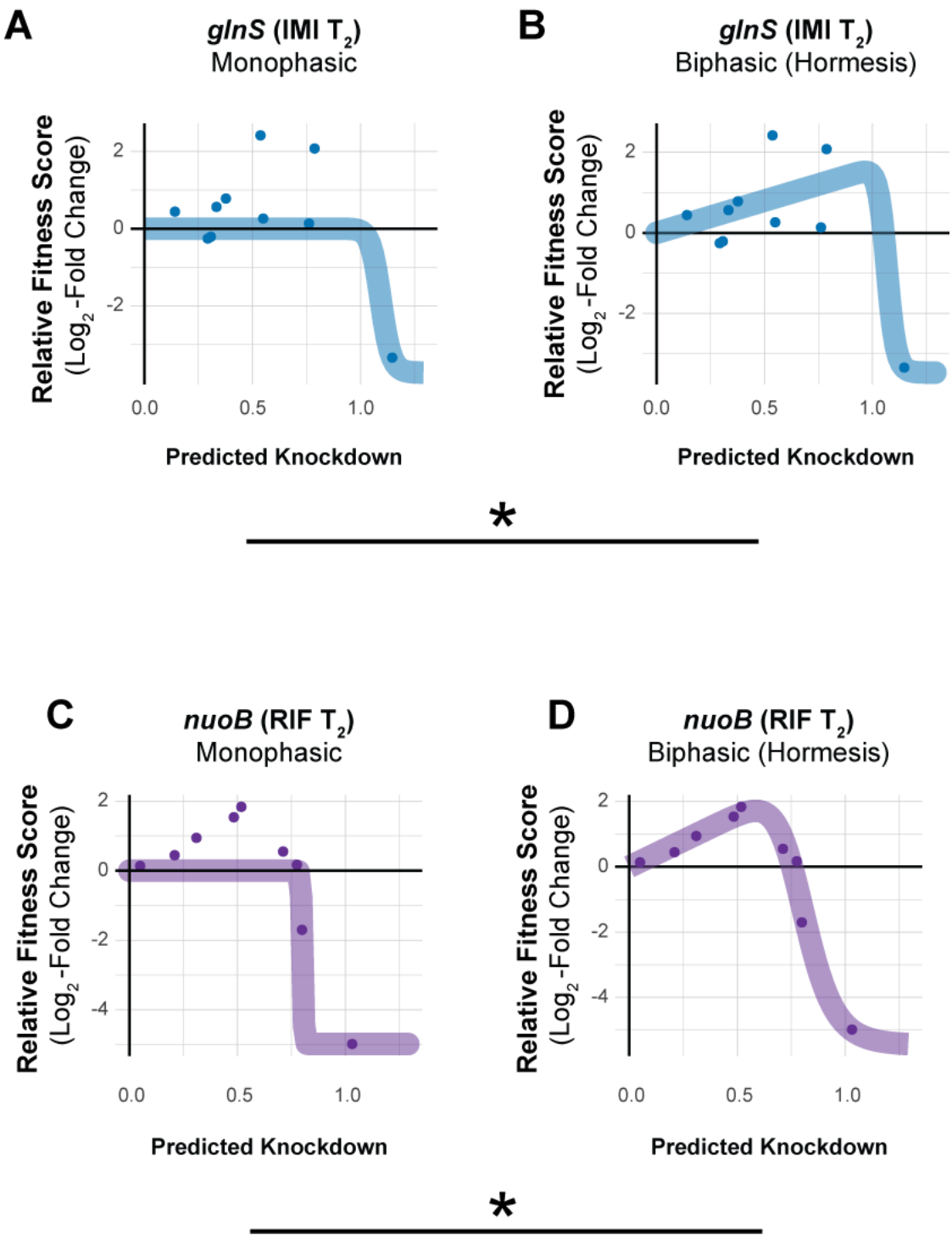
A
glnS (IMI T2)
Monophasic
B
glnS (IMI T2)
Biphasic (Hormesis)
Relative Fitness Score
(Log2-Fold Change)
2
0
-2
0.0
0.5
1.0
Predicted Knockdown
*
C
nuoB (RIF T2)
Monophasic
D
nuoB (RIF T2)
Biphasic (Hormesis)
-4
*

Figure 2.S11. COL and RIF are synergistic under our screening conditions in *A. baumannii*. 2-fold serial dilutions of drugs from minimum inhibitory concentrations (MICs) represented by gray wedges. Wells with red borders show synergy (*i.e.*, no growth & FIC index <0.5).

Figure 2.S11

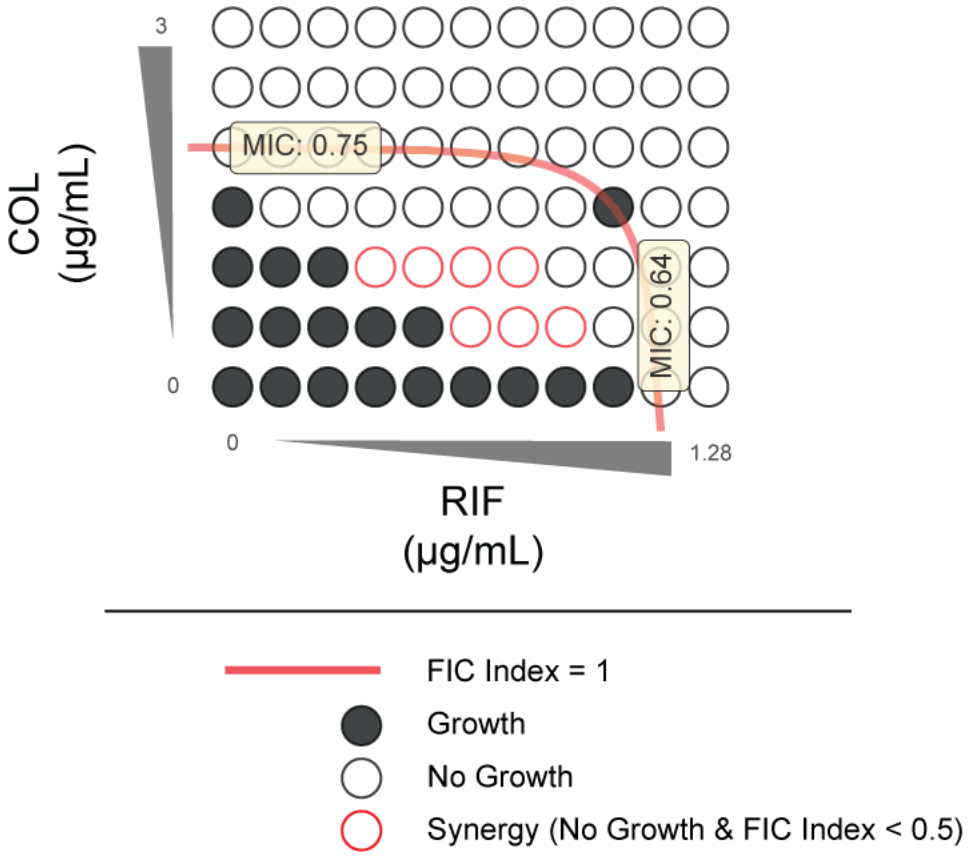
3
0
COL
(µg/mL)
MIC: 0.75
MIC: 0.64
0
1.28
RIF
(µg/mL)
FIC Index = 1
Growth
No Growth
Synergy (No Growth & FIC Index < 0.5)

Figure 2.S12 Essential gene knockdown phenotypes in versus colistin. Depletion of sgRNAs targeting transcription units (TUs) from the CRISPRi library during growth in inducer and RIF or COL at T_2. Vertical dashed lines indicate a two-fold loss in fitness score relative to non-targeting sgRNAs and horizontal dashed lines indicate a Stouffer's *p* value of ≤ 0.05. Stouffer's *p* values were calculated at the TU level by combining the false discovery rates (FDRs) of all individual sgRNAs targeting the TU. TUs related to pathways discussed in the text are colored according to the figure legend and the number of essential genes in a TU is indicated by point size.

Figure 2.S12

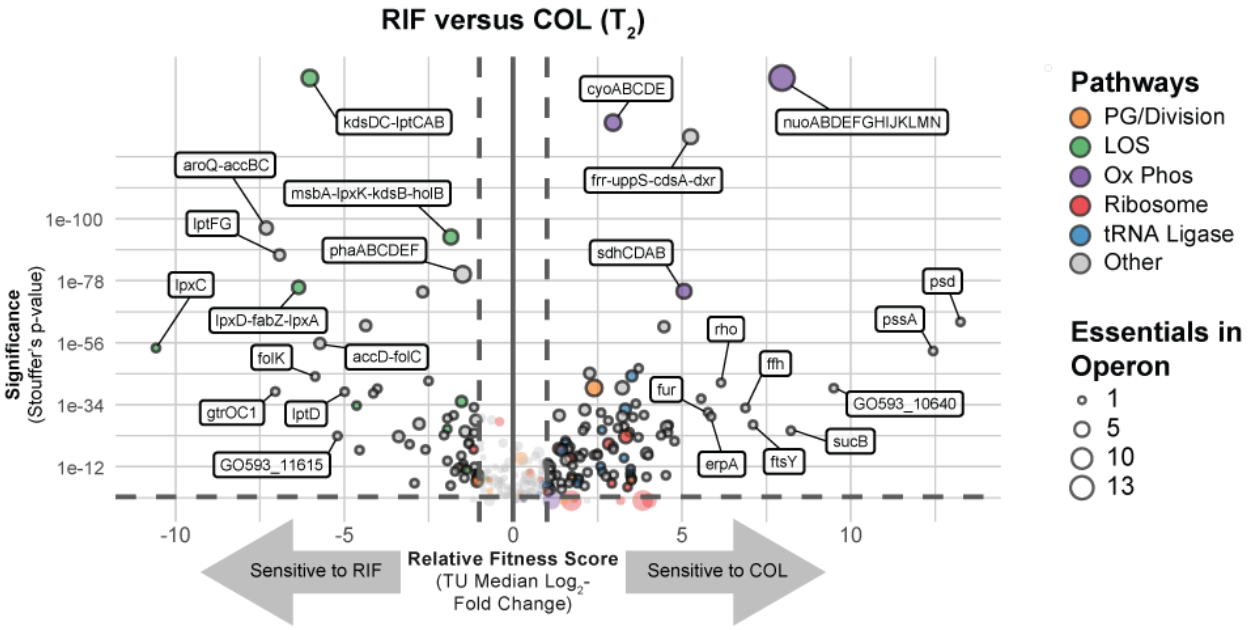
RIF versus COL (T_2)
kdsDC-lptCAB
cyoABCDE
nuoABDEFGHIJKLMN
aroQ-accBC
frr-uppS-cdsA-dxr
msbA-lpxK-kdsB-holB
lptFG
phaABCDEF
sdhCDAB
lpxC
psd
lpxD-fabZ-lpxA
pssA
rho
folK
accD-folC
ffh
fur
gtrOC1
lptD
GO593_10640
sucB
GO593_11615
erpA
ftsY
1e-100
1e-78
1e-56
1e-34
1e-12
Significance (Stouffer's p-value)
-10
-5
0
5
10
Sensitive to RIF
Relative Fitness Score (TU Median Log2-Fold Change)
Sensitive to COL
Pathways
PG/Division
LOS
Ox Phos
Ribosome
tRNA Ligase
Other
Essentials in Operon
1
5
10
13

Figure 2.S13 *nuoB* knockdown causes a subtle change in colistin MIC. Four independently constructed non-targeting (NT) or *nuoB* knockdown strains were plated as a lawn on LB + 1mM IPTG and grown in the presence of a COL MIC test strip. MIC values were read as the concentration line above the intersection between confluent growth and the test strip. The average MICs for NT and *nuoB* were 2 and 1.6 ng/µL, respectively (p = 0.02, 2 tailed t-test with equal variance).

Figure 2.S13

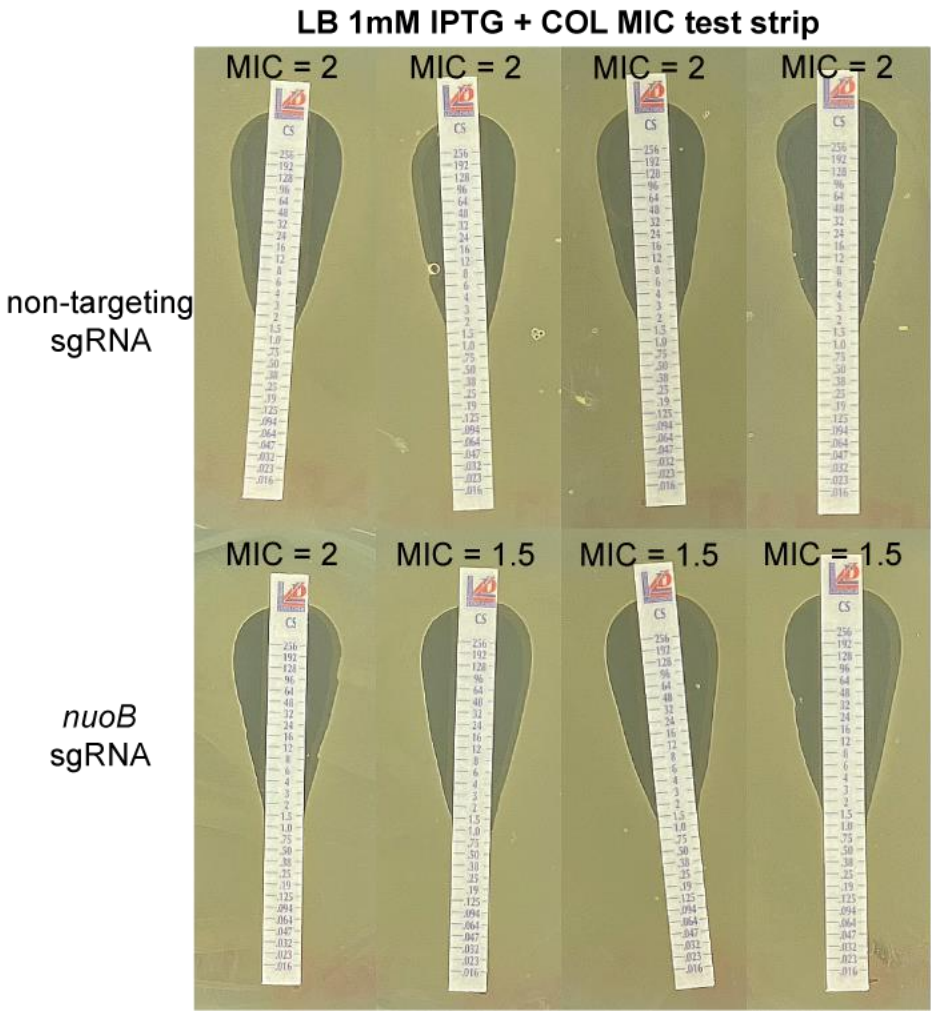
LB 1mM IPTG + COL MIC test strip
MIC = 2
MIC = 2
MIC = 2
MIC = 2
non-targeting sgRNA
MIC = 2
MIC = 1.5
MIC = 1.5
MIC = 1.5
nuoB sgRNA

Figure 2.S14. Membrane potential in non-targeting and *nuoB* knockdown strains. ThT fluorescence normalized to OD_{600} as a measurement of membrane potential (Δψ) in (A) non-targeting and *nuoB* knockdown strains with and without inducer. (B) Normalized ThT fluorescence in wildtype treated with CCCP at 0, 4, 6, and 8 ng/µL.

Figure 2.S14

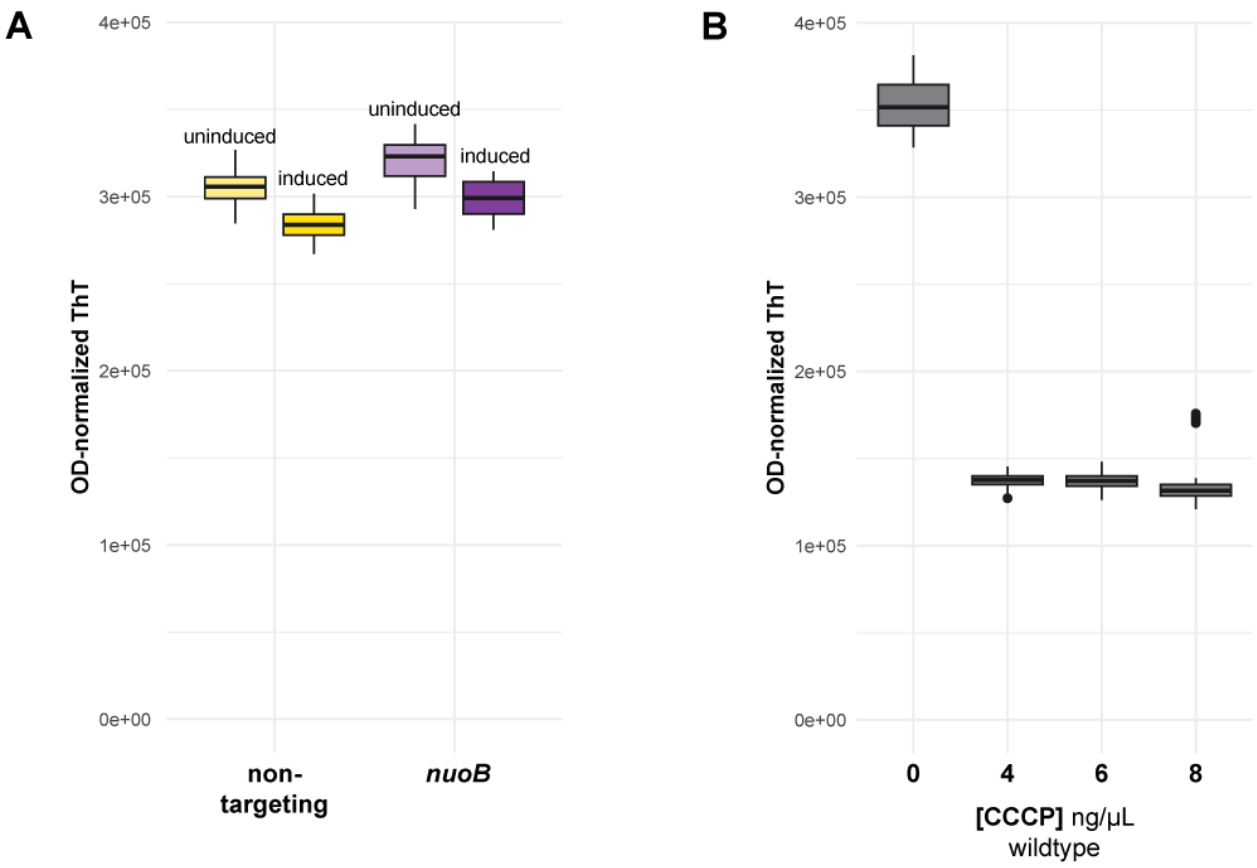
A
4e+05
3e+05
2e+05
1e+05
0e+00
OD-normalized ThT
uninduced
induced
uninduced
induced
non-
targeting
nuoB
B
4e+05
3e+05
2e+05
1e+05
0e+00
OD-normalized ThT
0
4
6
8
[CCCP] ng/µL
wildtype

Figure 2.S15. *nuoB* knockdown causes a subtle change in rifampicin MIC. Four independently constructed non-targeting (NT) or *nuoB* knockdown strains were plated as a lawn on LB + 1mM IPTG and grown in the presence of a RIF MIC test strip. MIC values were read as the concentration line above the intersection between confluent growth and the test strip. The average MICs for NT and *nuoB* were 2.25 and 3.25 ng/µL, respectively (*p* value = 0.03, 2 tailed t-test with equal variance).

Figure 2.S15

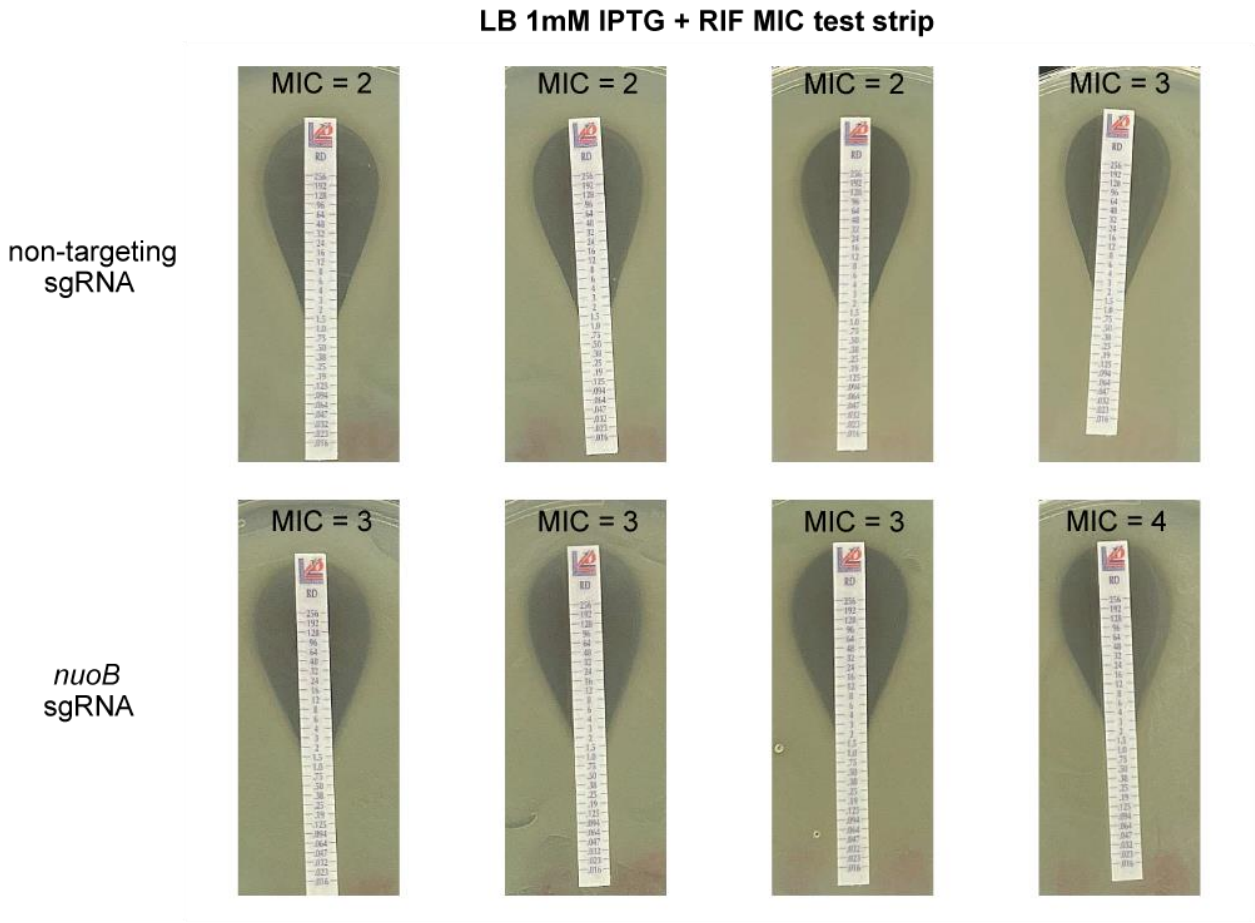
LB 1mM IPTG + RIF MIC test strip
non-targeting sgRNA
nuoB sgRNA
MIC = 2
MIC = 2
MIC = 2
MIC = 3
MIC = 3
MIC = 3
MIC = 3
MIC = 4

Figure 2.S16. COL/RIF interaction and physiological characterization of NDH-1 knockdown. (A-B) CoMBaT-seq experiments competing *nuoB* knockdown with a non-targeting strain in the presence or absence of (A) COL or (B) RIF; as the proportion of the non-targeting strain increases, the *nuoB* knockdown decreases and vice versa. Points are data from individual experiments (N=2).

Figure 2.S16

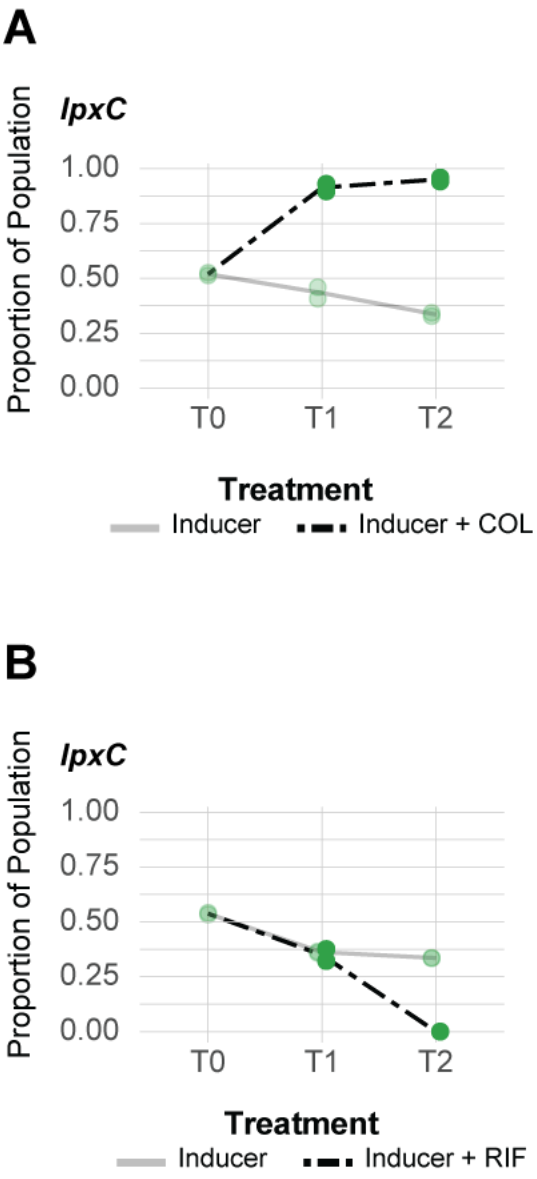
A
lpxC
Proportion of Population
1.00
0.75
0.50
0.25
0.00
T0
T1
T2
Treatment
Inducer
Inducer + COL
B
lpxC
Proportion of Population
1.00
0.75
0.50
0.25
0.00
T0
T1
T2
Treatment
Inducer
Inducer + RIF

Acknowledgements

This work was supported by a Career Transition Award from the NIH National Institute of Allergy and Infectious Diseases (K22AI137122). RDW was supported by the Predoctoral Training Program in Genetics (NIH 5T32GM007133). JST was supported by the Biotechnology Training Program (NIH 5T32GM135066) and a GRFP from the NSF. We thank ChatGPT for assistance in developing the CoMBaT-seq acronym. We thank Agilent Technologies for providing SurePrint Oligonucleotide libraries and Laura Whitman for oligo synthesis support and the University of Wisconsin Biotechnology Center for technical support with Illumina sequencing.

References

1. Prasad NK, Seiple IB, Cirz RT, Rosenberg OS. 2022. Leaks in the Pipeline: a Failure Analysis of Gram-Negative Antibiotic Development from 2010 to 2020. Antimicrobial Agents and Chemotherapy 66:e00054-22.

2. Centers for Disease Control and Prevention (U.S.). 2019. Antibiotic resistance threats in the United States, 2019. Centers for Disease Control and Prevention (U.S.).

3. Poirel L, Naas T, Nordmann P. 2010. Diversity, epidemiology, and genetics of class D beta-lactamases. Antimicrob Agents Chemother 54:24–38.

4. Héritier C, Poirel L, Lambert T, Nordmann P. 2005. Contribution of acquired carbapenem-hydrolyzing oxacillinases to carbapenem resistance in Acinetobacter baumannii. Antimicrob Agents Chemother 49:3198–3202.

5. Lupo A, Haenni M, Madec J-Y. 2018. Antimicrobial Resistance in Acinetobacter spp. and Pseudomonas spp. Microbiol Spectr 6.

6. Valentine SC, Contreras D, Tan S, Real LJ, Chu S, Xu HH. 2008. Phenotypic and molecular characterization of Acinetobacter baumannii clinical isolates from nosocomial outbreaks in Los Angeles County, California. J Clin Microbiol 46:2499–2507.

7. Zhao J, Zhu Y, Han J, Lin Y-W, Aichem M, Wang J, Chen K, Velkov T, Schreiber F, Li J. 2020. Genome-Scale Metabolic Modeling Reveals Metabolic Alterations of Multidrug-Resistant Acinetobacter baumannii in a Murine Bloodstream Infection Model. Microorganisms 8:E1793.

8. Holst O, Molinaro A. 2010. Chapter 3 - Core region and lipid A components of lipopolysaccharides, p. 29–55. *In* Holst, O, Brennan, PJ, Itzstein, M von, Moran, AP (eds.), Microbial Glycobiology. Academic Press, San Diego.

9. Boll JM, Crofts AA, Peters K, Cattoir V, Vollmer W, Davies BW, Trent MS. 2016. A penicillin-binding protein inhibits selection of colistin-resistant, lipooligosaccharide-deficient Acinetobacter baumannii. Proc Natl Acad Sci U S A 113:E6228–E6237.

10. Moffatt JH, Harper M, Harrison P, Hale JDF, Vinogradov E, Seemann T, Henry R, Crane B, St Michael F, Cox AD, Adler B, Nation RL, Li J, Boyce JD. 2010. Colistin resistance in Acinetobacter baumannii is mediated by complete loss of lipopolysaccharide production. Antimicrob Agents Chemother 54:4971–4977.

11. Bai J, Dai Y, Farinha A, Tang AY, Syal S, Vargas-Cuebas G, van Opijnen T, Isberg RR, Geisinger E. 2021. Essential Gene Analysis in Acinetobacter baumannii by High-Density Transposon Mutagenesis and CRISPR Interference. J Bacteriol 203:e0056520.

12. Gallagher LA, Ramage E, Weiss EJ, Radey M, Hayden HS, Held KG, Huse HK, Zurawski DV, Brittnacher MJ, Manoil C. 2015. Resources for Genetic and Genomic Analysis of Emerging Pathogen Acinetobacter baumannii. Journal of Bacteriology 197:2027–2035.

13. Geisinger E, Mortman NJ, Dai Y, Cokol M, Syal S, Farinha A, Fisher DG, Tang AY, Lazinski DW, Wood S, Anthony J, van Opijnen T, Isberg RR. 2020. Antibiotic susceptibility signatures identify potential antimicrobial targets in the Acinetobacter baumannii cell envelope. Nat Commun 11:4522.

14. Gallagher LA, Bailey J, Manoil C. 2020. Ranking essential bacterial processes by speed of mutant death. Proc Natl Acad Sci U S A 117:18010–18017.

15. Qi LS, Larson MH, Gilbert LA, Doudna JA, Weissman JS, Arkin AP, Lim WA. 2013. Repurposing CRISPR as an RNA-guided platform for sequence-specific control of gene expression. Cell 152:1173–1183.

16. Bikard D, Jiang W, Samai P, Hochschild A, Zhang F, Marraffini LA. 2013. Programmable repression and activation of bacterial gene expression using an engineered CRISPR-Cas system. Nucl Acids Res gkt520.

17. Peters JM, Colavin A, Shi H, Czarny TL, Larson MH, Wong S, Hawkins JS, Lu CHS, Koo B-M, Marta E, Shiver AL, Whitehead EH, Weissman JS, Brown ED, Qi LS, Huang KC, Gross CA. 2016. A Comprehensive, CRISPR-based Functional Analysis of Essential Genes in Bacteria. Cell 165:1493–1506.

18. Qu J, Prasad NK, Yu MA, Chen S, Lyden A, Herrera N, Silvis MR, Crawford E, Looney MR, Peters JM, Rosenberg OS. 2019. Modulating pathogenesis with Mobile-CRISPRi. J Bacteriol https://doi.org/10.1128/JB.00304-19.

19. Hawkins JS, Silvis MR, Koo B-M, Peters JM, Osadnik H, Jost M, Hearne CC, Weissman JS, Todor H, Gross CA. 2020. Mismatch-CRISPRi Reveals the Co-varying Expression-Fitness Relationships of Essential Genes in Escherichia coli and Bacillus subtilis. Cell Syst https://doi.org/10.1016/j.cels.2020.09.009.

20. Mathis AD, Otto RM, Reynolds KA. 2021. A simplified strategy for titrating gene expression reveals new relationships between genotype, environment, and bacterial growth. Nucleic Acids Res 49:e6.

21. Vigouroux A, Oldewurtel E, Cui L, Bikard D, Teeffelen S van. 2018. Tuning dCas9's ability to block transcription enables robust, noiseless knockdown of bacterial genes. Molecular Systems Biology 14:e7899.

22. Byun G, Yang J, Seo SW. 2023. CRISPRi-mediated tunable control of gene expression level with engineered single-guide RNA in Escherichia coli. Nucleic Acids Research 51:4650–4659.

23. Peters JM, Koo B-M, Patino R, Heussler GE, Hearne CC, Qu J, Inclan YF, Hawkins JS, Lu CHS, Silvis MR, Harden MM, Osadnik H, Peters JE, Engel JN, Dutton RJ, Grossman AD, Gross CA, Rosenberg OS. 2019. Enabling genetic analysis of diverse bacteria with Mobile-CRISPRi. Nature Microbiology 4:244–250.

24. Rock JM, Hopkins FF, Chavez A, Diallo M, Chase MR, Gerrick ER, Pritchard JR, Church GM, Rubin EJ, Sassetti CM, Schnappinger D, Fortune SM. 2017. Programmable transcriptional repression in mycobacteria using an orthogonal CRISPR interference platform. Nature Microbiology 2:16274.

25. Li S, Poulton NC, Chang JS, Azadian ZA, DeJesus MA, Ruecker N, Zimmerman MD, Eckartt KA, Bosch B, Engelhart CA, Sullivan DF, Gengenbacher M, Dartois VA, Schnappinger D, Rock JM. 2022. CRISPRi chemical genetics and comparative genomics identify genes mediating drug potency in Mycobacterium tuberculosis. 6. Nat Microbiol 7:766–779.

26. Tsubouchi T, Suzuki M, Niki M, Oinuma K-I, Niki M, Kakeya H, Kaneko Y. 2020. Complete Genome Sequence of Acinetobacter baumannii ATCC 19606T, a Model Strain of Pathogenic Bacteria Causing Nosocomial Infection. Microbiol Resour Announc 9:e00289-20.

27. Hullahalli K, Pritchard JR, Waldor MK. 2021. Refined Quantification of Infection Bottlenecks and Pathogen Dissemination with STAMPR. mSystems 6:e0088721.

28. Cui L, Vigouroux A, Rousset F, Varet H, Khanna V, Bikard D. 2018. A CRISPRi screen in E. coli reveals sequence-specific toxicity of dCas9. 1. Nature Communications 9:1912.

29. Bosch B, DeJesus MA, Poulton NC, Zhang W, Engelhart CA, Zaveri A, Lavalette S, Ruecker N, Trujillo C, Wallach JB, Li S, Ehrt S, Chait BT, Schnappinger D, Rock JM. 2021. Genome-wide gene expression tuning reveals diverse vulnerabilities of M. tuberculosis. Cell 184:4579-4592.e24.

30. Silver LL. 2017. Fosfomycin: Mechanism and Resistance. Cold Spring Harb Perspect Med 7:a025262.

31. Sharma A, Sharma R, Bhattacharyya T, Bhando T, Pathania R. 2017. Fosfomycin resistance in Acinetobacter baumannii is mediated by efflux through a major facilitator superfamily (MFS) transporter-AbaF. J Antimicrob Chemother 72:68–74.

32. Maguire BA, Wild DG. 1997. The roles of proteins L28 and L33 in the assembly and function of Escherichia coli ribosomes in vivo. Mol Microbiol 23:237–245.

33. Maguire BA, Wild DG. 1997. Mutations in the rpmBG operon of Escherichia coli that affect ribosome assembly. J Bacteriol 179:2486–2493.

34. Koo B-M, Kritikos G, Farelli JD, Todor H, Tong K, Kimsey H, Wapinski I, Galardini M, Cabal A, Peters JM, Hachmann A-B, Rudner DZ, Allen KN, Typas A, Gross CA. 2017. Construction and Analysis of Two Genome-Scale Deletion Libraries for Bacillus subtilis. Cell Syst 4:291-305.e7.

35. Sauer RT, Krovatin W, DeAnda J, Youderian P, Susskind MM. 1983. Primary structure of the immI immunity region of bacteriophage P22. J Mol Biol 168:699–713.

36. Young R. 2014. Phage lysis: three steps, three choices, one outcome. J Microbiol 52:243–258.

37. Bouz G, Zitko J. 2021. Inhibitors of aminoacyl-tRNA synthetases as antimycobacterial compounds: An up-to-date review. Bioorg Chem 110:104806.

38. Volynets GP, Usenko MO, Gudzera OI, Starosyla SA, Balanda AO, Syniugin AR, Gorbatiuk OB, Prykhod'ko AO, Bdzhola VG, Yarmoluk SM, Tukalo MA. 2022. Identification of dual-targeted Mycobacterium tuberculosis aminoacyl-tRNA synthetase inhibitors using machine learning. Future Med Chem 14:1223–1237.

39. Baba T, Ara T, Hasegawa M, Takai Y, Okumura Y, Baba M, Datsenko KA, Tomita M, Wanner BL, Mori H. 2006. Construction of Escherichia coli K-12 in-frame, single-gene knockout mutants: the Keio collection. Mol Syst Biol 2:2006.0008.

40. Papp-Wallace KM, Endimiani A, Taracila MA, Bonomo RA. 2011. Carbapenems: Past, Present, and Future ▿. Antimicrob Agents Chemother 55:4943–4960.

41. Kouidmi I, Levesque RC, Paradis-Bleau C. 2014. The biology of Mur ligases as an antibacterial target. Mol Microbiol 94:242–253.

42. Falagas ME, Kastoris AC, Karageorgopoulos DE, Rafailidis PI. 2009. Fosfomycin for the treatment of infections caused by multidrug-resistant non-fermenting Gram-negative bacilli: a systematic review of microbiological, animal and clinical studies. Int J Antimicrob Agents 34:111–120.

43. Lee AJ, Wang S, Meredith HR, Zhuang B, Dai Z, You L. 2018. Robust, linear correlations between growth rates and β-lactam–mediated lysis rates. Proceedings of the National Academy of Sciences 115:4069–4074.

44. Tuomanen E, Cozens R, Tosch W, Zak O, Tomasz A. 1986. The rate of killing of Escherichia coli by beta-lactam antibiotics is strictly proportional to the rate of bacterial growth. J Gen Microbiol 132:1297–1304.

45. Mathies AW, Leedom JM, Ivler D, Wehrle PF, Portnoy B. 1967. Antibiotic antagonism in bacterial meningitis. Antimicrob Agents Chemother (Bethesda) 7:218–224.

46. Calabrese EJ, Mattson MP. 2017. How does hormesis impact biology, toxicology, and medicine? 1. npj Aging Mech Dis 3:1–8.

47. Hogg GM, Barr JG, Webb CH. 1998. In-vitro activity of the combination of colistin and rifampicin against multidrug-resistant strains of Acinetobacter baumannii. J Antimicrob Chemother 41:494–495.

48. Vaara M. 1992. Agents that increase the permeability of the outer membrane. Microbiol Rev 56:395–411.

49. Harding CM, Hennon SW, Feldman MF. 2018. Uncovering the mechanisms of Acinetobacter baumannii virulence. 2. Nat Rev Microbiol 16:91–102.

50. Biswas S, Brunel J-M, Dubus J-C, Reynaud-Gaubert M, Rolain J-M. 2012. Colistin: an update on the antibiotic of the 21st century. Expert Rev Anti Infect Ther 10:917–934.

51. Deris ZZ, Akter J, Sivanesan S, Roberts KD, Thompson PE, Nation RL, Li J, Velkov T. 2014. A secondary mode of action of polymyxins against Gram-negative bacteria involves the inhibition of NADH-quinone oxidoreductase activity. 2. J Antibiot 67:147–151.

52. Thornsberry C, Hill BC, Swenson JM, McDougal LK. 1983. Rifampin: Spectrum of Antibacterial Activity. Reviews of Infectious Diseases 5:S412–S417.

53. The firA gene of Escherichia coli encodes UDP-3-O-(R-3-hydroxymyristoyl)-glucosamine N-acyltransferase. The third step of endotoxin biosynthesis - PubMed. https://pubmed.ncbi.nlm.nih.gov/8366125/. Retrieved 26 October 2022.

54. Luo H, Lin Y, Liu T, Lai F-L, Zhang C-T, Gao F, Zhang R. 2021. DEG 15, an update of the Database of Essential Genes that includes built-in analysis tools. Nucleic Acids Res 49:D677–D686.

55. Vinella D, Joseleau-Petit D, Thévenet D, Bouloc P, D'Ari R. 1993. Penicillin-binding protein 2 inactivation in Escherichia coli results in cell division inhibition, which is relieved by FtsZ overexpression. J Bacteriol 175:6704–6710.

56. Hards K, Adolph C, Harold LK, McNeil MB, Cheung C-Y, Jinich A, Rhee KY, Cook GM. 2020. Two for the price of one: Attacking the energetic-metabolic hub of mycobacteria to produce new chemotherapeutic agents. Progress in Biophysics and Molecular Biology 152:35–44.

57. Vilchèze C, Weisbrod TR, Chen B, Kremer L, Hazbón MH, Wang F, Alland D, Sacchettini JC, Jacobs WR. 2005. Altered NADH/NAD+ Ratio Mediates Coresistance to Isoniazid and Ethionamide in Mycobacteria. Antimicrobial Agents and Chemotherapy 49:708–720.

58. MacNair CR, Stokes JM, Carfrae LA, Fiebig-Comyn AA, Coombes BK, Mulvey MR, Brown ED. 2018. Overcoming mcr-1 mediated colistin resistance with colistin in combination with other antibiotics. 1. Nat Commun 9:458.

59. Olmeda-López H, Corral-Lugo A, McConnell MJ. 2021. Effect of Subinhibitory Concentrations of Antibiotics and Disinfectants on ISAba-Mediated Inactivation of Lipooligosaccharide Biosynthesis Genes in Acinetobacter baumannii. 10. Antibiotics 10:1259.

60. Schurek KN, Marr AK, Taylor PK, Wiegand I, Semenec L, Khaira BK, Hancock REW. 2008. Novel Genetic Determinants of Low-Level Aminoglycoside Resistance in *Pseudomonas aeruginosa*. Antimicrob Agents Chemother 52:4213–4219.

61. Santi I, Manfredi P, Maffei E, Egli A, Jenal U. 2021. Evolution of Antibiotic Tolerance Shapes Resistance Development in Chronic Pseudomonas aeruginosa Infections 12:17.

62. Zhao H, Sun Y, Peters JM, Gross CA, Garner EC, Helmann JD. 2016. Depletion of Undecaprenyl Pyrophosphate Phosphatases Disrupts Cell Envelope Biogenesis in Bacillus subtilis. J Bacteriol 198:2925–2935.

63. Johnson RA, Chan AN, Ward RD, McGlade CA, Hatfield BM, Peters JM, Li B. 2021. Inhibition of Isoleucyl-tRNA Synthetase by the Hybrid Antibiotic Thiomarinol. J Am Chem Soc 143:12003–12013.

64. Shelake RM, Pramanik D, Kim J-Y. 2023. Improved Dual Base Editor Systems (iACBEs) for Simultaneous Conversion of Adenine and Cytosine in the Bacterium Escherichia coli. mBio 14:e02296-22.

65. Banta AB, Ward RD, Tran JS, Bacon EE, Peters JM. 2020. Programmable Gene Knockdown in Diverse Bacteria Using Mobile-CRISPRi. Curr Protoc Microbiol 59:e130.

66. Szklarczyk D, Kirsch R, Koutrouli M, Nastou K, Mehryary F, Hachilif R, Gable AL, Fang T, Doncheva NT, Pyysalo S, Bork P, Jensen LJ, von Mering C. 2023. The STRING database in 2023: protein-protein association networks and functional enrichment analyses for any sequenced genome of interest. Nucleic Acids Res 51:D638–D646.

67. Datsenko KA, Wanner BL. 2000. One-step inactivation of chromosomal genes in Escherichia coli K-12 using PCR products. Proc Natl Acad Sci U S A 97:6640–6645.

68. Blodgett JAV, Thomas PM, Li G, Velasquez JE, van der Donk WA, Kelleher NL, Metcalf WW. 2007. Unusual transformations in the biosynthesis of the antibiotic phosphinothricin tripeptide. Nat Chem Biol 3:480–485.

69. de Boer PA, Crossley RE, Rothfield LI. 1989. A division inhibitor and a topological specificity factor coded for by the minicell locus determine proper placement of the division septum in E. coli. Cell 56:641–649.

70. Banta AB, Enright AL, Siletti C, Peters JM. 2020. A High-Efficacy CRISPR Interference System for Gene Function Discovery in Zymomonas mobilis. Appl Environ Microbiol 86:e01621-20.

71. Cherepanov PP, Wackernagel W. 1995. Gene disruption in Escherichia coli: TcR and KmR cassettes with the option of Flp-catalyzed excision of the antibiotic-resistance determinant. Gene 158:9–14.

72. Stabb EV, Ruby EG. 2002. RP4-based plasmids for conjugation between Escherichia coli and members of the Vibrionaceae. Methods Enzymol 358:413–426.

73. Robinson MD, McCarthy DJ, Smyth GK. 2010. edgeR: a Bioconductor package for differential expression analysis of digital gene expression data. Bioinformatics 26:139–140.

74. Cinar O, Viechtbauer W. 2022. The **poolr** Package for Combining Independent and Dependent p Values. J Stat Soft 101.

75. Ritz C, Baty F, Streibig JC, Gerhard D. 2015. Dose-Response Analysis Using R. PLoS One 10:e0146021.

76. Wickham H. 2016. ggplot2. Springer International Publishing, Cham. http://link.springer.com/10.1007/978-3-319-24277-4. Retrieved 17 July 2024.

77. Sprouffske K, Wagner A. 2016. Growthcurver: an R package for obtaining interpretable metrics from microbial growth curves. BMC Bioinformatics 17:172.

CHAPTER 3

Large-scale chemical-gene interaction profiling informs antibiotic and essential gene function in *Acinetobacter baumannii*

This chapter is in preparation for publication.

Jennifer S. Tran, Ryan D. Ward, Rubén Iruegas, Ingo Ebersberger, Jason M. Peters. 2024. Large-scale chemical-gene interaction profiling informs antibiotic and essential gene function in *Acinetobacter baumannii*. *In preparation*.

I performed all laboratory experiments, figure generation, and data analysis. RDW developed computational tools to count barcodes, calculate $\log_2$ fold changes, and analyze pathway-level fitness. RI performed conservation and evolutionary analyses. I wrote this chapter with edits and feedback from JMP. Supplementary figures can be found at the end of the chapter. Other supplementary information can be found at https://github.com/jentranxd.

Abstract

The Gram-negative pathogen *Acinetobacter baumannii* causes antibiotic resistant nosocomial infections that are a serious threat to human health. Despite this, our understanding of fundamental *A. baumannii* biology remains limited, as many essential genes are poorly characterized. Here, we systematically probe the function of essential genes by screening a CRISPR interference library against a diverse panel of antibiotics and other inhibitors. We found that the vast majority of essential genes showed chemical-gene interactions, enabling insights into both inhibitor and gene function. For instance, knockdowns of lipooligosaccharide transport genes were especially enriched for sensitive phenotypes due to lipooligosaccharide production-dependent hyper-permeability. We constructed a high-confidence essential gene network from chemical-gene interaction profiles that contained numerous connections between poorly- and well-characterized genes in cell division and other processes. Finally, we applied an unbiased, structure-function analysis to our chemical-gene interaction data, highlighting distinct cellular impacts among structurally related antibiotics and uncovering possible cellular targets for poorly characterized inhibitors. This study advances our understanding of essential gene and antibiotic function, providing a valuable resource for mechanistic studies, therapeutic strategies, and key future targets for antibiotic development.

Introduction

Systems biology provides a robust framework for deciphering the complex networks of interactions that govern cellular functions. This approach is especially pertinent in the study of infectious diseases and antibiotic resistance, offering sophisticated tools to analyze the multifaceted interactions between pathogens and their environments, including their responses to therapeutic interventions. The Gram-negative, hospital-acquired pathogen *Acinetobacter baumannii* is categorized as an 'urgent threat' due to certain clinical strains developing resistance to all known therapeutics and its ability to persist on surfaces in the hospital environment (1, 2). Despite the critical dangers posed by *A. baumannii*, our understanding of how the fundamental elements of its biology interact with antibiotics or other inhibitors remains limited. Essential genes, which are vital for the survival and virulence of bacteria, are promising targets for drug discovery. Essential genes in *A. baumannii* have been cataloged using methods like transposon sequencing (Tn-seq), which identifies genes with low or nonexistent insertion frequencies as critical for survival (3, 4). However, lethality caused by knocking out essential genes limits more detailed studies of gene function and interactions. CRISPR interference (CRISPRi), which allows for the knockdown of gene expression without eliminating gene function (5, 6), provides a solution for studying the function of essential genes (7). CRISPRi uses a deactivated Cas9 protein, dCas9, directed by a single guide RNA (sgRNA) to target and silence specific genes and has been used successfully in diverse bacteria including *A. baumannii*, non-*baumannii Acinetobacter* species, and other Gram-negative pathogens (8–13).

Chemical genomics, which combines gene perturbation libraries with chemical treatments, offers a strategy to explore gene function as changes in relative fitness of mutant or knockdown cells in response to chemical stresses (14, 15). This approach has been applied at a systems-level in bacteria to enhance the range of observable phenotypes and facilitate the identification of genetic

connections from Tn-seq or deletion libraries (3, 16, 17) as well as in CRISPRi libraries (18–21). Our previous work involved developing and characterizing a CRISPRi library in *A. baumannii*, which identified key vulnerabilities among essential genes and demonstrated how this library could be utilized to elucidate antibiotic-gene interactions (20).

In this study, we substantially expand this foundation by screening our *A. baumannii* essential gene CRISPRi library against a broad and varied set of chemical stressors (N = 45 conditions), allowing us to glean systems-level insights. With these data, we identified and characterized pathways that were highly sensitized to antibiotics and other inhibitors, created an essential gene network that informed the function of poorly characterized genes, and combined phenotypic and cheminformatic approaches to elucidate inhibitor target pathways. In doing so, this work furthers our understanding of the unique and complex biology of *A. baumannii* in the context of chemical stress.

Results

The vast majority of A. baumannii essential genes show significant chemical-gene interactions.

To investigate the relationship between chemical stressors and essential genes in *A. baumannii*, we conducted a large-scale chemical genomics screen using our established inducible CRISPRi library in *A. baumannii* strain ATCC19606 (19606 throughout) (20). This library consists of pooled CRISPRi strains with guides targeting 406 predicted essential genes and 1000 non-targeting controls. For each targeted gene, there are four perfect-match guides that exactly match the target sequence and ten mismatch guides with single-base variations from the target sequence that allow for titration of knockdown (22). We performed competition fitness assays by inducing CRISPRi knockdown and adding chemicals at sublethal concentrations that preserve library diversity and

size while allowing us to measure phenotypic responses to treatment (Fig 3.1A). The library was screened against diverse compounds, including clinically relevant antibiotics, heavy metals, and inhibitors with unknown mechanisms of action (Fig 3.1B). Knockdown strain abundance was analyzed by amplification and sequencing of the sgRNA spacer regions. To ensure guide count accuracy and to remove samples with excessive selective pressure or noise that would skew calculations, we improved our quantification of sgRNA barcodes using robust computational tools and implemented sample quality control metrics (Fig 3.S1A and B). Briefly, we implemented a position-aware counter that heuristically determines flanking sequences—ensuring accurate guide counts even for those with overlapping targets—and set replicate correlation and sample complexity cutoffs (see Material and Methods for details). We verified that chemical solvent impacts were negligible as DMSO-only and no-chemical control samples showed >95% correlation (Fig 3.S1C).

To determine chemical-gene phenotypes from the pooled screens, we calculated chemical-genetic (CG) scores for each gene, or median $\log_2$ fold change (medL_2FC) of perfect guides with chemical treatment compared to induction alone. Positive CG scores indicate gene knockdowns with improved growth under chemical conditions, whereas negative CG scores indicate further inhibition of growth. Strikingly, we found that 93% (378/406) of library genes exhibited at least one significant (medL_2FC ≥ |1|, Stouffer's $p < 0.05$) CG score when knocked down, with a median of 14 significant chemical interactions per gene. These skewed towards loss of relative fitness with ~73% (3895/5345) of significant CG scores being negative. No gene knockdown had significant, positive CG scores in more than 29% of the conditions (Fig 3.1D). This is consistent with previous studies in *Saccharomyces cerevisiae* showing essential genes are more frequently connected by negative interactions (23) and implies that no single knockdown shows generally improved growth under chemical exposure. Overall, this dataset provides thousands of unique chemical-gene phenotypes

Figure 3.1. Chemical genomics screen in *A. baumannii* essential gene library. (A) Schematic depicting experimental setup for chemical genomics. (B) Proportional area chart of reported mechanisms of action of screen chemicals. (C) Histogram showing significant chemical-gene scores (|median $\log_2$ fold change| ≥ 1 and Stouffer's $p < 0.05$, calculated from perfect-match guides), across chemical conditions in our screen. Darker bars to the right of the dotted line represent at least one significant chemical interaction in this screen. (D) Stacked bar chart showing the sum of significant positive (pink) and negative (blue) CG scores across screen chemicals for each gene in the library.

Figure 3.1

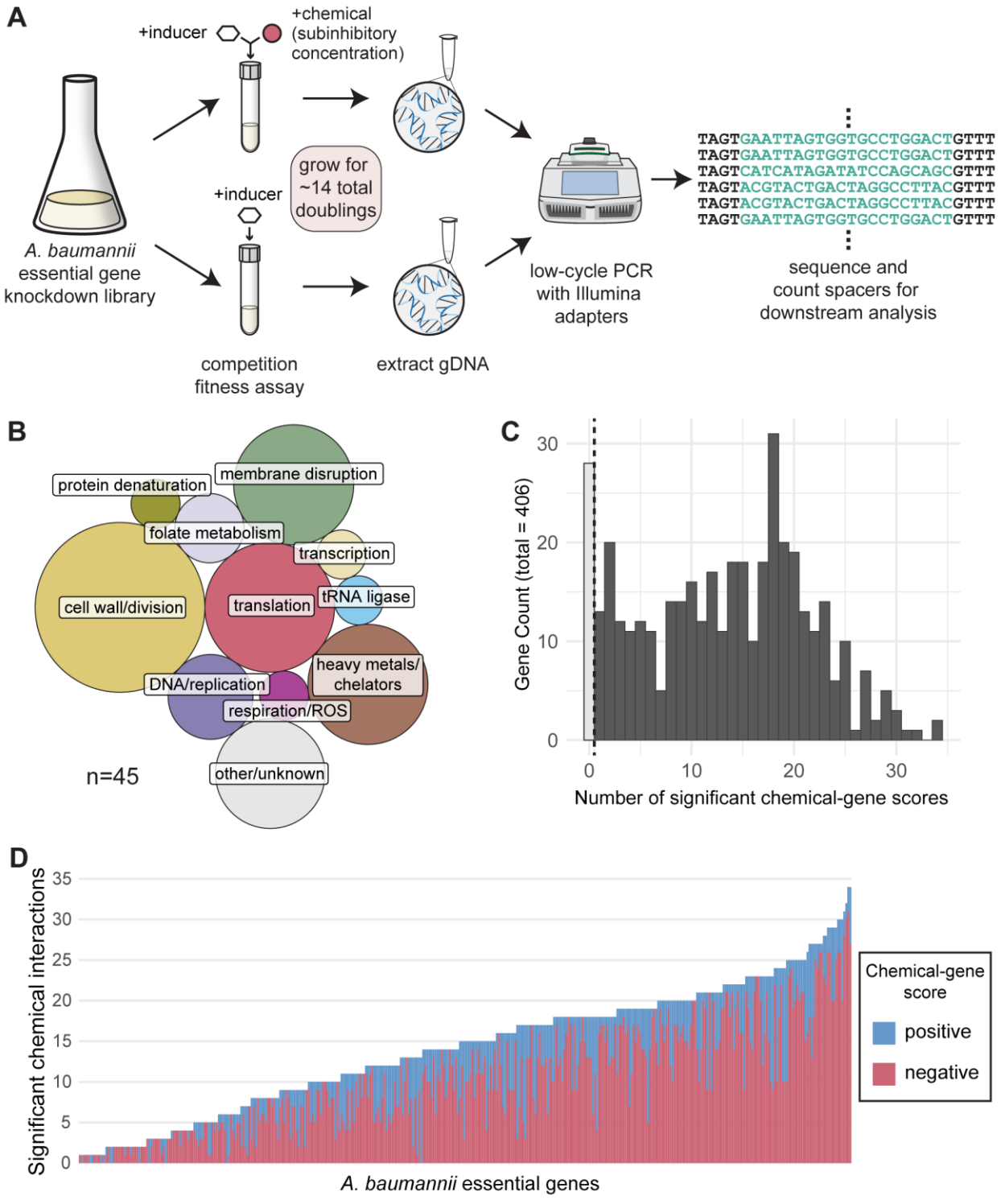
A
+inducer
+chemical
(subinhibitory
concentration)
grow for
~14 total
doublings
+inducer
A. baumannii
essential gene
knockdown library
competition
fitness assay
extract gDNA
low-cycle PCR
with Illumina
adapters
TAGTGAATTAGTGGTGCCTGGACTGTTT
TAGTGAATTAGTGGTGCCTGGACTGTTT
TAGTCATCATAGATATCCAGCAGCGTTT
TAGTACGTACTGACTAGGCCTTACGTTT
TAGTACGTACTGACTAGGCCTTACGTTT
TAGTGAATTAGTGGTGCCTGGACTGTTT
sequence and
count spacers for
downstream analysis
B
protein denaturation
membrane disruption
folate metabolism
transcription
cell wall/division
translation
tRNA ligase
heavy metals/
chelators
DNA/replication
respiration/ROS
other/unknown
n=45
C
Gene Count (total = 406)
Number of significant chemical-gene scores
D
Significant chemical interactions
A. baumannii essential genes
Chemical-gene
score
positive
negative

and serves as a robust and detailed resource for *A. baumannii* essential gene responses to chemical stress.

Lipooligosaccharide transport inhibition enhances drug susceptibility through increased membrane permeability

To identify *A. baumannii* essential pathways crucial for chemical resistance, we ranked genes based on significant negative CG scores (medL_2FC ≤-1, FDR <0.05) across conditions and performed functional enrichment using the STRING database (24). We found that knockdowns of the lipooligosaccharide transport (Lpt) system were substantially enriched (GO:0015920, enrichment score = 8.95, FDR = 1.04e-05), and showed sensitivity in 70% of all conditions in our screen (Fig 3.2B-C). Lpt is a highly conserved pathway required for lipopolysaccharide (LPS)/lipooligosaccharide (LOS) export to the outer leaflet of the outer membrane in Gram-negative bacteria. *A. baumannii* uses Lpt to transport LOS, which contains lipidA and core oligosaccharide moieties found in LPS but lacks O-polysaccharide repeats (Fig 3.2A) (25). Intriguingly, while LPS/LOS is essential in most Gram-negative bacteria, many strains of *A. baumannii* do not require LOS for survival, including the strain used for our library (19606) (26). Indeed, knockdowns of *lpx* genes responsible for LOS synthesis showed fewer phenotypes in our screen than knockdowns of *lpt* needed for LOS transport (Fig 3.S2A).

We validated our screen results by performing quantitative minimum inhibitory concentration (MIC) assays with antibiotic strips with individual knockdowns, showing that an *lptA* knockdown was sensitized to several clinically relevant antibiotics (Fig 3.2D) in contrast to an *lpxC* knockdown that was not (Fig 3.2D and 3.S2B); although loss of LOS has been shown to increase antibiotic sensitivity (27). Both the *lpxC* and *lptA* knockdowns remained sensitized to colistin (Fig 3.S2B)—a cationic lipopeptide that disrupts membranes by targeting the lipid A moiety of LOS (28) —suggesting that

Figure 3.2. *lpt* knockdowns are sensitized to antibiotics. (A) Graphical depiction of Lpt machinery and LOS trafficking to the outer membrane in *A. baumannii*. (B) Histogram of significant negative chemical interactions (medL_2FC ≤ -1 and Stouffer's $p < 0.05$) across conditions. Bold line indicates location of *lpt* genes. (C) Heatmap displaying CG scores for the *lpt* knockdown cluster. Y-axis clustering was conducted using the Ward method and Canberra distance across all library knockdowns. Chemical condition abbreviations can be found in Table 3.4. (D) Tigecycline and azithromycin MIC test strip assays for the *lptA* knockdown, *lpxC* knockdown, and control strain containing a nontargeting guide. Plates supplemented with 1mM IPTG; approximate MICs reported below images (μg/mL). (E) Ethidium bromide permeability assay for *lptA* knockdown and nontargeting control in 19606 or LOS^- backgrounds after induction; increased fluorescence over time indicates membrane permeability. Ribbons represent standard deviation (n=4).

Figure 3.2

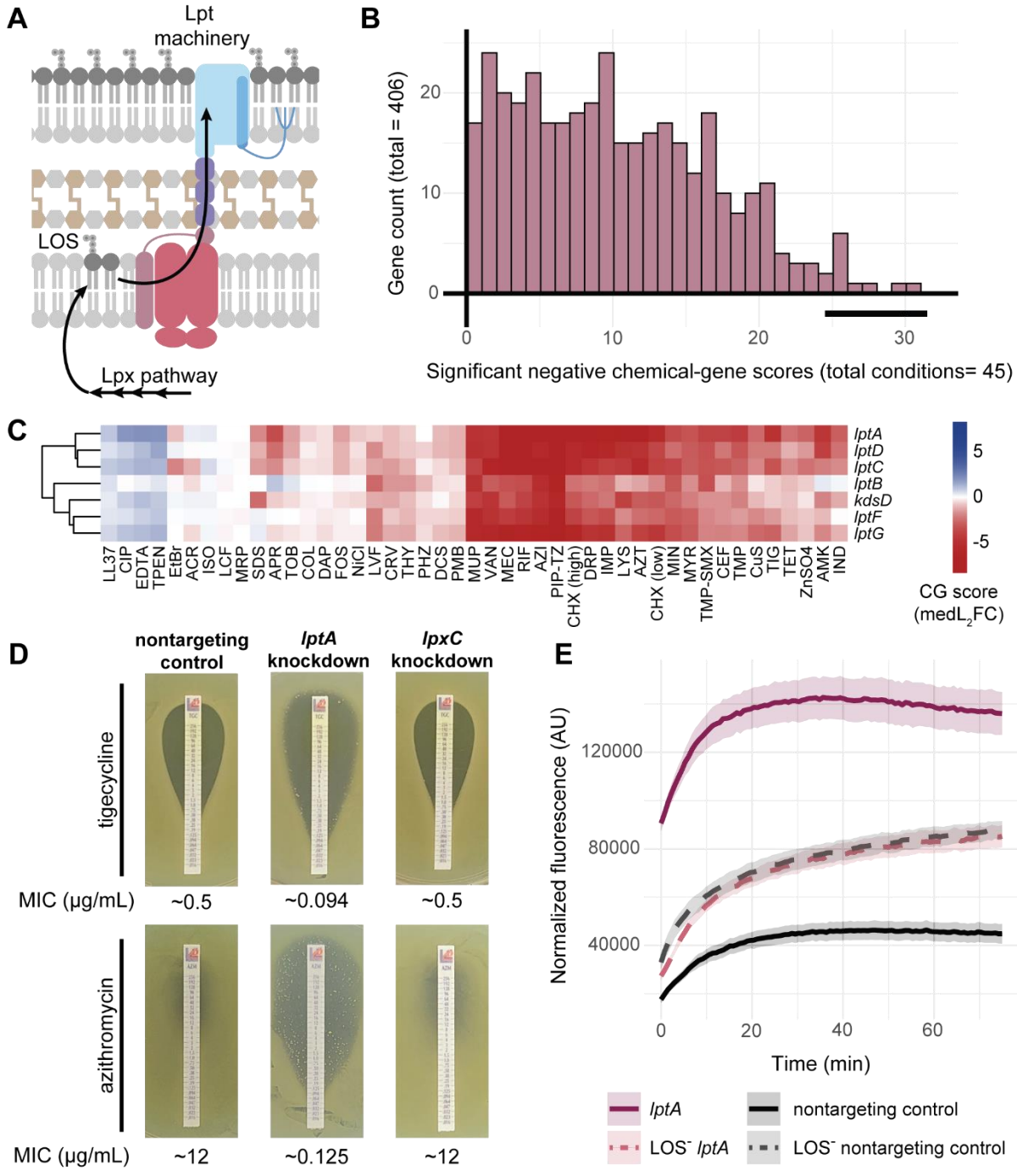
A
Lpt machinery
LOS
Lpx pathway
B
Gene count (total = 406)
Significant negative chemical-gene scores (total conditions= 45)
C
lptA
lptD
lptC
lptB
kdsD
lptF
lptG
CG score (medL2FC)
LL37 CIP EDTA TPEN EtBr ACR ISO LCF MRP SDS APR TOB COL DAP FOS NiCl LVF CRV THY PHZ DCS PMB MUP VAN MEC RIF AZI PIP-TZ CHX (high) DRP IMP LYS AZT CHX (low) MIN MYR TMP-SMX CEF TMP CuS TIG TET ZnSO4 AMK IND
D
nontargeting control
lptA knockdown
lpxC knockdown
tigecycline
azithromycin
MIC (µg/mL)
~0.5
~0.094
~0.5
~12
~0.125
~12
E
Normalized fluorescence (AU)
Time (min)
lptA
nontargeting control
LOS- lptA
LOS- nontargeting control

these knockdowns are not complete loss-of-function phenotypes and still maintain some level of LOS in the outer membrane that can be targeted by colistin (29). We therefore integrated CRISPRi either targeting *lptA* or containing a non-targeting control sgRNA into a mutant strain background that does not produce LOS, 19606 *lpxC(S106R*) (27). In contrast to the 19606 *lptA* and *lpxC* knockdowns, the LOS$^-$ strains were wholly resistant to colistin (Fig 3.S2B). Additionally, the LOS$^-$ strains showed considerable growth defects not exhibited by the 19606 knockdown strains (Fig 3.S2D). Yet, the *lptA* knockdown strain was as similarly sensitized as the LOS$^-$ strains to levofloxacin, an antibiotic that requires penetration into the cell cytoplasm (Fig 3.S2B).

The large number of sensitive phenotypes to chemically diverse inhibitors displayed by *lpt* knockdowns suggested a permeability defect. Therefore, we performed an ethidium bromide (EtBr) fluorescence assay to test for the knockdown's effect on membrane permeability; in this assay, cells are briefly exposed to EtBr, which fluoresces after passing through the outer and inner membranes and binding to DNA. More permeable membranes will have higher fluorescence readings, and as expected, the LOS$^-$ strains showed increased permeability compared to the 19606 nontargeting control. Surprisingly though, the 19606 *lptA* knockdown was substantially more permeable than the LOS$^-$ strains, including the LOS$^-$ *lptA* knockdown (Fig 3.2E and Fig 3.S2D). This indicates that Lpt deficiencies cause a further increase in membrane permeability when LOS is being synthesized, possibly due to LOS accumulation in the inner membrane. Taken together, these findings underscore the critical role of the LOS transport system in *A. baumannii* in maintaining membrane integrity and mediating resistance to chemicals.

Taxon-specific determinants of chemical susceptibility and resistance

Essential genes that are highly divergent in or unique to *A. baumannii* may provide additional insights into mechanisms underlying its distinct drug resistance and persistence and potentially

guide the development of more precise therapeutic targets. To identify genes that are highly divergent or exclusive to *A. baumannii* that contribute to chemical response, we examined library gene conservation using a feature-aware ortholog search across representative *Gammaproteobacteria* species (30). We identified a subset of 16 chemically responsive essential genes from *A. baumannii* that have orthologs in <40% of representative gammaproteobacterial species (~2500 species, excluding the *Moraxellales* family, which includes *Acinetobacter*) (Fig 3.3A). These genes exhibited significant CG scores in at least 10% of the tested conditions and likely play specialized yet substantial roles that impact growth under chemical stressors in *A. baumannii*. Notably, well-established genes involved in outer membrane biogenesis, *lptC* and *lpxL*, are highlighted here due to major divergence in their primary sequences between *A. baumannii* and other *Gammaproteobacteria*. Other less-established genes with possible roles in the cell envelope are also featured here: GO593_05760 (*advA*), GO593_03530 (*gtrOC1*), GO593_06865 (*wzx*), GO593_07665 (*blhA*), and GO593_11915 (*smc2*). When comparing genes only across *Acinetobacter* species, we identified three of these genes as predominantly biased towards *A. baumannii*: *gtrOC1, wzx,* and GO593_15125 (Fig 3.3B).

Genes *gtrOC1* and *wzx*, are both tied to cell surface components. Wzx is a known transporter of capsular polysaccharide in *A. baumannii*, but Wzx proteins generally exhibit poor conservation due to the diversity of the polysaccharides they transport (31, 32). The poor conservation of this *wzx* gene among *Acinetobacter* species even when using a feature-aware search suggests either high variation of the capsular polysaccharides transported by this machinery or horizontal acquisition. *gtrOC1* encodes for a predicted Elm1-like mitochondrial fission protein family, which contributes to non-conventional core oligosaccharide synthesis in *A. baumannii* (33). The lower conservation across even other *Acinetobacter* species (Fig 3.3B) supports the hypothesis that this gene supports a divergent mechanism of core oligosaccharide synthesis in *A. baumannii*. In our

Figure 3.3. Chemical interactions and conservation of essential genes. Dot plots depict library chemical-gene scores and conservation (ortholog frequency) across (A) representative non-*Moraxellales Gammaproteobacteria* or (B) non-*A. baumannii Acinetobacter* species. Dots in blue represent genes with <40% presence across representative groups and significant chemical-gene interactions in >10% of screen conditions. (C) Heatmap depicting CG scores for knockdowns of species-specific hits.

Figure 3.3

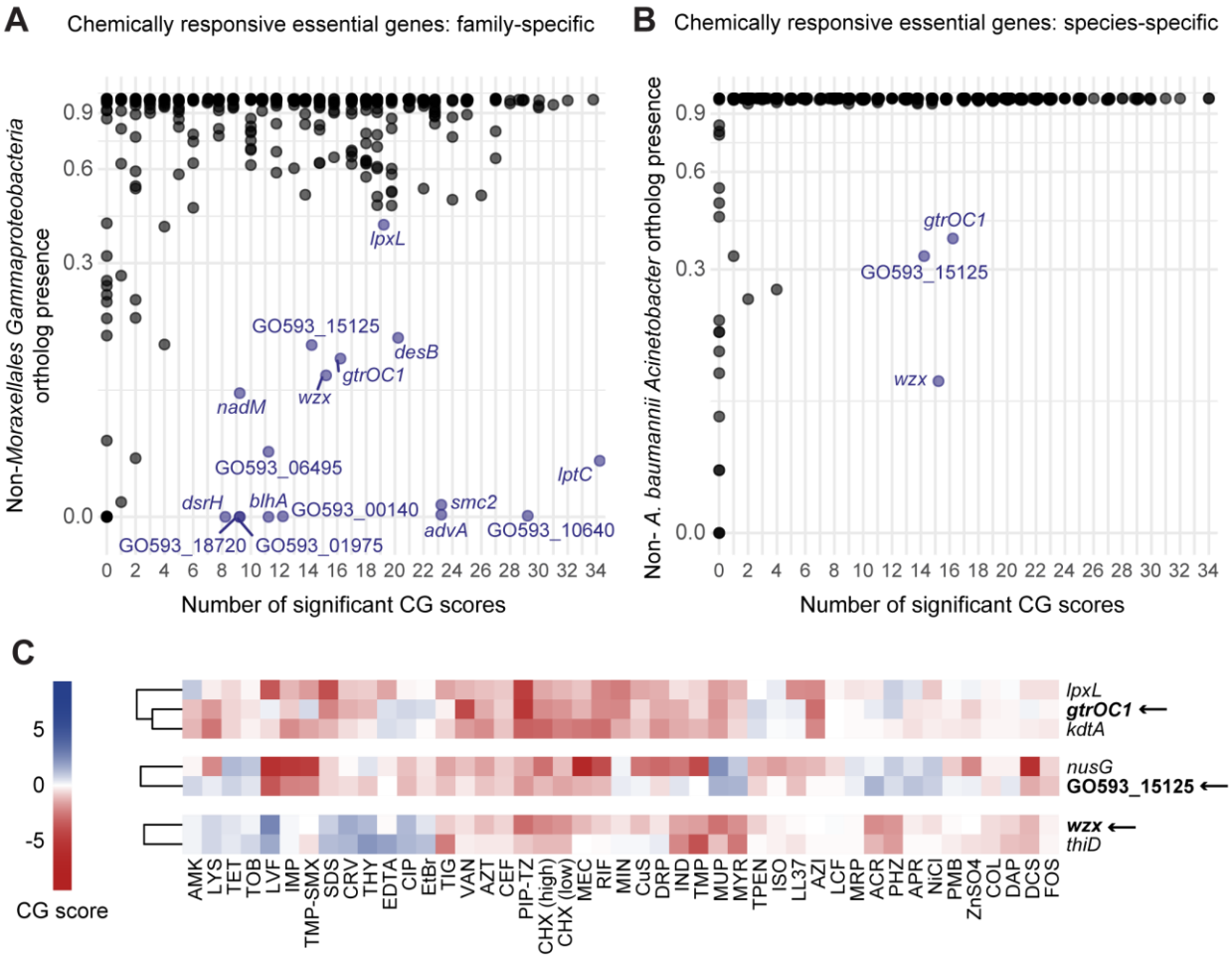
A
Chemically responsive essential genes: family-specific
Non-Moraxellales Gammaproteobacteria ortholog presence
Number of significant CG scores
lpxL
GO593_15125
desB
gtrOC1
wzx
nadM
GO593_06495
lptC
dsrH
blhA
GO593_00140
smc2
advA
GO593_10640
GO593_18720
GO593_01975
B
Chemically responsive essential genes: species-specific
Non- A. baumannii Acinetobacter ortholog presence
Number of significant CG scores
gtrOC1
GO593_15125
wzx
C
CG score
5
0
-5
lpxL
gtrOC1
kdtA
nusG
GO593_15125
wzx
thiD
AMK LYS TET TOB LVF IMP TMP-SMX SDS CRV THY EDTA CIP EtBr TIG VAN AZT CEF PIP-TZ CHX (high) CHX (low) MEC RIF MIN CuS DRP IND TMP MUP MYR TPEN ISO LL37 AZI LCF MRP ACR PHZ APR NiCl PMB ZnSO4 COL DAP DCS FOS

hierarchical clustering analysis of gene-level phenotypes across all chemical conditions, *gtrOC1* clusters with other genes tied to lipooligosaccharide synthesis supporting its role, but *wzx* interestingly does not, clustering with *thiD*, a thiamin synthesis gene for unknown reasons (Fig 3.3C).

GO593_15125 is an Arc-family repressor located upstream of a predicted transposase. In previous work, we identified a distinct, poorly conserved Arc-family prophage repressor as the most vulnerable gene in 19606, likely due to its role in repressing toxic prophage gene expression (20). The limited conservation of GO593_15125, which is only present in approximately 50% of *A. baumannii* strains, along with its association with a predicted transposase and an antiphage defense island (consisting of a type IIG restriction-modification gene (GO593_15130) and PD-T7-2 defense system (GO593_15155) (34, 35)) suggests a potential role in the regulation of mobile genetic elements that affect strain growth. Supporting this hypothesis, the most sensitive phenotype of GO593_15125 was observed with levofloxacin, a DNA-damaging antibiotic. Mobile genetic elements are known to modulate gene expression in response to DNA damage (36, 37) and can sometimes trigger DNA damage responses themselves (38). Additionally, the clustering of GO593_15125 with the transcription elongation factor *nusG* further implies a downstream effect on global gene regulation that may be related to DNA damage. In *E. coli*, the essential role of NusG is to negatively regulate prophage gene expression (39) and its depletion increases expression of genes involved in the DNA damage response (40). Taken together, these findings highlight unique and highly divergent genes with significant chemical interactions in *A. baumannii* that provide a potential intellectual foundation for more targeted therapeutics.

An essential gene network in A. baumannii identifies novel gene connections

To investigate functional connections for poorly conserved genes in *A. baumannii*,, we created a high-confidence essential gene network by calculating pairwise correlations between sets of gene

phenotypes and applying a stringent statistical threshold to define network edges, an approach previously applied in model bacteria (7, 16). Connections in this network were predominantly between rather than within operons, underscoring that the majority of our connections are not simply artifacts of CRISPRi polarity. As expected, we found that well-conserved pathways, such as ribosomal components and cell division, were interconnected (Fig 3.4A); however, complexes involved in oxidative phosphorylation were disconnected, indicating distinct functionalities (e.g., succinate dehydrogenase also functions in the TCA cycle). Notably, cytochrome bo_3 oxidase and the monovalent cation/H+ antiporter—complexes identified as absent in other *Moraxellales* (Fig 3.S3)—along with thiamin and ferrodoxin genes and *wzx* were found in the same subnetwork (Fig 3.S4A), hinting at possible regulatory or larger pathway connections. Lpt genes also formed a separate cluster, connected to the *A. baumannii*-specific glycosyltransferase *gtrOC1*, supporting the glycosyltransferase's role in LOS synthesis (Fig 3.S4B).

Connections between unannotated, poorly conserved genes and well-established genes suggest shared functions. We found that GO593_00140 and GO593_11615 were linked with multiple DNA replication genes (Fig 3.4B) and showed significant, negative CG scores in levofloxacin, which targets replication (Fig 3.S5A-B). Although GO593_00140 is poorly conserved outside *Moraxellales* (Fig 3.2A), Structural prediction using Alphafold2 showed that GO593_00140 contains a domain that is structurally similar to *E. coli* HolD, the psi subunit of the bacterial DNA polymerase III holoenzyme (Fig 3.S5C). A previous hidden Markov model (HMM)-based homology search identified similar putative psi subunits in other *Acinetobacter* species (41), and our work provides phenotypic evidence to further support that this gene is involved in DNA replication in *A. baumannii*. In comparison, GO593_11615 is likely a phage-associated transcriptional regulator, situated within an intact prophage as predicted by PHASTEST (42). This protein has domain architecture similar to LexA, a highly conserved protein that self-cleaves under DNA damage stress to activate SOS DNA

Figure 3.4. Essential gene network reveals functional connections. (A) Essential gene network in *A. baumannii*. Nodes (genes) are connected by edges (phenotypic correlations, r>0.76). Subnetworks of (B) DNA polymerase and replication-related genes, (C) signal-recognition, and (D) cell division and cell wall synthesis are shown. (E) Quantification of cell length of knockdowns from microscopy (N=200-400). (F) Representative microscopy images. Ruler is 5 μm.

Figure 3.4

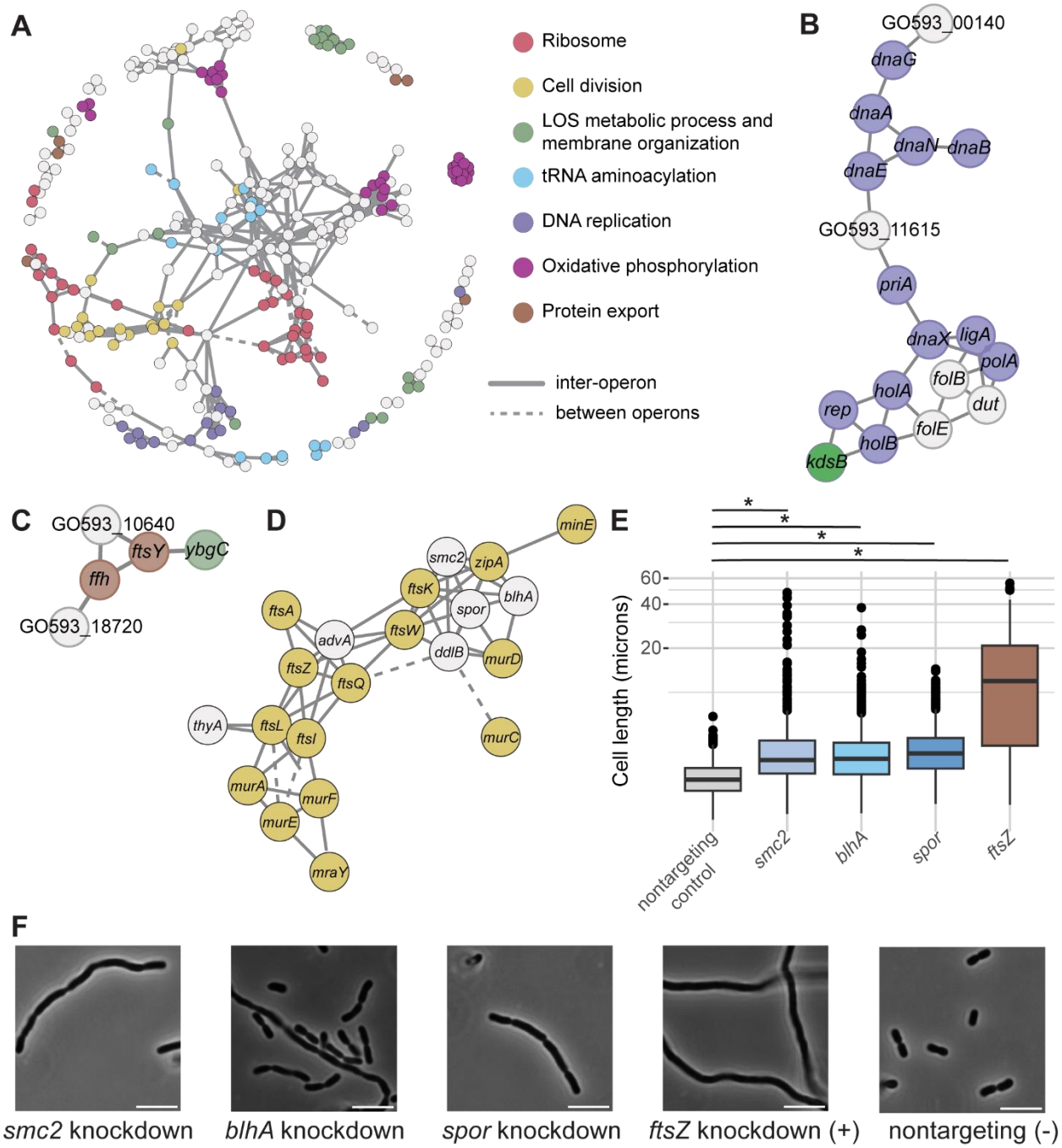
A
Ribosome
Cell division
LOS metabolic process and membrane organization
tRNA aminoacylation
DNA replication
Oxidative phosphorylation
Protein export
inter-operon
between operons
B
GO593_00140
dnaG
dnaA
dnaN
dnaB
dnaE
GO593_11615
priA
dnaX
ligA
polA
folB
holA
dut
rep
folE
holB
kdsB
C
GO593_10640
ftsY
ybgC
ffh
GO593_18720
D
minE
smc2
zipA
ftsK
blhA
spor
ftsA
advA
ftsW
ddlB
murD
ftsZ
ftsQ
thyA
ftsL
ftsI
murC
murA
murF
murE
mraY
E
Cell length (microns)
60
40
20
nontargeting control
smc2
blhA
spor
ftsZ
F
smc2 knockdown
blhA knockdown
spor knockdown
ftsZ knockdown (+)
nontargeting (-)

repair pathways (Fig 3.S5D). Prophages are known to hijack the SOS pathway: excising, synthesizing phage particles, and lysing the bacterial host cells when LexA is depleted (36). Interestingly, *A. baumannii* lacks *lexA* (43), suggesting this prophage encodes its own LexA-like protein as a strategy to overcome this absence.

GO593_10640 and GO593_18720, two poorly conserved genes, grouped with the conserved signal recognition particle (SRP) genes *ftsY* and *ffh* and *ybgC*, a Tol-Pal-associated thioesterase linked to membrane integrity (44) (Fig 3.4C). GO593_10640 shows structural similarities to ion transporters and significant chemical responses consistent with *ftsY* and *ffh* knockdowns (Fig 3.S6A-B). GO593_18720, however, showed subtle CG scores, indicating a possibly less critical or defined role (Fig 3.S6A). These genes may be directly or indirectly related to membrane protein localization and membrane integrity, though SRP mechanisms remain understudied in *A. baumannii*. We note some connections, such as *tusD* with GO593_17830, which lies upstream of a TusE-like gene, may be influenced by polar effects of this system (Fig 3.S6C-D).

The network analysis also revealed a cell wall and division subnetwork (Fig 3.4D), containing three genes poorly conserved across *Gammaproteobacteria* but present in *Acinetobacter*—GO593_05760 (*advA*), GO593_07665 (*blhA*), and GO593_11915 (*smc2* a.k.a. *SMC_prok_B*)—and a gene encoding for a SPOR domain-containing protein of unknown function, GO593_07290, annotated here as *spor*. These genes correlate with numerous well-characterized, highly conserved division genes, corroborating initial data from other studies suggesting roles for *advA*, *blhA*, and *smc2* in cell division (3, 45). While GO593_07290 contains a well-conserved SPOR domain, which interacts with peptidoglycan in the cell wall, functions of these SPOR domain-containing proteins vary considerably. Indeed, one of the most well-studied SPOR-domain proteins, FtsN from *E. coli*, does not require the SPOR domain for its essential function (46). The short periplasmic region required for FtsN function, ^{E}FtsN (47), does not appear to be present at the amino acid level in

GO593_07290, which is possibly functionally distinct from FtsN and performs an unknown role in cell division (Fig 3.S5E).

To further support the role of these genes in this pathway, we generated individual *blhA*, *smc2*, and *spor* CRISPRi knockdown strains and examined cell shape with microscopy. AdvA knockdowns have been previously shown to produce a filamentation phenotype, a hallmark of impaired cell division (12). Similarly, *blhA, smc2*, and *spor* knockdowns produced elongated or chained cells (Fig 3.4E-F), corroborating evidence seen previously in a *blhA* transposon mutant (45). We then looked to further characterize these proteins and their localization, expressing fluorescent fusions of these proteins *in trans*. Expression of the Smc2::sfGFP hybrid protein unexpectedly resulted in cell elongation and impaired division. The fluorescently tagged Smc2 protein was observed to form elongated aggregates within the chained cells (Fig 3.S7A); however, it remains unclear whether this represents true localization or is a consequence of toxic overexpression of the protein. The elongated cell phenotype was confirmed with the overexpression of Smc2 alone, suggesting that Smc2 protein levels must fall within a certain range for proper division (Fig 3.S7B). While *smc2* is directly upstream of known division gene, *zapA*, *trans* expression allowed us to disentangle its role in cell division from polar effects of knockdown. In contrast, the SPOR domain protein appeared to localize to both the membrane and septum (Fig 3.S7C), while the sfGFP::BlhA hybrid localized to the septum (Fig 3.S7D). The SPOR domain localization is unsurprising due to its peptidoglycan-binding domain, but suggests a more generalized cell wall synthesis function, while BlhA is primarily divisome-associated. Overall, this network reveals functional connections and underlying phenotypes linking crucial pathways in *A. baumannii*, such as cell division, and provides a basis for further targeted experiments to explore these connections.

Structure-informed clustering of chemical perturbations reveals insights into inhibitor function

We next sought to use our chemical genomics dataset to better characterize the functions of inhibitor molecules in *A. baumannii*. To broadly define inhibitor impacts on cell physiology, we analyzed chemical gene impacts at the pathway level rather than the individual gene level. This approach evaluated the L_2FCs of all guides, including mismatches, associated with a STRING functional pathway ("pathway effect") (48), increasing signal robustness. We then clustered the pathway-level interactions by chemical, showing the relationship between chemicals solely based on the cellular pathways they impacted in our screen (Fig 3.5A). Inhibitors from the same antibiotic classes, such as quinolones (ciprofloxacin and levofloxacin) or aminoglycosides (amikacin, apramycin, and tobramycin), clustered as expected, validating our method.

To more systematically compare inhibitors outside of established antibiotic classes, we performed molecular fingerprinting—a chemoinformatic approach that numerically represents unique chemical structure and properties of molecules as binary fingerprints (extended-connectivity fingerprints) (49, 50)—and measured similarity between chemicals using the Tanimoto coefficient (51, 52). Clustering using the Tanimoto coefficients again revealed that structurally similar molecules verified that antibiotics with similar core structures (beta-lactams, fluoroquinolones, aminoglycosides, etc.) do indeed group together (Fig 3.5B); however, there were important exceptions that we discuss below. Comparing pathway effects and molecular fingerprints allowed us to investigate (a) consistent chemical classes with a not-yet-established mechanism of action, (b) structurally similar chemicals that have different effects on *A. baumannii*, and (c) structurally dissimilar chemicals that affect *A. baumannii* physiology in the same way.

Figure 3.5. Chemical grouping by pathway effects and structure. (A) Dendrogram depicting hierarchical clustering (Ward method) of screen chemicals by similarities of effects across essential gene pathways. (B) Dendrogram displaying hierarchical clustering (Ward method) of chemical molecular fingerprints (ECFP6) by Tanimoto coefficient. Asterisks represent conditions with multiple chemical structures, in which a single structure was used (see Table S4). Chemical groups of interested are marked. (C) Sina plots with boxplots depict differential guide counts per million (CPMs) for protein translocation in carvacrol and thymol, or (D) for heme-copper terminal oxidase in tetracycline-class antibiotics, compared to corresponding no chemical controls. STRING group identifiers and representation are listed. Chemical-gene interactions are described above each graph—up (positive), down (negative), or no change—with FDR values. Guides are weighted in this calculation by predicted efficacy, with perfect guides at 100. Non-significant comparisons are shown with grey backgrounds.

Figure 3.5

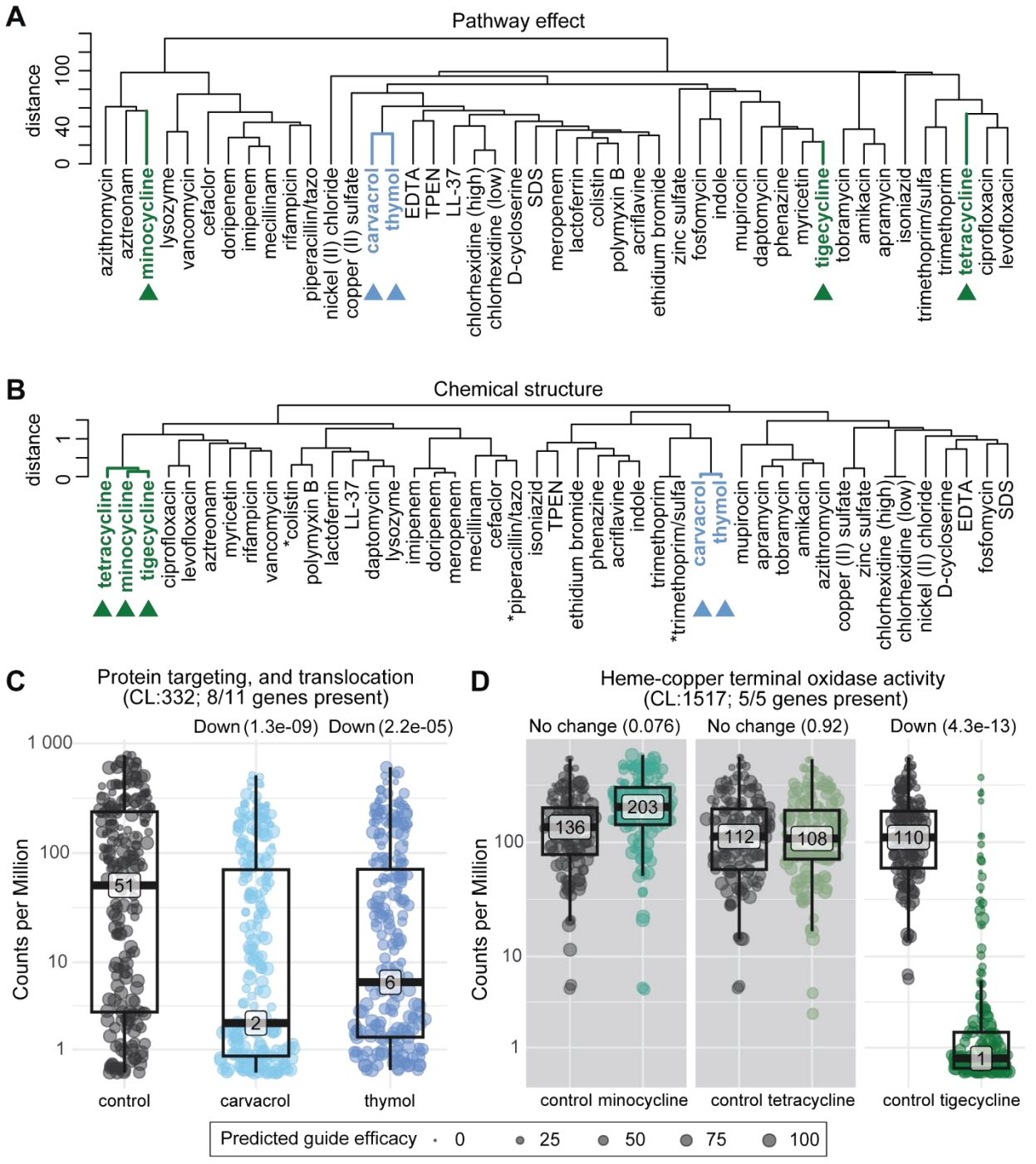
A
Pathway effect
distance
0
40
100
azithromycin
aztreonam
minocycline
lysozyme
vancomycin
cefaclor
doripenem
imipenem
mecillinam
rifampicin
piperacillin/tazo
nickel (II) chloride
copper (II) sulfate
carvacrol
thymol
EDTA
TPEN
LL-37
chlorhexidine (high)
chlorhexidine (low)
D-cycloserine
SDS
meropenem
lactoferrin
colistin
polymyxin B
acriflavine
ethidium bromide
zinc sulfate
fosfomycin
indole
mupirocin
daptomycin
phenazine
myricetin
tigecycline
tobramycin
amikacin
apramycin
isoniazid
trimethoprim/sulfa
trimethoprim
tetracycline
ciprofloxacin
levofloxacin
B
Chemical structure
distance
0
1
tetracycline
minocycline
tigecycline
ciprofloxacin
levofloxacin
aztreonam
myricetin
rifampicin
vancomycin
*colistin
polymyxin B
lactoferrin
LL-37
daptomycin
lysozyme
imipenem
doripenem
meropenem
mecillinam
cefaclor
*piperacillin/tazo
isoniazid
TPEN
ethidium bromide
phenazine
acriflavine
indole
trimethoprim
*trimethoprim/sulfa
carvacrol
thymol
mupirocin
apramycin
tobramycin
amikacin
azithromycin
copper (II) sulfate
zinc sulfate
chlorhexidine (high)
chlorhexidine (low)
nickel (II) chloride
D-cycloserine
EDTA
fosfomycin
SDS
C
Protein targeting, and translocation
(CL:332; 8/11 genes present)
Down (1.3e-09)
Down (2.2e-05)
Counts per Million
1 000
100
10
1
51
2
6
control
carvacrol
thymol
D
Heme-copper terminal oxidase activity
(CL:1517; 5/5 genes present)
No change (0.076)
No change (0.92)
Down (4.3e-13)
Counts per Million
100
10
1
136
203
112
108
110
1
control
minocycline
control
tetracycline
control
tigecycline
Predicted guide efficacy
0
25
50
75
100

One example from this dataset is carvacrol and thymol, which cluster tightly by both pathway effect and structure (Fig 3.S8). These compounds show antibacterial activity but do not have a defined mechanism of action. Our pathway analysis revealed protein transport (*ftsY, ffh,* and *sec* genes) and NADH dehydrogenase (*nuo* genes) knockdowns were significantly sensitized while ubiquinone (*ubi* genes) knockdowns were more resistant (Fig 3.5C, 3.S9). These pathways are affected by and contribute to membrane homeostasis and proton motive force (PMF), supporting previous studies stating that membrane disruption and depolarization underlie carvacrol and thymol antibacterial activity (53). However, the pathway-level effects of these two chemicals are related but distinct from other compounds that permeabilize and depolarize membranes like chlorhexidine and EDTA (54, 55) (Fig 3.5A). This suggests aspects of mechanisms of action for phenolic monoterpenes are unique from other membrane disruptors, perhaps due to effects on SRP-mediated protein transport or electron transport.

Structurally similar chemicals with varying pathway effects could reveal key alterations or R group modifications that alter impact on *A. baumannii* physiology. To investigate this, we scored how well chemical pairs clustered in pathway effect or in structure and mapped the differences (Fig 3.S10). Interestingly, the pathway effects of tetracycline, minocycline, and tigecycline diverged despite their strong structural similarity. Surprisingly, knockdowns associated with the known target, the ribosome, did not yield significant differences in tetracyclines (Fig 3.S11A). This is likely due to the lack of significant CG scores across ribosome genes in minocycline or tetracycline—potentially due to efflux mechanisms or other resistance factors impacting efficacy—and high variability in significant CG scores across ribosome genes for tigecycline, suggesting variability between ribosomal components (Fig 3.S11C). Indeed, knockdowns in the LOS transport pathway, Lpt, were generally sensitized to these antibiotics although the extent and confidence of the pathway effect varied (Fig 3.S12A). Additionally, pathways contributing to membrane potential and oxidative

phosphorylation, emerged as the most significant pathway-level divergences between these drugs in *A. baumannii*. ATP synthase knockdowns exhibited increased growth in tigecycline and tetracycline, but not to minocycline (Fig 3.S12B). RND efflux pumps in *A. baumannii* are often able to efflux tigecycline and tetracycline but not minocycline (56). However, a link between decreased RND-mediated efflux and ATP synthase knockdowns remains unclear, and other mechanisms may be affecting minocycline activity. Unlike other tetracyclines, tigecycline contains a unique structural modification making it a glycylcycline (57). This structural change may explain tigecycline's CG score variation for ribosomal genes and its unique effectiveness against heme-copper terminal oxidase (cytochrome bo_3 oxidase) knockdowns despite the shared core structure with minocycline or tetracycline (Fig 3.5D). Moreover, tigecycline clusters based on pathway effect with the structurally dissimilar chemicals phenazine and myricetin. While the exact mechanisms of action of phenazine and myricetin are unclear, both are known to affect oxidative phosphorylation and oxidative stress (58–61), suggesting tigecycline may similarly affect oxidative phosphorylation in *A. baumannii*.

We note that chemicals may display reduced pathway impacts in this analysis due to ineffective or noncomparable concentrations used and result in apparent divergence from their structural groups, as seen with meropenem (vs other carbapenems) in this screen (Fig 3.S13). Overall, however, we established a systematic method to group and compare chemicals by genetic interactions and structure, successfully highlighting effects of an understudied chemical group and uncovering unique effects of tetracycline-class antibiotics on *A. baumannii*.

Discussion

Essential cellular process are likely targets of future mono- and poly-therapies against antibiotic resistant pathogens. Despite the biological and clinical importance of essential genes, few studies

have comprehensively characterized their functions, especially in Gram-negative pathogens. This work advances our understanding of gene and antibiotic function in *A. baumannii* through large-scale, chemical genomic profiling of an essential gene knockdown library. The breadth and diversity of our chemical perturbations provided functional insights that could not be obtained with a smaller scope. We identified >5000 significant phenotypes for essential genes (Fig 3.1) and found that specific pathways, such as lipooligosaccharide transport, were highly enriched for sensitive phenotypes (Fig 3.2), representing potential compelling targets for combination therapies. Our evolutionary analysis revealed inhibitor-responsive essential genes that are unique to or highly divergent in *A. baumannii* (Fig 3.3), providing possible targets for narrow-spectrum therapeutics. Our essential gene network displayed robust connections between known and poorly characterized essential genes (Fig 3.4), hinting at new functions and corroborating prior work. Finally, our structure-function analysis of chemical-gene phenotypes uncovered surprising discordance in the physiological impacts of antibiotics with similar structures and targets (Fig 3.5), highlighting how genes outside of the direct target impact antibiotic efficacy. Moreover, this study provides a rich dataset of essential gene phenotypes to the *A. baumannii* and larger Gram-negative pathogen research communities, serving a resource and framework for further exploring essential gene function.

Our findings regarding the Lpt system's critical role in antibiotic resistance accentuate the potential of targeting LOS trafficking, especially in the context of recent pharmaceutical advances. Our observation that knockdown strains show a hyper-permeable phenotype that is dependent on LOS production suggests that increased permeability is caused by retention of fully synthesized LOS in the inner membrane, although additional work is needed to show this definitively. Other studies have suggested that inhibiting lipopolysaccharide transport results in toxic accumulation of LOS intermediates that cause membrane defects and antibiotic susceptibility (62–64). We note that

these hypotheses are not mutually exclusive. Moreover, the increased permeability of *lpt* knockdowns is consistent with classic *E. coli* mutations in *lptD* (imp4213 (65)) that are broadly permeable (66) and are often used in drug screening efforts (67). Recent studies have characterized novel Lpt-targeting macrocyclic peptides that selectively disrupt LOS transport in *Acinetobacter* species (68, 69). Interestingly, our conservation analyses revealed that *lptC* is far more divergent among *Gammaproteobacteria* than the other proteins involved in this complex, which may play a role in why these Lpt-targeting macrocyclic peptides are inactive against other Gram-negative organisms. Taken together, these data highlight the potential for recently described Lpt inhibitors to be effective in conjunction with other antibiotics as a combination therapeutic strategy for *A. baumannii*.

Our work also raises intriguing questions regarding the functions of poorly characterized essential genes in *A. baumannii*. Our gene network analysis revealed functional associations between established and poorly understood genes, generating hypotheses about gene function that can be addressed in future mechanistic studies. For example, GO593_10640 shows strong phenotypic similarity with components of the SRP. Whether GO593_10640 is a component required for activity of the SRP or a key substrate involved in antibiotic resistance is unknown. GO593_10640 contains a predicted signal sequence, and, thus, is a potential substrate of SRP itself. In general, the SRP is poorly characterized in *A. baumannii*, although relatively recent work is beginning to decipher its functions (70). Combining structural predictions with gene phenotyping uncovered GO593_00140 has a possible *holD* analog in *A. baumannii*. Although GO593_00140 is highly divergent from *E. coli* HolD at the primary sequence level, GO593_00140 contains similar predicted folds to HolD and responds to similar chemicals as other knockdowns of DNA polymerase III subunits. Advances in protein structural modeling have caused a paradigm shift in contemporary biology (71); synthesizing structural predictions with systematic phenotyping will likely continue to pay

dividends in elucidating gene functions. Notably, our work corroborates previous in silico findings suggesting that GO593_00140 has a HolD-like function (41). Although *A. baumannii* has a distinct SOS response that does not rely on LexA, we found a possible LexA analog inside what appears to be a prophage (GO593_11615) with phenotypes consistent with a disruption of DNA polymerase function or DNA damage. These findings suggest that mobile genetic elements may serve as a resource to better understand DNA damage responses and to identify proteins particularly toxic to *A. baumannii*. Finally, our ortholog and phenotype analyses suggest that *A. baumannii* contains many unique or divergent genes associated with cell division. Synthesizing our work with prior observations in the field (3, 45) raises the possibility that *A. baumannii* may contain a unique divisome with AdvA and BlhA appearing to localize primarily to the division septum and additional genes participating either directly or indirectly in the division process (*spor* and *smc2*). The precise functions and order of assembly into the divisome (72) of these proteins has yet to be elucidated.

Our structure-function studies combining cheminformatics, bioinformatics, and experimentally determined gene phenotype data revealed important insights into the function of known and poorly characterized inhibitors. Our results with carvacrol and thymol, two inhibitors of unknown mechanism, suggest that growth inhibition occurs through either disruption of membrane and PMF (53), or disruption of specific membrane complexes. Disruption of protein secretion, including specific targeting of the SRP, are also possible interpretations of our data. We further show how drugs within the same antibiotic class, tetracyclines, can have divergent effects on *A. baumannii*. In particular, minocycline showed no change in efficacy for ATP synthase knockdowns, while tigecycline exhibited a unique and substantial increase in efficacy for cytochrome bo_3 oxidase knockdowns. Despite tigecycline being a newer antibiotic, it is often less effective against *A. baumannii* than minocycline due to efflux (56), which may explain why knockdowns of ATP synthase, which contributes to PMF and efflux (73), would not affect fitness in minocycline.

Previous work suggests that tigecycline is more prone to inactivation by dissolved oxygen in media than other tetracyclines (74) and is known to have anti-cancer activities due to induction of mitochondrial oxidative stress (75). Cytochrome bo_3 oxidase, as the main terminal oxidase in *A. baumannii*, has an important role in reducing oxygen that could impact tigecycline stability. It is important to note that these genes are essential in *A. baumannii* because of its obligate aerobic lifestyle, and knockdowns of ATP synthase or cytochrome bo_3 oxidase may be causing complex compensation or stress responses that affect observed phenotypes. This approach identified differing genetic impacts that explain the observed efficacy differences of tetracycline-class antibiotics with minor structural changes. This underscores the utility of this method in larger chemical or small-molecule screens to elucidate mechanistic differences between compounds.

Overall, this study enhances our understanding of essential genes and processes in *A. baumannii*, establishing a useful resource and highlighting unique aspects of the organism's biology. A limitation of our approach is dependence on CRISPRi, which is polar and can have off-target effects, although our experimental design and statistics mitigate some of the risks of toxic or otherwise off-target guides. Additionally, much of our computational analysis relies on similarity to known proteins and functional predictions, particularly from the STRING database (24). *A. baumannii* ATCC 19606 has a poorly characterized proteome compared to model bacteria; despite this, our approach still successfully identified expected gene connections, likely due to the high level of conservation seen in essential gene sequences and functions. Future approaches could integrate custom annotations and network analyses from this dataset and others to enhance the breadth and coverage of predicted genetic pathways. Beyond this dataset, the approaches used here provide an important framework to understanding compound effects on bacterial genetic pathways. While this screen focuses on essential genes and utilized a curated set of chemicals known to cause growth defects in *A. baumannii*, these systems biology and chemical

characterization approaches can be further applied to full knockdown libraries or small-molecule screens in other pathogens.

Materials and methods

Bacterial strains and growth

Strains (listed in Table 3.1) were grown in EZ Rich Defined Media (Teknova) with 40 mM sodium succinate (AbRDM) or AbRDM + 1.5% agar at 37°C, unless otherwise noted. Selective antibiotics used when required: 100 µg/mL ampicillin (amp) or carbenicillin (carb), 15 µg/mL gentamicin (gent), or 30 µg/mL kanamycin (kan) for *E. coli*; 10 µg/mL polymyxin B (pmb), 150 µg/mL gent, 60 µg/mL kan for *A. baumannii*. Diaminopimelic acid (DAP) was added at 300 µM to support growth of *E. coli* dap- donor strains. IPTG (isopropyl b-D-1-thiogalactopyranoside) (0 to 1 mM) was added as indicated.

General molecular biology techniques and plasmid construction

Plasmids, oligos, and construction details are listed in Tables 3.2 and 3.3. Oligonucleotides were synthesized by Integrated DNA Technologies (Coralville, IA). Plasmid DNA was purified using the GeneJet plasmid miniprep kit (K0503; Thermo Scientific). Genomic DNA (gDNA) purification used the GeneJet gDNA purification kit (K0721; Thermo Scientific). DNA fragments were amplified with Q5 DNA polymerase (M0491; New England Biolabs (NEB)) or OneTaq DNA Polymerase (NEB). All restriction enzymes were from NEB. DNA fragments were spin-purified using DNA Clean & Concentrator kit (D4004; Zymo Research) after digestion or amplification. Ligations used T4 DNA ligase (M0202; NEB). Plasmids were assembled from linearized vector and PCR products or synthetic DNA fragments using the NEBuilder Hifi DNA assembly kit (E2621; NEB). Plasmids were transformed into electrocompetent *E. coli* cells using a Bio-Rad Gene Pulser Xcell on the EC1 setting. Sanger DNA sequencing was performed by Functional Biosciences (Madison, WI); full plasmid sequencing was performed by Plasmidsaurus.

Library growth experiment

The *A. baumannii* essential gene CRISPRi library (sJMP2949) was diluted 1000-fold from frozen stock in 50 mL AbRDM (starting OD600= 0.015) and incubated in 250 mL flasks at 37°C with shaking until mid-log (OD600=0.2; ~3.5 hrs) (t0). This culture was then diluted to OD600=0.02 in 4 mL media with 1mM IPTG and antibiotics (see Table S4) in 14 mL snapcap culture tubes (Falcon 352051) and incubated with shaking at 37°C. At 18 hours, saturated cultures were serially diluted to OD600=0.02 into fresh media and incubated for another 18 hours at 37°C with shaking, for a total of ~14 doublings. Cells were pelleted from 1 mL culture in duplicate before and after growth.

Sample preparation and sequencing

As previously described (20), sample gDNA was extracted, and the sgRNA-encoding region was amplified using Q5 DNA polymerase (NEB) in a 100 µL reaction with ~100 ng gDNA and primers oJMP697 and oJMP698, using a BioRad C1000 thermocycler: 30s at 98°C;16 cycles of 15s at 98°C, 15s at 65°C, 15s at 72°C; 72°C for 5 min. PCR products were spin-purified, and samples sequenced by the UW-Madison Biotech Center Next Gen Sequencing Core. PCR products were amplified with nested primers containing i5 and i7 indexes and Illumina TruSeq adapters, cleaned, quantified, pooled, and run on a Novaseq 6000 (150 bp paired-end reads).

Sequencing read quality control and processing

Guides were counted using a custom Python script that samples sequencing reads to identify and correct for barcode diversity, read orientations, offsets, and flanking sequences, ensuring accurate identification of overlapping guide sequences and both listed and unlisted guides. Only counts for library barcodes were used in downstream analyses.

Coefficients of determination (R^2) between samples were calculated from guide CPMs. Conditions with $R^2 < 0.5$ were removed to ensure replicate agreement. Samples with population diversity (Nb)

less than 10,000 for nontargeting control guides were also excluded. Log_2 fold changes and confidence values were computed using edgeR. Gene-level values (CG scores) were calculated by taking the median guide-level log_2 fold change for perfect match guides; confidence was calculated by using Stouffer's p-value using guide-level FDR values (poolr R package). Functional enrichment analyses were performed with STRING-db (v.11.5) with custom 19606 proteome (Organism ID: STRG0060QIE). Transcriptional unit predictions were obtained from BioCyc (76).

Creation of knockdown strains

As previously described (20, 77), sgRNA-encoding sequences were cloned between the BsaI restriction sites of the MCi plasmid pJMP2776. Two oligonucleotides encoding an sgRNA were designed to overlap, allowing their ends to be complementary to the BsaI-cut ends on the vector. The Mobile-CRISPRi system was then transferred to the attTn*7* site on the chromosome of *A. baumannii* via quad-parental conjugation. This involved three donor strains, containing either pTn*7*C1, pEVS104, or the plasmid containing the Tn*7* transposon encoding the CRISPRi system, and the *A. baumannii* recipient strain. 100 µL cultures of donor and recipient strains were mixed with 600 µL LB, pelleted at ~8,000 × g, washed twice with LB, deposited on a nitrocellulose filter (Millipore HAWP02500) on an LB plate, and incubated at 37°C for ~4 h. Cells were then removed from the filter by vortexing in 500 µL PBS and grown on selective plates at 37°C.

MIC test strip assays

500 µL of culture (OD=0.1, or 0.5 for LOS- strains) was spread on Mueller-Hinton agar plates and allowed to dry for 30 minutes. A sterile MIC test strip was added to the plate and incubated overnight at 37°C. The MIC was determined as the value where the zone of inhibition meets the strip.

Spot assays

Strains were grown on LB agar overnight. Cell scrapes were resuspended from plates into 500 µL PBS and normalized to an OD_{600} of ~1.0. 10 µL of ten-fold dilutions of these resuspensions were then spotted on AbRDM and AbRDM +1mM IPTG agar plates.

Membrane permeability assay

ATCC 19606 and LOS- strains containing sgRNAs targeting *lptA* or a non-targeting control (sJMP4539 and 4324, respectively) were grown on LB agar or LB agar containing 1mM IPTG overnight. Cell scrapes were resuspended from plates into 500 µL PBS and normalized to an OD600 of 0.3. Ethidium bromide (EtBr; Bio-Rad #1610433) was added to cell suspensions at a final concentration of 10 ug/mL, and OD600 and fluorescence at 545nm excitation/600 emission were read in a plate reader (Tecan Infinite 200 Pro M Plex). Readings occurred over 100 cycles (~75 min).

Ortholog analyses

Genome assemblies of *Gammaproteobacteria* were collected from the NCBI Reference Sequence database (RefSeq release 213). The dataset comprises 2792 isolates distributed among 474 genera and 18 taxonomic orders.

Essential genes represented in the library were pulled from the genome assembly for *A. baumannii* ATCC 19606 (GCA_009759685.1). Orthology assignment was computed with the phylogenetic profiling tool fDOG v.0.1.26 (30), compiling a maximum of 25 core-orthologs for each gene using a taxonomic distance minimum of genus and maximum of class.

Evolutionary conservation was measured for each gene on a taxonomic group, considering the number of isolates with at least one ortholog divided by the number of analyzed isolates. We analyzed the evolutionary conservation at the genus level with non-ACB (*Acinetobacter*

calcoaceticus-baumannii complex) isolates, at the order level with non-*Acinetobacter Moraxellales*, and at the class level with non-*Moraxellales Gammaproteobacteria*.

Network generation

Pairwise correlations of CG scores were calculated, resulting in ~165k gene-gene correlations. As previously described (7), a cutoff (85% confidence interval, r>0.758) was determined through estimating background distribution of correlations through 5000 random permutations of gene identities relative to CG scores. The resulting 630 connections were visualized using Cytoscape v3.10.2 (Cytoscape Consortium).

Chemical comparison analyses

After importing, organizing, filtering, and normalizing counts using edgeR, gene set testing was performed with the limma package and voom method, utilizing functional groups predicted by STRING-db (Organism ID: STRG0060QIE). Chemical effects on pathways were scored for direction and significance, then transformed into a correlation matrix. Chemicals were hierarchically clustered (Ward method) based on pathway effect and visualized as a dendrogram. SMILES strings for each chemical were parsed using the rcdk package to generate molecular fingerprints (ECFP6). For combination or mixed-structure antibiotics, a representative structure was selected (e.g., trimethoprim for trimethoprim-sulfamethoxazole). A Tanimoto similarity matrix was generated, converted to a distance matrix, and clustered using the Ward method to create a chemical structure dendrogram.

Dendrograms were iteratively cut at all k-values (1-45), scoring chemical pairs (+1) if clustered together. Final association scores were calculated as fractions of the maximum possible score, ranging from 0 to 1. Differences in association scores between pathway-effect and structure were

plotted to highlight disparities, and sums of association scores were plotted to highlight similarities.

Protein structural prediction

Structures of GO593_10640 and GO593_00140 (with chi subunit ortholog) were predicted from amino acid sequence using Alphafold2 (71, 78) and AlphaFold-Multimer (79). Predicted structures were visualized using PyMOL (Schrödinger).

Cell division protein localization and microscopy

Expression vector plasmids were transferred by conjugation into *A. baumannii* ATCC 17978; briefly, 100 µL of culture of donor and recipient strains were mixed and deposited on a nitrocellulose filter (Millipore HAWP02500) on an LB plate, and incubated at 37°C, ~2 h. Cells were removed from the filter by vortexing in 500 µL PBS and grown on selective plates at 37°C.

Cultures were grown from a starting OD600~0.01 to mid-log at 37°C for ~3 hours in AbRDM + 1mM IPTG (or 500 µM IPTG for Smc2 and Smc2::sfGFP overexpression strains, due to toxicity). 1 mL of culture was centrifuged (8000xg for 2 min) and resuspended in equal volume PBS. Cells were fixed with paraformaldehyde (final concentration 5%) and quenched with equal volume 2.5M glycine. 10 µL of each sample were spotted on a glass slide for microscopy. Bacteria were imaged with a Nikon Ti-E inverted microscope with an Orca Fusion BT digital CMOS camera (Hamamatsu) using NIS-Elements. Fluorescence images were collected using Prior Lumen 200 metal halide light source and a FITC-specific filter set. Cell length analysis was done with MicrobeJ (80).

Table 3.1. Strains used in this study.

Strain name	Description[1]	Source
sJMP4001	*Acinetobacter baumannii* ATCC19606 WT	ATCC
sJMP4002	*Acinetobacter baumannii* ATCC17978 WT	ATCC
sJMP2949	*A. baumannii* 19606 (sJMP4001) with MCi pooled library inserted into the Tn*7 att* site, gmR (*A. baumannii* essential gene Mobile-CRISPRi pooled library)	Ward et al. (20)
sJMP3049	E*scherichia coli* (derived from WM6026, sJMP3043) lacIq, rrnB3, DElacZ4787, hsdR514, DE(araBAD)567, DE(rhaBAD)568, rph-1 att-lambda::pAE12-del (oriR6K/cat::frt5), del 4229(dapA)::FRT (DAP-), del(endA)::FRT, uidA(DMluI)::pir(wt), attHK::pJK1006::del1/2(del oriR6K-cat::FRT5, del trfA::FRT), FRT inserted between mltB and srlA, recA1, attTn7::acrIIA4 (cms) (pir+, recAI mating strain with anti-CRISPR)	Ward et al. (20)
sJMP3053	*Escherichia coli* (derived from BW25141, sJMP3034) Δ(araD-araB)567, ΔlacZ4787(::rrnB-3), Δ(phoB-phoR)580, l-, galU95, ΔuidA3::pir+, recA1, endA9(del-ins)::FRT, rph-1, Δ(rhaD-rhaB)568, hsdR514, attTn7::acrIIA4 (pir+, recAI cloning strain with anti-CRISPR)	Ward et al. (20)
sJMP4061	*E. coli* mating strain sJMP3049 with pEVS104 (helper strain; sJMP2935); kanR, dap-	Ward et al. (20)
sJMP4062	*E. coli* mating strain sJMP3049 with pJMP1039 (Tn7 transposase expression strain; sJMP2644); ampR, dap-	Ward et al. (20)
sJMP4324	*A. baumannii* 19606 (sJMP4001) with MCi system inserted into the Tn7 *att* site, gmR (non-targeting control sgRNA)	Ward et al. (20)
sJMP4395	*A. baumannii* 19606 (sJMP4001) with Mci system from pJMP4379 inserted into the Tn*7 att* site, gmR (*smc2* sgRNA)	this study
sJMP4408	*A. baumannii* 19606 (sJMP4001) with Mci system from pJMP4396 inserted into the Tn*7 att* site, gmR (*blhA* sgRNA)	this study
sJMP4414	*A. baumannii* 19606 (sJMP4001) with Mci system from pJMP4248 inserted into the Tn*7 att* site, gmR (*ftsZ* sgRNA)	this study
sJMP4431	*A. baumannii* 19606 (sJMP4001) with Mci system from pJMP4415 inserted into the Tn*7 att* site, gmR (GO593_07290 sgRNA)	this study
sJMP4501	sJMP3719; *A. baumannii* 17978 (sJMP4002) with empty vector expression plasmid; kanR	Bacon et al. (81)
sJMP4507	sJMP3720; *A. baumannii* 17978 (sJMP4002) with sfGFP expression plasmid; kanR	Bacon et al. (81)
sJMP4498	*A. baumannii* 17978 (sJMP4002) with smc2::sfGFP expression plasmid; kanR	this study

sJMP4500	*A. baumannii* 17978 (sJMP4002) with sfGFP::GO593_07290 expression plasmid; kanR	this study
sJMP4519	*A. baumannii* 17978 (sJMP4002) with sfGFP::blhA expression plasmid; kanR	this study
sJMP4520	*A. baumannii* 17978 (sJMP4002) with smc2 expression plasmid; kanR	this study
sJMP4521	*A. baumannii* 19606 (sJMP4001) with Mci system inserted into the Tn*7 att* site, gmR (*lptA* sgRNA)	this study
sJMP4532	*A. baumannii* ATCC19606 *lpxC*(S106R)	Powers and Trent (27)
sJMP4539	*A. baumannii* 19606 *lpxC*(S106R) (sJMP4532) with Mci system inserted into the Tn*7 att* site, gmR (*lptA* sgRNA)	this study
sJMP4543	*A. baumannii* 19606 *lpxC*(S106R) (sJMP4532) with Mci system inserted into the Tn*7 att* site, gmR (nontargeting sgRNA)	this study
sJMP10076	*A. baumannii* 19606 (sJMP4001) with MCi system inserted into the Tn7 *att* site, gmR (*lpxC* sgRNA)	Ward et al. (20)

[1]gmR = gentamicin-resistant; kanR = kanamycin-resistant; ampR = ampicillin-resistant; dap- = requires diaminopimelic acid; pmbR = polymyxin B-resistant; vanS = vancomycin-sensitive; MCi = Mobile-CRISPRi

Table 3.2. Plasmids used in this study.

Plasmid	Description[1]	Construction/Notes[2]	Source
pJMP2776	MCi plasmid for *A. baumannii* for cloning new guides	BsaI sites to insert guides; ampR (backbone), gmR (transposon)	Ward et al. (20); Addgene: 208890
pJMP4189	MCi plasmid for *A. baumannii*; nontargeting guide	pJMP2776 digested with BsaI and ligated with oJMP834/835; ampR (backbone), gmR (transposon)	Ward et al. (20)
pJMP2768	MCi test plasmid. GFP targeting spacer, GFP expression.	Used to PCR *sfgfp* fragment; ampR (backbone), gmR (transposon)	Ward et al. (20); Addgene: 208889
pEVS104	R6K ori helper plasmid for conjugation into *A. baumannii*	kanR	Stabb et al. (80)
pJMP4480	pJMP3654; *A. baumannii* sfGFP vector	multiple cloning site downstream of strong promoter (PabstBR) and RBS; kanR	Bacon et al. (81); Addgene: 222349
pJMP4481	pJMP3653; *A. baumannii* replicative vector for overexpression; empty vector	multiple cloning site downstream of strong promoter (PabstBR) and RBS; kanR	Bacon et al. (81); Addgene: 222348
pJMP3407	*A. baumannii* replicative vector for expression; weak promoter, empty vector	multiple cloning site downstream of weak promoter (Pabst) and RBS - expression too low for microscopy; kanR	Bacon et al. (81)
pJMP4253	MCi plasmid for *A. baumannii*; *lptA* guide	pJMP2776 digested with BsaI and ligated with oJMP767/787; ampR (backbone), gmR (transposon)	this study
pJMP4396	MCi plasmid for *A. baumannii*; *blhA* guide	pJMP2776 digested with BsaI and ligated with oJMP1883/1884; ampR (backbone), gmR (transposon)	this study
pJMP4379	MCi plasmid for *A. baumannii*; *smc2* guide	pJMP2776 digested with BsaI and ligated with oJMP1853/1854; ampR (backbone), gmR (transposon)	this study

pJMP4248	MCi plasmid for *A. baumannii*; *ftsZ* guide	pJMP2776 digested with BsaI and ligated with oJMP778/779; ampR (backbone), gmR (transposon)	this study
pJMP4415	MCi plasmid for *A. baumannii*; GO593_07290 guide	pJMP2776 digested with BsaI and ligated with oJMP1959/1960; ampR (backbone), gmR (transposon)	this study
pJMP4461	*A. baumannii* sfGFP::GO593_07290 vector; weak promoter	Hifi assemble GO593_07290 PCR amplified from A. baumannii 19606 gDNA with oJMP1991/1992, *sfgfp* amplified from p2768 with oJMP1989/1990, and pJMP3407 cut with NcoI and BamHI; kanR	this study
pJMP4479	*A. baumannii* sfGFP::GO593_07290 expression vector	Site-directed mutagenesis of pJMP4461 with oJMP2219 to convert to strong promoter for overexpression and microscopy (P_{abst} to P_{abstBR}); kanR	this study
pJMP4457	*A. baumannii* Smc2::sfGFP vector; weak promoter	Hifi assemble *smc2* PCR amplified from A. baumannii 19606 gDNA with oJMP1983/1984, *sfgfp* PCR amplified from pJMP2768 with oJMP1985/1986, and pJMP3407 cut with NcoI and BamHI; kanR	this study
pJMP4477	*A. baumannii* Smc2::sfGFP overexpression vector	Site-directed mutagenesis of pJMP4457 with oJMP2219 to convert to strong promoter for overexpression and microscopy (P_{abst} to P_{abstBR}); kanR	this study
pJMP4513	*A. baumannii* Smc2 vector	PCR *smc2* (GO593_11915) from A. baumannii 19606 gDNA with oJMP1983/2320; clone into pJMP4481 with NcoI and BamHI; kanR	this study
pJMP4511	*A. baumannii* sfGFP::BlhA vector	Hifi assemble *blhA* gblock (oJMP2321), *sfgfp* PCR amplified from pJMP4461 with oJMP2318/2319, and pJMP4481 cut with NcoI and BamHI; kanR	this study

[1]MCi = Mobile-CRISPRi

[2]gmR = gentamicin resistant; kanR = kanamycin resistant; ampR = ampicillin resistant

Table 3.3. Oligos used in this study.

Oligo	Sequence (5' to 3')	Description/Usage[1]
oJMP834	TAGTGGGTCATAACATACTTCGTC	nontargeting top; anneal oligos to clone guides into BsaI sites in Mci vector
oJMP835	AAACGACGAAGTATGTTATGACCC	nontargeting bottom; anneal oligos to clone guides into BsaI sites in Mci vector
oJMP786	TAGTTAATTACCGCAGCTTGTTTT	*lptA* top; anneal oligos to clone guides into BsaI sites in Mci vector
oJMP787	AAACAAAACAAGCTGCGGTAATTA	*lptA* bottom; anneal oligos to clone guides into BsaI sites in Mci vector
oJMP1883	TAGTCACAGTTGAATAGGGGTCTG	GO593_07665 - *blhA* top; anneal oligos to clone guides into BsaI sites in Mci vector
oJMP1884	AAACCAGACCCCTATTCAACTGTG	GO593_07665 - *blhA* bottom; anneal oligos to clone guides into BsaI sites in Mci vector
oMP1853	TAGTCTGAAAACGATTTTTTAAAT	GO593_11915 - *smc2* top; anneal oligos to clone guides into BsaI sites in Mci vector
oJMP1854	AAACATTTAAAAAATCGTTTTCAG	GO593_11915 - *smc2* bottom; anneal oligos to clone guides into BsaI sites in Mci vector
oJMP778	TAGTATCTTCTATAAATTCAAATG	*ftsZ* top; anneal oligos to clone guides into BsaI sites in Mci vector
oJMP779	AAACCATTTGAATTTATAGAAGAT	*ftsZ* bottom; anneal oligos to clone guides into BsaI sites in Mci vector
oJMP1959	TAGTACAAGTGTCCCTAACCATTT	GO593_07290 top; anneal oligos to clone guides into BsaI sites in Mci vector
oJMP1960	AAACAAATGGTTAGGGACACTTGT	GO593_07290 bottom; anneal oligos to clone guides into BsaI sites in Mci vector
oJMP2219	GTCGTAAAGACGTCTCATTAATCAGATAAAAT ATTGACAATGTGAGCGGATAACAAG	primer for site-directed mutagenesis of P_{abst} to P_{abstBR} (81); used to create pJMP4477 and pJMP4479
oJMP2321	TGGCATGGATGAGCTCTACAAAGGCTCAGG CTCAATGGTGGCATTAAATGTCGGGCAAGAT TTTAAAAAAAGATGGTTAAATGCGCCTGAAG CTGTCCGTCATGCTTATCAACAGGATTTGGC TCGTATTTGTGATTTATTAGAGCCTCAGACCC CTATTCAACTGTGGGTTTTAAATGACGAAAAA GCGCAATTAGAATCACAACAAAATATTGAAAA GGCATATGCTGACTTAAAGGCAGAGTTAATC	gblock containing *A. baumannii* ATCC19606 *blhA* and ends overlapping with sfGFP and pJMP4481 for pJMP4511 Hifi assembly

	GAGCAAGCGCGAATACGTCGCCAACTTGCT TTAGAAAAAGCTCTTGCAGATAAGCGCGCAA AGGAAGCAGCTTATGCTGCTGAATTACAAGC TGACGAAGTTCGTAAATTTAGTGAACAAACG GAAGCTTTGCAGGCTTTACGCAGTCATTTAG AACAAGAAGTTGCTGAACATACTGCACGTTA TCAAAAAAACCCTGAAACGCCAGCAATTGA CTATTCTTCTGGTACAAAACTTAGCATTACTGA CGATCAAATCTTATCTGAGCTTGAAAGTGTAC GCGTTCGCCTAGAACTTGAAGCTGAAAGCTT AATTGAACAGGCGGTAACAGTTTTCCGTGCC AAACTGCATGCTGCGGCTCAAGAAGAAATT GAATATATTTTAAAGAATTCTAACTTTTCTGATG AAAAAATAGAAAAGTAATAAGGATCCTCTAGA GTCGACCTGCAGGCATGCAAGCTT	
oJMP1991	GCAACGCGGTGTATCTGAAA	PCR GO593_07290 gene from *A. baumannii* ATCC19606 genomic DNA for pJMP4461 Hifi assembly; primer 1
oJMP1992	CAGGTCGACTCTAGAGGATCCTTATTATCTG CGTTTAATCACAATAGAGTCA	PCR GO593_07290 gene from *A. baumannii* ATCC19606 genomic DNA for pJMP4461 Hifi assembly; primer 2
oJMP1983	GCAGCACACAGGAAACAGACCATGTTAGAA CAATTACAGCGTCTACA	PCR *smc2* gene from *A. baumannii* ATCC19606 genomic DNA for pJMP4513 or pJMP4457 construction; primer 1
oJMP2320	CTTGCATGCCTGCAGGTCGACTCTAGAGGA TCCTTACACTCATGATTGTGTCTCCTC	PCR *smc2* gene from *A. baumannii* ATCC19606 genomic DNA for pJMP4513 construction; primer 2
oJMP1984	GATTGTGTCTCCTCACCAGC	PCR *smc2* gene from *A. baumannii* ATCC19606 genomic DNA for pJMP4457 construction; primer 2
oJMP1985	GCTGGTGAGGAGACACAATCAGGCTCAGG CTCAATGAGCAAAGGAGAAGAACTTTTCA	PCR *sfgfp* from pJMP2768 for pJMP4457 Hifi assembly; primer 1
oJMP1986	CCTGCAGGTCGACTCTAGAGGATCCTTATTA TTTGTAGAGCTCATCCATGCC	PCR *sfgfp* from pJMP2768 for pJMP4457 Hifi assembly; primer 2
oJMP2319	GCACATCAGCAGCACACAG	PCR *sfgfp* from pJMP4461 for pJMP4511 Hifi assembly; primer 1
oJMP2318	GCCTGAGCCTTTGTAGAGC	PCR *sfgfp* from pJMP4461 for pJMP4511 Hifi assembly; primer 2
oJMP1989	CAGCACACAGGAAACAGACCATGAGCAAA GGAGAAGAACTTTTCA	PCR *sfgfp* from pJMP2768 for pJMP4461 Hifi assembly; primer 1

oJMP1990	TTTCAGATACACCGCGTTGCGTTTTGCCAAA CACTGAGCCTGAGCCTTTGTAGAGCTCATCC ATGCC	PCR *sfgfp* from pJMP2768 for pJMP4461 Hifi assembly; primer 2

[1]MCi = Mobile-CRISPRi

Table 3.4. Final concentrations and abbreviations for chemicals used in this screen.

Chemical	Abbreviation[1]	Solvent[2]	Final concentration	Notes[3]
acriflavine	ACR	DMSO	2 µg/mL	
amikacin	AMK	water	1.75 µg/mL	
apramycin	APR	water	7 µg/mL	
azithromycin	AZI	DMSO	0.2 µg/mL	
aztreonam	AZT	water	1 µg/mL	
carvacrol	CRV	DMSO	40 µg/mL	
cefaclor	CEF	water	72 µg/mL	
chlorhexidine (high)	CHX (high)	DMSO	5 µg/mL	
chlorhexidine (low)	CHX (low)	DMSO	6 µg/mL	
ciprofloxacin	CIP	DMSO	5 µg/mL	
colistin	COL	water	0.5 µg/mL	Colistin is a mix of polymyxin E molecules. PubChem CID: 24825758 SMILES used
copper(II) sulfate	CuS	water	100 µg/mL	
daptomycin	DAP	water	100 µg/mL	
D-cycloserine	DCS	water	60 µg/mL	
doripenem	DRP	water	0.05 µg/mL	
EDTA	EDTA	water	0.125 mM	
ethidium bromide	EtBr	water	10 µg/mL	
fosfomycin	FOS	water	32 µg/mL	
imipenem	IMP	DMSO	.05 µg/mL	
indole	IND	DMSO	200 µg/mL	
isoniazid	ISO	water	100 µg/mL	
lactoferrin	LCF	water	100 µg/mL	SMILES for active portion of lactoferrin used
levofloxacin	LVF	DMSO	.125 µg/mL	
LL-37	LL37	water	4 µg/mL	
lysozyme	LYS	water + 0.02M sodium acetate-acetic acid buffer (pH=4.6)	50 µg/mL	
mecillinam	MEC	DMSO	25 µg/mL	
meropenem	MRP	DMSO	0.15 µg/mL	
minocycline	MIN	water	0.005 µg/mL	

mupirocin	MUP	DMSO	250 µg/mL	
myricetin	MYR	DMSO	15 µg/mL	
nickel(II) chloride	NiCl	water	400 µg/mL	
phenazine	PHZ	water	5 µg/mL	
polymyxin B	PMB	water	0.5 µg/mL	Polymyxin B1; Aerosporin
rifampicin	RIF	DMSO	1.2 µg/mL	
SDS	SDS	water	50 µg/mL	
piperacillin/tazobactam	PIP-TZ; piperacillin/ tazo	DMSO	4 µg/mL; 0.5 µg/mL	used SMILES for piperacillin (sodium salt)
tetracycline	TET	water	0.5 µg/mL	
thymol	THY	DMSO	30 µg/mL	
tigecycline	TIG	DMSO	.03125 µg/mL	
tobramycin	TOB	water	0.4 µg/mL	
TPEN	TPEN	DMSO	1 µg/mL	
trimethoprim	TMP	DMSO	2 µg/mL	
trimethoprim/ sulfamethoxazole	TMP-SMX; trimethoprim/ sulfa	DMSO	5 µg/mL; 25 µg/mL	used SMILES for trimethoprim
vancomycin	VAN	water	5 µg/mL	
zinc sulfate	ZnSO4	water	250 µg/mL	
DMSO (control)	DMSO	DMSO	1% final	

[1]Shorthand used throughout in figures.

[2]Solvent used for resuspension of stock chemical solutions and dilution of working stocks, ~1% final of sample media.

[3]additional information about chemicals; SMILES = simplified molecular-input line-entry system, used for chemical structure analyses

Figure 3.S1. Replicate agreement and sample diversity as quality metrics. (A) Correlation of library spacer counts per million (CPM) across the two biological replicates for samples containing polymyxin B at concentrations of 0.5 ug/mL (left) or 1 ug/mL (right). Count density represented by contour map; right graph shows over-depletion of guides. (B) Population diversity (N_b) for polymyxin B replicates. Samples with nontargeting guide complexity below the cutoff (dotted line) were excluded from analyses. (C) Heatmap showing correlations of spacer CPMs between solvent controls. All solvent control samples show r≥0.97.

Figure 3.S1

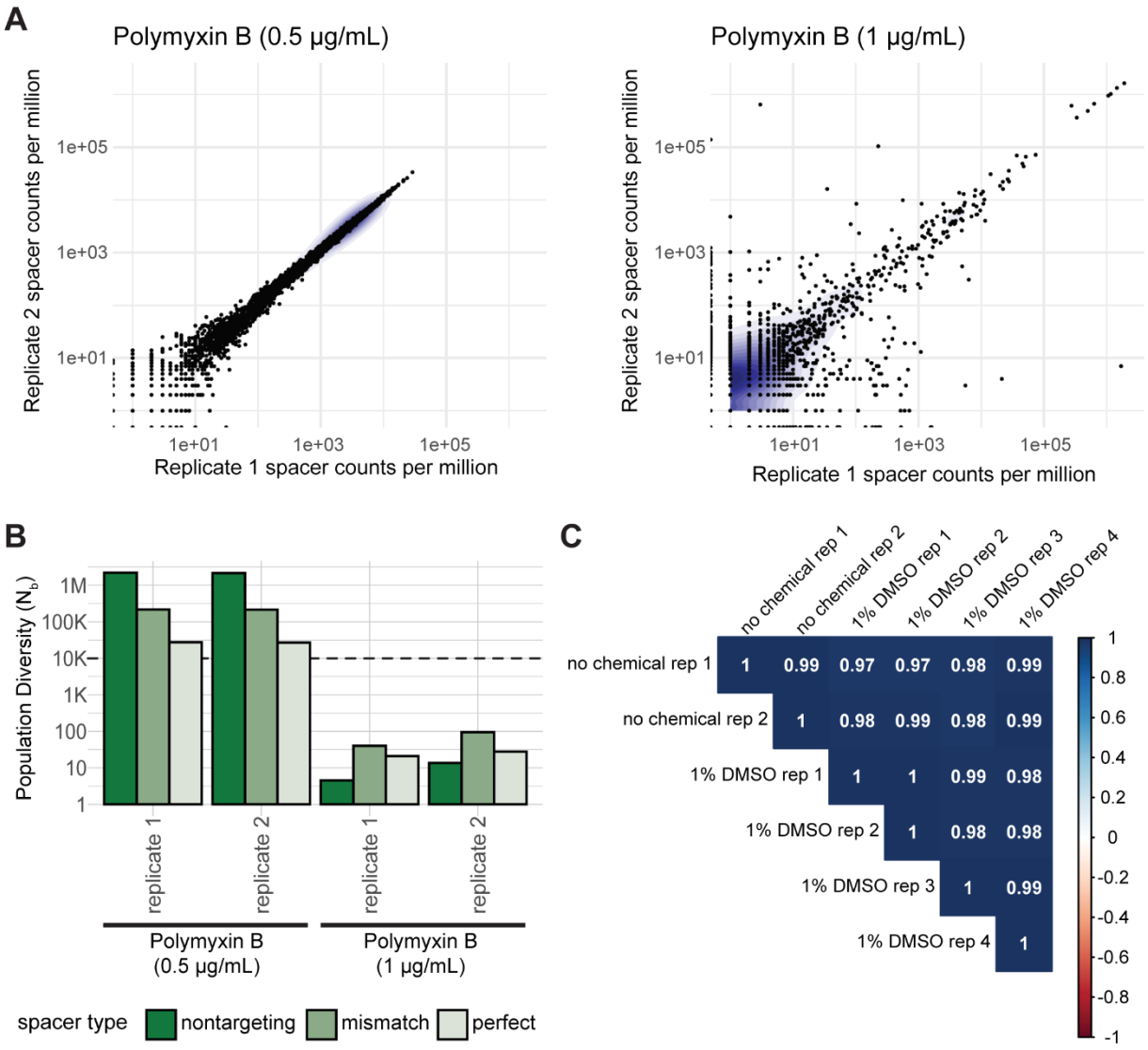
A
Polymyxin B (0.5 µg/mL)
Replicate 2 spacer counts per million
1e+05
1e+03
1e+01
1e+01
1e+03
1e+05
Replicate 1 spacer counts per million
Polymyxin B (1 µg/mL)
Replicate 2 spacer counts per million
1e+05
1e+03
1e+01
1e+01
1e+03
1e+05
Replicate 1 spacer counts per million
B
Population Diversity (N_b)
1M
100K
10K
1K
100
10
1
replicate 1
replicate 2
replicate 1
replicate 2
Polymyxin B (0.5 µg/mL)
Polymyxin B (1 µg/mL)
spacer type
nontargeting
mismatch
perfect
C
no chemical rep 1
no chemical rep 2
1% DMSO rep 1
1% DMSO rep 2
1% DMSO rep 3
1% DMSO rep 4
no chemical rep 1 1 0.99 0.97 0.97 0.98 0.99
no chemical rep 2 1 0.98 0.99 0.98 0.99
1% DMSO rep 1 1 1 0.99 0.98
1% DMSO rep 2 1 0.98 0.98
1% DMSO rep 3 1 0.99
1% DMSO rep 4 1
1
0.8
0.6
0.4
0.2
0
-0.2
-0.4
-0.6
-0.8
-1

Figure 3.S2. Growth and permeability assays for *lpt* and *lpx* knockdowns. (A) Box plot of significant negative CG scores for *lpt* or *lpx* genes. Asterisk denotes $p < 0.05$ (Student's *t*-test). (B) Colistin and levofloxacin MIC test strip assays for *lptA* or *lpxC* knockdown, LOS^-, or nontargeting guide control strains. Plates supplemented with 1mM IPTG. Approximate MICs indicated below images. (C) Heatmap of CG scores of *lpx* knockdowns across conditions, showing muted phenotypes compared to *lpt* knockdowns. (D) 10µL spots of ten-fold serial dilutions on plates with and without induction (N=3 biological replicates). The *lptA* knockdown, but not the *lpxC* knockdown, exhibits a minor growth defect upon induction. LOS^- strains show major growth defects. (E) Ethidium bromide permeability assay for *lptA* knockdown and nontargeting control in 19606 or LOS- backgrounds without induction; increased fluorescence over time indicates membrane permeability. Ribbons represent standard deviation (N=4 biological replicates). Without induction, the strain containing the *lptA* guide behaves similarly to a nontargeting guide control.

Figure 3.S2

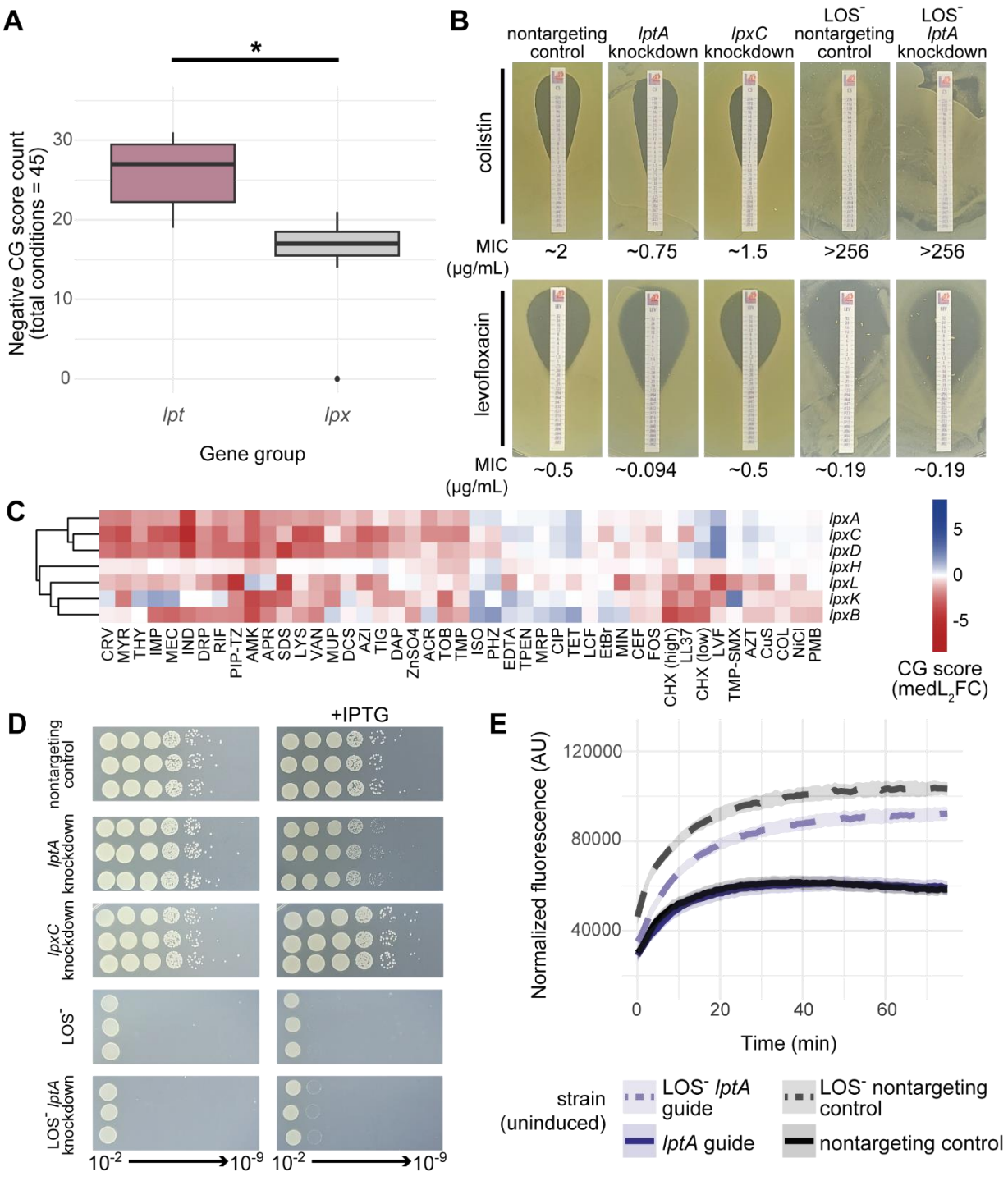
A
*
Negative CG score count (total conditions = 45)
30
20
10
0
lpt
lpx
Gene group
B
nontargeting control
lptA knockdown
lpxC knockdown
LOS- nontargeting control
LOS- lptA knockdown
colistin
MIC (μg/mL)
~2
~0.75
~1.5
>256
>256
levofloxacin
MIC (μg/mL)
~0.5
~0.094
~0.5
~0.19
~0.19
C
lpxA
lpxC
lpxD
lpxH
lpxL
lpxK
lpxB
CRV MYR THY IMP MEC IND DRP RIF PIP-TZ AMK APR SDS LYS VAN MUP DCS AZI TIG DAP ZnSO4 ACR TOB TMP ISO PHZ EDTA TPEN MRP CIP TET LCF EtBr MIN CEF FOS CHX (high) LL37 CHX (low) LVF TMP-SMX AZT CuS COL NiCl PMB
5
0
-5
CG score (medL2FC)
D
+IPTG
nontargeting control
lptA knockdown
lpxC knockdown
LOS-
LOS- lptA knockdown
10-2 → 10-9
10-2 → 10-9
E
Normalized fluorescence (AU)
120000
80000
40000
0
20
40
60
Time (min)
strain (uninduced)
LOS- lptA guide
LOS- nontargeting control
lptA guide
nontargeting control

Figure 3.S3. Chemical-gene scores and conservation in *Moraxellales*. Dot plot depicting significant CG scores and ortholog frequency across representative non-*Acinetobacter* *Moraxellales* for library essential genes.

Figure 3.S3

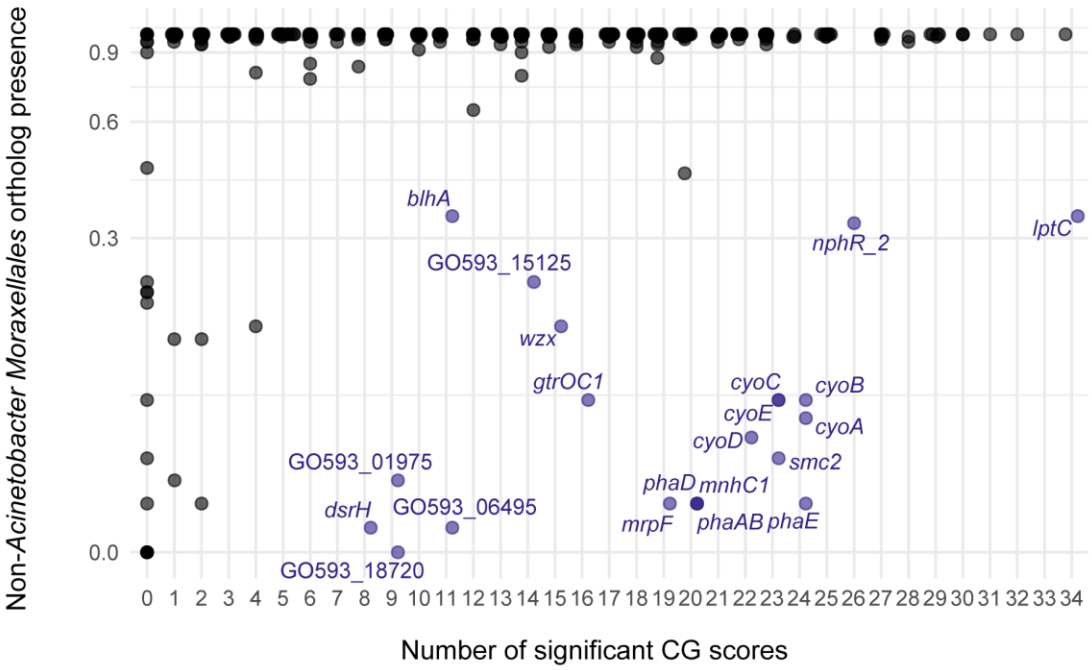
Non-Acinetobacter Moraxellales ortholog presence
0.9
0.6
0.3
0.0
blhA
GO593_15125
wzx
gtrOC1
nphR_2
lptC
cyoC
cyoB
cyoE
cyoA
cyoD
smc2
phaD
mnhC1
mrpF
phaAB
phaE
GO593_01975
dsrH
GO593_06495
GO593_18720
0 1 2 3 4 5 6 7 8 9 10 11 12 13 14 15 16 17 18 19 20 21 22 23 24 25 26 27 28 29 30 31 32 33 34
Number of significant CG scores

Figure 3.S4. Essential gene subnetworks. Sections from the essential gene network for (A) cytochrome bo3 oxidase (*cyo*), ion transporter (*phaAB, mnhC1, phaD, mrpF*), and related genes or (B) *lpt*-associated genes, including *gtrOC1*.

Figure 3.S4

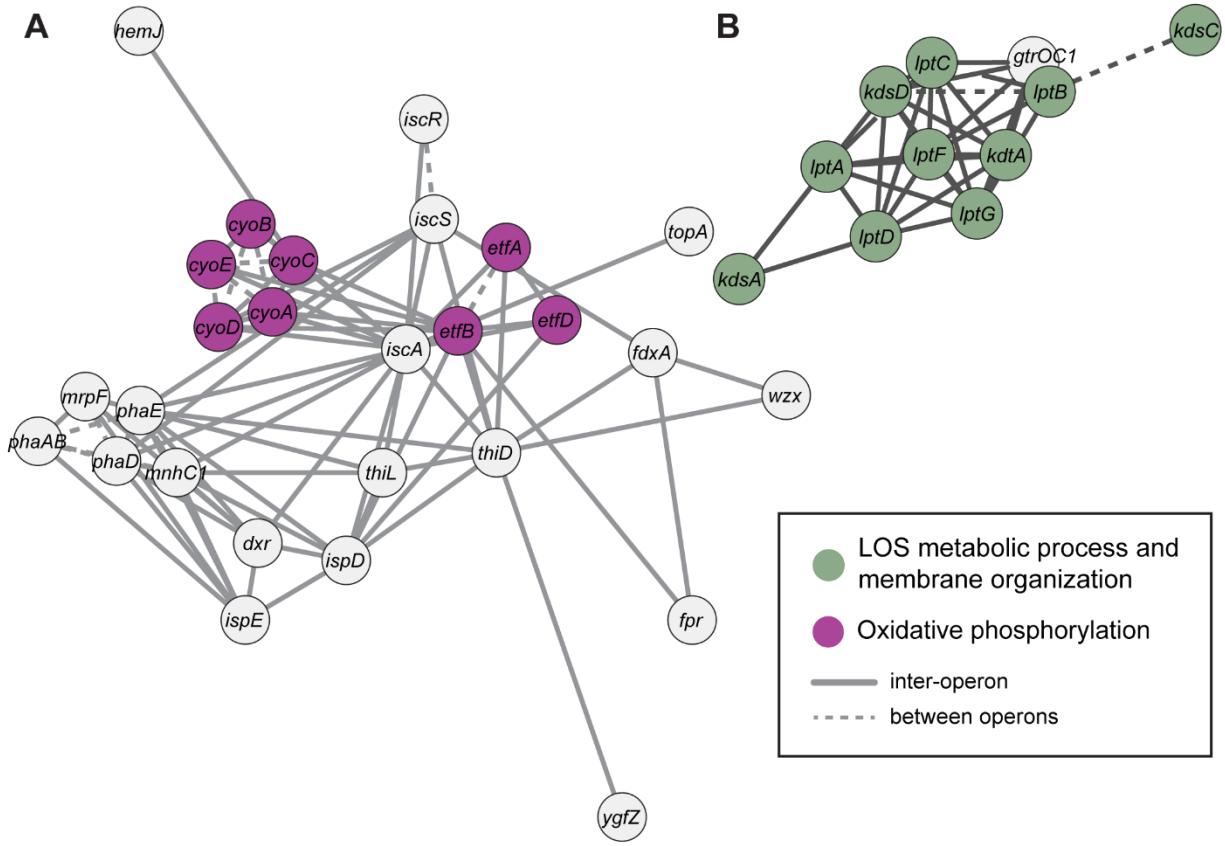
A
B
hemJ
iscR
iscS
cyoB
cyoE
cyoC
cyoD
cyoA
etfA
etfB
etfD
topA
iscA
fdxA
wzx
mrpF
phaE
phaAB
phaD
mnhC1
thiL
thiD
dxr
ispD
ispE
fpr
ygfZ
kdsC
gtrOC1
lptC
kdsD
lptB
lptA
lptF
kdtA
lptG
lptD
kdsA
LOS metabolic process and membrane organization
Oxidative phosphorylation
inter-operon
between operons

Figure 3.S5. Characterization of unannotated, poorly conserved genes. Heatmaps of CG scores for clusters containing (A) GO593_00140 or (B) GO593_11615. Y-axis clustering was conducted using the Ward method and Canberra distance across all library knockdowns. (C) Heterodimer structural prediction (Alphafold2) for GO593_00140 and the chi subunit of DNA Polymerase III in *A. baumannii* (left) and the solved structure for the *E. coli* psi-chi subunit heterodimer (right). GO593_00140 has a lengthy unstructured N-terminal end absent in *E. coli* HolD. (D) Domain architecture map from InterProScan analysis, comparing *E. coli* LexA to GO593_11615. Both have a DNA-binding domain and S24 peptidase/LexA domain but differ in overall protein length and specific type of DNA-binding domain. (E) Domain architectures for *E. coli* FtsN and *A. baumannii* GO593_07290. GO593_07290 lacks similarity to the short ^{E}FtsN region required for function (47). BLAST-aligned amino acid sequences (24% identity) are depicted with dotted lines.

Figure 3.S5

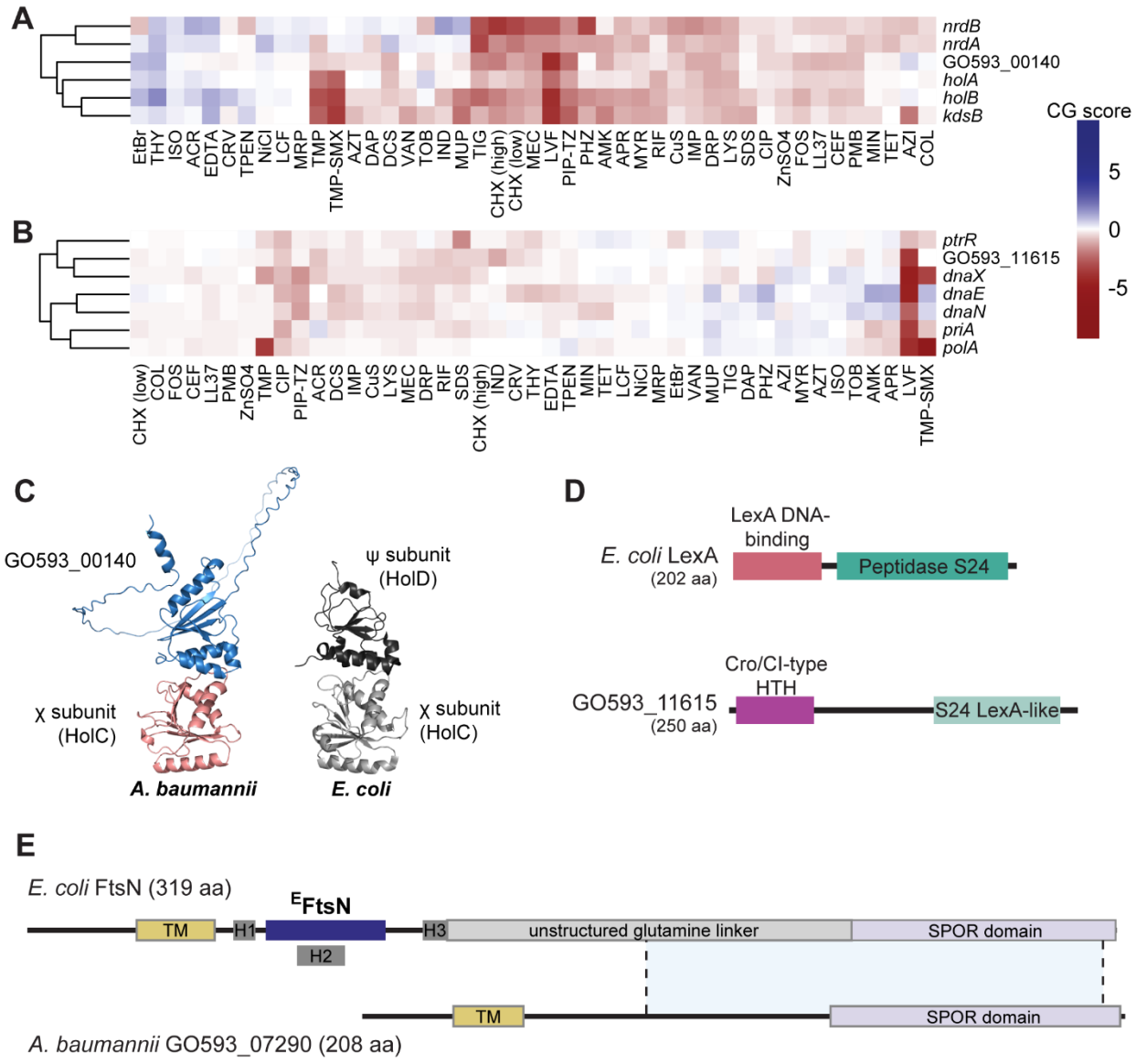
A
nrdB
nrdA
GO593_00140
holA
holB
kdsB
EtBr THY ISO ACR EDTA CRV TPEN NiCl LCF MRP TMP TMP-SMX AZT DAP DCS VAN TOB IND MUP TIG CHX (high) CHX (low) MEC LVF PIP-TZ PHZ AMK APR MYR RIF CuS IMP DRP LYS SDS CIP ZnSO4 FOS LL37 CEF PMB MIN TET AZI COL
CG score
5
0
-5
B
ptrR
GO593_11615
dnaX
dnaE
dnaN
priA
polA
CHX (low) COL FOS CEF LL37 PMB ZnSO4 TMP CIP PIP-TZ ACR DCS IMP CuS LYS MEC DRP RIF SDS CHX (high) IND CRV THY EDTA TPEN MIN TET LCF NiCl MRP EtBr VAN MUP TIG DAP PHZ AZI MYR AZT ISO TOB AMK APR LVF TMP-SMX
C
GO593_00140
ψ subunit (HolD)
χ subunit (HolC)
χ subunit (HolC)
A. baumannii
E. coli
D
E. coli LexA (202 aa)
LexA DNA-binding
Peptidase S24
GO593_11615 (250 aa)
Cro/CI-type HTH
S24 LexA-like
E
E. coli FtsN (319 aa)
EFtsN
TM
H1
H2
H3
unstructured glutamine linker
SPOR domain
TM
SPOR domain
A. baumannii GO593_07290 (208 aa)

Figure 3.S6. Functional phenotypes for network genes of unknown function. (A) Heatmaps display CG scores for the signal-recognition cluster containing *ftsY, ffh,* and GO593_10640. GO593_18720 does not cluster in the heatmap with these genes due to muted phenotypes but is connected in the network. (B) GO593_10640 is a predicted transmembrane protein similar to a transporter. Predicted structure (Alphafold) and orientation in the membrane (TMHMM) are shown. (C) GO593_17830 is connected to *tus* genes in the network, but this could be due to polar effects as (D) the gene is upstream of a TusE/DsrC-like protein in a predicted operon.

Figure 3.S6

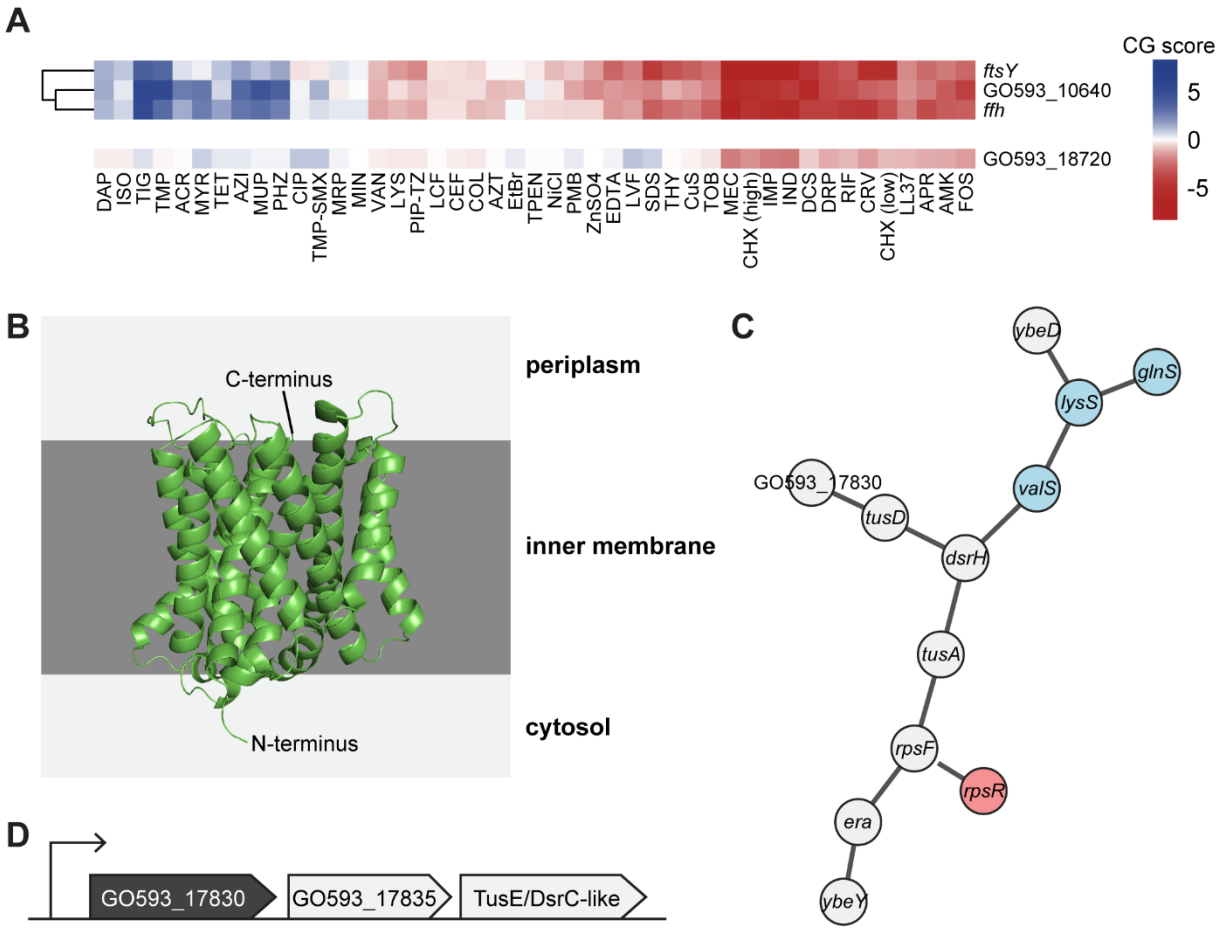
A
CG score
5
0
-5
ftsY
GO593_10640
ffh
GO593_18720
DAP
ISO
TIG
TMP
ACR
MYR
TET
AZI
MUP
PHZ
CIP
TMP-SMX
MRP
MIN
VAN
LYS
PIP-TZ
LCF
CEF
COL
AZT
EtBr
TPEN
NiCl
PMB
ZnSO4
EDTA
LVF
SDS
THY
CuS
TOB
MEC
CHX (high)
IMP
IND
DCS
DRP
RIF
CRV
CHX (low)
LL37
APR
AMK
FOS
B
C-terminus
periplasm
inner membrane
cytosol
N-terminus
C
ybeD
glnS
lysS
GO593_17830
valS
tusD
dsrH
tusA
rpsF
rpsR
era
ybeY
D
GO593_17830
GO593_17835
TusE/DsrC-like

Figure 3.S7. Microscopy of fluorescently tagged cell division proteins. 3 representative images for each construct are shown with corresponding empty vector controls. (A) Smc2::sfGFP expression leads to elongated cells, with fluorescently tagged proteins aggregating inconsistently within the cells. (B) Expression of Smc2 from a replicative plasmid produces elongated cells. (C) sfGFP::BlhA localizes at sites of division at the mid-cell at either existing or forming septa. (D) Fluorescently tagged SPOR-domain protein shows localization at the cell membrane and at septa for dividing cells. All bars are 5 μm; GFP fluorescence/phase contrast channels merged in composite images for all except (B).

Figure 3.S7

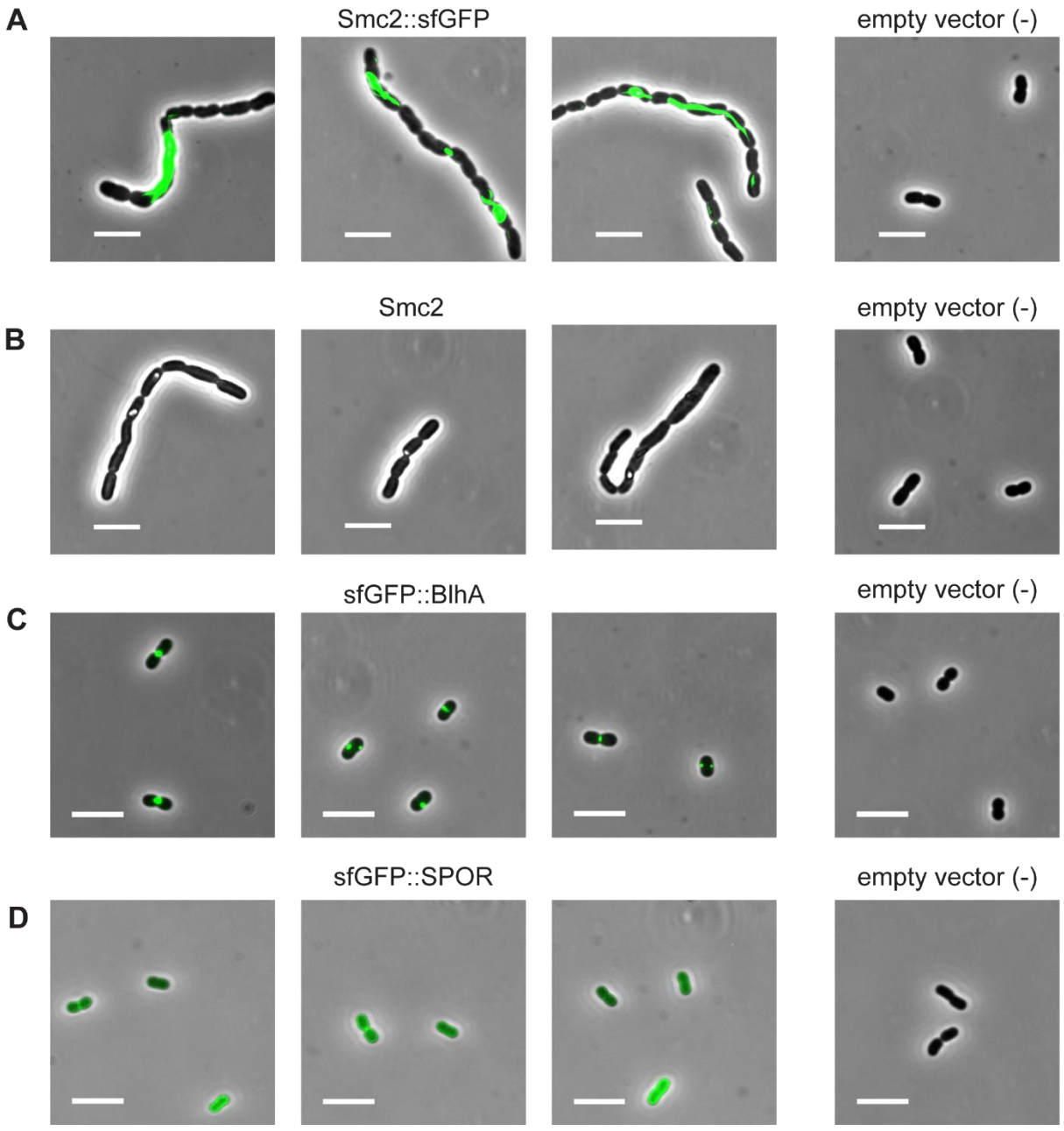
A
Smc2::sfGFP
empty vector (-)
B
Smc2
empty vector (-)
C
sfGFP::BlhA
empty vector (-)
D
sfGFP::SPOR
empty vector (-)

Figure 3.S8. Chemical pairs similar in pathway effect and structure. Heatmap shows the normalized sum of pathway effect and structure association scores for chemical pairs, highlighting chemicals similar in both structure and pathway effect.

Figure 3.S8

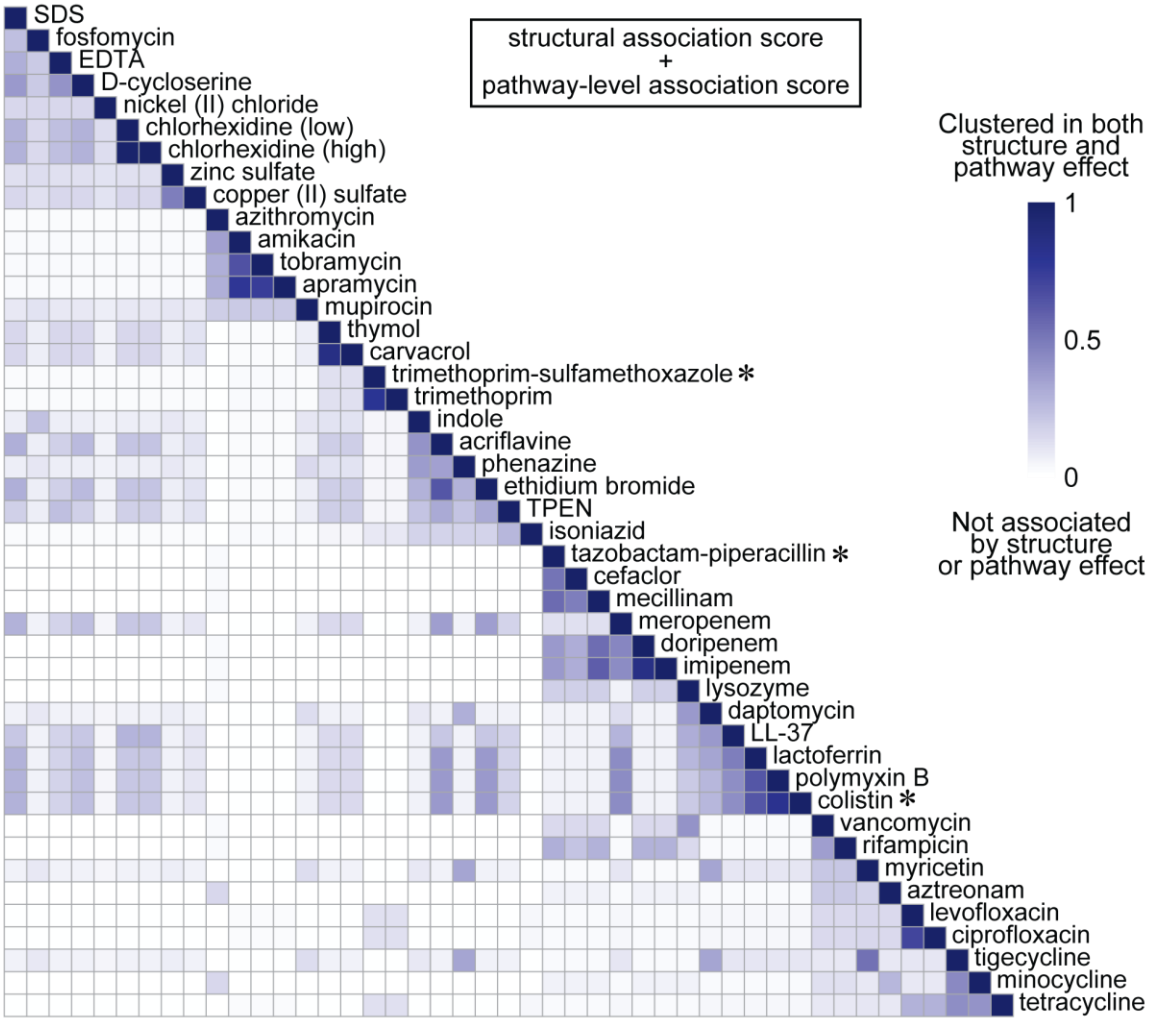
SDS
fosfomycin
EDTA
D-cycloserine
nickel (II) chloride
chlorhexidine (low)
chlorhexidine (high)
zinc sulfate
copper (II) sulfate
azithromycin
amikacin
tobramycin
apramycin
mupirocin
thymol
carvacrol
trimethoprim-sulfamethoxazole *
trimethoprim
indole
acriflavine
phenazine
ethidium bromide
TPEN
isoniazid
tazobactam-piperacillin *
cefaclor
mecillinam
meropenem
doripenem
imipenem
lysozyme
daptomycin
LL-37
lactoferrin
polymyxin B
colistin *
vancomycin
rifampicin
myricetin
aztreonam
levofloxacin
ciprofloxacin
tigecycline
minocycline
tetracycline
structural association score
+
pathway-level association score
Clustered in both structure and pathway effect
1
0.5
0
Not associated by structure or pathway effect

Figure 3.S9. Pathways impacted by carvacrol and thymol. Sina plots with boxplots depict differential guide CPMs for (A) NADH dehydrogenase and (B) ubiquinone pathways in carvacrol and thymol compared to no chemical control. STRING identifiers and representation of pathways listed. Chemical-gene interactions are described above each graph—up (positive), down (negative), or no change—with FDR values. Guides are weighted in this calculation by predicted efficacy, with perfect guides at 100. Volcano plots show relative fitness and FDRs at the gene-level in (C) carvacrol or (D) thymol, with genes in pathways of interest highlighted.

Figure 3.S9

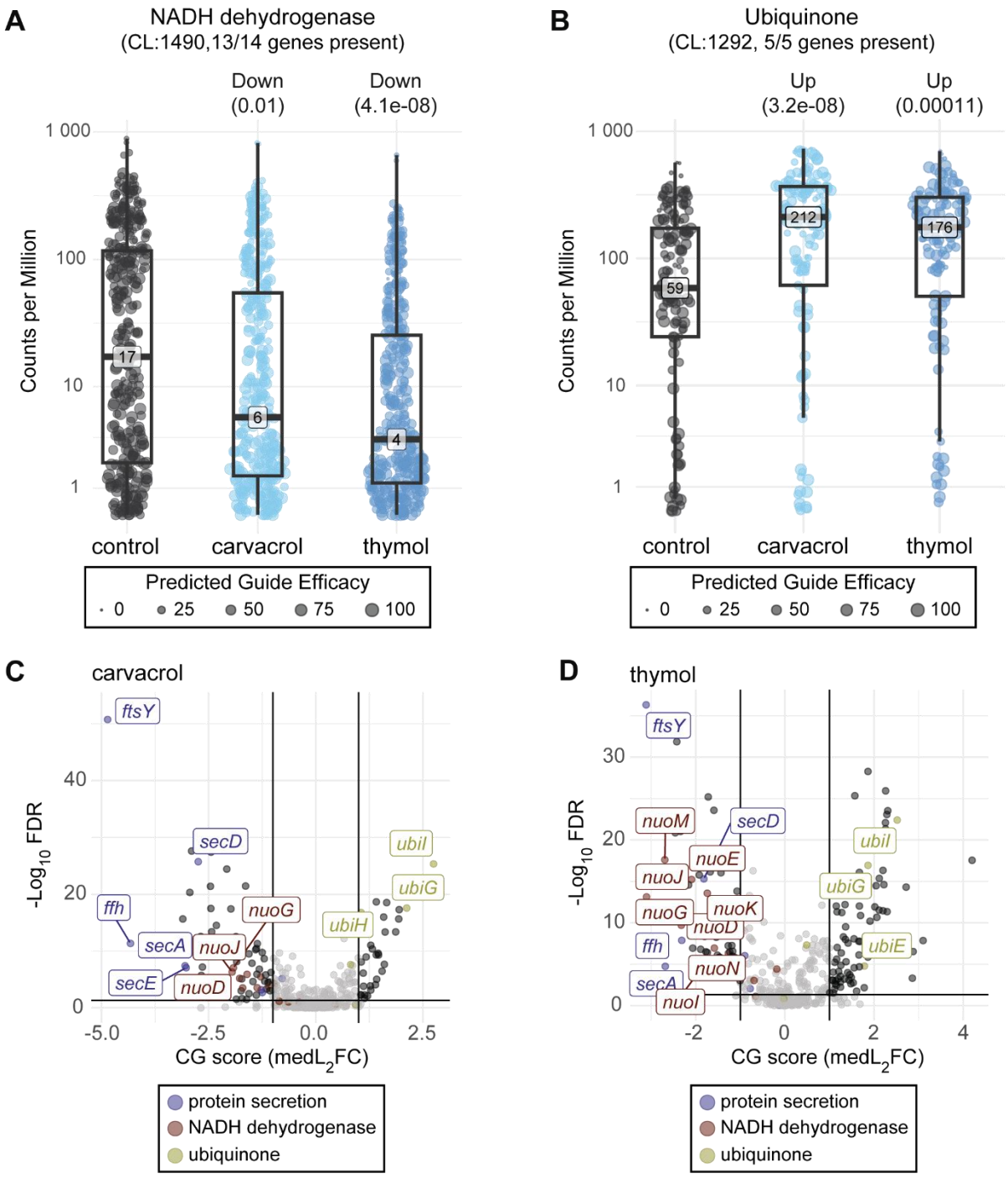
A
NADH dehydrogenase
(CL:1490,13/14 genes present)
Down
(0.01)
Down
(4.1e-08)
1 000
100
10
1
Counts per Million
17
6
4
control
carvacrol
thymol
Predicted Guide Efficacy
0
25
50
75
100
B
Ubiquinone
(CL:1292, 5/5 genes present)
Up
(3.2e-08)
Up
(0.00011)
59
212
176
C
carvacrol
ftsY
secD
ubiI
ubiG
ffh
nuoG
ubiH
secA
nuoJ
secE
nuoD
40
20
0
-Log10 FDR
-5.0
-2.5
0.0
2.5
CG score (medL2FC)
protein secretion
NADH dehydrogenase
ubiquinone
D
thymol
ftsY
30
nuoM
secD
20
nuoE
ubiI
nuoJ
ubiG
nuoG
nuoK
10
nuoD
ffh
ubiE
nuoN
secA
nuoI
0
-2
0
2
4

Figure 3.S10. Chemical pairs opposed in pathway effect and structure. Heatmap shows the normalized differences between pathway effect and structure association scores for chemical pairs, highlighting chemicals that cluster in only structure or only pathway effect.

Figure 3.S10

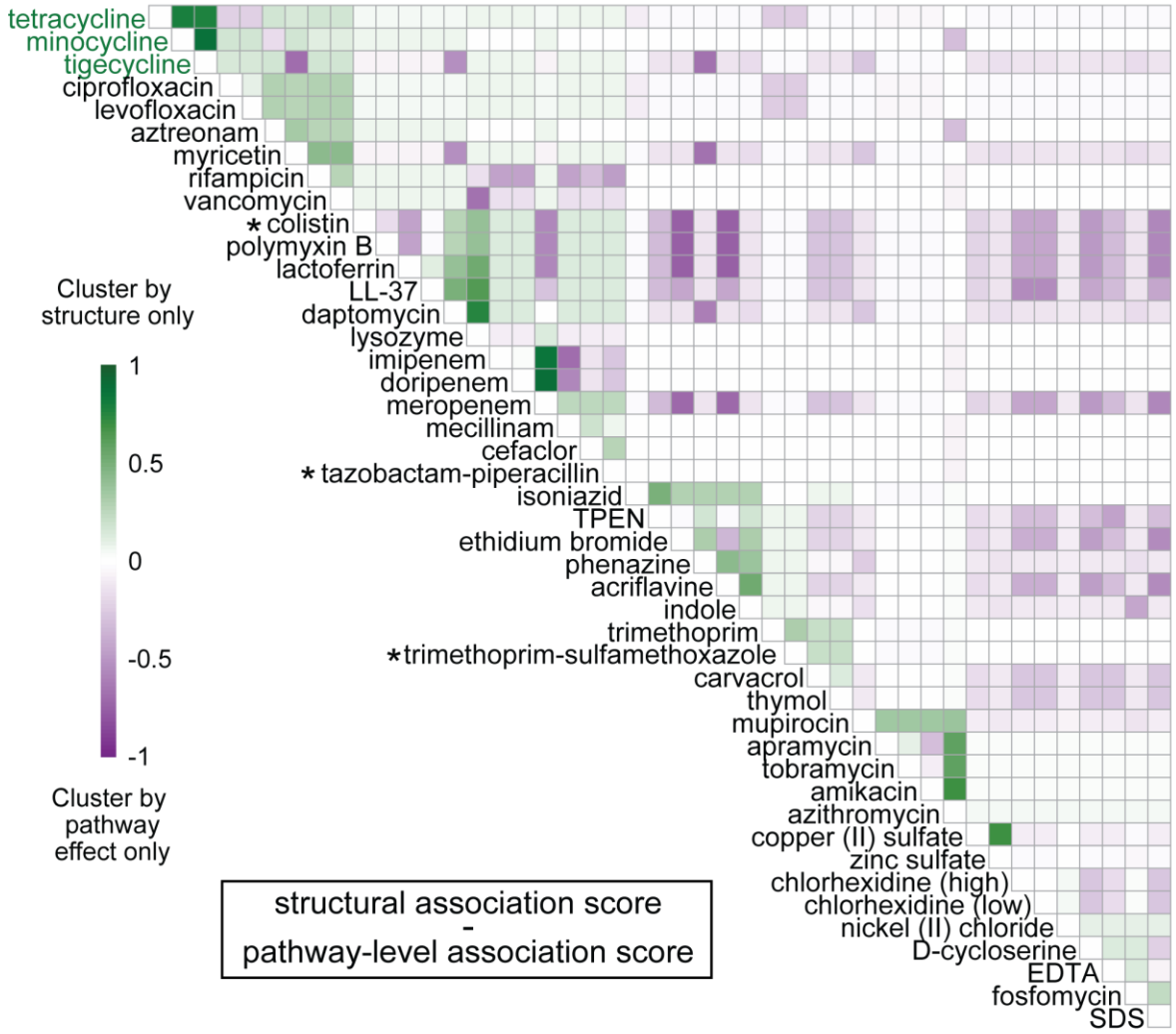
tetracycline
minocycline
tigecycline
ciprofloxacin
levofloxacin
aztreonam
myricetin
rifampicin
vancomycin
*colistin
polymyxin B
lactoferrin
LL-37
daptomycin
lysozyme
imipenem
doripenem
meropenem
mecillinam
cefaclor
*tazobactam-piperacillin
isoniazid
TPEN
ethidium bromide
phenazine
acriflavine
indole
trimethoprim
*trimethoprim-sulfamethoxazole
carvacrol
thymol
mupirocin
apramycin
tobramycin
amikacin
azithromycin
copper (II) sulfate
zinc sulfate
chlorhexidine (high)
chlorhexidine (low)
nickel (II) chloride
D-cycloserine
EDTA
fosfomycin
SDS
Cluster by structure only
1
0.5
0
-0.5
-1
Cluster by pathway effect only
structural association score
-
pathway-level association score

Figure 3.S11. Target pathway effects for tetracycline-class antibiotics. (A) Sina plots with boxplots depict differential guide CPMs for ribosome genes (STRING identifier CL:113) in minocycline, tetracycline, or tigecycline compared to no chemical control. Chemical-gene interactions are described above each graph—up (positive), down (negative), or no change—with FDR values. Guides are weighted in this calculation by predicted efficacy, with perfect guides at 100. Non-significant comparisons are shown with grey backgrounds. (B) Heatmap shows relative fitness scores (log_2 fold changes) of ribosomal gene knockdowns after growth compared to T0. Ribosome knockdowns have substantial loss of fitness. (C) Volcano plots of library gene CG scores for minocycline, tetracycline, and tigecycline. Lines depict defining cutoffs for CG score significance. Genes in the ribosome group are colored green.

Figure 3.S11

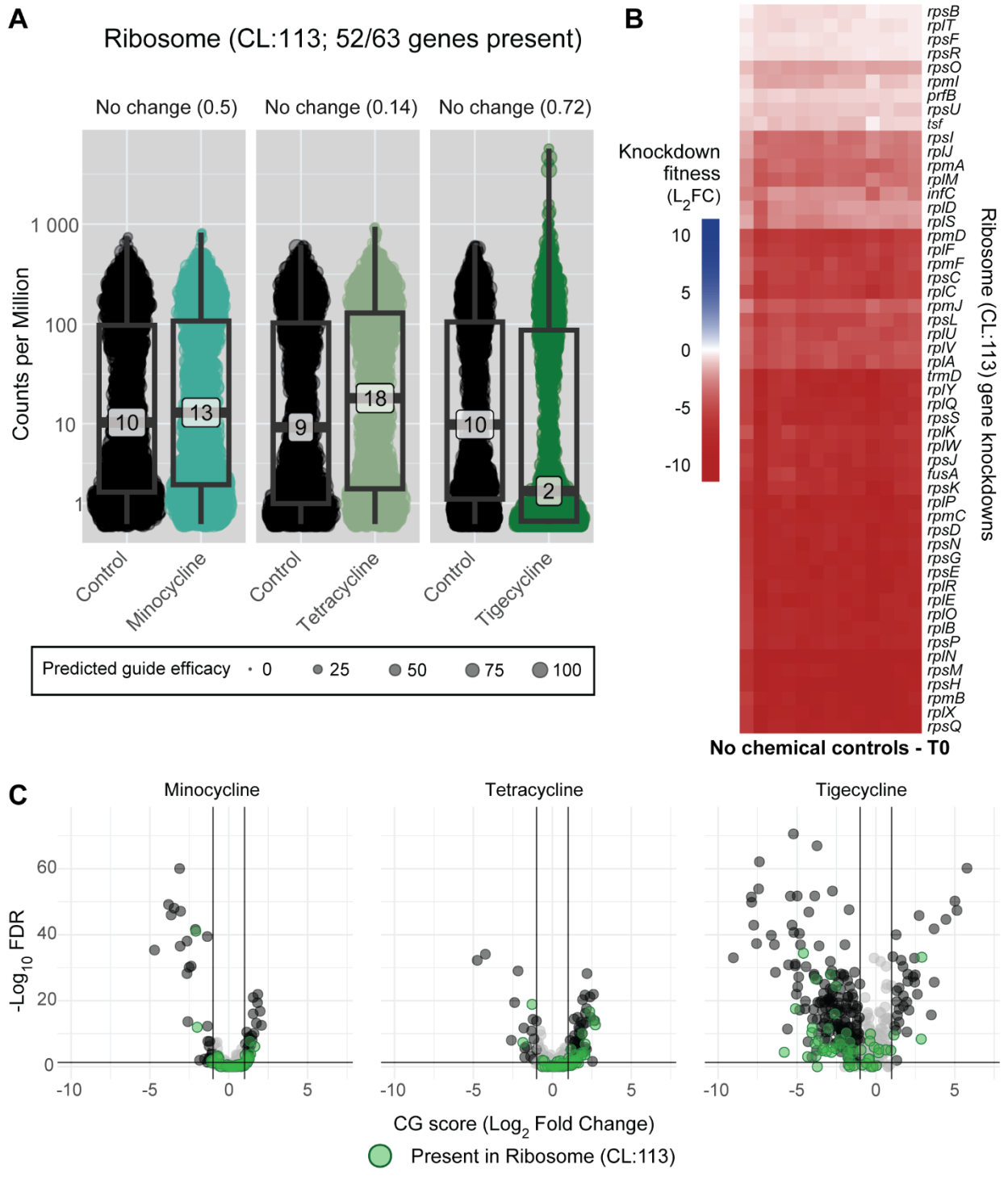
A
Ribosome (CL:113; 52/63 genes present)
No change (0.5)
No change (0.14)
No change (0.72)
Counts per Million
1 000
100
10
1
10
13
9
18
10
2
Control
Minocycline
Control
Tetracycline
Control
Tigecycline
Predicted guide efficacy
0
25
50
75
100
B
Knockdown fitness (L2FC)
10
5
0
-5
-10
rpsB
rplT
rpsF
rpsR
rpsO
rpmI
prfB
rpsU
tsf
rpsI
rplJ
rpmA
rplM
infC
rplD
rplS
rpmD
rplF
rpmF
rpsC
rplC
rpmJ
rpsL
rplU
rplV
rplA
trmD
rplY
rplQ
rpsS
rplK
rplW
rpsJ
fusA
rpsK
rplP
rpmC
rpsD
rpsN
rpsG
rpsE
rplR
rplE
rplO
rplB
rpsP
rplN
rpsM
rpsH
rpmB
rplX
rpsQ
Ribosome (CL:113) gene knockdowns
No chemical controls - T0
C
Minocycline
Tetracycline
Tigecycline
-Log10 FDR
60
40
20
0
-10
-5
0
5
CG score (Log2 Fold Change)
Present in Ribosome (CL:113)

Figure 3.S12. Lpt and ATP synthesis pathway effects in tetracycline-class antibiotics. Sina plots with boxplots of differential guide CPMs for listed STRING identifiers in tetracycline-class antibiotics: (A) lipopolysaccharide (lipooligosaccharide in *A. baumannii*) transport or (B) ATP synthesis pathways. Guides are weighted by predicted efficacy, with perfect guides at 100. Chemical interactions compared to no chemical control (up, down, or no change) and FDRs are listed. Non-significant comparisons are shown with grey backgrounds.

Figure 3.S12

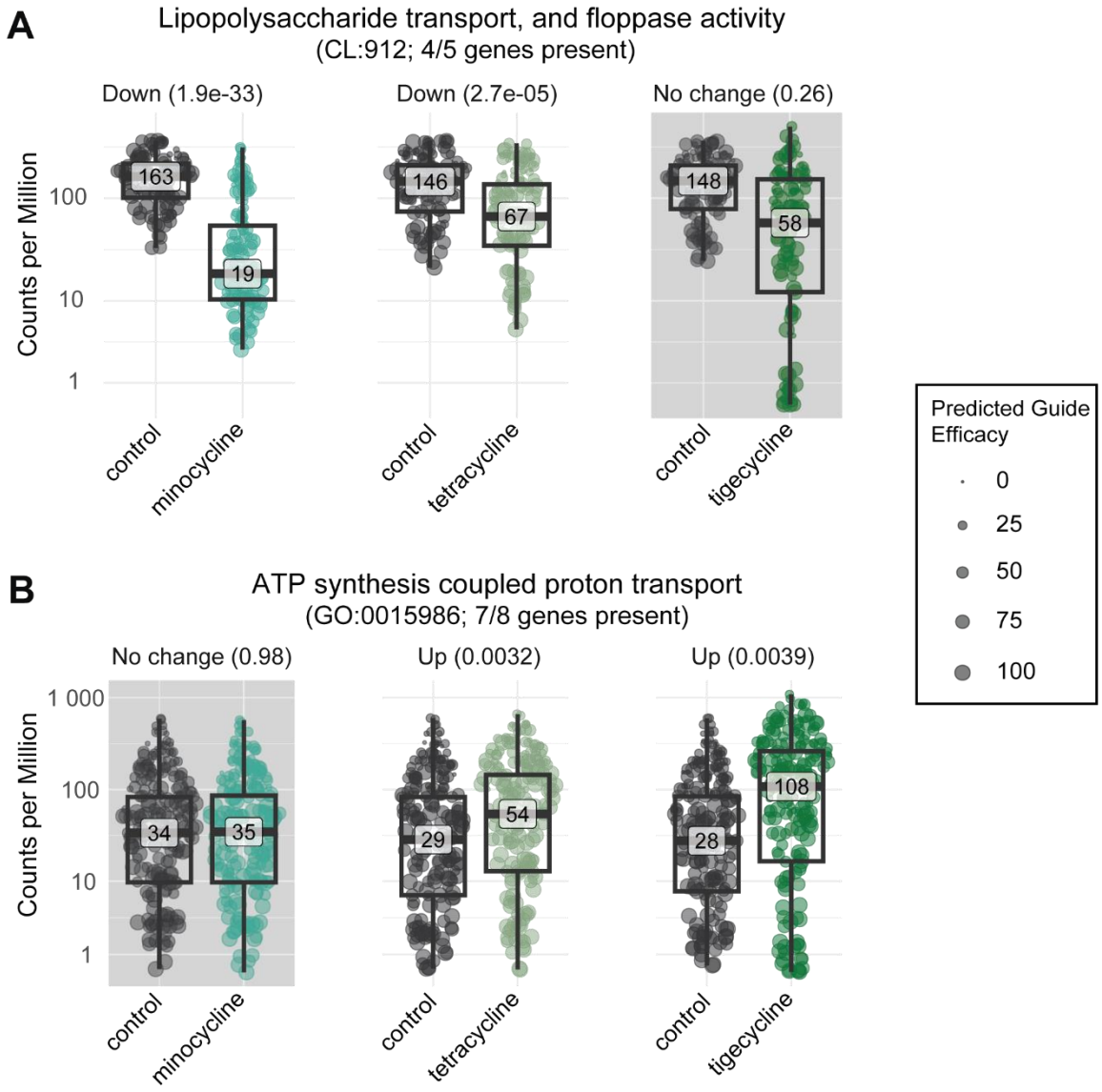
A
Lipopolysaccharide transport, and floppase activity
(CL:912; 4/5 genes present)
Down (1.9e-33)
Down (2.7e-05)
No change (0.26)
Counts per Million
100
10
1
163
19
146
67
148
58
control
minocycline
control
tetracycline
control
tigecycline
B
ATP synthesis coupled proton transport
(GO:0015986; 7/8 genes present)
No change (0.98)
Up (0.0032)
Up (0.0039)
1 000
100
10
1
34
35
29
54
28
108
control
minocycline
control
tetracycline
control
tigecycline
Predicted Guide Efficacy
0
25
50
75
100

Figure 3.S13. Ineffective chemical concentrations lack significant pathway effects. (A) Volcano plots of genes in meropenem, imipenem, or doripenem compared to no drug control. Genes with significant CG scores are shown in black. Meropenem has very few significant CG scores, suggesting insufficient chemical dosage. (B) Sina plots with boxplots of differential guide CPMs for target pathway in doripenem, imipenem, or meropenem. Chemical interactions compared to no chemical control (up, down, or no change) and FDRs are listed. Non-significant comparison for meropenem is shown with grey background. Doripenem and imipenem are significantly impacted.

Figure 3.S13

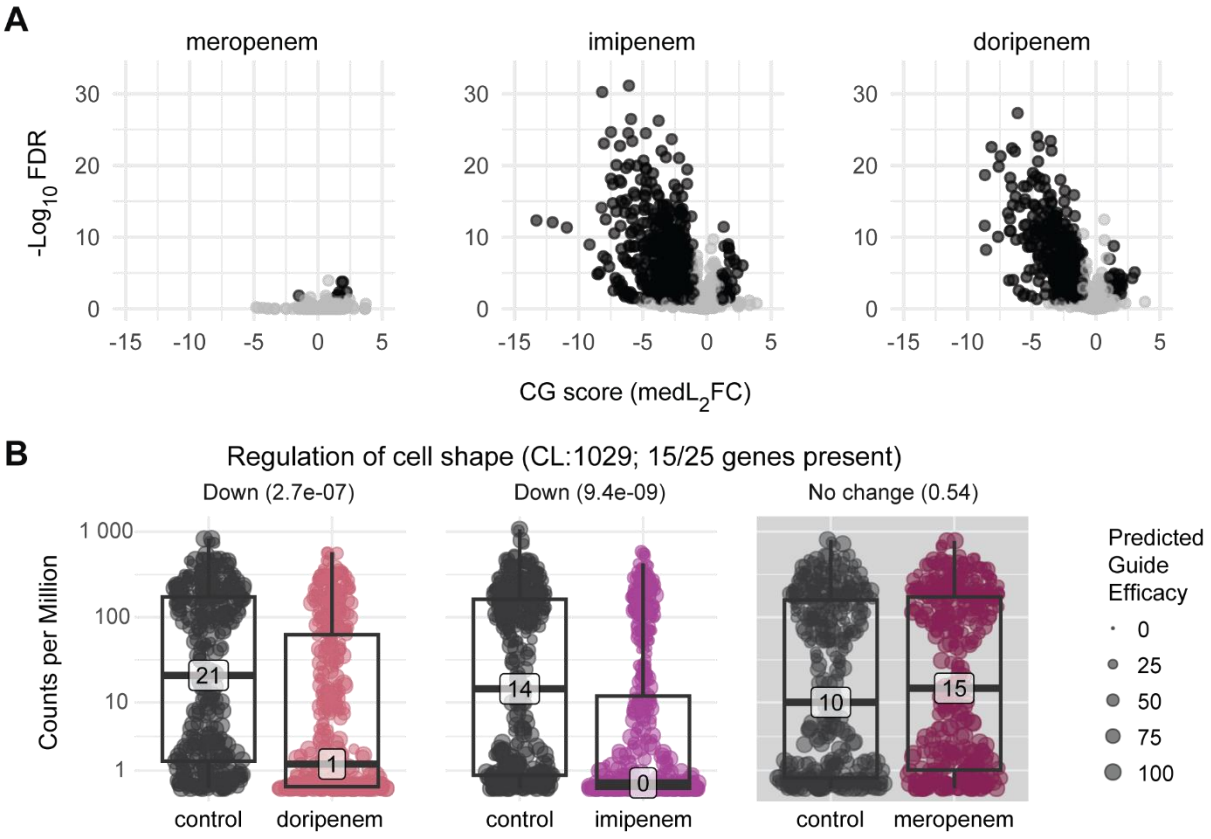
A
meropenem
imipenem
doripenem
-Log10 FDR
CG score (medL2FC)
B
Regulation of cell shape (CL:1029; 15/25 genes present)
Down (2.7e-07)
Down (9.4e-09)
No change (0.54)
Counts per Million
control
doripenem
imipenem
meropenem
Predicted Guide Efficacy
0
25
50
75
100

Acknowledgments

We thank the UW-Madison Biotech Center for their assistance with sequencing. Special thanks to Rachel Salemi and Alex Goetsch for their assistance and training with microscopy. The LOS$^-$ strain was a gift from Stephen Trent and Brent Simpson. This work is supported by the National Institutes of Health under award numbers K22AI137122 and 1R35GM150487-01. JST is supported by the Biotechnology Training Program (NIH 5T32GM135066), SciMED Graduate Research Scholars, and an NSF GRFP. RDW is supported by the Predoctoral Training Program in Genetics (NIH 5T32GM007133) and SciMED Graduate Research Scholars.

References

1. 2019. Acinetobacter in Healthcare Settings | HAI | CDC. https://www.cdc.gov/hai/organisms/acinetobacter.html. Retrieved 11 July 2023.

2. Wong D, Nielsen TB, Bonomo RA, Pantapalangkoor P, Luna B, Spellberg B. 2017. Clinical and Pathophysiological Overview of Acinetobacter Infections: a Century of Challenges. Clin Microbiol Rev 30:409–447.

3. Geisinger E, Mortman NJ, Dai Y, Cokol M, Syal S, Farinha A, Fisher DG, Tang AY, Lazinski DW, Wood S, Anthony J, van Opijnen T, Isberg RR. 2020. Antibiotic susceptibility signatures identify potential antimicrobial targets in the Acinetobacter baumannii cell envelope. 1. Nat Commun 11:4522.

4. Gallagher LA, Ramage E, Weiss EJ, Radey M, Hayden HS, Held KG, Huse HK, Zurawski DV, Brittnacher MJ, Manoil C. 2015. Resources for Genetic and Genomic Analysis of Emerging Pathogen Acinetobacter baumannii. J Bacteriol 197:2027–2035.

5. Qi LS, Larson MH, Gilbert LA, Doudna JA, Weissman JS, Arkin AP, Lim WA. 2013. Repurposing CRISPR as an RNA-Guided Platform for Sequence-Specific Control of Gene Expression. Cell 152:1173–1183.

6. Bikard D, Jiang W, Samai P, Hochschild A, Zhang F, Marraffini LA. 2013. Programmable repression and activation of bacterial gene expression using an engineered CRISPR-Cas system. Nucl Acids Res gkt520.

7. Peters JM, Colavin A, Shi H, Czarny TL, Larson MH, Wong S, Hawkins JS, Lu CHS, Koo B-M, Marta E, Shiver AL, Whitehead EH, Weissman JS, Brown ED, Qi LS, Huang KC, Gross CA. 2016. A Comprehensive, CRISPR-based Functional Analysis of Essential Genes in Bacteria. Cell 165:1493–1506.

8. Peters JM, Koo B-M, Patino R, Heussler GE, Hearne CC, Qu J, Inclan YF, Hawkins JS, Lu CHS, Silvis MR, Harden MM, Osadnik H, Peters JE, Engel JN, Dutton RJ, Grossman AD, Gross CA, Rosenberg OS. 2019. Enabling genetic analysis of diverse bacteria with Mobile-CRISPRi. Nat Microbiol 4:244–250.

9. Geyman L, Tanner M, Rosario-Melendez N, Peters J, Mandel MJ, van Kessel JC. 2024. Mobile-CRISPRi as a powerful tool for modulating Vibrio gene expression. bioRxiv 2024.01.17.575898.

10. Zhou D, Huang G, Xu G, Xiang L, Huang S, Chen X, Zhang Y, Wang D. 2022. CRISPRi-Mediated Gene Suppression Reveals Putative Reverse Transcriptase Gene PA0715 to Be a Global Regulator of Pseudomonas aeruginosa. Infect Drug Resist 15:7577–7599.

11. Hogan AM, Rahman ASMZ, Lightly TJ, Cardona ST. 2019. A Broad-Host-Range CRISPRi Toolkit for Silencing Gene Expression in Burkholderia. ACS Synth Biol 8:2372–2384.

12. Bai J, Dai Y, Farinha A, Tang AY, Syal S, Vargas-Cuebas G, van Opijnen T, Isberg RR, Geisinger E. Essential Gene Analysis in Acinetobacter baumannii by High-Density Transposon Mutagenesis and CRISPR Interference. J Bacteriol 203:e00565-20.

13. Luo J, Efimova E, Volke DC, Santala V, Santala S. 2022. Engineering cell morphology by CRISPR interference in Acinetobacter baylyi ADP1. Microb Biotechnol 15:2800–2818.

14. Zheng XFS, Chan T-F. 2002. Chemical genomics: a systematic approach in biological research and drug discovery. Curr Issues Mol Biol 4:33–43.

15. Alaimo PJ, Shogren-Knaak MA, Shokat KM. 2001. Chemical genetic approaches for the elucidation of signaling pathways. Curr Opin Chem Biol 5:360–367.

16. Nichols RJ, Sen S, Choo YJ, Beltrao P, Zietek M, Chaba R, Lee S, Kazmierczak KM, Lee KJ, Wong A, Shales M, Lovett S, Winkler ME, Krogan NJ, Typas A, Gross CA. 2011. Phenotypic landscape of a bacterial cell. Cell 144:143–156.

17. Cain AK, Barquist L, Goodman AL, Paulsen IT, Parkhill J, van Opijnen T. 2020. A decade of advances in transposon-insertion sequencing. Nat Rev Genet 21:526–540.

18. Enright AL, Banta AB, Ward RD, Rivera Vazquez J, Felczak MM, Wolfe MB, TerAvest MA, Amador-Noguez D, Peters JM. 2023. The genetics of aerotolerant growth in an alphaproteobacterium with a naturally reduced genome. mBio 14:e0148723.

19. Li S, Poulton NC, Chang JS, Azadian ZA, DeJesus MA, Ruecker N, Zimmerman MD, Eckartt KA, Bosch B, Engelhart CA, Sullivan DF, Gengenbacher M, Dartois VA, Schnappinger D, Rock JM. 2022. CRISPRi chemical genetics and comparative genomics identify genes mediating drug potency in Mycobacterium tuberculosis. Nat Microbiol 7:766–779.

20. Ward RD, Tran JS, Banta AB, Bacon EE, Rose WE, Peters JM. Essential gene knockdowns reveal genetic vulnerabilities and antibiotic sensitivities in Acinetobacter baumannii. mBio 15:e02051-23.

21. Rousset F, Cabezas-Caballero J, Piastra-Facon F, Fernández-Rodríguez J, Clermont O, Denamur E, Rocha EPC, Bikard D. 2021. The impact of genetic diversity on gene essentiality within the Escherichia coli species. Nat Microbiol 6:301–312.

22. Hawkins JS, Silvis MR, Koo B-M, Peters JM, Osadnik H, Jost M, Hearne CC, Weissman JS, Todor H, Gross CA. 2020. Mismatch-CRISPRi Reveals the Co-varying Expression-Fitness Relationships of Essential Genes in Escherichia coli and Bacillus subtilis. Cell Systems 11:523-535.e9.

23. Costanzo M, VanderSluis B, Koch EN, Baryshnikova A, Pons C, Tan G, Wang W, Usaj M, Hanchard J, Lee SD, Pelechano V, Styles EB, Billmann M, van Leeuwen J, van Dyk N, Lin Z-Y, Kuzmin E, Nelson J, Piotrowski JS, Srikumar T, Bahr S, Chen Y, Deshpande R, Kurat CF, Li SC, Li Z, Usaj MM, Okada H, Pascoe N, San Luis B-J, Sharifpoor S, Shuteriqi E, Simpkins SW, Snider J, Suresh HG, Tan Y, Zhu H, Malod-Dognin N, Janjic V, Przulj N, Troyanskaya OG, Stagljar I, Xia T, Ohya Y, Gingras A-C, Raught B, Boutros M, Steinmetz LM, Moore CL, Rosebrock AP, Caudy AA, Myers CL, Andrews B, Boone C. 2016. A global genetic interaction network maps a wiring diagram of cellular function. Science 353:aaf1420.

24. Szklarczyk D, Kirsch R, Koutrouli M, Nastou K, Mehryary F, Hachilif R, Gable AL, Fang T, Doncheva NT, Pyysalo S, Bork P, Jensen LJ, von Mering C. 2023. The STRING database in 2023: protein-protein association networks and functional enrichment analyses for any sequenced genome of interest. Nucleic Acids Res 51:D638–D646.

25. Preston A, Mandrell RE, Gibson BW, Apicella MA. 1996. The lipooligosaccharides of pathogenic gram-negative bacteria. Crit Rev Microbiol 22:139–180.

26. Boll JM, Crofts AA, Peters K, Cattoir V, Vollmer W, Davies BW, Trent MS. 2016. A penicillin-binding protein inhibits selection of colistin-resistant, lipooligosaccharide-deficient Acinetobacter baumannii. Proceedings of the National Academy of Sciences 113:E6228–E6237.

27. Powers MJ, Trent MS. 2018. Phospholipid retention in the absence of asymmetry strengthens the outer membrane permeability barrier to last-resort antibiotics. Proc Natl Acad Sci U S A 115:E8518–E8527.

28. Sabnis A, Hagart KL, Klöckner A, Becce M, Evans LE, Furniss RCD, Mavridou DA, Murphy R, Stevens MM, Davies JC, Larrouy-Maumus GJ, Clarke TB, Edwards AM. 2021. Colistin kills bacteria by targeting lipopolysaccharide in the cytoplasmic membrane. eLife 10:e65836.

29. Moffatt JH, Harper M, Harrison P, Hale JDF, Vinogradov E, Seemann T, Henry R, Crane B, St. Michael F, Cox AD, Adler B, Nation RL, Li J, Boyce JD. 2010. Colistin Resistance in Acinetobacter baumannii Is Mediated by Complete Loss of Lipopolysaccharide Production. Antimicrobial Agents and Chemotherapy 54:4971–4977.

30. 2024. BIONF/fDOG. Python. BIONF.

31. Hong Y, Liu MA, Reeves PR. 2017. Progress in Our Understanding of Wzx Flippase for Translocation of Bacterial Membrane Lipid-Linked Oligosaccharide. J Bacteriol 200:e00154-17.

32. Hong Y, Reeves PR. 2014. Diversity of o-antigen repeat unit structures can account for the substantial sequence variation of wzx translocases. J Bacteriol 196:1713–1722.

33. VanOtterloo LM, Macias LA, Powers MJ, Brodbelt JS, Trent MS. 2024. Characterization of Acinetobacter baumannii core oligosaccharide synthesis reveals novel aspects of lipooligosaccharide assembly. mBio 15:e03013-23.

34. Vassallo CN, Doering CR, Littlehale ML, Teodoro GIC, Laub MT. 2022. A functional selection reveals previously undetected anti-phage defence systems in the E. coli pangenome. Nat Microbiol 7:1568–1579.

35. Tesson F, Hervé A, Mordret E, Touchon M, d'Humières C, Cury J, Bernheim A. 2022. Systematic and quantitative view of the antiviral arsenal of prokaryotes. Nat Commun 13:2561.

36. Fornelos N, Browning DF, Butala M. 2016. The Use and Abuse of LexA by Mobile Genetic Elements. Trends in Microbiology 24:391–401.

37. Auchtung JM, Lee CA, Monson RE, Lehman AP, Grossman AD. 2005. Regulation of a Bacillus subtilis mobile genetic element by intercellular signaling and the global DNA damage response. Proc Natl Acad Sci U S A 102:12554–12559.

38. Lane D, Cavaillé J, Chandler M. 1994. Induction of the SOS response by IS1 transposase. J Mol Biol 242:339–350.

39. Cardinale CJ, Washburn RS, Tadigotla VR, Brown LM, Gottesman ME, Nudler E. 2008. Termination Factor Rho and Its Cofactors NusA and NusG Silence Foreign DNA in E. coli. Science 320:935–938.

40. Yakhnin AV, Bubunenko M, Mandell ZF, Lubkowska L, Husher S, Babitzke P, Kashlev M. 2023. Robust regulation of transcription pausing in Escherichia coli by the ubiquitous elongation factor NusG. Proc Natl Acad Sci U S A 120:e2221114120.

41. Robinson A, Brzoska AJ, Turner KM, Withers R, Harry EJ, Lewis PJ, Dixon NE. 2010. Essential Biological Processes of an Emerging Pathogen: DNA Replication, Transcription, and Cell Division in Acinetobacter spp. Microbiol Mol Biol Rev 74:273–297.

42. Wishart DS, Han S, Saha S, Oler E, Peters H, Grant JR, Stothard P, Gautam V. 2023. PHASTEST: faster than PHASTER, better than PHAST. Nucleic Acids Res 51:W443–W450.

43. Hare JM, Bradley JA, Lin C-L, Elam TJ. 2012. Diverse responses to UV light exposure in Acinetobacter include the capacity for DNA damage-induced mutagenesis in the opportunistic pathogens Acinetobacter baumannii and Acinetobacter ursingii. Microbiology (Reading) 158:601–611.

44. Hubloher JJ, Van der Sande L, Schaudinn C, Müller V, Averhoff B. 2023. The Tol-Pal system of Acinetobacter baumannii is important for cell morphology, antibiotic resistance and virulence. Int Microbiol 26:543–550.

45. Knight Daniel, Dimitrova Daniela D., Rudin Susan D., Bonomo Robert A., Rather Philip N. 2016. Mutations Decreasing Intrinsic β-Lactam Resistance Are Linked to Cell Division in the Nosocomial Pathogen Acinetobacter baumannii. Antimicrobial Agents and Chemotherapy 60:3751–3758.

46. Ursinus A, van den Ent F, Brechtel S, de Pedro M, Höltje J-V, Löwe J, Vollmer W. 2004. Murein (peptidoglycan) binding property of the essential cell division protein FtsN from Escherichia coli. J Bacteriol 186:6728–6737.

47. Gerding MA, Liu B, Bendezú FO, Hale CA, Bernhardt TG, de Boer PAJ. 2009. Self-enhanced accumulation of FtsN at Division Sites and Roles for Other Proteins with a SPOR domain (DamX, DedD, and RlpA) in Escherichia coli cell constriction. J Bacteriol 191:7383–7401.

48. Law CW, Alhamdoosh M, Su S, Dong X, Tian L, Smyth GK, Ritchie ME. 2016. RNA-seq analysis is easy as 1-2-3 with limma, Glimma and edgeR. F1000Res 5:ISCB Comm J-1408.

49. Rogers D, Hahn M. 2010. Extended-Connectivity Fingerprints. J Chem Inf Model 50:742–754.

50. Guha R. 2007. Chemical Informatics Functionality in *R*. J Stat Soft 18.

51. Tanimoto, TT. 1957. IBM Internal Report.

52. Rogers DJ, Tanimoto TT. 1960. A Computer Program for Classifying Plants: The computer is programmed to simulate the taxonomic process of comparing each case with every other case. Science 132:1115–1118.

53. Xu J, Zhou F, Ji B-P, Pei R-S, Xu N. 2008. The antibacterial mechanism of carvacrol and thymol against Escherichia coli. Lett Appl Microbiol 47:174–179.

54. Epand RF, Pollard JE, Wright JO, Savage PB, Epand RM. 2010. Depolarization, bacterial membrane composition, and the antimicrobial action of ceragenins. Antimicrob Agents Chemother 54:3708–3713.

55. Rzycki M, Drabik D, Szostak-Paluch K, Hanus-Lorenz B, Kraszewski S. 2021. Unraveling the mechanism of octenidine and chlorhexidine on membranes: Does electrostatics matter? Biophys J 120:3392–3408.

56. Lashinsky JN, Henig O, Pogue JM, Kaye KS. 2017. Minocycline for the Treatment of Multidrug and Extensively Drug-Resistant A. baumannii: A Review. Infect Dis Ther 6:199–211.

57. Rose WE, Rybak MJ. 2006. Tigecycline: first of a new class of antimicrobial agents. Pharmacotherapy 26:1099–1110.

58. Stewart-Tull DE, Armstrong AV. 1972. The effect of 1-hydroxyphenazine and pyocyanin from Pseudomonas aeruginosa on mammalian cell respiration. J Med Microbiol 5:67–73.

59. Bisschop A, Bergsma J, Konings WN. 1979. Site of interaction between phenazine methosulphate and the respiratory chain of Bacillus subtilis. Eur J Biochem 93:369–374.

60. Donadio G, Mensitieri F, Santoro V, Parisi V, Bellone ML, De Tommasi N, Izzo V, Dal Piaz F. 2021. Interactions with Microbial Proteins Driving the Antibacterial Activity of Flavonoids. Pharmaceutics 13:660.

61. Taheri Y, Suleria HAR, Martins N, Sytar O, Beyatli A, Yeskaliyeva B, Seitimova G, Salehi B, Semwal P, Painuli S, Kumar A, Azzini E, Martorell M, Setzer WN, Maroyi A, Sharifi-Rad J. 2020. Myricetin bioactive effects: moving from preclinical evidence to potential clinical applications. BMC Complement Med Ther 20:241.

62. Zhang G, Baidin V, Pahil KS, Moison E, Tomasek D, Ramadoss NS, Chatterjee AK, McNamara CW, Young TS, Schultz PG, Meredith TC, Kahne D. 2018. Cell-based screen for discovering lipopolysaccharide biogenesis inhibitors. Proc Natl Acad Sci U S A 115:6834–6839.

63. Richie DL, Takeoka KT, Bojkovic J, Metzger LE, Rath CM, Sawyer WS, Wei J-R, Dean CR. 2016. Toxic Accumulation of LPS Pathway Intermediates Underlies the Requirement of LpxH for Growth of Acinetobacter baumannii ATCC 19606. PLoS One 11:e0160918.

64. Wang H, Ishchenko A, Skudlarek J, Shen P, Dzhekieva L, Painter RE, Chen Y-T, Bukhtiyarova M, Leithead A, Tracy R, Babaoglu K, Bahnck-Teets C, Buevich A, Cabalu TD, Labroli M, Lange H, Lei Y, Li W, Liu J, Mann PA, Meng T, Mitchell HJ, Mulhearn J, Scapin G, Sha D, Shaw AW, Si Q, Tong L, Wu C, Wu Z, Xiao JC, Xu M, Zhang L-K, McKenney D, Miller RR, Black TA, Cooke A, Balibar CJ, Klein DJ, Raheem I, Walker SS. 2024. Cerastecins inhibit membrane lipooligosaccharide transport in drug-resistant Acinetobacter baumannii. Nat Microbiol 9:1244–1255.

65. Sampson BA, Misra R, Benson SA. 1989. Identification and characterization of a new gene of Escherichia coli K-12 involved in outer membrane permeability. Genetics 122:491–501.

66. Ruiz N, Falcone B, Kahne D, Silhavy TJ. 2005. Chemical conditionality: a genetic strategy to probe organelle assembly. Cell 121:307–317.

67. Singh MP, Petersen PJ, Weiss WJ, Janso JE, Luckman SW, Lenoy EB, Bradford PA, Testa RT, Greenstein M. 2003. Mannopeptimycins, new cyclic glycopeptide antibiotics produced by Streptomyces hygroscopicus LL-AC98: antibacterial and mechanistic activities. Antimicrob Agents Chemother 47:62–69.

68. Zampaloni C, Mattei P, Bleicher K, Winther L, Thäte C, Bucher C, Adam J-M, Alanine A, Amrein KE, Baidin V, Bieniossek C, Bissantz C, Boess F, Cantrill C, Clairfeuille T, Dey F, Di Giorgio P, du Castel P, Dylus D, Dzygiel P, Felici A, García-Alcalde F, Haldimann A, Leipner M, Leyn S, Louvel S, Misson P, Osterman A, Pahil K, Rigo S, Schäublin A, Scharf S, Schmitz P, Stoll T, Trauner A, Zoffmann S, Kahne D, Young JAT, Lobritz MA, Bradley KA. 2024. A novel antibiotic class targeting the lipopolysaccharide transporter. Nature 625:566–571.

69. Pahil KS, Gilman MSA, Baidin V, Clairfeuille T, Mattei P, Bieniossek C, Dey F, Muri D, Baettig R, Lobritz M, Bradley K, Kruse AC, Kahne D. 2024. A new antibiotic traps lipopolysaccharide in its intermembrane transporter. Nature 625:572–577.

70. Faoro C, Wilkinson-White L, Kwan AH, Ataide SF. 2018. Discovery of fragments that target key interactions in the signal recognition particle (SRP) as potential leads for a new class of antibiotics. PLoS One 13:e0200387.

71. Jumper J, Evans R, Pritzel A, Green T, Figurnov M, Ronneberger O, Tunyasuvunakool K, Bates R, Žídek A, Potapenko A, Bridgland A, Meyer C, Kohl SAA, Ballard AJ, Cowie A, Romera-Paredes B, Nikolov S, Jain R, Adler J, Back T, Petersen S, Reiman D, Clancy E, Zielinski M, Steinegger M, Pacholska M, Berghammer T, Bodenstein S, Silver D, Vinyals O, Senior AW, Kavukcuoglu K, Kohli P, Hassabis D. 2021. Highly accurate protein structure prediction with AlphaFold. Nature 596:583–589.

72. Goehring NW, Beckwith J. 2005. Diverse paths to midcell: assembly of the bacterial cell division machinery. Curr Biol 15:R514-526.

73. Amaral L, Martins A, Spengler G, Molnar J. 2014. Efflux pumps of Gram-negative bacteria: what they do, how they do it, with what and how to deal with them. Front Pharmacol 4:168.

74. Hope R, Warner M, Mushtaq S, Ward ME, Parsons T, Livermore DM. 2005. Effect of medium type, age and aeration on the MICs of tigecycline and classical tetracyclines. J Antimicrob Chemother 56:1042–1046.

75. Xiong Y, Liu W, Huang Q, Wang J, Wang Y, Li H, Fu X. 2018. Tigecycline as a dual inhibitor of retinoblastoma and angiogenesis via inducing mitochondrial dysfunctions and oxidative damage. Sci Rep 8:11747.

76. Romero PR, Karp PD. 2004. Using functional and organizational information to improve genome-wide computational prediction of transcription units on pathway-genome databases. Bioinformatics 20:709–717.

77. Banta AB, Ward RD, Tran JS, Bacon EE, Peters JM. 2020. Programmable Gene Knockdown in Diverse Bacteria Using Mobile-CRISPRi. CP Microbiology 59:e130.

78. Varadi M, Anyango S, Deshpande M, Nair S, Natassia C, Yordanova G, Yuan D, Stroe O, Wood G, Laydon A, Žídek A, Green T, Tunyasuvunakool K, Petersen S, Jumper J, Clancy E, Green R, Vora A, Lutfi M, Figurnov M, Cowie A, Hobbs N, Kohli P, Kleywegt G, Birney E, Hassabis D, Velankar S. 2022. AlphaFold Protein Structure Database: massively expanding the structural coverage of protein-sequence space with high-accuracy models. Nucleic Acids Res 50:D439–D444.

79. Evans R, O'Neill M, Pritzel A, Antropova N, Senior A, Green T, Žídek A, Bates R, Blackwell S, Yim J, Ronneberger O, Bodenstein S, Zielinski M, Bridgland A, Potapenko A, Cowie A, Tunyasuvunakool K, Jain R, Clancy E, Kohli P, Jumper J, Hassabis D. 2021. Protein complex prediction with AlphaFold-Multimer https://doi.org/10.1101/2021.10.04.463034.

80. Ducret A, Quardokus EM, Brun YV. 2016. MicrobeJ, a tool for high throughput bacterial cell detection and quantitative analysis. Nat Microbiol 1:16077.

81. Bacon EE, Tran JS, Nadig N, Peters JM. 2024. Modular, inducible, and titratable expression systems for *Escherichia coli* and *Acinetobacter baumannii*. bioRxiv 2024.05.28.596346.

CHAPTER 4

Modular, inducible, and titratable expression systems for *Escherichia coli* and *Acinetobacter baumannii*

A version of this chapter has been submitted for publication:

Emily E. Bacon*, Jennifer S. Tran*, Nischala Nadig, Jason M. Peters. 2024. Modular, inducible, and titratable expression systems for *Escherichia coli* and *Acinetobacter baumannii*. bioRxiv [Preprint]. 2024 May 29:2024.05.28.596346. doi: 10.1101/2024.05.28.596346.

I performed flow experiments, created the P_{abstBR} promoter, analyzed data, and generated figures. EEB constructed initial plasmids and performed expression experiments. NN created additional plasmids and validated expression and transfer efficiencies. I wrote the text with EEB, and JMP provided feedback and edits. Supplementary figures can be found at the end of the chapter.

Abstract

Gene expression systems that transcend species barriers are needed for cross-species analysis of gene function. In particular, expression systems that can be utilized in both model and pathogenic bacteria underpin comparative functional approaches that inform conserved and variable features of bacterial physiology. Here, we develop replicative and integrative vectors alongside a novel, IPTG-inducible promoter that can be used in the model bacterium *Escherichia coli* K-12 as well as strains of the antibiotic-resistant pathogen, *Acinetobacter baumannii*. We generate modular vectors that transfer by conjugation at high efficiency and either replicate or integrate into the genome, depending on design. Embedded in these vectors, we also developed a synthetic, IPTG-inducible promoter, P_{abstBR}, that induces to a high level, but is less leaky than the commonly used *trc* promoter. We show that P_{abstBR} is titratable at both the population and single cell level, regardless of species, highlighting the utility of our expression systems for cross-species functional studies. Finally, as a proof of principle, we use our integrating vector to develop a reporter for the *E. coli* envelope stress σ factor, RpoE, and deploy the reporter in *E. coli* and *A. baumannii*, finding that *A. baumannii* does not recognize RpoE-dependent promoters unless RpoE is heterologously expressed. We envision that these vector and promoter tools will be valuable for the community of researchers that study fundamental biology of *E. coli* and *A. baumannii*.

Importance

Acinetobacter baumannii is a multidrug-resistant, hospital-acquired pathogen with the ability to cause severe infections. Understanding the unique biology of this non-model bacterium may lead to the discovery of new weaknesses that can be targeted to treat antibiotic-resistant infections. Here, we provide expression tools that can be used to study gene function in *A. baumannii*, including in drug-resistant clinical isolates. These tools are also compatible with the model bacterium, *Escherichia coli*, enabling cross-species comparisons of gene function. We anticipate that the use of these tools by the scientific community will accelerate our understanding of *Acinetobacter* biology.

Introduction

Historically, research in bacterial genetics focused on specific model organisms, such as *Escherichia coli* K-12, due to a lack of techniques, tools, reagents, genome sequences, and general knowledge of non-model bacteria (1, 2). As a result, much of our current understanding about the basic physiology of Gram-negative bacteria comes from *E. coli* (3, 4). Although most core cellular processes are likely conserved, gene function and regulation can vary subtly or even dramatically across species boundaries (4, 5). Such deviation is obvious in pathogens such as *Acinetobacter baumannii*, which has adopted many traits that are distinct from *E. coli* K-12—most notably extreme antibiotic resistance (6-8). With advances in DNA sequencing and synthesis as well as tools that democratize genetic analysis across species (e.g., CRISPR approaches (9)), there now exists an enormous opportunity to shrink the knowledge and technique gaps between model bacteria and clinically relevant pathogens. One simple approach to bridge the gap would be to develop systems capable of assessing gene function in both model and pathogenic bacteria, such that the function of any gene could be readily compared in different strain or species backgrounds.

Here, we focus on genetic tools that function in the antibiotic-resistant pathogen, *A. baumannii*. *A. baumannii* is considered an "urgent threat" by the Centers for Disease Control and Prevention due to its ability to resist nearly all available antibiotic treatments (10). Although some promising new anti-*Acinetobacter* compounds have recently been discovered (11, 12), more work is needed in this area as *Acinetobacter* is adept at acquiring and developing new resistance mechanisms (13-15). *A. baumannii* is poorly studied compared to *E. coli* K-12 and even other Gram-negative pathogens such as *Pseudomonas aeruginosa*; however, understanding the distinct physiology of *A. baumannii* is critical to developing new treatments (16, 17). For instance, lipid A, an essential component of the outer membrane in most Gram-negatives and a binding site for the antibiotic colistin (18), is not

essential for viability in many *A. baumannii* strains including clinical isolates (19). Further, regulation of stress pathways that could play roles in antibiotic resistance, tolerance, or persistence is distinct in *A. baumannii* compared to other γ-proteobacteria, as *A. baumannii* lacks conserved transcription factors such as the stationary phase sigma (σ) factor, RpoS (20, 21).

Vectors that are capable of replicating in or integrating into *E. coli* and *A. baumannii* have been previously described, but also share important limitations. Replicative shuttle vectors typically use a high-copy, ColE1 origin of replication for *E. coli* and either the pWH1266 (22) or pRSF1010 (23) origin for *A. baumannii*. The pWH1266 and pRSF1010 origins are compatible in *A. baumannii*, enabling expression from two replicative vectors in the same cell (23). Integrative vectors based on the site-specific transposon Tn*7* insert DNA cargo into the genome downstream of the *glmS* gene and have been used extensively in *E. coli* (24), *A. baumannii* (25-27), and many other species (28, 29). However, many of these vectors were not designed to contain easily swappable modules (e.g., different antibiotic markers) outside of standard multiple cloning sites (MCS). Existing vectors typically employ inducible promoters that are either native to or designed for use in *E. coli* (30, 31). These include *E. coli* native promoters such as P_{lac} and P_{araBAD} that can be induced with IPTG or arabinose, respectively (22, 32), or semi-synthetic promoters such as P_{tac} and P_{trc} which are IPTG-inducible (23). Unfortunately, characteristics of these promoters pose challenges for precise control of expression. For instance, P_{araBAD} expression cannot be titrated with sub-saturating concentrations of its inducer, arabinose, due to "all or nothing" effects that result in a fraction of cells inducing at high level while others show minimal activity (33-35). P_{tac} and P_{trc} are sufficiently leaky that genes placed under their control often complement deletion phenotypes in the absence of inducer (30, 36, 37), and full induction often results in overexpression toxicity (38). A titratable promoter with less leakiness and a lower maximal level of expression would be ideal for physiological expression and gene function studies in *A. baumannii*.

In this work, we generate useful reagents for gene function studies in *A. baumannii* and *E. coli*. We create modular vectors that replicate or integrate in both species, and carry the novel promoter P_{abstBR}, which can be induced and titrated with IPTG. In a proof of principle experiment, we combine all three reagents to probe the activity of the *E. coli* envelope stress σ factor, RpoE, in both species.

Results and Discussion

Modular replicative and integrating vectors for E. coli and A. baumannii

We sought to construct a modular set of replicative and integrative vectors that could be used to examine gene function in *A. baumannii* and *E. coli*. Our shuttle vector (Fig 4.1A) replicates in *E. coli* using the medium copy origin, p15A (20-30 copies per cell (39)), and in *A. baumannii* using the low copy origin pWH1266 (~9 copies per cell (40)). Our integrating vector (Fig 4.1A) inserts into the genomes of *E. coli* and *A. baumannii* downstream of *glmS* using the Tn*7* transposase (provided on a separate plasmid (9, 28)). Both vectors have an antibiotic module flanked by XhoI sites, which provide a facile way of removing the existing resistance marker while simultaneously linearizing the plasmid as a substrate for Gibson assembly (41). Here, we have provided hygromycin, apramycin, and kanamycin versions of both replicative and integrative vectors. We note that hygromycin and apramycin are attractive resistance markers for studying multidrug-resistant pathogens given that neither antibiotic is used against *A. baumannii* clinically (25, 42). FRT sites in the integrative vector allow for optional FLP recombinase-mediated excision of the antibiotic marker (43, 44). The cloning module, or multiple cloning site (MCS), has several restriction sites for cloning genes of interest (Fig 4.1B-C). Although other sites can be used, we recommend cloning into NcoI because it contains a translation start codon (ATG) in alignment with a strong upstream ribosome binding site (RBS) taken from the classic expression vector pTrc99a (45). The promoter module exists between AatII and NcoI sites for the replicating vector and SpeI and NcoI sites for the integrating vector. We provide

Figure 4.1. Modular replicative and integrative expression vectors. (A) Circular plasmid map and features of the replicative shuttle vector containing both *E. coli* and *A. baumannii* origins of replication (top) and the Tn*7* expression vector containing a transposon that will integrate into the chromosomal att_{Tn7} site (bottom). Available antibiotic resistance cassettes (AbR) are listed. Maps are adapted from SnapGene (GSL Biotech). (B and C) Linear maps showing the modular promoter region and multiple cloning sites (MCS) for the replicative plasmid and Tn*7* vector. NcoI site provides an ATG start codon optimally proximal to a strong ribosome binding site (RBS).

Figure 4.1

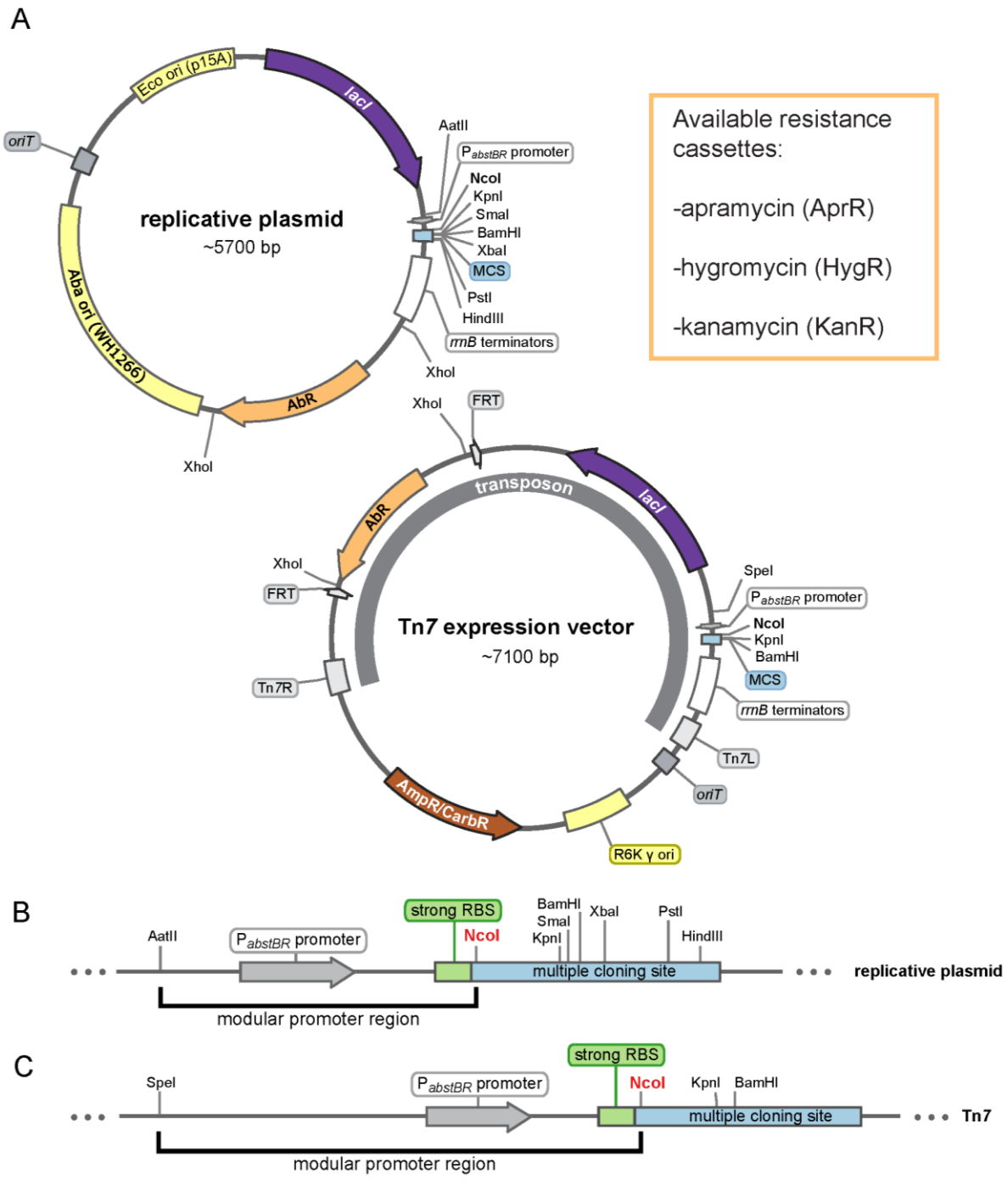
A
Eco ori (p15A)
lacI
oriT
AatII
PabstBR promoter
NcoI
KpnI
SmaI
BamHI
XbaI
MCS
PstI
HindIII
rrnB terminators
XhoI
replicative plasmid
~5700 bp
Aba ori (WH1266)
AbR
XhoI
Available resistance cassettes:
-apramycin (AprR)
-hygromycin (HygR)
-kanamycin (KanR)
XhoI
FRT
transposon
lacI
AbR
XhoI
FRT
SpeI
PabstBR promoter
NcoI
KpnI
BamHI
MCS
rrnB terminators
Tn7 expression vector
~7100 bp
Tn7R
Tn7L
oriT
AmpR/CarbR
R6K γ ori
B
strong RBS
BamHI
SmaI
KpnI
XbaI
PstI
HindIII
AatII
PabstBR promoter
NcoI
multiple cloning site
replicative plasmid
modular promoter region
C
strong RBS
SpeI
PabstBR promoter
NcoI
KpnI
BamHI
multiple cloning site
Tn7
modular promoter region

these vectors with a novel, IPTG-inducible promoter (P_{abstBR}, described below), but other promoters and RBSs of interest can be readily swapped into the module. Additionally, both the replicative and integrative vectors can be used in the same strain as multiple markers are available and only one vector replicates, ruling out compatibility issues.

We next determined the efficiency of transfer for both vectors into *E. coli* and *A. baumannii*. Both vectors contain *oriT* sites, enabling transfer by conjugation from *E. coli* cells that are auxotrophic for diaminopimelic acid (DAP^-) to DAP^+ recipient bacteria followed by antibiotic selection to recover only vector-containing recipients. Additionally, both vectors can be transferred by electroporation into competent recipient cells, if desired. To quantify efficiency of transfer by conjugation, we mated DAP^- *E. coli* donor cells (*E. coli* K-12 WM6026) with model strains of *E. coli* K-12 (BW25113) and *A. baumannii* (ATCC 17978). We found that both vectors were transferred at efficiencies consistent with use in downstream experiments ranging in scale from individual genes to large libraries (Fig 4.S1A-B). Transfers of both the replicative and integrative vectors were highly efficient in *E. coli* ($>10^{-1}$ efficiencies for both vectors) and *A. baumannii* ($>10^{-2}$ and 10^{-4} efficiencies for replicative and integrative vectors, respectively). Importantly, our observed transfer efficiencies were on par with those needed for library construction for genome-scale experiments (9). We note that we observed instances of unintended integration of the Tn*7* vector backbone in both *E. coli* and *A. baumannii* (i.e., co-integrates (46)). The presence of such co-integrates in recipient colonies can be tested by screening for the *ampR*/*bla* gene (which confers carbenicillin resistance) present in the vector backbone. We patched 40 transconjugants for each organism, and while the frequency of integration with the vector backbone was relatively low (≤3/40 for each), we recommend testing transconjugants to verify insertion accuracy (Fig 4.S1C). Taken together, we have created modular replicative and integrative vectors for *E. coli* and *A. baumannii* that can be transferred at efficiencies that are useful for a variety of applications.

A tightly regulated, IPTG-inducible promoter for E. coli and A. baumannii

We sought to develop an IPTG-inducible promoter with low leakiness and high expression for *A. baumannii*. We previously found that a broadly utilized synthetic promoter in *E. coli*, $P_{LlacO-1}$, was unstable when used to express a toxic protein in *A. baumannii* (dCas9) (27). When we selected for mutants with stable expression of dCas9, we found that *lacO* repeats in the promoter had collapsed, creating a new IPTG-regulated promoter (Fig 4.2A, *Acinetobacter* Suppressor of Toxicity or P_{abst}). We hypothesized this promoter was weaker due to its success at repressing toxicity. To measure promoter activity in *A. baumannii*, we cloned P_{abst} upstream of a gene encoding Superfolder Green Fluorescent Protein (*sfgfp*) in our replicative vector (Fig 4.2B). Our measurements confirmed that P_{abst} expression was very weak, with less than 2-fold increase in expression at saturating levels of inducer. This weak activity is likely due to divergence between the P_{abst} -35 element (TTATAA) and the consensus σ^{70} -35 (TTGACA), especially at the -33 position (A versus G, respectively).

To generate a new promoter with higher activity but without repeating *lacO* elements, we used site-directed mutagenesis to replace the P_{abst} -35 sequence with a consensus -35 (Fig 4.2A). We found that the new promoter, P_{abstBR} (*Acinetobacter* Suppressor of Toxicity with Better Regulation), showed significantly higher induction than P_{abst} (~150-fold; Welch's *t*-test, p=0.003) in *A. baumannii* (Fig 4.2B). P_{abstBR} also showed ~3-fold reduced leakiness compared to P_{trc}, a popular IPTG-inducible promoter used in both *E. coli* (30) and *A. baumannii* (23); although induction at saturating levels of IPTG was somewhat lower (~3-fold) than P_{trc}. With reduced leakiness and a more physiologically appropriate expression range, P_{abstBR} has advantages for complementation and expression with reduced toxicity (36, 47).

Figure 4.2. P_{abstBR} promoter construction and expression. (A) Promoter sequences showing the homologous recombination event in *lacO* repeat regions (red) of the $P_{LlacO-1}$ sequence that produces P_{abst}, which contains a -35-like region (yellow). Site-directed mutagenesis reverts the -35 region back to consensus (orange) to create P_{abstBR}. (B) Dot plots showing sfGFP fluorescence from replicative vectors containing *sfgfp* under P_{abst}, P_{abstBR}, or P_{trc} promoters in *A. baumannii* ATCC 17978 with no IPTG (left) or 1 mM IPTG (right). Values were normalized to empty vector controls, and sample means are represented by a solid horizontal line (n=3 biological replicates). Asterisks and ns indicate significant and not significant sample differences, respectively (Welch's *t*-tests; p-values < 0.05).

Figure 4.2

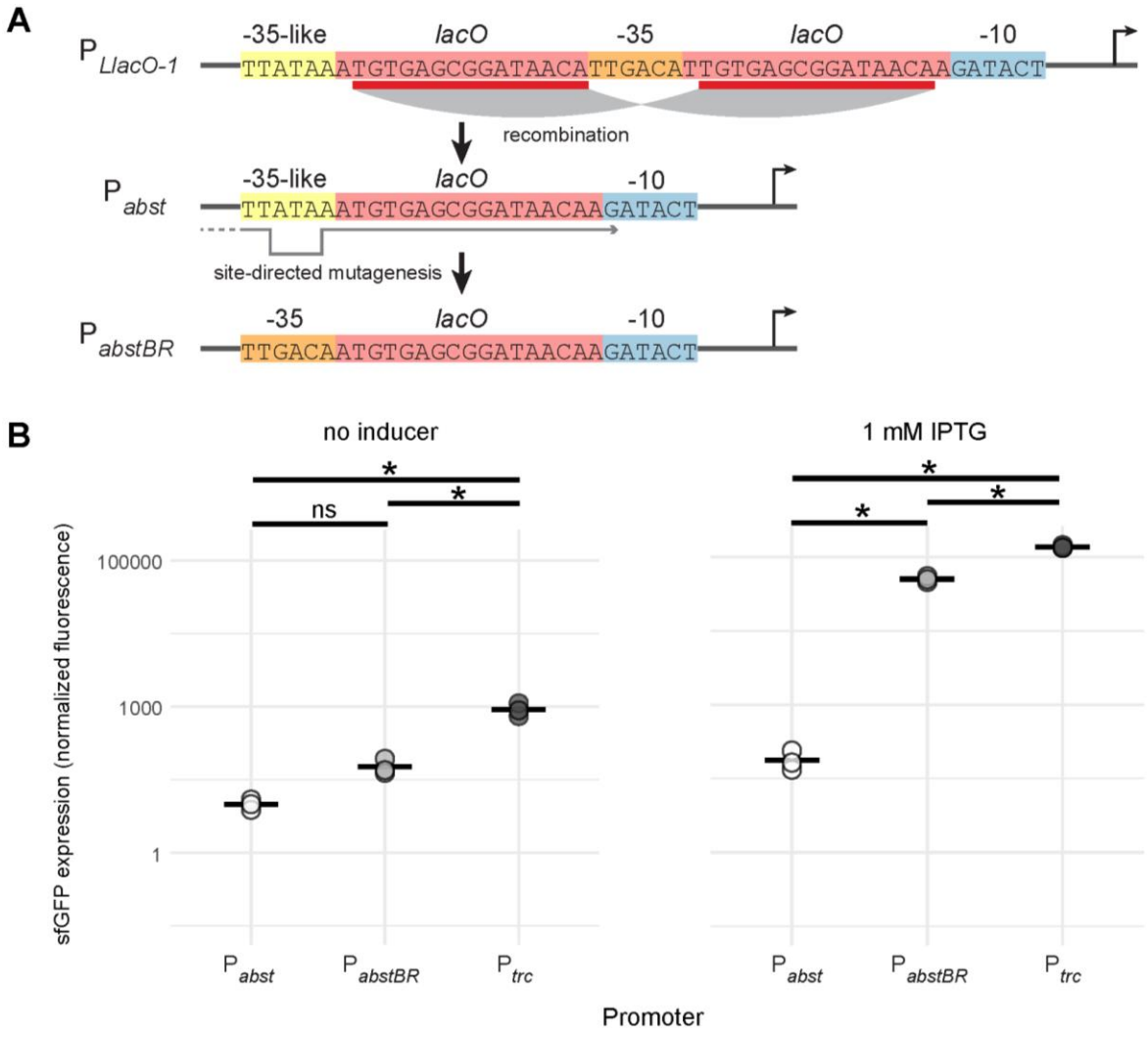
A
P LlacO-1
-35-like
lacO
-35
lacO
-10
TTATAAATGTGAGCGGATAACATTGACATTGTGAGCGGATAACAAGATACT
recombination
P abst
-35-like
lacO
-10
TTATAAATGTGAGCGGATAACAAGATACT
site-directed mutagenesis
P abstBR
-35
lacO
-10
TTGACAATGTGAGCGGATAACAAGATACT
B
no inducer
1 mM IPTG
ns
*
sfGFP expression (normalized fluorescence)
100000
1000
1
P abst
P abstBR
P trc
Promoter

P_{abstBR} expression is titratable at the population and single cell level

Investigators frequently titrate promoter activity to determine expression-phenotype relationships and avoid toxic overexpression. To determine if P_{abstBR} expression is titratable at the population level, we induced expression of P_{abstBR}-*sfgfp* at varying concentrations of IPTG from both our replicative and integrative vectors in *E. coli* K-12 BW25113 and *A. baumannii* ATCC 17978 (Fig 4.3A and 3B). We found that P_{abstBR} was titratable in all tested contexts. Plasmid-borne P_{abstBR} showed similar patterns of IPTG induction in both *E. coli* and *A. baumannii* and had ~10-fold higher level of maximal expression compared to an integrated copy. Unexpectedly, Tn*7* integrated P_{abstBR} showed a higher apparent level of expression in *A. baumannii* compared to *E. coli* at nearly every concentration of IPTG, including saturating concentrations (Fig 4.3B). In addition to 17978, the *A. baumannii* field uses strains ATCC 19606 and AB5075 as antibiotic susceptible and resistant models, respectively. To test P_{abstBR} titratability in those strain backgrounds, we again expressed P_{abstBR}-*sfgfp* at varying IPTG concentrations (Fig 4.S2). As expected, we found that P_{abstBR} was titratable at the population level.

Inducible promoters can erroneously appear to be titratable at the population level due to varying subpopulations of fully induced cells, as is seen in systems with active transport and feedback of inducer molecules (e.g., arabinose and P_{araBAD} (33)). To rule out this possibility, we measured induction of P_{abstBR}-*sfgfp* at varying concentrations of IPTG in single cells using flow cytometry (Fig 4.4A and 4B). We measured P_{abstBR} expression from replicative vectors as we reasoned that variations in plasmid copy number would be more likely to have a subpopulation effect. We found that P_{abstBR} was fully titratable at the single cell level in *E. coli* K-12 BW25113 and *A. baumannii* ATCC 17978. Distributions of sfGFP fluorescence were unimodal at all IPTG concentrations in both species, consistent with relatively uniform induction of P_{abstBR} at the single cell level. Although increasing concentrations of IPTG fully shifted the sfGFP distributions in *A. baumannii*, the

Figure 4.3. Titration of P_{abstBR} expression at the population level. Titration of expression from (A) the replicative plasmid or (B) the Tn*7* transposon. Plots shown are normalized sfGFP levels expressed from P_{abstBR} across IPTG concentrations for *E. coli* BW25113 and *A. baumannii* ATCC 17978. Error bars represent standard deviation (n=3 biological replicates for replicative vector, n=6 biological replicates for Tn*7* transposon).

Figure 4.3

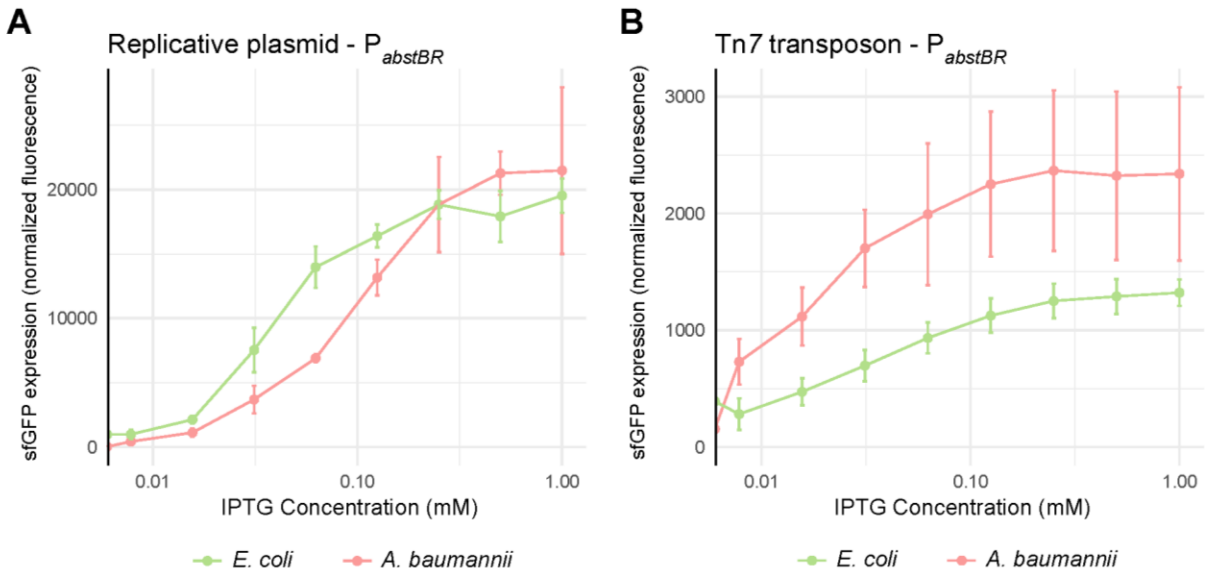
A
Replicative plasmid - P abstBR
sfGFP expression (normalized fluorescence)
20000
10000
0
0.01
0.10
1.00
IPTG Concentration (mM)
E. coli
A. baumannii
B
Tn7 transposon - P abstBR
sfGFP expression (normalized fluorescence)
3000
2000
1000
0
0.01
0.10
1.00
IPTG Concentration (mM)
E. coli
A. baumannii

Figure 4.4. Titration of P_{abstBR} expression at the single-cell level. Titration of expression in (A) *E. coli* BW25113 or (B) *A. baumannii* ATCC 17978. Ridgeline plots depict overlapping density plots of sfGFP fluorescence for cells induced at different IPTG concentrations, measured by flow cytometry and expressed from the replicative expression vector under control of P_{abstBR}. EV are empty vector (no GFP) control samples in 1 mM IPTG.

Figure 4.4

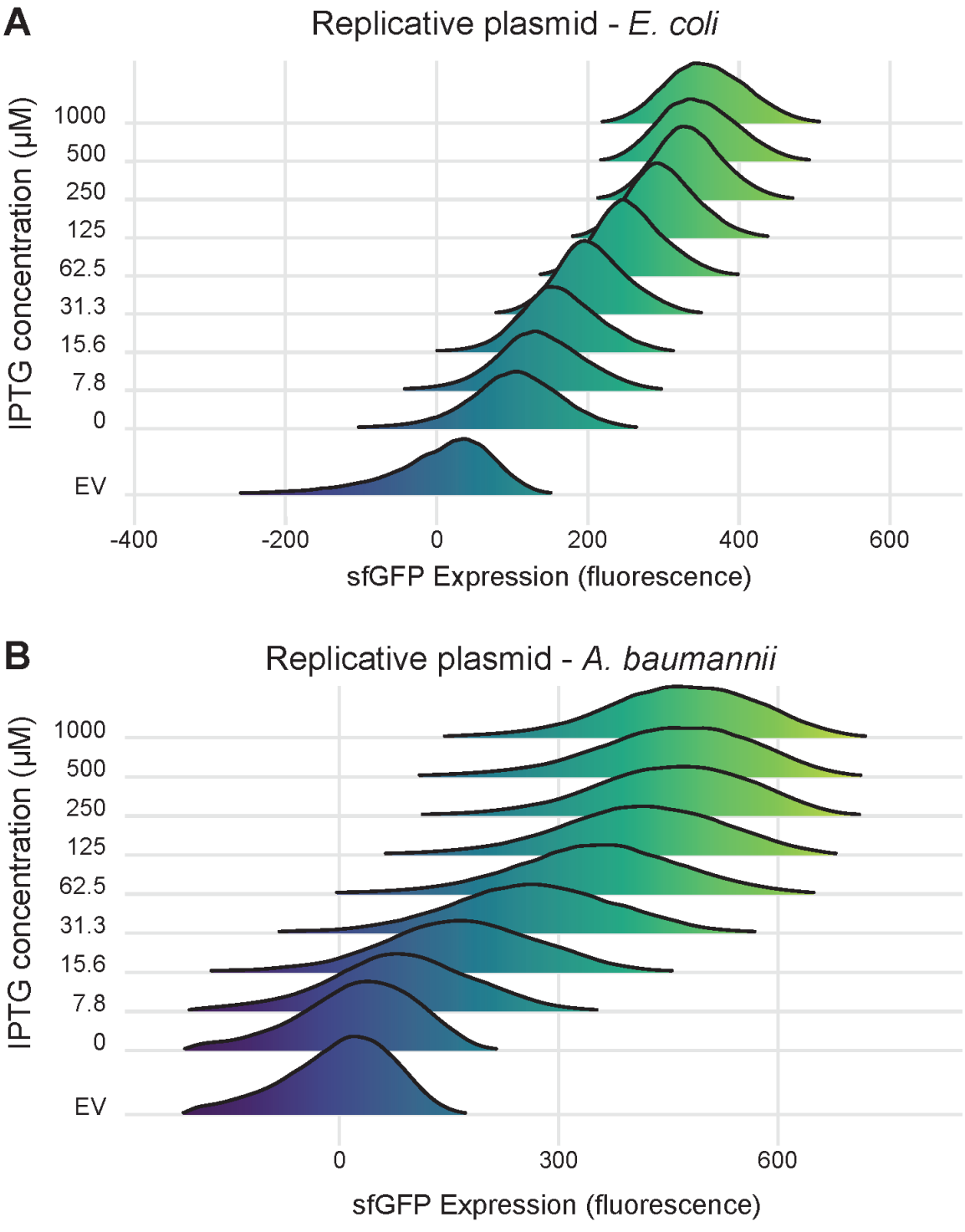
A
Replicative plasmid - E. coli
IPTG concentration (μM)
1000
500
250
125
62.5
31.3
15.6
7.8
0
EV
-400
-200
0
200
400
600
sfGFP Expression (fluorescence)
B
Replicative plasmid - A. baumannii
IPTG concentration (μM)
1000
500
250
125
62.5
31.3
15.6
7.8
0
EV
0
300
600
sfGFP Expression (fluorescence)

distributions were wider than those seen in *E. coli* for unknown reasons (Fig 4.4B). One possibility to explain increased expression variation in *A. baumannii* is simply that the pWH1266 origin has intrinsically greater plasmid copy number variation than p15A, although testing plasmid copy number at the single cell level is fraught with challenges (48). We conclude that P_{abstBR} is titratable at the single cell level, enabling gene function studies with precise levels of expression.

Modular vectors and P_{abstBR} enable gene regulation studies in E. coli and A. baumannii

As a proof of principle to demonstrate the utility of our P_{abstBR} vector set in studying gene function, we investigated RpoE promoter activity in *E. coli* and *A. baumannii*. RpoE, also known as σ^E, is an extracytoplasmic function (ECF) σ factor that regulates the envelope stress response in *E. coli* and related γ-proteobacteria (49-52). Species as distant from *E. coli* as *Pseudomonas aeruginosa* have a functional ortholog (AlgU, 66% identity) that recognizes the same DNA sequence as RpoE (53); however, a BLAST search of the *A. baumannii* genome recovered no hits for RpoE. To determine if *A. baumannii* recognizes RpoE-dependent promoters, we cloned the autoregulated *rpoE* promoter (P_{rpoE}) from *E. coli* into our integration vector upstream of a gene encoding monomeric Red Fluorescent Protein (*mrfp*) as a reporter. We integrated this construct into both *E. coli* and *A. baumannii* and found P_{rpoE} was only active in *E. coli* (Fig 5a and 5b). To determine if the promoter could be recognized in *A. baumannii* in the presence of RpoE, we cloned the *rpoE* gene into our replicating vector under the control of P_{abstBR}. We found that expression of RpoE in *A. baumannii* was sufficient to drive expression from P_{rpoE} (Fig 5a). This suggests that *A. baumannii* has no RpoE activity and that no other factors in *A. baumannii* can recognize RpoE promoters. As expected, we also found that overexpression of RpoE in *E. coli* resulted in increased P_{rpoE} activity (Fig 4.5B). Importantly, these results demonstrate the ability to utilize our integrative and replicative expression systems together, in the same strain, to better understand biology and gene function in both *E. coli* and *A. baumannii*.

Figure 4.5. Modular integrative and replicative vectors facilitate a functional reporter assay. (A) Graphical depiction of reporter assay experiments. Strains contain an mRFP reporter under control of the *E. coli*-native *rpoE* promoter (P_{rpoE}) in the att_{Tn7} site (constructed using the Tn*7* vector) and either a P_{abstBR}-*rpoE* overexpression vector or empty vector control (replicative plasmid). (B and C) Bar graphs of mRFP fluorescence from P_{rpoE} with and without expression of RpoE *in trans* from the replicative plasmid in *E. coli* or *A. baumannii*. As RpoE is native to *E. coli*, the *E. coli* strains also carry a copy of the *rpoE* gene on the chromosome. Fluorescence is normalized to no mRFP controls, and individual data points and standard deviation are displayed (n=6 biological replicates). Asterisks and ns indicate significant and not significant sample differences, respectively (Welch's *t*-tests; p-values < 0.05)

Figure 4.5

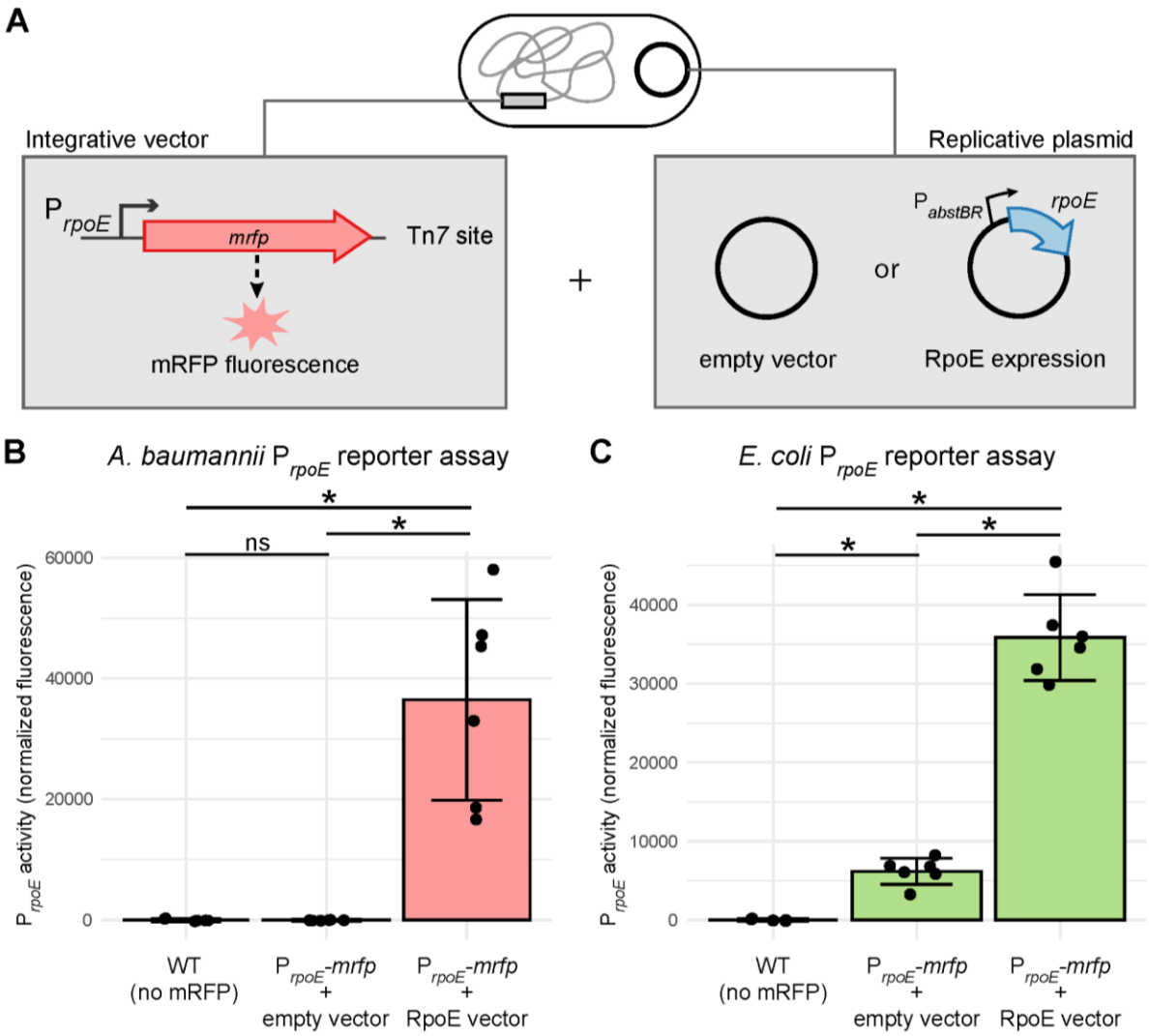
A
Integrative vector
Replicative plasmid
P rpoE
mrfp
Tn7 site
mRFP fluorescence
+
or
P abstBR
rpoE
empty vector
RpoE expression
B
A. baumannii P rpoE reporter assay
C
E. coli P rpoE reporter assay
P rpoE activity (normalized fluorescence)
ns
*
60000
40000
20000
0
30000
10000
WT
(no mRFP)
P rpoE-mrfp
+
empty vector
P rpoE-mrfp
+
RpoE vector

Conclusion

Here, we have provided modular vectors that replicate and integrate into *E. coli* and *A. baumannii*, and a titratable, IPTG-inducible promoter, P_{abstBR}. We envision that our vectors will be valuable for complementation studies, particularly for comparing the function of genes in *E. coli* to those found in *A. baumannii*. We predict that our tools will allow for precise tuning of gene expression to achieve physiological or somewhat higher levels of expression while avoiding toxicity from extreme high-level overexpression. As such, our vectors could also be used for expressing gene fusions with fluorescent proteins for localization studies. The high integration efficiencies make library scale experiments possible, as we have previously shown for Tn*7*-based CRISPRi work (9). Given the host ranges of our vector components, we expect our vectors to be broadly useful for gene function studies in *Acinetobacter* species not tested here, including multidrug-resistant isolates.

Materials and Methods

Strains and growth conditions

Strains are listed in Table 4.1. *Escherichia coli* and *Acinetobacter baumannii* were grown in Lennox lysogeny broth (LB) at 37°C shaking in a flask at 250 rpm, in a culture tube on a rollerdrum at max speed, in a 96-well plate shaking at 900 rpm, or in a plate reader shaking (Tecan Infinite Mplex or Tecan Sunrise). Culture medium was solidified with 1.5% agar for growth on plates. Antibiotics were added when necessary: 100 µg/mL ampicillin (amp), 30 µg/mL kanamycin (kan), 50 µg/mL apramycin (apr), and 150 µg/mL hygromycin (hyg) for *E. coli* and 150 µg/mL carbenicillin (carb), 60 µg/mL kanamycin (kan), 100 µg/mL apramycin (apr), 150 µg/mL hygromycin (hyg) for *A. baumannii*. Diaminopimelic acid (DAP) was added at 300 µM to support growth of *E. coli* dap^- donor strains. IPTG (isopropyl b-D-1-thiogalactopyranoside) was added at varying concentrations from 0 to 1 mM as indicated in the figures or figure legends. Strains were preserved in 15% glycerol at -80°C.

Plasmids were propagated in *E. coli* strain BW25141 att_{Tn7}::acrIIA4 (sJMP3053) or in *E. coli* strain DH10B (sJMP1) for DNA extraction and analysis or in *E. coli* strain WM6026 att_{Tn7}::acrIIA4 (sJMP3257) for conjugation.

General molecular biology techniques

A complete list of plasmids and oligonucleotides are listed in Tables 4.2 and 4.3. Oligonucleotides were synthesized by Integrated DNA Technologies (Coralville, IA). Plasmid DNA was purified using GeneJet Plasmid Miniprep kit (Thermo) or the Purelink HiPure Plasmid Midiprep kit (Invitrogen K210005). PCR was performed according to manufacturer directions using Q5, OneTaq, or Phusion DNA Polymerases (NEB). DNA was digested with restriction enzymes from NEB. PCR products were purified with DNA Spin and Concentrate kit (Zymo Research) following manufacturer instructions or gel-purified from kit (Zymo Research). Plasmids were assembled using NEBuilder HiFi DNA assembly kit (NEB). DNA was quantified on a Nanodrop Lite or Qubit. Plasmids and recombinant strains were sequenced via Sanger sequencing by Functional Biosciences or Oxford Nanopore sequencing by Plasmidsaurus.

Construction of replicative expression vectors

Details for construction of expression vectors are listed under “Construction/notes” for corresponding vectors (Table 4.2). Briefly, base replicative expression plasmid construction was performed using HiFi assembly with: (i) p15A origin of replication and *oriT* from pJMP3262, (ii) pWH1266 origin of replication from pJMP3347, (iii) pTrc99a plasmid base including *lacI* and MCS from pJMP3067, and (iv) *kanR* marker from pJMP3341 to create plasmid pJMP3649. To swap the promoters, pJMP3649 was cut with AatII and NcoI enzymes and HiFi assembled with gblocks containing the desired promoters, to create plasmids pJMP3651 (P_{abst}, *kanR*) and pJMP3653 (P_{abstBR}, *kanR*). To swap the resistance markers, pJMP3653 was cut with XhoI enzyme and HiFi assembled

with gblocks containing the desired resistance markers, to create plasmids pJMP3664 (P_{abstBR}, *aprR*) and pJMP3665 (P_{abstBR}, *hygR*). To test expression of genes from these vectors, the *kanR* versions of the vectors with P_{trc}, P_{abst}, and P_{abstBR} (pJMP3649, pJMP3651, and pJMP3653, respectively) were cut with NcoI and BamHI enzymes and HiFi assembled with the *sfgfp* gene amplified from pJMP2748 to create plasmids pJMP3650, pJMP3652, and pJMP3654.

Construction of P_{abstBR}

Site-directed mutagenesis of the P_{abst} promoter was performed by single-primer high-fidelity Phusion PCR using pJMP3407 and oJMP2167. The PCR product was treated with DpnI, electroporated into sJMP3053, and selected on kan to make plasmid pJMP4481 containing the P_{abstBR} promoter. The mutation was verified by whole-plasmid sequencing with Plasmidsaurus.

Conjugative-based transfer of expression vectors

Replicative vector*:* Donor Dap$^-$ *E. coli* mating strain containing desired replicative expression vector and recipient strain (*A. baumannii* or *E. coli*) were both scraped off an agar plate into LB at OD600 of ~3. Strains were mixed at equal ratios, placed on a 0.45 µm filter on an LB plate, and incubated upright at 37°C for ~3 hrs. Filters were vortexed in LB media to remove cells and plated onto LB plates supplemented with appropriate antibiotic.

Tn*7* integrating vector*:* Conjugation was performed similarly to above, except with the addition of a donor Dap$^-$ *E. coli* strain carrying a Tn*7* transposase plasmid (tri-parental mating) for *E. coli*, *A. baumannii* ATCC 17978, and AB5075 strains. For *A. baumannii* ATCC 19606, quad-parental mating was performed, using an additional Dap$^-$ donor *E. coli* strain (sJMP4061) harboring a helper plasmid that contains extra mating machinery to improve efficiency. Tn*7* matings were performed for ~4 hrs before plating on LB plates supplemented with appropriate antibiotic.

Ten-fold serial dilutions were spotted (10 µL) on LB and LB with antibiotic. Transfer efficiencies were calculated as transformants or transconjugants (colony forming units or CFUs on selective plates) divided by total cells (CFUs on LB only).

Promoter activity assays

Promoter activities were assayed using the sfGFP expression vectors. Promoter-*sfgfp* or empty vector strains were grown to saturation in LB supplemented with appropriate antibiotic and IPTG inducer, washed several times with 1xPBS to remove all media, and GFP fluorescence and OD_{600} were measured in a Tecan Infinite Mplex plate reader. Values were normalized to OD_{600} readings and were background-subtracted using empty vector cells.

Flow cytometry

Cells containing either a P_{absBR}-*sfgfp* vector or empty vector control were grown in LB supplemented with kan and varying concentrations of IPTG to saturation overnight in tubes. Cells were formaldehyde fixed, washed, and resuspended in 1xPBS. GFP fluorescence was measured by flow cytometry on a LSR Fortessa instrument (BD Biosciences) at 100,000 events/sample. Data were analyzed in FlowJo (FlowJo, LLC) using singlet gates and dead cell or debris exclusion gates, as previously described (54).

Data availability

Plasmids and their sequences are available from Addgene under accession numbers 222348-222357. R code for data analysis and graphs can be found at https://github.com/jasonpeterslab/. Data available on request.

Table 4.1. Strains used in this study.

Strain name	Description[1]	Source
sJMP3053	*Escherichia coli* (derived from BW25141) pir+, recAI cloning strain with anti-CRISPR (attTn7::acrIIA4); Δ*(araD-araB)*567, Δ*lacZ4787*(::*rrnB-3*), Δ(*phoB-phoR*)580, l-, *galU95*, Δ*uidA3*::pir+, recA1, endA9(del-ins)::FRT, *rph-1*, Δ(*rhaD-rhaB*)*568*, *hsdR514, attTn7::acrIIA4*	Ward et al. (27)
sJMP3075	*Escherichia coli* MG1655 wild type (sJMP163, CAG80011)	Carol Gross, UCSF
sJMP3076	*Escherichia coli* BW25113 (sJMP6, CAG74538); F-, Δ(araD-araB)567, ΔlacZ4787(::rrnB-3), λ-, rph-1, Δ(rhaD-rhaB)568, hsdR514	Carol Gross, UCSF
sJMP3257	*Escherichia coli* (derived from WM6026) pir+, dap- mating strain with anti-CRISPR (attTn7::acrIIA4); lacIq, rrnB3, DElacZ4787, hsdR514, DE(araBAD)567, DE(rhaBAD)568, rph-1 att-lambda::pAE12-del (oriR6K/cat::frt5), del 4229(dapA)::frt(DAP-), del(endA)::frt, uidA(delMluI)::pir(wt), attHK::pJK1006::del1/2(del oriR6K-cat::frt5, del trfA::frt), attTn7::acrIIA4	Banta et al. (55)
sJMP3261	*Escherichia coli* sJMP3257 mating strain with plasmid pTn7C1 (pJMP1039) transposase expression; ampR, dap-	Banta et al. (55)
sJMP3329	*Acinetobacter baumannii* ATCC 19606 WT	ATCC
sJMP3348	*Acinetobacter baumannii* ATCC 17978 WT	ATCC
sJMP3518	*Acinetobacter baumannii* AB5075 WT	Colin Manoil, UW
sJMP3683	*E. coli* sJMP3257 mating strain with plasmid pJMP3649 (Ptrc EV); kanR, dap-	this study
sJMP3684	*E. coli* sJMP3257 mating strain with plasmid pJMP3650 (Ptrc sfGFP); kanR, dap-	this study
sJMP3685	*E. coli* sJMP3257 mating strain with plasmid pJMP3651 (Pabst EV); kanR, dap-	this study
sJMP3686	*E. coli* sJMP3257 mating strain with plasmid pJMP3652 (Pabst sfGFP); kanR, dap-	this study
sJMP3687	*E. coli* sJMP3257 mating strain with plasmid pJMP3653 (PabstBR EV kan); kanR, dap-	this study
sJMP3688	*E. coli* sJMP3257 mating strain with plasmid pJMP3654 (PabstBR sfGFP kan); kanR, dap-	this study
sJMP3689	*E. coli* sJMP3257 mating strain with plasmid pJMP3664 (PabstBR EV apr); aprR, dap-	this study

sJMP3690	*E. coli* sJMP3257 mating strain with plasmid pJMP3666 (PabstBR sfGFP apr); aprR, dap-	this study
sJMP3691	*E. coli* sJMP3257 mating strain with plasmid pJMP3665 (PabstBR EV hyg); hygR, dap-	this study
sJMP3692	*E. coli* sJMP3257 mating strain with plasmid pJMP3667 (PabstBR sfGFP hyg); hygR, dap-	this study
sJMP3715	*A. baumannii* 17978 (sJMP3348) with plasmid pJMP3649 (Ptrc EV); kanR	this study
sJMP3716	*A. baumannii* 17978 (sJMP3348) with plasmid pJMP3650 (Ptrc sfGFP); kanR	this study
sJMP3717	*A. baumannii* 17978 (sJMP3348) with plasmid pJMP3651 (Pabst EV); kanR	this study
sJMP3718	*A. baumannii* 17978 (sJMP3348) with plasmid pJMP3652 (Pabst sfGFP); kanR	this study
sJMP3719	*A. baumannii* 17978 (sJMP3348) with plasmid pJMP3653 (PabstBR EV); kanR	this study
sJMP3720	*A. baumannii* 17978 (sJMP3348) with plasmid pJMP3654 (PabstBR sfGFP); kanR	this study
sJMP3721	*A. baumannii* 19606 (sJMP3329) with plasmid pJMP3664 (PabstBR EV); aprR	this study
sJMP3722	*A. baumannii* 19606 (sJMP3329) with plasmid pJMP3666 (PabstBR sfGFP); aprR	this study
sJMP3725	*A. baumannii* AB5075 (sJMP3518) with plasmid pJMP3665 (PabstBR EV); hygR	this study
sJMP3726	*A. baumannii* AB5075 (sJMP3518) with plasmid pJMP3667 (PabstBR sfGFP); hygR	this study
sJMP3733	*E. coli* BW25113 (sJMP3076) with plasmid pJMP3653 (PabstBR EV); kanR	this study
sJMP3734	*E. coli* BW25113 (sJMP3076) with plasmid pJMP3654 (PabstBR sfGFP); kanR	this study
sJMP3844	*A. baumannii* 17978 (sJMP3348) with attTn7::PrpoE-mRFP reporter (Tn7 from pJMP3748; rpoE promoter sequence from E. coli), aprR	this study
sJMP3845	*E. coli* (sJMP3075) with attTn7::PrpoE-mRFP reporter (Tn7 from pJMP3748; rpoE promoter sequence from E. coli), aprR	this study

sJMP4061	*E. coli* mating strain with helper plasmid pEVS104 (sJMP2935; helper strain); kanR, dap-	Ward et al. (27)
sJMP12051	*A. baumannii* 17978 (sJMP3348) with attTn7::PabstBR-sfGFP (Tn7 from pJMP12049); aprR	this study
sJMP12053	*A. baumannii* 17978 (sJMP3348) with attTn7::PabstBR-empty (Tn7 from pJMP12042); aprR	this study
sJMP12055	*A. baumannii* 19606 (sJMP3329) with attTn7::PabstBR-sfGFP (Tn7 from pJMP12049); aprR	this study
sJMP12057	*A. baumannii* 19606 (sJMP3329) with attTn7::PabstBR-empty (Tn7 from pJMP12042); aprR	this study
sJMP12059	*E. coli* BW25113 (sJMP3076) with attTn7::PabstBR-sfGFP (Tn7 from pJMP12049); aprR	this study
sJMP12061	*E. coli* BW25113 (sJMP3076) with attTn7::PabstBR-empty (Tn7 from pJMP12042); aprR	this study
sJMP12063	*E. coli* sJMP3257 mating strain with plasmid pJMP12042 (Tn7 PabstBR EV); ampR, aprR, dap-	this study
sJMP12065	*E. coli* sJMP3257 mating strain with plasmid pJMP12049 (Tn7 PabstBR sfGFP); ampR, aprR, dap-	this study
sJMP12070	*E. coli* mating strain with plasmid pJMP3853 (PabstBR RpoE OE vector); kanR, dap-	this study
sJMP12074	*A. baumannii* 17978 (sJMP3348) with attTn7::PrpoE-mRFP reporter (Tn7 from pJMP3748; rpoE promoter sequence from E. coli) and rpoE OE vector (pJMP3853), aprR, kanR	this study
sJMP12076	*E. coli* (sJMP3075) with attTn7::PrpoE-mRFP reporter (Tn7 from pJMP3748; rpoE promoter sequence from E. coli) and rpoE OE vector (pJMP3853), aprR, kanR	this study
sJMP12083	*A. baumannii* AB5075 (sJMP3518) with attTn7::PabstBR-empty (Tn7 from pJMP12042); aprR	this study
sJMP12085	A. baumannii AB5075 (sJMP3518) with attTn7::PabstBR-sfGFP (Tn7 from pJMP12049); aprR	this study

[1]ampR, ampicillin resistant; aprR, apramycin resistant; kanR, kanamycin resistant; hygR, hygromycin resistant; dap-, requires diaminopimelic acid.

Table 4.2. Plasmids used in this study.

Plasmid #	Description	Construction/notes[1]	Source
pJMP0631	Tiny Tn*7* vector	pTinyTn*7* plasmid, R6k ori vector with Tn*7* transposon with kanR cassette; ampR, kanR	Hall et al. (56)
pJMP1039	pTn*7*C1	Tn*7* transposase expression; ampR	Peters et al. (9), Addgene: 119239
pJMP2748	vector that contains GFP	sfGFP is on this vector for amplification; ampR, gentR	Ward et al. (27)
pJMP3067	pTrc99a	pTrc99a expression plasmid, pBR322 ori expression vector containing IPTG-inducible trc promoter; ampR	Rhodius et al. (49)
pJMP3262	pJQ200SK with p15A ori	pJQ200SK, gent-sacB vector containing *E. coli* p15A origin of replication; gentR	Quandt et al. (57), Addgene: 78497
pJMP3341	Tiny Tn7 with NcoI site removed	Tiny-Tn*7* plasmid; HiFi assembly to delete NcoI sites from pJMP631 with o1255/1258 and o1256/1257 amplified from pJMP631; ampR, kanR	this study
pJMP3347	pSGAb-km with pWH1266 ori	plasmid containing pWH1266 *A. baumannii* origin of replication; kanR	Wang et al. (58), Addgene: 121999
pJMP3352	Old Ptrc-EV expression vector, R6k version	overexpression plasmid containing pTrc99a expression system, *E. coli* R6K gamma origin, *A. baumannii* pWH1266 origin; (requires pir to replicate in *E. coli*); kanR	this study
pJMP3361	Old Ptrc-GFP expression vector, R6k version	overexpression plasmid containing Ptrc promoter expressing GFP, *E, coli* R6K gamma origin, *A. baumannii* pWH1266 origin; HiFi assembled sfGFP gene amplified from pJMP2748 with oJMP1253/oMP1254 into pJMP3352 cut with NcoI/BamHI; (requires pir to replicate in *E. coli*); kanR	this study
pJMP3407	Old Pabst-EV expression vector, R6k version	overexpression plasmid containing Pabst promoter, *E. coli* R6K ori, *A. baumannii* pWH1266 ori; constructed by PCR amplifying pJMP3352 with oJMP2040 and oJMP2041, and HiFi assembling with gblock oJMP2039 and pJMP3352 digested with EcoRI (used larger piece from digest via gel purification); (requires pir to replicate in *E. coli*); kanR	this study
pJMP3434	Old Pabst-GFP expression vector, R6k version	overexpression plasmid containing Pabst promoter expressing GFP, *E. coli* R6K gamma origin, *A. baumannii* pWH1266 origin; HiFi assembled sfGFP gene amplified from pJMP2748 with oJMP1253/oMP1254 into pJMP3407 cut with NcoI/BamHI; (requires pir to replicate in *E. coli*); kanR	this study

pJMP3649	Ptrc EV kan - replicative vector used in this study	Ptrc OE empty vector with p15A(ACYC) and pWH1266 origins; constructed by digesting pJMP3352 with AscI/PmeI, and HiFi assembling with PCR product of oJMP2134 and oJMP2135 amplified from pJQ200SK; kanR	this study
pJMP3650	Ptrc GFP kan - replicative vector used in this study	Ptrc-GFP expression vector with p15A(ACYC) and pWH1266 origins; constructed by digesting pJMP3361 with AscI/PmeI, and HiFi assembling with PCR product of oJMP2134 and oJMP2135 amplified from pJQ200SK; kanR	this study
pJMP3651	Pabst EV kan - replicative vector used in this study	Pabst OE empty vector with p15A(ACYC) and pWH1266 origins; constructed by digesting pJMP3407 with AscI/PmeI, and HiFi assembling with PCR product of oJMP2134 and oJMP2135 amplified from pJQ200SK; kanR	this study
pJMP3652	Pabst GFP kan - replicative vector used in this study	Pabst-GFP expression vector with p15A(ACYC) and pWH1266 origins; constructed by digesting pJMP3434 with AscI/PmeI, and HiFi assembling with PCR product of oJMP2134 and oJMP2135 amplified from pJQ200SK; kanR	this study
pJMP3653	PabstBR EV kan - replicative vector used in this study	PabstBR OE empty vector with p15A(ACYC) and pWH1266 origins; constructed by digesting pJMP4481 with AscI/PmeI, and HiFi assembling with PCR product of oJMP2134 and oJMP2135 amplified from pJQ200SK; kanR	this study, Addgene: 222348
pJMP3654	PabstBR GFP kan - replicative vector used in this study	PabstBR-GFP expression vector with p15A(ACYC) and pWH1266 origins; constructed by digesting pJMP4491 with AscI/PmeI, and HiFi assembling with PCR product of oJMP2134 and oJMP2135 amplified from pJQ200SK; kanR	this study, Addgene: 222349
pJMP3664	PabstBR EV apr - replicative vector used in this study	Apramycin version of pJMP3653 (PabstBR-empty vector); digested pJMP3653 with XhoI, HiFi assembled with gblock oJMP1946; aprR	this study, Addgene: 222350
pJMP3665	PabstBR EV hyg - replicative vector used in this study	Hygromycin version of pJMP3653 (PabstBR-empty vector); digested pJMP3653 with XhoI, HiFi assembled with gblock oJMP2117; hygR	this study, Addgene: 222351
pJMP3666	PabstBR GFP apr - replicative vector used in this study	Apramycin version of pJMP3654 (PabstBR-empty vector); digested pJMP3654 with XhoI, HiFi assembled with gblock oJMP1946; aprR	this study, Addgene: 222352
pJMP3667	PabstBR GFP hyg - replicative vector used in this study	Hygromycin version of pJMP3654 (PabstBR-empty vector); digested pJMP3654 with XhoI, HiFi assembled with gblock oJMP2117; hygR	this study, Addgene: 222353
pJMP3748	Tn7 PrpoE-mRFP reporter vector	Integrative expression vector with PrpoE-mRFP reporter on Tn*7* transposon; derived from pJMP8602 by adding PrpoE in front of mRFP reporter using oligos oJMP2369 and oJMP2370; ampR, aprR	this study
pJMP3853	PabstBR rpoE OE vector kan	PabstBR-RpoE expression vector, parent pJMP3653; HiFi assembled rpoE gene amplified from E. coli sJMP3075	this study

		gDNA with oJMP2634 and oJMP2635 into pJMP3653 digested with NcoI/BamHI; kanR	
pJMP4003	pEVS104 helper plasmid	pEVS104(R6K ori, KanR, Tra+); kanR	Stabb and Ruby (59)
pJMP4481	Old PabstBR-EV expression vector, R6k version	Overexpression plasmid containing PabstBR promoter, *E. coli* R6K ori, *A. baumannii* pWH1266 ori; constructed by site-directed mutagenesis using pJMP3407 and oJMP2167; (requires pir to replicate in *E. coli*); kanR	this study
pJMP4491	Old PabstBR-GFP expression vector, R6k version	Overexpression plasmid containing PabstBR promoter expressing GFP, *E. coli* R6K gamma origin, *A. baumannii* pWH1266 origin; HiFi assembled sfGFP gene amplified from pJMP2748 with oJMP1253/oMP1254 into pJMP4481 cut with NcoI/BamHI; (requires pir to replicate in *E. coli*); kanR	this study
pJMP8602	Old vector containing Tn7 base	Tn*7* expression vector with mRFP reporter on Tn*7* transposon; kanR	Hall et al. (56)
pJMP12042	Tn7 PabstBR EV apr - integrative vector used in this study	Integrative expression vector with PabstBR empty vector on Tn*7* transposon; constructed by amplifying pJMP3653 with oJMP2539 and oJMP2540, pJMP8602 with oJMP2541 and oJMP2542, pJMP3352 with oJMP2543 and oJMP2544, and HiFi assembling with pJMP3539 digested with SpeI/NotI; ampR, aprR	this study, Addgene: 222354
pJMP12049	Tn7 PabstBR GFP apr - integrative vector used in this study	Integrative expression vector with PabstBR-GFP on Tn*7* transposon; constructed by digesting pJMP12042 with NcoI/BamHI, and HiFi assembling with PCR product of oJMP1254 and oJMP2078 amplified from pJMP2748; ampR, aprR	this study, Addgene: 222355
pJMP12068	Tn7 PabstBR EV kan - integrative vector used in this study	Kanamycin version of pJMP12042 (Tn*7*-PabstBR-empty vector); HiFi assembled PCR product of pJMP3653 with oJMP0193 and oJMP0194 into pJMP12042 digested with XhoI; ampR, kanR	this study, Addgene: 222356
pJMP12089	Tn7 PabstBR EV hyg - integrative vector used in this study	Hygromycin version of pJMP12042 (Tn*7*-PabstBR-empty vector); digested pJMP12042 with XhoI, HiFi assembled with gblock oJMP2117; ampR, hygR	this study, Addgene: 222357

[1]ampR, ampicillin resistant; aprR, apramycin resistant; gentR, gentamycin resistant; kanR, kanamycin resistant

Table 4.3. Oligos used in this study.

Oligo #	Sequence (5' to 3')	Usage
oJMP0193	TCCTGAACGGCCATAAGAAC	amplifying kanR marker for swapping A
oJMP0194	GAGCGCTTTTGAAGCTGATG	amplifying kanR marker for swapping B
oJMP1253	CGGATAACAATTTCACACAGGAAACAGACCATGAGCAAAGGAGA AGAACT	amplify GFP A
oJMP1254	TGCATGCCTGCAGGTCGACTCTAGAGGATCTTTGTAGAGCTCATC CATGC	amplify GFP B
oJMP1255	TTCGGCAAGCAGGCATCGCCGTGGGTCACGACGAGATCCT	remove NcoI sites from pJMP631 A
oJMP1256	GAGGATCTCGTCGTGACCCACGGCGATGCCTGCTTGCCGA	remove NcoI sites from pJMP631 C
oJMP1257	CTGACATGGGAATTAGCCACGGCATCACAGTATCGTGATG	remove NcoI sites from pJMP631 D
oJMP1258	ATCACGATACTGTGATGCCGTGGCTAATTCCCATGTCAGC	remove NcoI sites from pJMP631 B
oJMP1946	TCCTGAACGGCCATAAGAACGAAGGCTGTCTGTTGAACTCTCGA GCCTTGTCGCCTTGCGTATAATATTTGCTCATGGACGCACACCGT GGAAACGGATGAAGGCACGAACCCAGTTGACATAAGCCTGTTCG GTTCGTAAACTGTAATGCAAGTAGCGTATGCGCTCACGCAACTGG TCCAGAACCTTGACCGAACGCAGCGGTGGTAACGGCGCAGTGG CGGTTTTCATGGCTTGTTATGACTGTTTTTTCGTACAGTCTATGCCTC GGGCATCCAAGCAGCAAGCGCGTTACGCCGTGGGTCGATGTTT GATGTTATGGAGCAGCAACGATGTCATCAGCGGTGGAGTGCAATG TCGTGCAATACGAATGGCGAAAAGCCGAGCTGATCGGTCAGCTT CTCAACCTTGGGGTTACCCCCGGCGGTGTGCTGCTGGTCCACA GCTCCTTCCGTAGCGTCCGGCCCCTCGAAGATGGGCCACTTGG ACTGATCGAGGCCCTGCGTGCTGCACTGGGTCCGGGAGGGAC GCTCGTCATGCCATCGTGGTCAGGTCTGGACGACGAGCCGTTCG ATCCTGCCACGTCGCCCGTTACACCGGACCTTGGAGTTGTCTCT GACACATTCTGGCGTCTGCCAAATGTAAAGCGCAGCGCCCATCC ATTTGCCTTTGCGGCAGCGGGGCCACAGGCAGAGCAGATCATC TCTGATCCATTGCCCCTGCCACCTCACTCGCCTGCAAGCCCGGT CGCCCGTGTCCATGAACTCGATGGGCAGGTACTTCTCCTCGGCG TGGGACACGATGCCAACACGACGCTGCATCTTGCCGAGTTGATG GCAAAGGTTCCCTATGGGGTGCCGAGACACTGCACCATTCTTCA GGATGGCAAGTTGGTACGTGTCGATTATCTGGAGAATGACCACTG CTGTGAGCGCTTTGCCTTGGCGGACAGGTGGCTCAAGGAGAAC AGCCTTCAGAAGGAAGGTCCAGTCGGTCATGCCTTTGCTCGGTT GATCCGCTCCCGCGACATTGTGGCGACAGCCCTGGGTCAACTG GGCCGAGATCCGTTGATCTTCCTGCATCCGCCAGAGGCGGGAT GCGAAGAATGCGATGCCGCTCGCCAGTCGATTGGCTAACAATTC GTTCAAGCCGAGATCTCGAGCATCAGCTTCAAAAGCGCTC	apramycin (aprR) gblock
oJMP2039	AGCCATCGGAAGCTGTGGTATGGCTGTGCAGGTCGTAAAGACGT CTCATTAATCAGATAAAATATTATAAATGTGAGCGGATAACAAGATAC TGAGCACATCAGCAGCACACAGGAAACAGACCATGGAATTCGAG CTCGGTACCCGGGGATCCTCTAGAGTCGACC	making Pabst replicative vector gblock

oJMP2040	TGATACCTCTGGCTCAGCG	making Pabst replicative vector A
oJMP2041	TTTACGACCTGCACAGCCAT	making Pabst replicative vector B
oJMP2117	TCCTGAACGGCCATAAGAACGAAGGCTGTCTGTTGAACTCTCGA GCCTTGTCGCCTTGCGTATAATATTTGCTCATGGACGCACACCGT GGAAACGGATGAAGGCACGAACCCAGTTGACATAAGCCTGTTCG GTTCGTAAACTGTAATGCAAGTAGCGTATGCGCTCACGCAACTGG TCCAGAACCTTGACCGAACGCAGCGGTGGTAACGGCGCAGTGG CGGTTTTCATGGCTTGTTATGACTGTTTTTTCGTACAGTCTATGCCTC GGGCATCCAAGCAGCAAGCGCGTTACGCCGTGGGTCGATGTTT GATGTTATGGAGCAGCAACGATGACCCAAGAAAGCCTGCTGCTG CTGGATCGTATTGATAGTGATGATAGCTATGCAAGCCTGCGCAATG ATCAAGAATTTTGGGAACCGCTGGCACGTCGTGCACTGGAAGAA CTGGGTCTGCCGGTTCCGCCTGTTCTGCGTGTTCCGGGTGAAAG CACCAATCCGGTTCTGGTTGGTGAACCTGATCCTGTTATTAAACTG TTTGGTGAACATTGGTGTGGTCCGGAAAGCCTGGCAAGCGAAAG CGAAGCCTATGCAGTTCTGGCAGATGCACCGGTTCCGGTTCCTC GTCTGTTAGGTCGTGGTGAACTGCGTCCTGGTACAGGTGCATGGC CGTGGCCGTATCTGGTTATGAGCCGTATGACCGGCACCACCTGG CGTAGCGCAATGGATGGCACCACCGATCGTAATGCACTGCTGGC ACTGGCACGTGAACTGGGACGTGTTCTGGGTCGTCTGCATCGTGT TCCGCTGACCGGTAATACCGTTCTGACACCGCATAGCGAAGTTTT TCCGGAACTGCTGCGTGAACGTCGTGCCGCAACCGTTGAAGATC ATCGTGGTTGGGGTTATCTGAGTCCGCGTCTGCTGGACCGTCTGG AAGATTGGCTGCCGGATGTTGATACCCTGCTGGCAGGTCGCGAA CCGCGTTTTGTTCATGGTGATCTGCATGGCACCAACATTTTTGTTG ATCTGGCAGCAACCGAAGTTACCGGTATTGTTGATTTCACCGATGT TTATGCCGGTGATAGCCGTTATAGCCTGGTTCAGCTGCATCTGAAT GCATTTCGTGGTGATCGTGAAATTCTGGCAGCCCTGCTGGATGGT GCACAGTGGAAACGTACCGAAGATTTTGCCCGTGAACTGCTGGC CTTTACCTTTCTGCATGATTTTGAAGTGTTTGAAGAAACACCGCTG GATCTGAGCGGTTTTACCGATCCGGAAGAATTAGCACAGTTTCTGT GGGGTCCGCCTGATACCGCACCGGGTGCATAATAACAATTCGTT CAAGCCGAGATCTCGAGCATCAGCTTCAAAAGCGCTC	hygromycin (hygR) gblock
oJMP2134	GCCTTCCGTTTGGGCCTAGAATTCCGGTTTAACAGGGAAGTGAGA GGGC	swapping to p15A ori A
oJMP2135	TGGCTTGCAGCCCTTATGTCCTCAGGCGCGCACAAAACAGCAG GGAAGC	swapping to p15A ori B
oJMP2167	CAAGAAGATCATCTTATTAATCAGATAAAATATTGACAATGTGAGCG GATAACAAG	making PabstBR Quikchange primer
oJMP2369	CTAGAAACAAAAACAGATGCGTTACGGAACTTTACAAAAACGAGA CACTCTAACCCTTTG	PrpoE cloning A
oJMP2370	TCGTCAAAGGGTTAGAGTGTCTCGTTTTTGTAAAGTTCCGTAACGC ATCTGTTTTTGTTT	PrpoE cloning B
oJMP2539	CACGCCGCTTTTTTTACGTCTGCAGACTAGTCAGGCAGCCATCG GAAGCT	amplify MCS A
oJMP2540	TGTCGACTAGGCCATGATGCTCATTCTGTGAAAAGGCCATCCGTC AGGAT	amplify MCS B
oJMP2541	CACAGAATGAGCATCATGGC	amplify Tn7 cassette A
oJMP2542	GGGTCAGTGAGCGAGGAAG	amplify Tn7 cassette B

oJMP2543	TTTAAAACTTCATTTTTAATTTTTGCGGCCGATCTGAAGATCAGCAG TTC	amplify R6k and oriT A
oJMP2544	GGGCTCTTCCGCTTCCTCGCTCACTGACCCTATCAGAGCTTATCG GCCAG	amplify R6k and oriT B

Figure 4.S1. Conjugation and transposition efficiencies. (A) Dot plot of conjugation efficiency of the replicative vector to the recipient strain (*A. baumannii* ATCC 17978 or *E. coli* BW25113) after ~3-hour incubations. Bars represent mean efficiencies (n=3 biological replicates). Dashed line is drawn at the limit of detection, defined by the maximum number of colony-forming units (CFUs) observed on non-selective plates in each experiment. (B) Dot plot showing transposition efficiency of the Tn*7* transposon into the att_{Tn7} site of *A. baumannii* ATCC 17978 or *E. coli* BW25113 after ~4-hour incubation with donor strains, one carrying the Tn*7* transposon vector and another carrying the Tn*7* transposase vector. Bars represent mean efficiencies (n=3 biological replicates); dashed line shows limit of detection. (C) Table showing instances of carbenicillin-resistant (CarbR) transconjugants of 40 isolates tested for Tn*7* co-integrates in *A. baumannii* and *E. coli*.

Figure 4.S1

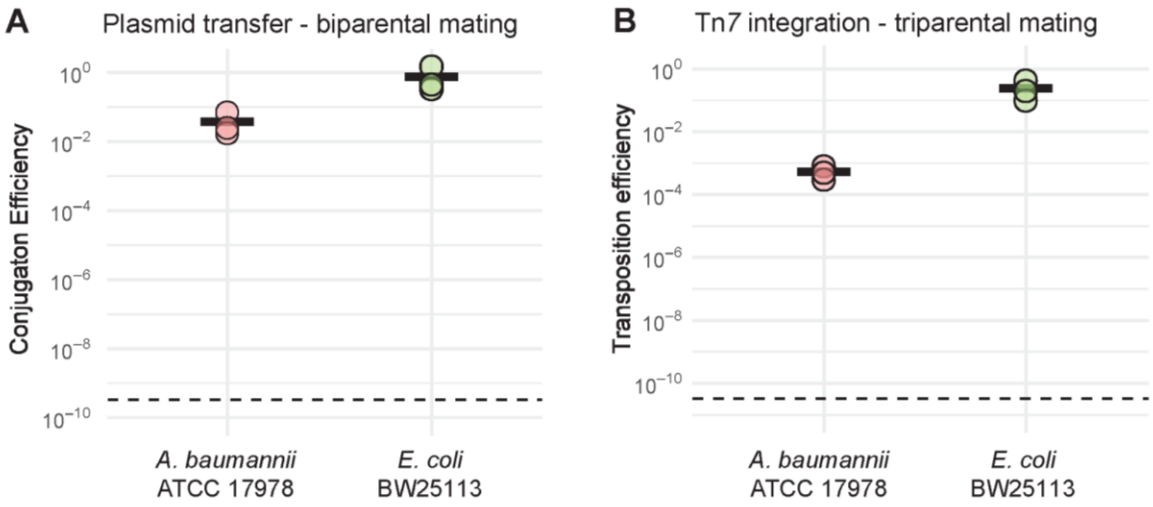

C

Co-integrates: CarbR Tn7 transconjugants

	Strain	
	A. baumannii ATCC 17978	*E. coli* BW25113
Tn7 vector - empty	2/40	0/40
Tn7 vector - sfGFP	3/40	1/40

Figure 4.S2. Titration of P_{abstBR} expression. Expression from **(A)** the replicative plasmid vector or **(B)** the Tn*7* transposon. Plots shown are normalized sfGFP levels expressed from P_{abstBR} across IPTG concentrations for *A. baumannii* ATCC 19606 and *A. baumannii* AB5075. Error bars represent standard deviation (n=3 biological replicates for replicative vector, n=6 biological replicates for Tn*7* transposon).

Figure 4.S2

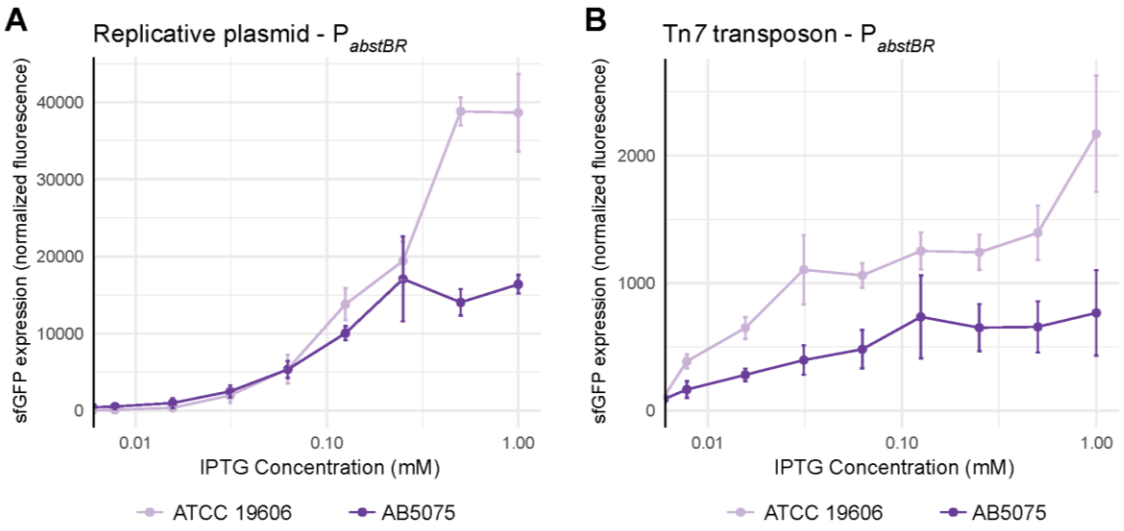
A
Replicative plasmid - P abstBR
sfGFP expression (normalized fluorescence)
40000
30000
20000
10000
0
0.01
0.10
1.00
IPTG Concentration (mM)
ATCC 19606
AB5075
B
Tn7 transposon - P abstBR
sfGFP expression (normalized fluorescence)
2000
1000
0
0.01
0.10
1.00
IPTG Concentration (mM)
ATCC 19606
AB5075

Acknowledgements

We thank Colin Manoil for providing AB5075 WT strain and Quanjiang Ji for pSGAb-km (Addgene plasmid #121999). We also thank the UWCCC Flow Cytometry lab for equipment access and assistance (NIH Special BD LSR Fortessa Project: 1S100OD018202-01). This work was supported by the National Institutes of Health under award numbers K22AI137122 and 1R35GM150487-01. J.S.T. was funded by an NSF GRFP and the SciMed Graduate Research Scholars program.

References

1. Blount ZD. 2015. The unexhausted potential of E. coli. Elife 4.

2. Nora LC, Westmann CA, Guazzaroni ME, Siddaiah C, Gupta VK, Silva-Rocha R. 2019. Recent advances in plasmid-based tools for establishing novel microbial chassis. Biotechnol Adv 37:107433.

3. Ruiz N, Silhavy TJ. 2022. How Escherichia coli Became the Flagship Bacterium of Molecular Biology. J Bacteriol 204:e0023022.

4. Hanage WP. 2016. Not So Simple After All: Bacteria, Their Population Genetics, and Recombination. Cold Spring Harb Perspect Biol 8.

5. Ramon C, Stelling J. 2023. Functional comparison of metabolic networks across species. Nat Commun 14:1699.

6. Peleg AY, Seifert H, Paterson DL. 2008. Acinetobacter baumannii: emergence of a successful pathogen. Clin Microbiol Rev 21:538-82.

7. Nowak J, Zander E, Stefanik D, Higgins PG, Roca I, Vila J, McConnell MJ, Cisneros JM, Seifert H. 2017. High incidence of pandrug-resistant Acinetobacter baumannii isolates collected from patients with ventilator-associated pneumonia in Greece, Italy and Spain as part of the MagicBullet clinical trial. J Antimicrob Chemother 72:3277-3282.

8. Wong D, Nielsen TB, Bonomo RA, Pantapalangkoor P, Luna B, Spellberg B. 2017. Clinical and Pathophysiological Overview of Acinetobacter Infections: a Century of Challenges. Clin Microbiol Rev 30:409-447.

9. Peters JM, Koo BM, Patino R, Heussler GE, Hearne CC, Qu J, Inclan YF, Hawkins JS, Lu CHS, Silvis MR, Harden MM, Osadnik H, Peters JE, Engel JN, Dutton RJ, Grossman AD, Gross CA, Rosenberg OS. 2019. Enabling genetic analysis of diverse bacteria with Mobile-CRISPRi. Nat Microbiol 4:244-250.

10. Anonymous. 2019. Antibiotic resistance threats in the United States, 2019.

11. Zampaloni C, Mattei P, Bleicher K, Winther L, Thäte C, Bucher C, Adam JM, Alanine A, Amrein KE, Baidin V, Bieniossek C, Bissantz C, Boess F, Cantrill C, Clairfeuille T, Dey F, Di Giorgio P, du Castel P, Dylus D, ..., Bradley KA. 2024. A novel antibiotic class targeting the lipopolysaccharide transporter. Nature 625:566-571.

12. Falcone M, Tiseo G, Leonildi A, Della Sala L, Vecchione A, Barnini S, Farcomeni A, Menichetti F. 2022. Cefiderocol- Compared to Colistin-Based Regimens for the Treatment of Severe Infections Caused by Carbapenem-Resistant Acinetobacter baumannii. Antimicrob Agents Chemother 66:e0214221.

13. Héritier C, Poirel L, Lambert T, Nordmann P. 2005. Contribution of acquired carbapenem-hydrolyzing oxacillinases to carbapenem resistance in Acinetobacter baumannii. Antimicrob Agents Chemother 49:3198-202.

14. Lupo A, Haenni M, Madec JY. 2018. Antimicrobial Resistance in Acinetobacter spp. and Pseudomonas spp. Microbiol Spectr 6.

15. Valentine SC, Contreras D, Tan S, Real LJ, Chu S, Xu HH. 2008. Phenotypic and molecular characterization of Acinetobacter baumannii clinical isolates from nosocomial outbreaks in Los Angeles County, California. J Clin Microbiol 46:2499-507.

16. Zhao J, Zhu Y, Han J, Lin YW, Aichem M, Wang J, Chen K, Velkov T, Schreiber F, Li J. 2020. Genome-Scale Metabolic Modeling Reveals Metabolic Alterations of Multidrug-Resistant Acinetobacter baumannii in a Murine Bloodstream Infection Model. Microorganisms 8.

17. Moffatt JH, Harper M, Harrison P, Hale JD, Vinogradov E, Seemann T, Henry R, Crane B, St Michael F, Cox AD, Adler B, Nation RL, Li J, Boyce JD. 2010. Colistin resistance in Acinetobacter baumannii is mediated by complete loss of lipopolysaccharide production. Antimicrob Agents Chemother 54:4971-7.

18. Moran AP. 2009. Microbial glycobiology: structures, relevance and applications. Elsevier.

19. Boll JM, Crofts AA, Peters K, Cattoir V, Vollmer W, Davies BW, Trent MS. 2016. A penicillin-binding protein inhibits selection of colistin-resistant, lipooligosaccharide-deficient Acinetobacter baumannii. Proc Natl Acad Sci U S A 113:E6228-e6237.

20. Robinson A, Brzoska AJ, Turner KM, Withers R, Harry EJ, Lewis PJ, Dixon NE. 2010. Essential biological processes of an emerging pathogen: DNA replication, transcription, and cell division in Acinetobacter spp. Microbiol Mol Biol Rev 74:273-97.

21. Casella LG, Weiss A, Pérez-Rueda E, Antonio Ibarra J, Shaw LN. 2017. Towards the complete proteinaceous regulome of Acinetobacter baumannii. Microb Genom 3:mgen000107.

22. Lucidi M, Runci F, Rampioni G, Frangipani E, Leoni L, Visca P. 2018. New Shuttle Vectors for Gene Cloning and Expression in Multidrug-Resistant Acinetobacter Species. Antimicrob Agents Chemother 62.

23. Jie J, Chu X, Li D, Luo Z. 2021. A set of shuttle plasmids for gene expression in Acinetobacter baumannii. PLoS One 16:e0246918.

24. McKenzie GJ, Craig NL. 2006. Fast, easy and efficient: site-specific insertion of transgenes into enterobacterial chromosomes using Tn7 without need for selection of the insertion event. BMC Microbiol 6:39.

25. Sykes EME, Deo S, Kumar A. 2020. Recent Advances in Genetic Tools for Acinetobacter baumannii. Front Genet 11:601380.

26. Pérez-Varela M, Tierney ARP, Kim JS, Vázquez-Torres A, Rather P. 2020. Characterization of RelA in Acinetobacter baumannii. J Bacteriol 202.

27. Ward RD, Tran JS, Banta AB, Bacon EE, Rose WE, Peters JM. 2024. Essential gene knockdowns reveal genetic vulnerabilities and antibiotic sensitivities in Acinetobacter baumannii. mBio 15:e0205123.

28. Choi KH, Gaynor JB, White KG, Lopez C, Bosio CM, Karkhoff-Schweizer RR, Schweizer HP. 2005. A Tn7-based broad-range bacterial cloning and expression system. Nat Methods 2:443-8.

29. Banta AB, Enright AL, Siletti C, Peters JM. 2020. A High-Efficacy CRISPR Interference System for Gene Function Discovery in Zymomonas mobilis. Appl Environ Microbiol 86.

30. Terpe K. 2006. Overview of bacterial expression systems for heterologous protein production: from molecular and biochemical fundamentals to commercial systems. Appl Microbiol Biotechnol 72:211-22.

31. Lozano Terol G, Gallego-Jara J, Sola Martínez RA, Martínez Vivancos A, Cánovas Díaz M, de Diego Puente T. 2021. Impact of the Expression System on Recombinant Protein Production in Escherichia coli BL21. Front Microbiol 12:682001.

32. Müller-Hill B, Crapo L, Gilbert W. 1968. Mutants that make more lac repressor. Proc Natl Acad Sci U S A 59:1259-64.

33. Siegele DA, Hu JC. 1997. Gene expression from plasmids containing the araBAD promoter at subsaturating inducer concentrations represents mixed populations. Proc Natl Acad Sci U S A 94:8168-72.

34. Mäkelä J, Kandhavelu M, Oliveira SM, Chandraseelan JG, Lloyd-Price J, Peltonen J, Yli-Harja O, Ribeiro AS. 2013. In vivo single-molecule kinetics of activation and subsequent activity of the arabinose promoter. Nucleic Acids Res 41:6544-52.

35. Megerle JA, Fritz G, Gerland U, Jung K, Rädler JO. 2008. Timing and dynamics of single cell gene expression in the arabinose utilization system. Biophys J 95:2103-15.

36. Chaperon DN. 2006. Construction and complementation of in-frame deletions of the essential Escherichia coli thymidylate kinase gene. Appl Environ Microbiol 72:1288-94.

37. Mutsuda M, Michel KP, Zhang X, Montgomery BL, Golden SS. 2003. Biochemical properties of CikA, an unusual phytochrome-like histidine protein kinase that resets the circadian clock in Synechococcus elongatus PCC 7942. J Biol Chem 278:19102-10.

38. Hannig G, Makrides SC. 1998. Strategies for optimizing heterologous protein expression in Escherichia coli. Trends Biotechnol 16:54-60.

39. Lutz R, Bujard H. 1997. Independent and tight regulation of transcriptional units in Escherichia coli via the LacR/O, the TetR/O and AraC/I1-I2 regulatory elements. Nucleic Acids Res 25:1203-10.

40. Anderson SE, Chin CY, Weiss DS, Rather PN. 2020. Copy Number of an Integron-Encoded Antibiotic Resistance Locus Regulates a Virulence and Opacity Switch in Acinetobacter baumannii AB5075. mBio 11.

41. Gibson DG, Young L, Chuang RY, Venter JC, Hutchison CA, 3rd, Smith HO. 2009. Enzymatic assembly of DNA molecules up to several hundred kilobases. Nat Methods 6:343-5.

42. Drew RH. 2022. Aminoglycosides. Wolters Kluwe, UpToDate.

43. Hoang TT, Karkhoff-Schweizer RR, Kutchma AJ, Schweizer HP. 1998. A broad-host-range Flp-FRT recombination system for site-specific excision of chromosomally-located DNA sequences: application for isolation of unmarked Pseudomonas aeruginosa mutants. Gene 212:77-86.

44. Choi KH, Schweizer HP. 2006. mini-Tn7 insertion in bacteria with single attTn7 sites: example Pseudomonas aeruginosa. Nat Protoc 1:153-61.

45. Amann E, Ochs B, Abel KJ. 1988. Tightly regulated tac promoter vectors useful for the expression of unfused and fused proteins in Escherichia coli. Gene 69:301-15.

46. May EW, Craig NL. 1996. Switching from cut-and-paste to replicative Tn7 transposition. Science 272:401-4.

47. Wen X, Zhang Y, Cheng H, An J, Guo Y, Wang L, Wang M. 2021. A CRISPR/dCas9-assisted system to clone toxic genes in Escherichia coli. Biochim Biophys Acta Gen Subj 1865:129994.

48. Tal S, Paulsson J. 2012. Evaluating quantitative methods for measuring plasmid copy numbers in single cells. Plasmid 67:167-73.

49. Rhodius VA, Suh WC, Nonaka G, West J, Gross CA. 2006. Conserved and variable functions of the sigmaE stress response in related genomes. PLoS Biol 4:e2.

50. Lima S, Guo MS, Chaba R, Gross CA, Sauer RT. 2013. Dual molecular signals mediate the bacterial response to outer-membrane stress. Science 340:837-41.

51. Firoved AM, Boucher JC, Deretic V. 2002. Global genomic analysis of AlgU (sigma(E))-dependent promoters (sigmulon) in Pseudomonas aeruginosa and implications for inflammatory processes in cystic fibrosis. J Bacteriol 184:1057-64.

52. Mathur J, Davis BM, Waldor MK. 2007. Antimicrobial peptides activate the Vibrio cholerae sigmaE regulon through an OmpU-dependent signalling pathway. Mol Microbiol 63:848-58.

53. Schulz S, Eckweiler D, Bielecka A, Nicolai T, Franke R, Dötsch A, Hornischer K, Bruchmann S, Düvel J, Häussler S. 2015. Elucidation of sigma factor-associated networks in Pseudomonas aeruginosa reveals a modular architecture with limited and function-specific crosstalk. PLoS Pathog 11:e1004744.

54. Staats J, Divekar A, McCoy JP, Maecker HT. 2019. Guidelines for Gating Flow Cytometry Data for Immunological Assays, p 81-104. In McCoy JJP (ed), Immunophenotyping: Methods and Protocols. Springer New York, New York, NY.

55. Banta AB, Myers KS, Ward RD, Cuellar RA, Place M, Freeh CC, Bacon EE, Peters JM. 2024. A Targeted Genome-scale Overexpression Platform for Proteobacteria. bioRxiv.

56. Hall AN, Hall BW, Kinney KJ, Olsen GG, Banta AB, Noguera DR, Donohue TJ, Peters JM. 2023. Tools for Genetic Engineering and Gene Expression Control in Novosphingobium aromaticivorans and Rhodobacter sphaeroides. bioRxiv.

57. Quandt J, Hynes MF. 1993. Versatile suicide vectors which allow direct selection for gene replacement in gram-negative bacteria. Gene 127:15-21.

58. Wang Y, Wang Z, Chen Y, Hua X, Yu Y, Ji Q. 2019. A Highly Efficient CRISPR-Cas9-Based Genome Engineering Platform in Acinetobacter baumannii to Understand the H(2)O(2)-Sensing Mechanism of OxyR. Cell Chem Biol 26:1732-1742.e5.

59. Stabb EV, Ruby EG. 2002. RP4-based plasmids for conjugation between Escherichia coli and members of the Vibrionaceae. Methods Enzymol 358:413-26.

CHAPTER 5

Chapter for the Public: A Journey through the Genetics of a Drug-Resistant Bacterium

I wrote this chapter as part of the Wisconsin Initiative for Science Literacy Award for Communicating PhD Research to the Public.

Introduction

As graduate students and scientists, we are traditionally trained to communicate primarily with other experts in our field, focusing on a niche audience. As a result, academic research can sometimes be insular, with researchers working in isolation within very specialized areas. However, to truly advance science, solve complex problems, and create meaningful real-world change, we need to break out of these silos and engage with diverse perspectives and disciplines. Clear communication not only inspires collaboration but also encourages more people to join and support science, contributing to a better and more inclusive scientific future.

My goal for this chapter is to share my six years of graduate work with the people in my life and beyond, who come from all walks of life, and hopefully spark an interest in microbiology. Many of these people may not consider themselves scientists but have the potential to be, or already are.

I'm thankful for the Wisconsin Initiative for Science Literacy (WISL) and Professor Bassam Shakhashiri, for giving me the opportunity to write this chapter, and Cayce Osborne and Elizabeth Reynolds for their writing guidance and editing assistance.

Discovering the World of Superbugs

While working towards my undergraduate degree in Biochemistry and Genetics at Texas A&M University, I had the opportunity to perform research in the lab of Dr. Ry Young. People often equate viruses and bacteria when thinking about infectious diseases, but my undergraduate research taught me that there are distinct differences. Bacteria, like *E. coli* or *Salmonella*, are single-celled microorganisms that can live, survive, and multiply independently. In contrast, viruses, like those causing the flu or common cold, require a host to infect. They hijack host cell machinery to multiply and eventually escape back into the environment to reinfect others. In the Young lab, I studied viruses that only infect bacteria, called bacteriophages or 'phages' for short. During my time there, members of the lab were asked to isolate phages as an experimental treatment for a patient with an immediately life-threatening bacterial infection that was unresponsive to any antibiotics or treatments. These phages targeted and killed the bacteria causing the infection and helped save the patient's life.[1]

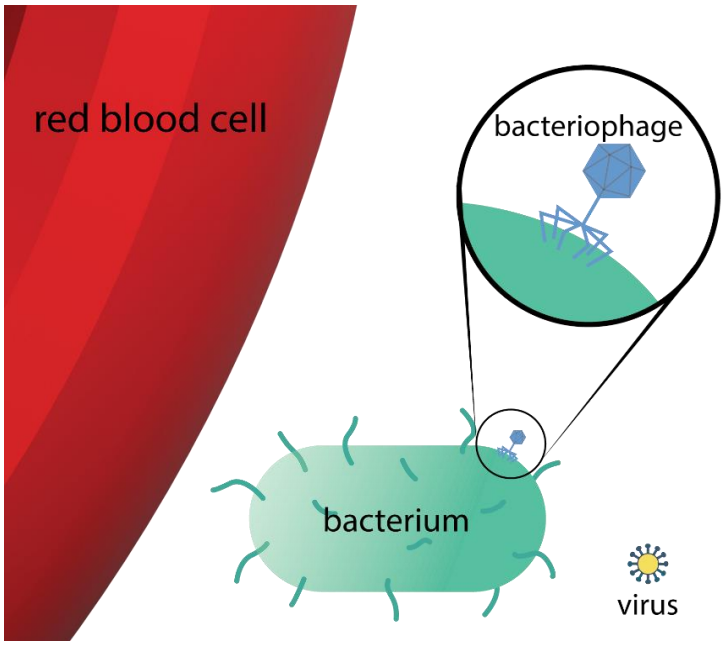

Figure 5.1 A bacterium and viruses to scale compared to a red blood cell. Bacteria are typically 1-5 micrometers, or microns, in length, where viruses are typically 0.02-0.5 microns. Red blood cells in comparison are ~25 microns.

This experience was my first real exposure to superbugs—disease-causing bacteria resistant to all known antibiotics that pose a significant threat to global public health. These pathogens have evolved to withstand multiple antibiotics, rendering standard treatments ineffective and leading to

[1] 1. Steffanie A. Strathdee, Teresa Barker, and Thomas L. Patterson, *The Perfect Predator: A Scientist's Race to Save Her Husband from a Deadly Superbug: A Memoir* (New York, NY: Hachette Books, 2020).

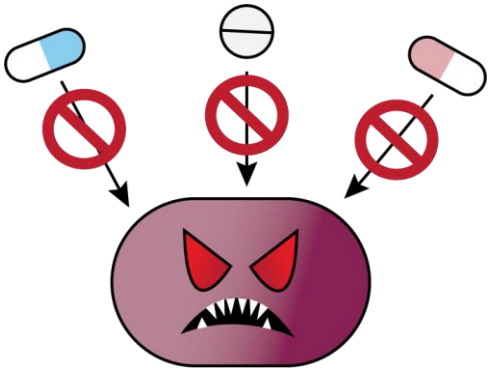

Figure 5.2 A cartoon of a superbug. This bacterium is depicted as super-resistant to antibiotic treatment.

persistent, hard-to-treat infections. The overuse and misuse of antibiotics have accelerated this resistance, resulting in bacteria that are nearly impossible to treat with existing drugs. According to the World Health Organization (WHO), antibiotic resistance is one of the biggest threats to global health, food security, and development today.[2] Superbug infections can cause severe illness, longer hospital stays, increased mortality rates, and higher healthcare costs. The rise of superbugs underscores the urgent need for new antibiotics and innovative treatment strategies to combat these resilient pathogens and safeguard public health.

I was inspired by my time in the Young Lab to pursue a PhD in Microbiology and further study these superbugs and their genetics. My thesis work in Dr. Jason Peters' lab, here at the University of Wisconsin-Madison, focuses on *Acinetobacter baumannii* or *A. baumannii*—the same bacteria that caused that deadly infection treated with Young Lab phages. By studying *A. baumannii* genetics and physiology and how it responds to antibiotics, our lab hopes to eventually develop better treatments.

The Good, The Bad, and The Neutral Bacteria: Where does *A. baumannii* fit in?

Not all bacteria are harmful. 'Good' bacteria in our intestines aid in digesting foods, producing vitamins, and even protecting us from infectious bacteria. Soil and compost bacteria help break down leaf litter and waste, while others help plants get nutrients by growing in their roots. These microorganisms are everywhere and play important roles in human health, agriculture, and more.

---

[2] World Health Organization. *WHO bacterial priority pathogens list, 2024: Bacterial pathogens of public health importance to guide research, development and strategies to prevent and control antimicrobial resistance*. World Health Organization, 2024.

In contrast, some bacteria are 'neutral' and free-living in the environment, not designed for human infection or benefit. Yet, these neutral bacteria can sometimes cause serious infections in individuals with weakened immune systems—these are known as opportunistic pathogens.[3] *A. baumannii* is one such pathogen. It can take advantage of the weakened defenses of immunocompromised individuals, such as those undergoing chemotherapy, patients with serious wounds or illnesses, or patients with chronic autoimmune diseases. Infections caused by *A. baumannii* can lead to severe conditions such as pneumonia, bloodstream infections (bacteremia), and septic shock. Commonly found in soil and water, *Acinetobacter* species have evolved to grow under a variety of conditions and protect themselves from harsh environments. This resilience makes *A. baumannii* a formidable pathogen, particularly in healthcare settings where it can infect patients

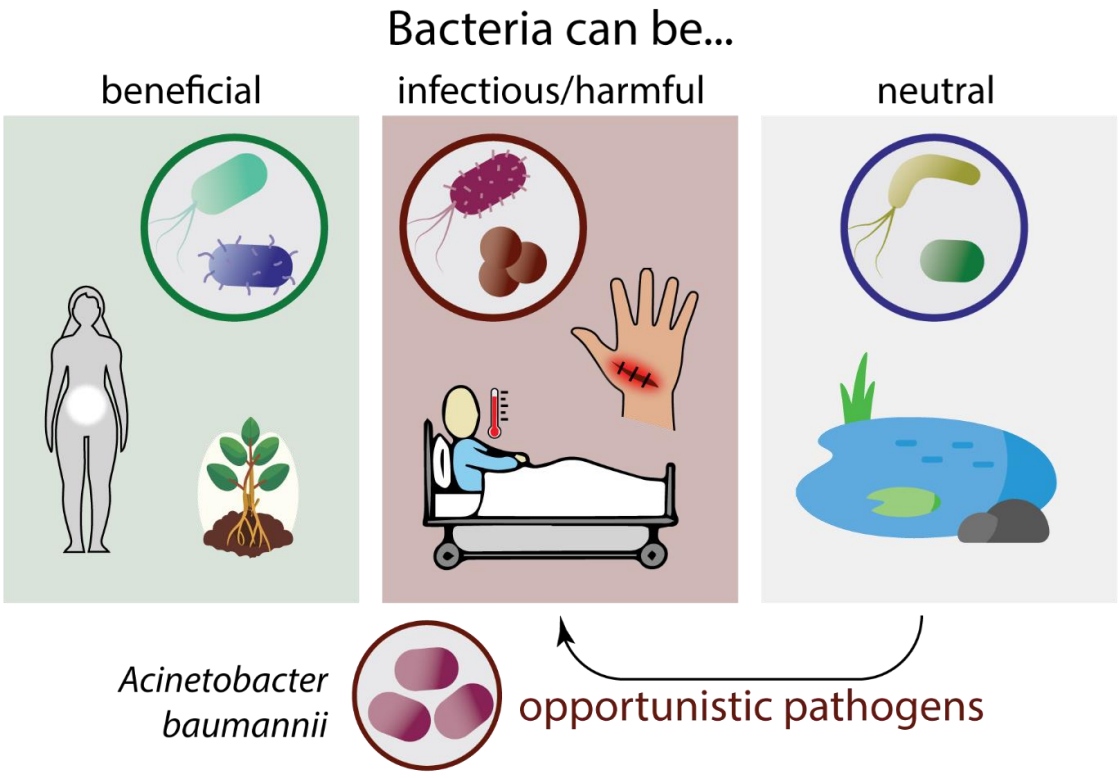

Figure 5.3 Good, bad, and neutral bacteria. Depiction of beneficial or 'good' bacteria, infectious/harmful bacteria, and bacteria which are typically neutral and do not benefit or infect other organisms. An arrow depicts how opportunistic pathogens, which are typically neutral, can become infectious or harmful to immunocompromised individuals. *Acinetobacter baumannii* is one of these opportunistic pathogens.

[3] Wassenaar, Trudy M. 2012. *Bacteria : The Benign, the Bad, and the Beautiful.* Hoboken, N.J: Wiley-Blackwell.

with weakened immune systems and survive on hospital surfaces for long periods without nutrients or water.

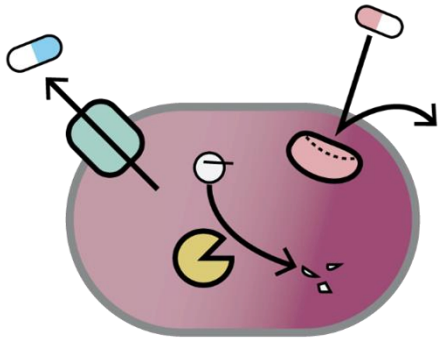

Figure 5.4 Antibiotic resistance mechanisms of *A. baumannii*. These include efflux pumps (green) that pump out antibiotics, proteins (yellow) that degrade or break down antibiotics, and changes to the target (pink) to prevent antibiotic binding.

The Challenge of Antibiotic Resistance

The difficulty in treating *A. baumannii* infections lies in its remarkable ability to develop resistance to antibiotics. Antibiotics typically work by targeting essential processes that bacteria need to survive, like DNA replication or production of the envelope that surrounds and encapsulates the cell. However, *A. baumannii* has evolved several mechanisms to evade these drugs. It can produce molecules that degrade antibiotics, pump out antibiotics before they can take effect, and alter its cellular targets to reduce drug binding. These survival tactics, coupled with its ability to acquire antibiotic resistance genes from other bacteria, have led to the emergence of multidrug-resistant superbug strains.[4]

Understanding the genetic and molecular basis of *A. baumannii*'s resistance mechanisms is crucial for developing new strategies to combat these infections. My research focuses specifically on genes involved in those essential processes necessary for the bacteria to survive, which are often the target for antibiotics. By pinpointing these essential genes, I hope to learn more about *A. baumannii* biology, find new ways to disrupt the bacteria's defenses, and develop more effective treatments.

[4] Kyriakidis, Ioannis, Eleni Vasileiou, Zoi Dorothea Pana, and Athanasios Tragiannidis. 2021. "Acinetobacter Baumannii Antibiotic Resistance Mechanisms." *Pathogens* 10 (3): 373. https://doi.org/10.3390/pathogens10030373.

The Scientist's Toolkit: how (and why) do we study *A. baumannii* genetics?

To understand and combat superbugs like *A. baumannii*, researchers use a variety of techniques from genetics and molecular biology - like DNA sequencing to determine the genetic code, PCR (Polymerase Chain Reaction) to amplify specific DNA segments, and gene cloning to introduce DNA copies or new DNA into a cell. We can use these techniques to create bacterial mutants that have undergone changes or mutations in their DNA, which allow us to study how specific genes contribute to *A. baumannii's* ability to cause disease, survive in hostile environments, or resist antibiotics.

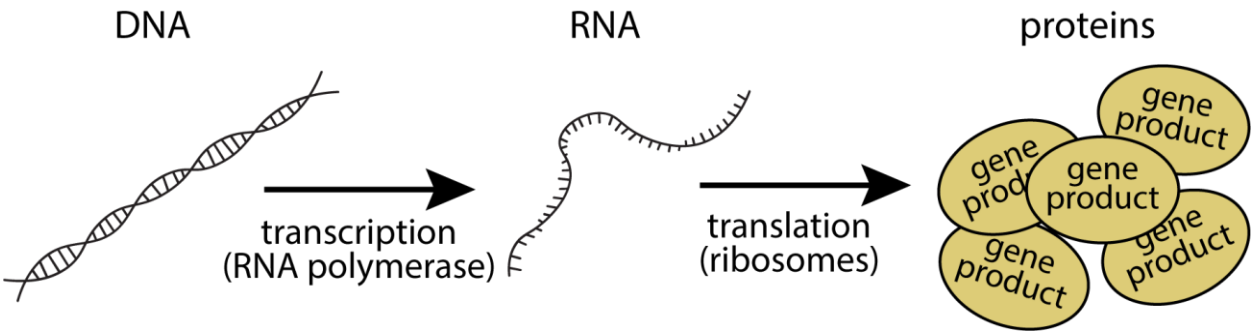

Figure 5.5 The Central Dogma of Biology. This illustrates the flow of genetic information within a biological system, where DNA or genetic material is transcribed by RNA polymerase into RNA, which is then translated by ribosomes into large molecules called proteins that perform functions in the cell. Changing or mutating the DNA affects everything downstream, causing cellular differences that can be seen or measured.

In the lab, my colleagues and I use additional CRISPR tools to create *A. baumannii* essential gene mutants. CRISPR (Clustered Regularly Interspaced Short Palindromic Repeats, after the DNA sequences that first pointed scientists to this naturally occurring system) is a revolutionary genetic engineering tool that allows scientists to make precise changes to the DNA of living organisms. It works like a pair of molecular scissors that can cut DNA at specific locations, allowing for the addition, removal, or alteration of genetic material. However, because these genes are essential, cutting them with CRISPR kills the bacteria, preventing further studies.

CRISPRi, or CRISPR interference, is a variation of the CRISPR technique.[5] CRISPRi does not cut DNA and is more like a broken pair of scissors. Imagine trying to cut paper with scissors that have blunt, non-cutting blades. You can still 'grab' the paper, but you can't cut it. Similarly, CRISPRi uses a modified version of the CRISPR system that binds to a gene without cutting the DNA. This method blocks gene expression, lowering the number of gene products made, almost like a genetic dimmer switch. This approach causes the bacterial cells to be sick but does not totally kill them when we target essential genes, allowing us to conduct more experiments and learn more about essential gene functions. We call these CRISPRi mutants "knockdowns."

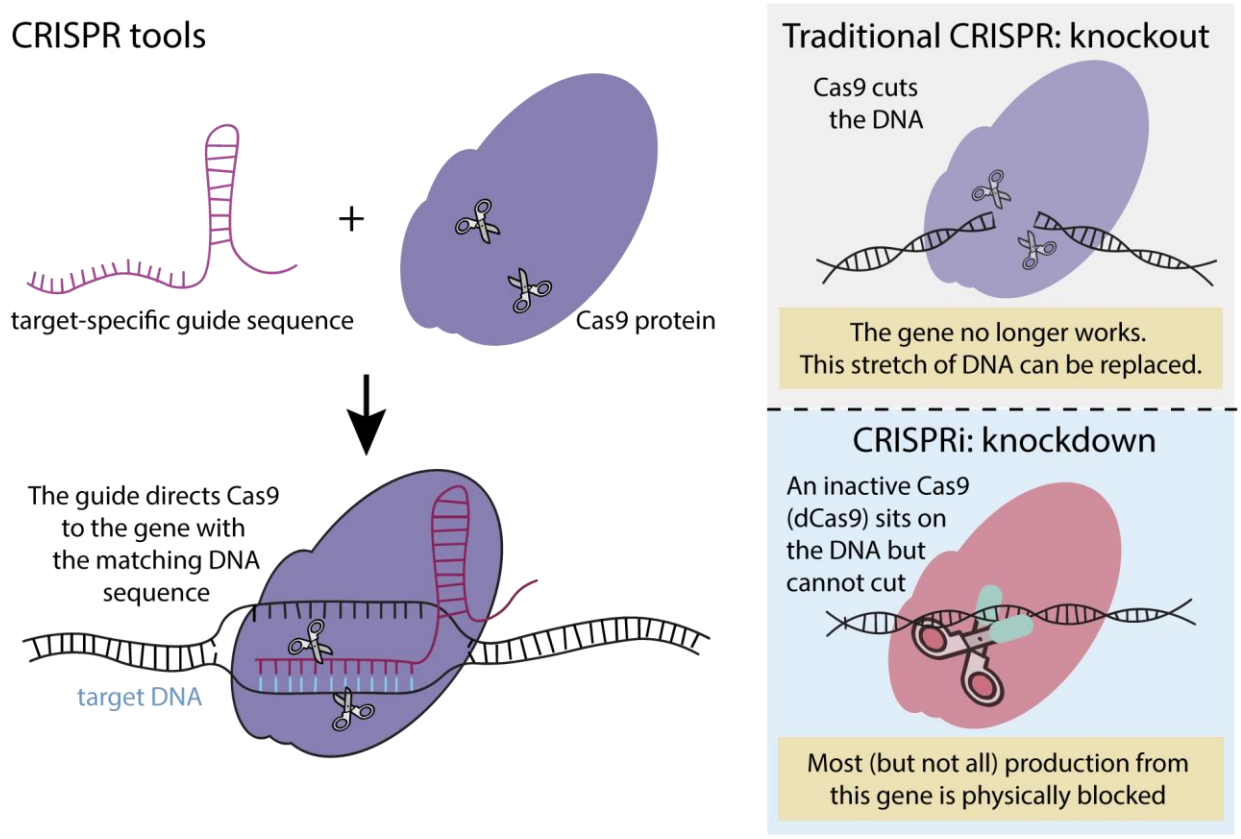

Figure 5.6 CRISPR tools. This involves a guide RNA and the protein Cas9. We can engineer the guide sequence to match any DNA target of interest. The guide will direct Cas9 to matching sequences, where it will cut the DNA and inactivate genes. In some systems, new DNA sequences can be inserted. In our experiments, using normal CRISPR would kill the bacteria we want to study. Instead, we use CRISPRi, which uses a deactivated Cas9 (dCas9). Instead of cutting, this dCas9 will sit on the DNA and block transcription of the gene.

[5] Qi, Lei S., Matthew H. Larson, Luke A. Gilbert, Jennifer A. Doudna, Jonathan S. Weissman, Adam P. Arkin, and Wendell A. Lim. 2013. "Repurposing CRISPR as an RNA-Guided Platform for Sequence-Specific Control of Gene Expression." *Cell* 152 (5): 1173–83. https://doi.org/10.1016/j.cell.2013.02.022.

I teamed up with other members of our lab to use CRISPRi to make a pooled collection of *A. baumannii* mutants, each with a different essential gene knocked down. This collection, known as a genetic 'library', allows us to study over 400 genes at once. By observing how well these mutants grow, we could identify which genes are crucial for the bacteria's survival. For example, if a mutant grows poorly or dies, it suggests that the gene we knocked down is important for the bacteria to thrive. Additionally, by treating the library with antibiotics, we can see which mutants are most affected. For instance, if a particular mutant becomes more susceptible to penicillin-like drugs, it indicates that the targeted gene plays a role in penicillin resistance. This helps us determine which genes are specifically involved in antibiotic resistance and could be targeted by new drugs. Studying over 400 genes at once, in multiple conditions, generates a lot of scientific data! While this data is a treasure trove of genetic information, I could not possibly study all of it in-depth within a single PhD. Instead, I focused on some key findings from these experiments that I will share here.

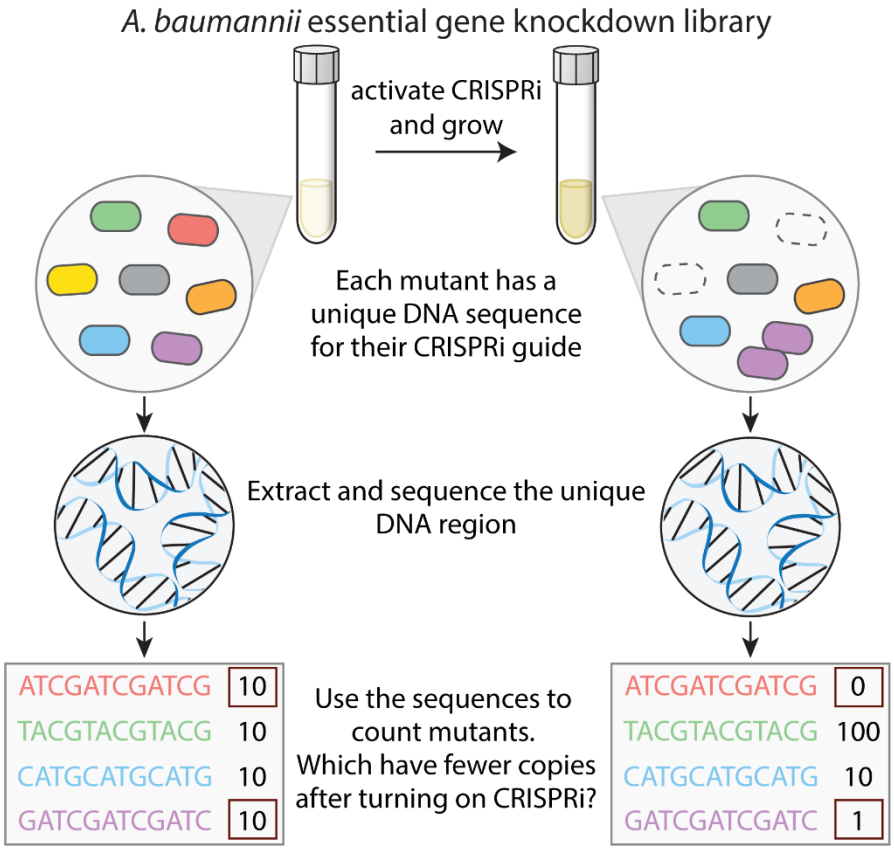

Figure 5.7 Experimental setup to find the essential genes most important for *A. baumannii* survival. Our group looked for knockdowns that were the most depleted after turning on the CRISPRi system.

Finding the best targets: the most vulnerable essential genes

For the first part of this project, our team grew the bacteria in our *A. baumannii* essential gene library, turning on the CRISPRi system and incubating the mutants in culture tubes filled with nutrient-rich liquid. We collected samples from before and after growth and used DNA sequencing to determine the composition of mutants in our samples, looking for gene knockdowns that were sicker compared to the other mutants in the mix. From this experiment, we discovered that *A. baumannii* cells became very sick when we knocked down genes for tRNA synthetases, which are needed for the cell to properly make proteins. Importantly, tRNA synthetases can be targeted with mupirocin, an antibiotic not currently prescribed for *A. baumannii* infections. Although mupirocin is used for different bacterial infections, our data suggested it could potentially treat *A. baumannii* as well. Our team also identified other genes that when targeted or knocked down also made *A. baumannii* sick.

Our team was surprised to find that the gene causing the largest and most significant growth defect was unidentified, its function unknown despite its crucial role in the bacteria's survival. Upon further investigation into the gene, I discovered that it was a phage repressor. Phages - those bacterial viruses I had studied in my undergraduate work - can have two lifestyles: a lytic lifestyle, where they replicate and then burst the host cell to escape and reinfect, and a lysogenic lifestyle, where they integrate their own DNA into the host's and lie dormant until later. This phage repressor was part of one of these lysogenic phages and was actively maintaining the phage's dormant lifestyle.[6] Targeting this phage repressor with CRISPRi caused the phage to switch to the lytic lifestyle, expressing toxic genes that killed the host *A. baumannii* cells. Phages that target and stow away in *A. baumannii* are surprisingly common, and this finding opens the door to discovering proteins produced by these

[6] Britannica, T. Editors of Encyclopaedia. "bacteriophage." *Encyclopedia Britannica*, May 31, 2024. https://www.britannica.com/science/bacteriophage.

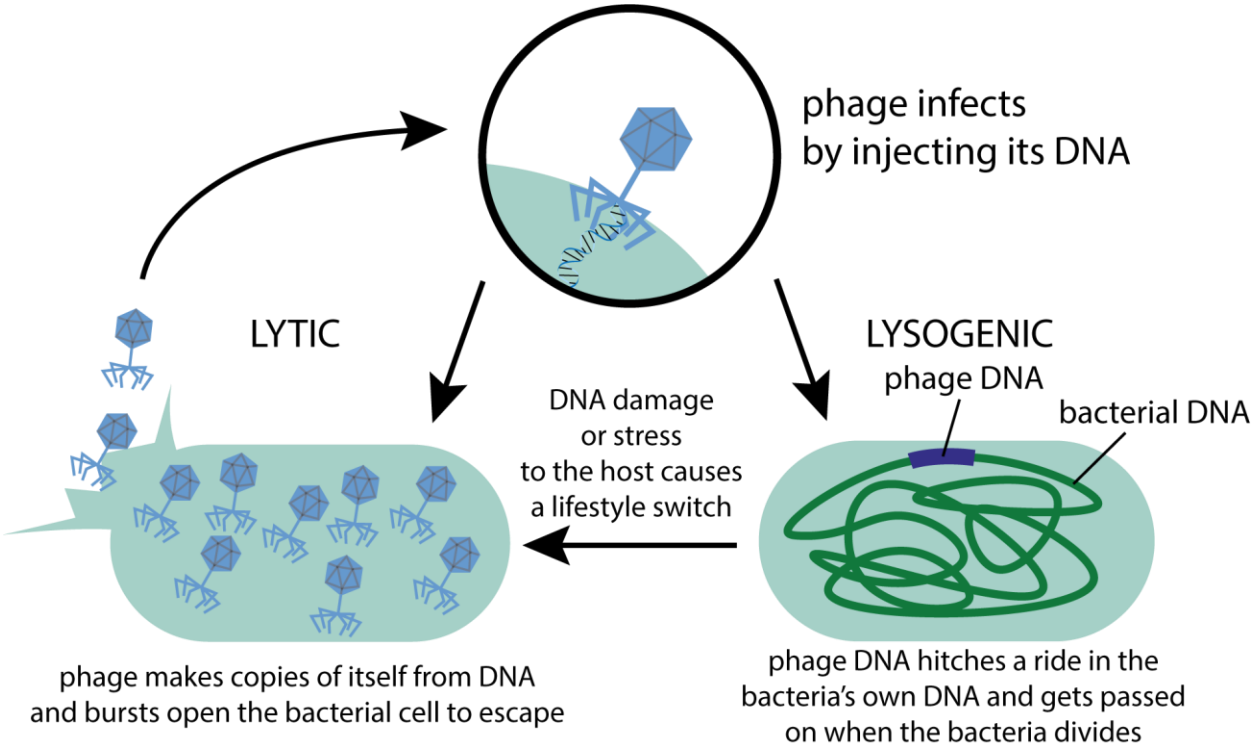

Figure 5.8 The two main lifestyles of bacteriophages. In the lytic cycle, phages infect bacteria, replicate, and then burst open or lyse the host to release new phage progeny. This requires phages to carry genes that can kill their bacterial host from the inside. Some phages have an alternate lifestyle known as lysogenic, in which they integrate their DNA into the bacterial genome. They remain dormant and pass on as the bacteria divides until they are triggered by DNA damage or other stress that causes them to switch lifestyles, like an "eject" button. The phage repressor in our screen was keeping the phage infecting our *A. baumannii* strain in the lysogenic lifestyle. By knocking it down, we essentially hit the "eject" button and killed the *A. baumannii* host.

phages that are exceptionally good at killing *A. baumannii*. Engineered versions of these proteins could potentially be used as future treatments for infection.

Genes in antibiotic resistance

I then wanted to see how *A. baumannii* essential genes interact with antibiotics. To do this, I grew this library of *A. baumannii* mutants again, but this time with low levels of antibiotics added. I tested 45 different antibiotics in separate

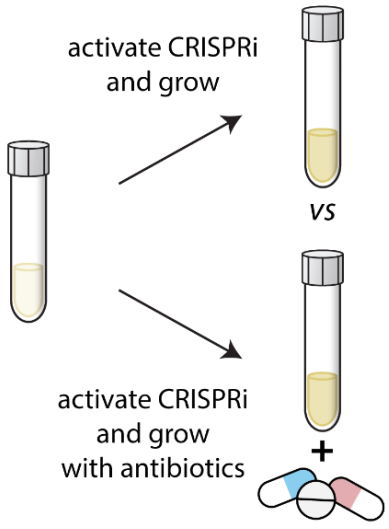

Figure 5.9 Genes in antibiotics. I compare the library grown with antibiotics to the library grown without them to find genes especially sensitive to antibiotics.

tubes, looking specifically for gene knockdowns that became sicker, or died, in antibiotics. This would indicate that these genes are needed for drug resistance.

I discovered that knocking down genes involved in lipooligosaccharide (LOS) transport caused *A. baumannii* to be sensitized to a wide array of antibiotics. LOS makes up the outermost layer of the envelope that surrounds and protects *A. baumannii* cells. This LOS layer, the outer membrane, acts as a crucial barrier, preventing harmful substances – like antibiotics – from entering the bacterial cell. The LOS transport system functions like a shuttle, moving LOS from its production site inside the cell

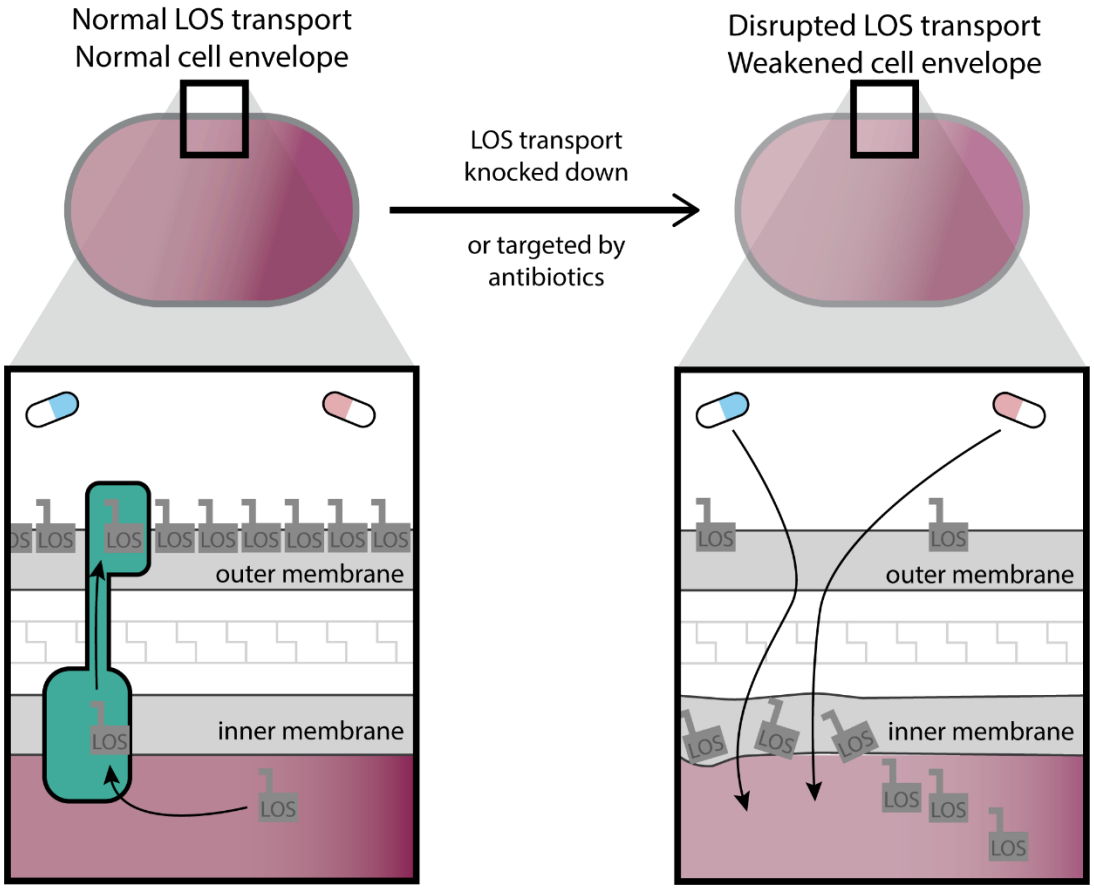

Figure 5.10 A. baumannii's cell envelope, which separates the inside of the cell from the outside, has an inner membrane and an outer membrane. The outer membrane contains LOS that forms a tight barrier to antibiotics. These cartoons depict the cell envelope with normal LOS transport (left) or with disrupted LOS transport (right). LOS is typically transported to the outer membrane by the LOS transport machinery (teal). When LOS transport is knocked down or targeted with antibiotics, LOS builds up in the inner membrane and inside the cell. The inner membrane is weakened by the unexpected backup of LOS, and the outer membrane is missing its important outer component, allowing other antibiotics to pass through both barriers.

to its proper place in the outermost layer. I found that knocking down the LOS transport system causes a traffic jam of LOS in the cell. Surprisingly, this backup doesn't just disrupt the destination of LOS (the outer membrane) but also the stop along the way (the inner membrane), allowing antibiotics to get through both barriers and reach the cell's interior more easily. This finding is especially important in the context of other scientists' work. Recently, new drugs have been developed that specifically target this LOS transport system.[7] My discovery suggests that these drugs, which also cause an LOS backup, could actually enhance the effectiveness of other antibiotics, helping them reach their targets. This tells us that these new drugs targeting LOS transport could be extremely useful in combination therapies – where clinicians prescribe multiple antibiotics together for patient infections – and work simultaneously with existing antibiotics to create a more powerful strategy to combat *A. baumannii* infections.

Connecting the dots with gene functions

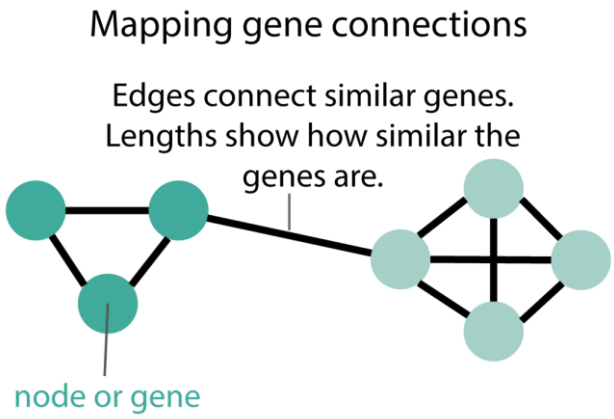

Figure 5.11 Mapping gene connections. I used this large dataset to draw an essential gene network for *A. baumannii*, where each node is a gene. Genes are connected by lines or edges when they behave similarly. Lengths of those edges are related to how similar the genes are. Connected genes are likely to be involved in the same cellular processes.

These types of experiments generate large amounts of data; for each of the 400+ gene knockdowns, I know if they are sensitized, more resistant, or have no change when treated with 45 different antibiotics. Because of the sizable number of observations, patterns start to emerge across the antibiotics. Some of the genes in

[7] Pahil, Karanbir S., Morgan S. A. Gilman, Vadim Baidin, Thomas Clairfeuille, Patrizio Mattei, Christoph Bieniossek, Fabian Dey, et al. 2024. "A New Antibiotic Traps Lipopolysaccharide in Its Intermembrane Transporter." *Nature* 625 (7995): 572–77. https://doi.org/10.1038/s41586-023-06799-7; Zampaloni, Claudia, Patrizio Mattei, Konrad Bleicher, Lotte Winther, Claudia Thäte, Christian Bucher, Jean-Michel Adam, et al. 2024. "A Novel Antibiotic Class Targeting the Lipopolysaccharide Transporter." *Nature* 625 (625): 1–6. https://doi.org/10.1038/s41586-023-06873-0.

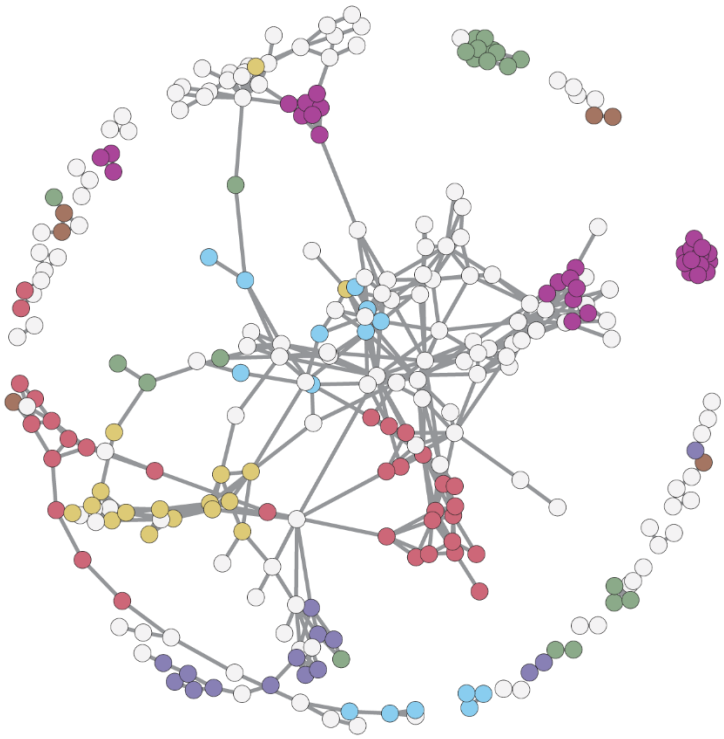

Figure 5.12 An *A. baumannii* essential gene network created using this dataset. Genes that are the same color are involved in the same well-known processes and are mostly interconnected. Uncolored genes fall into an "other" category.

our essential gene library behave similarly to each other when they are knocked down– that is, the knockdown mutants react in the same way across all the antibiotics. Genes with similar patterns have similar functions, or are working towards the same end goal in the cell.[8] I visually represented these similarities in a network, which is like a map of genes, that shows which genes are closely related and interact with each other. By analyzing these connections, I was able to identify the functions of several previously unknown genes.

I additionally focused on a group of genes involved in cell shape and cell division. Cell shape and cell division are closely related processes in bacteria. Cells grow lengthwise before cell division, during which the cell splits into two daughter cells. This process is

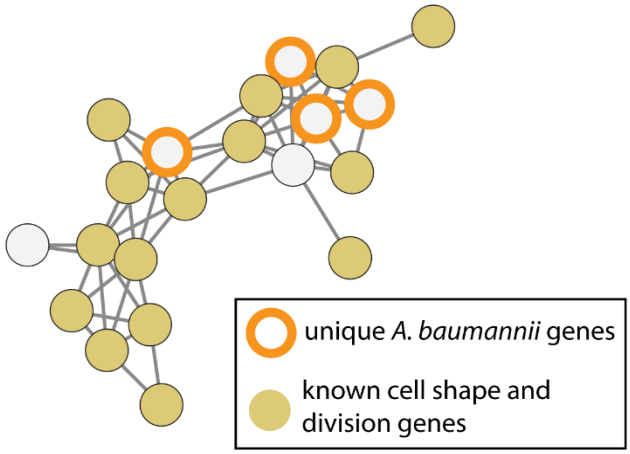

Figure 5.13 The cell division genes from the larger essential gene network. Unique *A. baumannii* genes are circled in orange and are clearly connected to known cell division genes (yellow).

[8] Peters, Jason M., Alexandre Colavin, Handuo Shi, Tomasz L. Czarny, Matthew H. Larson, Spencer Wong, John S. Hawkins, et al. 2016. "A Comprehensive, CRISPR-Based Functional Analysis of Essential Genes in Bacteria." *Cell* 165 (6): 1493–1506. https://doi.org/10.1016/j.cell.2016.05.003.

tightly regulated to ensure that each new cell receives the correct genetic material and maintains the proper shape and size.[9] While the process of cell division has many commonalities across bacterial species, I found that *A. baumannii* has unique genes for cell shape and division machinery that are distinct from other species. *A. baumannii* has a unique potato-like shape, and my research shows that this different machinery for cell division could be the explanation. I used microscopy to confirm that these *A. baumannii*-specific genes were indeed involved in division, observing that knocking down these genes significantly prevented the cells from dividing. Cell division is an important target for antibiotics, such as beta-lactams (like penicillin), but clinical strains of *A. baumannii* are often resistant to the drugs currently available. This discovery opens avenues for developing new, effective antibiotics that target these unique cell division genes.

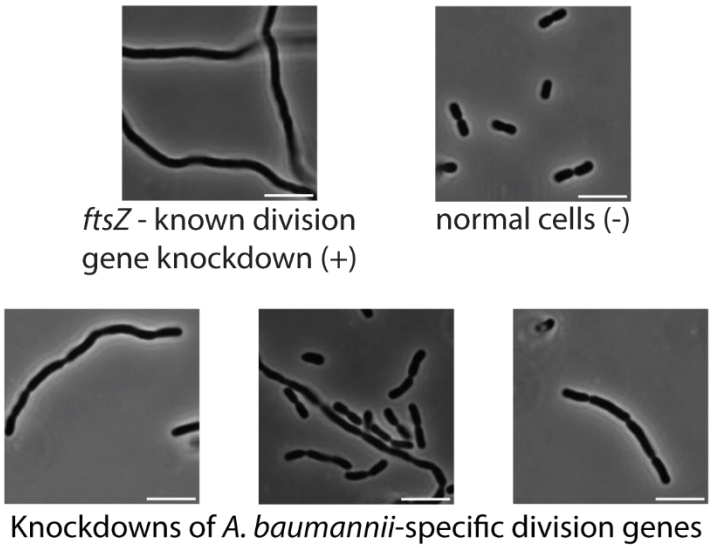

Figure 5.14 Microscopy of the knockdowns of unique division genes in *A. baumannii*. The top left shows a known division gene knockdown. These cells cannot divide and form long strings, compared to normal cells (top right), which are short and almost rounded. Knockdowns of these *A. baumannii*-specific division genes are also elongated and chained, confirming that these genes are needed for proper division. The small line in the bottom right indicates 5 microns.

New weapons in the arsenal: from genetics to therapeutics

My thesis research, using CRISPRi to investigate essential genes in *A. baumannii*, revealed important insights into the bacterium's unique biology and weaknesses. This work is part of a broader trend in genetic research that's opening new doors for drug development against superbugs. By

[9] Margolin, William. 2009. "Sculpting the Bacterial Cell." *Current Biology* 19 (17): R812–22. https://doi.org/10.1016/j.cub.2009.06.033.

understanding how bacteria resist antibiotics and survive in harsh conditions, scientists can find new strategies to target and treat bacterial infections. For instance, by identifying genes that are particularly sensitive when knocked down, our lab pinpointed specific weaknesses that can be used to develop new drugs. These discoveries pave the way for creating new antibiotics to target these critical pathways. I also showed that targeting one pathway can make other antibiotics more effective, potentially guiding future combination therapies for these infections.

This research, which combines large-scale, 'one-step' genetic screening with antibiotic testing, not only has the potential to lead to more effective treatments against multidrug-resistant bacteria, but also exemplifies collaborative scientific efforts. Researchers across academic institutions, pharmaceutical companies, and biotech startups are working together and using these techniques to develop powerful new tools in the fight against antibiotic-resistant infections. With a continued focus on exploring and targeting the ways bacteria survive, infect, and resist antibiotics, we can hopefully overcome multidrug resistance and one of the biggest public health challenges of our time.

Reflections on the PhD journey

My thesis research, presented here, was the backbone of my PhD. I've only shared a small part of our findings here as there was far more work (and struggle) beneath the surface: learning how to ask the right questions, designing experiments to answer them, and handling the large amounts of data these experiments generated. Over the past six years, I've learned to manage, analyze, and interpret vast and confusing data, turning it into coherent stories and visual presentations. Research doesn't happen in a vacuum either. One of my favorite aspects of my thesis project has been collaborating with others who have complementary skills and discussing my research and experiences with peers.

While my thesis research was a major focus during my PhD, it was far from the entirety of my graduate experience. Alongside my research, I embraced various roles that broadened my perspective and

skills. I became actively involved in my graduate program's committees, collaborating with students, staff, and faculty to plan annual student retreats and recruitment and address important program issues like diversity, equity, and inclusion. I delved into the world of entrepreneurship and the intersection of science and business through the Morgridge Entrepreneurial Bootcamp and through the Biotechnology Training Program (BTP). Through BTP, I interned with the Air Force Research Labs, offering me a glimpse into US government research. In more recent years, I've become an active member of WiSolve Consulting Group, a nonprofit run by UW-Madison graduate students and postdocs, helping local startups address challenges through market research, grant writing, and more. I've even had the chance to fundraise and organize major events for fellow graduate students, like UW-Madison Life Sciences Career Day and the Midwest Healthcare Case Competition. These experiences provided unique opportunities that only a graduate student could have, and greatly enriched my personal and professional development. I strongly encourage anyone pursuing a PhD to seek out experiences like this as well. For me, they have been invaluable.

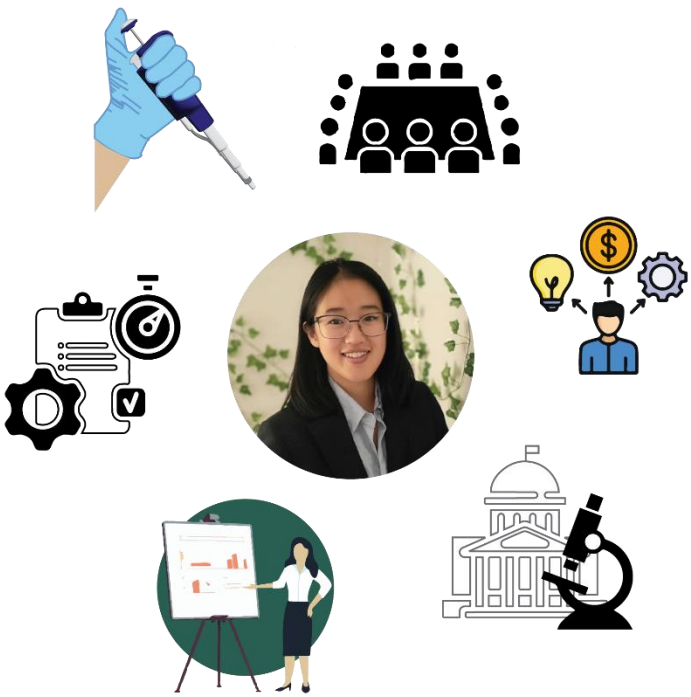

Figure 5.15 The PhD journey. My thesis project is only one aspect of my time in graduate school. My experiences outside of the lab helped me build additional soft skills, meet students in other programs, and work with professionals outside of UW-Madison.

All these experiences have led me down a slightly different path than I initially planned when I started graduate school. I found that I genuinely enjoyed computational analyses, giving presentations, and meeting and chatting with diverse teams far more than spending time at the lab bench in my lab coat.

After my PhD, I will be starting a position as a management consultant, applying the skills I've gained in graduate school to areas outside of science experiments. While my thesis project focused on a specific scientific question and allowed me to become an expert in that niche, I now look forward to broadening my experiences across various business sectors. Nevertheless, microbiology, especially bacteria and bacteriophages, will always hold a special place in my heart.

CHAPTER 6

Conclusions and future directions

Conclusions

The objective of this thesis was to utilize advanced systems-level approaches to investigate and characterize essential genes in *Acinetobacter baumannii*. Despite its clinical significance, the genetic landscape of *A. baumannii*, especially its essential genes, remains largely unexplored. Initially, the focus of the field was predominantly on non-essential genes due to the limitations of transposon-based tools used in systems-level studies of this pathogen. My research addresses this knowledge gap by employing a CRISPRi essential gene knockdown library to examine gene vulnerabilities, drug-gene interactions, and gene functions within the unique biological context of *A. baumannii*. My findings provide significant phenotypic data and analytical tools, serving as a valuable resource for exploring *A. baumannii* essential biology in therapeutic interventions.

In Chapter 2, we constructed and validated an essential gene CRISPRi library in *A. baumannii* ATCC 19606, identifying essential genes and pathways sensitive to knockdown, including NDH-1 (*nuo*), highlighting potential targets for antibiotic development. We also developed models examining the relationship between gene knockdown and fitness, which elucidate how gene product levels impact function and resistance phenotypes at sub-inhibitory antibiotic concentrations. Additionally, we discovered that tRNA genes influence carbapenem sensitivity and uncovered anticorrelated phenotypes underlying the synergistic interaction between rifampicin and colistin.

I expand on this in Chapter 3 by establishing a comprehensive dataset of chemical-gene interactions using the same library, revealing that the vast majority of essential genes interact with at least one chemical condition. Notably, I found that lipooligosaccharide transport is crucial for generalized antibiotic resistance, as inhibiting this transport increases membrane permeability and drug sensitivity. This finding is particularly relevant in the context of recently discovered Lpt-targeting drugs and their potential for combination therapeutics. I also identified poorly

characterized genes unique to *A. baumannii* that may play roles in its distinctive biology and used an essential gene network to functionally connect many of these genes to pathways such as cell division. Finally, I develop a method to analyze this dataset by combining cheminformatics with genetic pathway effects, observing that phenolic monoterpenes appear to have unique mechanisms of action and that tetracycline class antibiotics exert different effects on *A. baumannii*.

Chapter 4 introduces and characterizes a suite of novel expression vectors designed for studying *A. baumannii* essential genes. These vectors, used in Chapter 3 for the expression of cell division genes and fluorescent constructs, include a novel promoter that allows for controlled gene expression in *A. baumannii* and *E. coli*, facilitating genetic studies.

Chapter 5 summarizes my graduate work for a general audience, as part of the Wisconsin Initiative for Science Literacy. This chapter aims to communicate important concepts and findings from this thesis to those not specifically trained in science, bridging the gap between scholarly work and public knowledge. Through this chapter, I strive to make the complexities of microbiology and my research accessible, to foster a greater appreciation and understanding of the ongoing efforts to combat antibiotic-resistant pathogens.

The findings presented in this thesis advance our understanding of *A. baumannii* genetics from a binary focus on essentiality to a more nuanced comprehension of genetic vulnerability. We created and validated a CRISPRi knockdown library as a robust tool for studying *A. baumannii* biology. Our analyses in Chapters 2 and 3 detail the general fitness of essential genes upon knockdown and their chemical-specific vulnerabilities across more than 45 different conditions. Remarkably, over 93% of essential genes exhibited at least one significant chemical interaction, with over 5000 total

significant interactions. These datasets are invaluable for further characterizing the 400+ essential genes in *A. baumannii*.

The roles of mobile genetic elements (MGEs) are particularly intriguing. In Chapter 2, we identified GO593_00515, a phage repressor, as the most vulnerable gene in *A. baumannii* 19606. In Chapter 3, we found a transposon-associated regulatory gene and another Arc-type phage repressor unique to *A. baumannii*, with strong phenotypes or associations with global regulation and DNA damage. Considering the significant role MGEs play in antibiotic resistance in *A. baumannii*, and their diversity and ubiquity, there are compelling questions regarding whether MGEs could be therapeutically exploited. These elements often contain endolysins or toxic genes and cause global regulatory effects that could potentially be leveraged.

While findings in Chapters 2 and 3 identify novel genes and provide functional phenotyping, the exact mechanisms for many of these genes within their respective pathways remain unclear. For instance, NDH-1 contributes to overall fitness, colistin sensitivity, and rifampin resistance in Chapter 2. In Chapter 3, cytochrome bo_3 oxidase is identified as having multiple significant phenotypes, particularly in contributing to tigecycline resistance. The nuances of electron transport and remodeling in *A. baumannii*, frequently appearing in our datasets, warrant further investigation.

Taken as a whole, this thesis presents a suite of biological and computational tools for studying *A. baumannii*. The CRISPRi library and expression vectors developed here establish a foundation for future genetic studies in this organism, a non-model pathogen with limited genetic tools compared to more extensively studied organisms. The fitness data presented constitutes a significant phenotypic resource for future research. Additionally, we developed multiple computational tools to manage and interpret this data, which will be valuable for future applications. The data analysis pipeline created for handling sequencing data, interpreting sgRNA counts, and modeling

knockdown responses validates the effectiveness of mismatch guide predictions and links transcriptional levels to fitness effects. Our chemical analyses offer a framework for understanding genetic perturbations in the context of chemical structures. In conclusion, this thesis lays a robust groundwork for advancing our understanding of *A. baumannii* and informs future research efforts aimed at uncovering specific bacterial physiology and developing effective therapeutic strategies against this formidable pathogen.

Future directions

Mobile genetic elements and their regulation of host lysis in A. baumannii ATCC19606

We identified regulators of mobile genetic elements as particularly vulnerable in A. baumannii ATCC 19606 (GO593_00515 in Chapter 2) and critical for fitness under chemical stress (GO593_15125 and GO593_11615 in Chapter 3). Knocking down these repressors led to decreased fitness, suggesting toxic genes within their respective mobile genetic elements may be expressed. Intact phages typically contain lysis cassettes, which often include endolysins or holins – enzymes that degrade the host cell wall or form pores, leading to cell lysis (1). Future work could identify which genes, when expressed, cause host cell lysis. Specifically, we could use bioinformatic tools, such as MGEfinder (2), to better identify MGEs and search within predicted MGEs for proteins with domains characteristic of endolysins (3) or other toxic proteins (4). Using expression vectors in *A. baumannii* (see Chapter 4), we can express proteins of interest to identify genes that cause cells to lyse or cease growth after induction.

Additionally, I discovered that the prophage containing GO593_00515 is excised from the genome at some frequency in the ATCC 19606 strain. However, it remains unclear if phage progeny are being synthesized and assembled. Quantitative PCR (qPCR) can be utilized to quantify any increase in phage locus copies following knockdown (5), and improved purification techniques and electron

microscopy could be used to detect phage particles (6). If phage production is confirmed, further characterization of this phage could be performed using bioinformatic tools and screening across a wider variety of *A. baumannii* strains to identify the host range. Additionally, RNA-seq in WT and after induction of knockdown of GO593_00515 could provide important information on what, if any, of these phage genes are expressed under normal growth conditions and how this phage is regulated.

LexA-like proteins as newly discovered regulation of phage lysogeny

Acinetobacter species lack LexA, a canonical DNA damage response (or SOS response) regulator, instead employing the combined actions of a repressor protein UmuDAb and a small regulator protein DdrR (7, 8). We identified GO593_11615 in *A. baumannii* ATCC 19606 as a phage-associated regulator that has a LexA-like domain, suggesting it may carry a LexA analog to compensate for the absence of native LexA, which other phages exploit as a signal to switch to the lytic cycle during host DNA damage. Data in Chapter 3 showed that knocking down GO593_11615 caused fitness defects both upon induction of the CRISPRi system and in levofloxacin, a DNA-damaging antibiotic, suggesting that depletion of the phage regulator may be inducing the lytic cycle. To identify what genes are upregulated upon induction of GO593_11615 knockdown and determine the role of the repressor in overall phage regulation, we could perform RNA-seq to measure transcriptional changes (9, 10). In addition, we could perform ChIP-seq (Chromatin Immunoprecipitation sequencing)—a technique that identifies DNA binding sites by crosslinking protein-DNA interactions, shearing the DNA, immunoprecipitating the protein of interest, and sequencing the associated DNA fragments (11)—to identify direct binding sites of GO593_11615. Combining RNA-seq and ChIP-seq data (12) allows for thorough promoter and DNA-binding sequence analyses to provide important information about downstream GO593_11615 regulation.

Typically, the protein RecA induces cleavage of LexA in response to DNA damage to initiate the SOS response, and it is possible that *A. baumannii* RecA or other SOS response proteins induce cleavage of GO593_11615. A previous study in *A. baumannii* ATCC 17978 found that DdrR interacts with one putative LexA-like phage repressor but not with another in the same strain (7). This study also showed that activated RecA* (*A. baumannii* RecA in complex with ATP and ssDNA) was unable to induce self-cleavage of these phage repressors, suggesting RecA* may only recognize the repressor bound to DNA, similar to RecA-mediated cleavage of an *E. coli* phage repressor (13). We could similarly test whether GO593_11615 interacts with the *A. baumannii* SOS response by testing for binding between GO593_11615 and activated RecA or DdrR with a pull-down assay in cells or with purified components using surface plasmon resonance as previously described (14). We could test for cleavage of GO593_11615 *in vitro* as previously described (7, 13). The proposed RNA-seq and ChIP-seq experiments may identify DNA binding sequences, enabling additional autoproteolysis assays with DNA-bound GO593_11615.

Although phage repressors with LexA-like domains have been identified in the lab strains *A. baumannii* ATCC 19606 and ATCC 17978, the evolution of this possible phage regulation mechanism has not been well-characterized. Our analyses in Chapter 3 revealed that this phage repressor has orthologs in ~25% of Gammaproteobacteria. However, further analyses are needed to better describe coevolution among hosts and host-encoded LexA to determine whether LexA-like phage regulators are more prevalent in species lacking the canonical LexA. Such studies could highlight a possible evolutionary path for phages that utilize these regulators.

LptC$_{Ab}$ and its role in Lpt-targeting antibiotics

LptC is one of the periplasmic proteins of the lipopolysaccharide transport system (Lpt), responsible for transfer of lipopolysaccharides (LPS) – or in *A. baumannii*, lipooligosaccharide (LOS) – between

the Lpt inner and outer membrane complexes (15). In Chapter 3, we found that LptC from *A. baumannii* ($LptC_{Ab}$) had few hits from our orthology search in Gammaproteobacteria, even though the Lpt pathway was generally highly conserved. Indeed, the primary sequence of $LptC_{Ab}$ diverged heavily although structural prediction of $LptC_{Ab}$ was highly confident in its identity. Recently, novel antibiotics targeting Lpt in *A. baumannii* have been well-characterized (16, 17), but these macrocyclic peptide antibiotics have poor activity in non-*Acinetobacter* species, likely due to differences in the Lpt proteins (e.g., *A. baumannii* LptFG are <25% identical to their *E. coli* counterparts) (16).

To better understand Lpt differences and to potentially identify other target species for these antibiotics, we could perform a thorough evolutionary analysis of these genes. While LptC had few orthologs in our initial search, other Lpt proteins were considered highly conserved across Gammaproteobacteria. By examining the evolution of these genes combined with structural prediction software, we could potentially identify species where Lpt is somewhat similar, using species known to be resistant to macrocyclic peptides (e.g., *E. coli, P. aeruginosa, K. pneumoniae*) as a baseline. It is likely that there are other species in the Moraxellales order against which these drugs are effective, and we could further characterize whether there are direct relationships between Lpt machinery, structure, and the components they transport (i.e., LOS vs LPS).

Additionally, Pahil et al. found the inner membrane complex of Lpt, $LptB_2FG$, bound *E. coli* LPS despite the structural differences affecting macrocyclic peptide binding (16). To test whether Lpt from *A. baumannii* could functionally replace that of *E. coli*, we could delete the Lpt genes from *E. coli* and attempt to complement them with the corresponding *A. baumannii* Lpt genes to better understand the functional differences between these complexes. Multimeric protein predictions using AlphaFold Multimer (18) or AlphaFold3 (19) could inform whether individual Lpt proteins could be substituted before testing them experimentally. This would provide more information about the

functionality and species-specificity of these components. If successful, we could evaluate the activity of macrocyclic peptides against *E. coli* with *A. baumannii* Lpt to reveal whether Lpt structural differences alone prevent drug activity or if there are other contributing factors.

$HolD_{Ab}$ subunit interactions and role in DNA Polymerase activity

In bacteria, DNA polymerase III is responsible for DNA synthesis and replication. For DNA replication to occur, DNA polymerase must be properly tethered to the template DNA with the clamp-loading complex, composed of the beta sliding clamp – a ring-shaped protein complex that encircles the DNA - and the clamp loader, which hydrolyzes ATP to assemble the beta sliding clamp onto primed DNA (20, 21).

We found that the psi subunit (HolD) of DNA polymerase III is highly divergent in *A. baumannii* at the sequence level. Because of this divergence, it was unable to be identified by feature-aware ortholog analyses (22). However, previous work identified homologs of $HolD_{Ab}$ as the likely psi subunits for *Acinetobacter* species (23). Additionally, structural prediction software (24) identified the *A. baumannii* protein as HolD with high confidence, and we mapped the predicted *A. baumannii* HolD ($HolD_{Ab}$) structure to the structure of *E. coli* HolD ($HolD_{Eco}$) to confirm the similarities in structure. The most striking difference between the predicted structure of $HolD_{Ab}$ and the $HolD_{Eco}$ crystal structure was that an additional unstructured loop region in $HolD_{Ab,}$ which could affect interactions or binding with other DNA polymerase subunits.

To further investigate, we could model $HolD_{Ab}$ with the other clamp-loading complex subunits from *A. baumannii* using multimeric protein prediction software (18, 19) to compare predicted interactions to those in *E. coli*. The multimeric protein prediction may resolve the unstructured loop to provide more information about its function. In conjunction, we would attempt to purify these proteins and solve the structure of the clamp-loading complex.

Furthermore, we would test if $HolD_{Ab}$ expression from a replicative plasmid or integrating Tn*7* vector could complement a deletion of the native HolD in *E. coli* and vice versa. Since these proteins are essential in both species, unsuccessful complementation should result in non-viable cells from the HolD deletion strains. Complementation or the lack thereof would provide important functional information about HolD in these organisms, and whether the functional interactions of these proteins differ significantly. Understanding why HolD is divergent and what specific functions it plays in DNA synthesis in *A. baumannii* could elucidate important differences in an essential process, which plays a direct role in growth and pathogenicity and could affect efficacy of antibiotics targeting this pathway.

Further characterization of cell wall synthesis and cell division genes in A. baumannii

In the *A. baumannii* essential gene network in Chapter 3, I identified three poorly characterized genes of interest – *blhA, smc2,* and *spor* – associated with cell division and cell wall synthesis. I propose multiple experiments to further characterize the roles of these genes.

I showed that BlhA could be fluorescently tagged with sfGFP and appeared to be localized to the septum, or site of division in *A. baumannii.* The question remains whether BlhA functionally interacts with the divisome, the protein complex responsible for coordinating bacterial cell division and cell wall synthesis at the septum. Following previously described protocols (25), we could perform a pulldown assay with BlhA, with a His-tag or other tag for affinity purification, to identify interacting partners. In addition, we can perform bacterial two-hybrid assays (26) to validate hits from the pulldown assay or test for interactions with known *A. baumannii* divisome-associated proteins—such as AdvA (27, 28) or BonA (29)—or with highly conserved divisome proteins, such as FtsZ or FtsA (30). This experiment would provide insights into the role BlhA plays in cell division and confirm any direct interactions with the divisome complex.

Overexpression of Smc2 revealed chained cells with impaired division, and fluorescently tagged Smc2 appeared to form elongated aggregates from either localization or because of toxic overexpression of the protein. However, these microscopy experiments were done with cells fixed at mid-log, with a single concentration of inducer for expression from replicative plasmids. It is possible that Smc2 dynamics were obscured due to the methods we employed or because protein levels are crucial; the possibility of cell-to-cell variation of replicative plasmid copy could affect the phenotypes I observed. To better characterize the effects of Smc2 protein levels on cell division, I propose expressing Smc2 or Smc2::sfGFP from an integrative vector under control of an IPTG-inducible promoter (see Chapter 4), varying the level of induction to control the increase of Smc2 expression. Additionally, we could express Smc2::sfGFP under control of its native promoter, and—as long as essential functions remain unimpaired—create a clean deletion of the native *smc2* as previously described (31). In conjunction with knockdown of Smc2::sfGFP, titrated with mismatch guides, we could perform parallel live-cell time-lapse fluorescence microscopy experiments. This should allow us to visualize phenotypic effects of both knocking down and increasing Smc2 levels in conjunction with protein dynamics and localization throughout division.

Smc2 is named because of similarities to Structural maintenance of chromosomes (SMC) proteins, which are highly conserved across all domains of life and are important for organizing and segregating chromosomes (32, 33). In eukaryotic cells, SMC proteins are found as heterodimers of six core SMC proteins, but these proteins are not typically found in prokaryotes (34). Most bacteria have a single SMC complex, comprising of a homodimer of SMC (also known as MukB) interacting with two accessory subunits, ScpA and ScpB (MukE and MukF in *E. coli*) (35). *A. baumannii* has a separate gene encoding for the orthologous SMC/MukB protein (*smc*) that was called non-essential by previous Tn-seq screens (27, 36, 37) as well as orthologs for *scpA* and *scpB*. Phenotypes upon deletion of *smc, scpA,* and/or *scpB* along with pulldown assays of Smc2 would point to Smc2

interactions with this highly conserved complex. Alone, the structure of Smc2 could not be predicted using Alphafold (24) or Phyre2 (38), but multimeric protein structural predictions (18, 19), including homo- or hetero-oligomerization (39–41), with Smc2 or SMC2 with SMC, ScpA, and/or ScpB may provide information. To determine if Smc2 – or Smc2 in complex with other proteins – binds DNA or has DNA condensation activity, we could additionally perform DNA electrophoretic mobility shift assays (EMSA) and microfuge DNA aggregation assays, respectively (42).

Finally, I propose further experiments to determine the role of *spor* in *A. baumannii.* Due to high conservation of the SPOR domain, another study suggested that this gene is *ftsN*, concluding that the protein interacts with AdvA in the divisome (28). However, the region required for function in *E. coli* FtsN ($FtsN_{Eco}$) is not conserved in this SPOR-domain-containing protein (SPOR), and it is unclear if these two proteins perform the same function. I propose creating mutants for all regions of the SPOR-domain protein, similar to the approach used with FtsN in *E. coli* (43), to identify the region necessary for its function. As SPOR is essential, truncations or mutations in the essential functional regions would lead to non-viability. Time-lapse microscopy or even super resolution microscopy (44) with the fluorescently tagged SPOR construct and functional domain fusions, if possible, can be used to track localization and movement throughout cell division. Comparing the data to that from *E. coli* FtsN (43, 45) would help uncover the role of SPOR in *A. baumannii*.

Tetracycline-class antibiotic efficacy and the electron transport chain

Our chemical genomics screen showed that tetracycline, minocycline, and tigecycline had divergent effects on *A. baumannii* essential genes despite being within the same antibiotic class. Notably, knockdowns of cytochrome bo_3 oxidase genes (*cyo*) were uniquely sensitive to tigecycline, whereas knockdowns of ATP synthase genes (*atp*) showed increased resistance to both tigecycline and tetracycline, but not minocycline. Cytochrome bo_3 oxidase serves as the terminal oxidase in

the *A. baumannii* electron transport chain, while ATP synthase utilizes the proton motive force (PMF) generated by the electron transport chain to produce energy. As an obligate aerobe, *A. baumannii* depends on these aerobic respiration complexes for ATP production. Although it is known that tetracycline uptake and efflux can exhibit specificity (46), the direct impact of cytochrome bo_3 oxidase and ATP synthase remains unclear.

First, we could examine the role of efflux pumps that recognize tetracycline-class antibiotics. One explanation for these phenotypes is that *cyo* and *atp* knockdowns affect efflux pump activity, which are often PMF- or ATP-dependent. Because efflux pumps in *A. baumannii* have been extensively characterized (47–49), we could determine if the minimum inhibitory concentrations (MICs) of tetracycline-class antibiotics with *cyo* and *atp* knockdowns differ in strain backgrounds with systematically deleted tetracycline efflux pumps. Beyond effects on efflux, uptake of tetracyclines is known to be affected by membrane potential (46, 50); to test this, we would need to accurately measure membrane potential for *cyo* and *atp* knockdowns. While I present preliminary data for the effect of these knockdowns on membrane potential and ATP levels (see Appendix C), the exact effects remain uncertain. Experiments with alternative fluorescent probes to assess membrane potential (51) or measurements of external pH (52) would more precisely determine degree of impact on membrane potential and proton-motive force. Additionally, liquid chromatography-mass spectrometry (LC-MS) approaches allow for direct measurement of extracellular drug concentration, enabling exact measurement of drug uptake (53), which would further clarify uptake and efflux of these tetracyclines in *cyo* or *atp* knockdowns.

We also observed that, based on effects on essential gene pathways, tigecycline clustered with phenazine and myricetin, which are known to affect oxidative phosphorylation and cause oxidative stress (54–57). To determine if oxidative stress links *cyo* knockdowns with tigecycline sensitivity and to better understand the role of cytochrome bo_3 oxidase, we can measure redox potential (58),

reactive oxygen species (ROS) (59), and oxygen uptake kinetics (60) with or without tigecycline in WT *A. baumannii* and in *cyo* knockdowns.

Beyond the three tetracycline-class antibiotics in this screen, we could additionally screen this essential gene library against a wider range of tetracycline derivatives (61) or similar small molecules. This, combined with MIC assays, would lead to a more comprehensive understanding of the minor changes in tetracycline chemical structures causing differences in efficacy and impact on *A. baumannii*.

Broadening applications: full genome libraries and small molecule screens

Finally, the tools developed in Chapters 2 and 3 lend themselves to dissecting broad swaths of chemical-gene interaction space, despite the limitations of this essential gene CRISPRi library and the chemical set used (e.g., polar effects and varying representation from chemical classes). Expanding to a full genome CRISPRi knockdown library or creating targeted overexpression or knockout libraries using CRISPR-associated transposon systems (62) in *A. baumannii* for chemical genomics would provide far more comprehensive genetic data, increasing the potential for discovering new drug targets and allowing for a more complete look at *A. baumannii* biology.

With careful considerations for library size and sequencing coverage (63) – the approaches presented here could additionally be adapted for high-throughput small molecule screens, utilizing thousands of organic compounds. This would enable us to observe the effects of an even wider range of chemicals, facilitating the identification of novel drug-gene interactions as well as allowing for far more comprehensive analysis of relationships between chemical structures and impact on *A. baumannii* genetic pathways. Using this approach, we could potentially find drugs with unique mechanisms of action that would be missed under classical approaches that prioritize efficacy over uniqueness.

Finally, while this thesis focuses on *A. baumannii* due to its clinical relevance, these libraries and high-throughput molecule screens could be adapted for many different bacterial species. The tools developed here would still be applicable for resulting data analyses, thereby expanding the scope of research and enhancing our ability to investigate bacterial biology and drug interactions on a broad scale.

References

1. Young R. 2014. Phage lysis: three steps, three choices, one outcome. J Microbiol 52:243–258.

2. Durrant MG, Li MM, Siranosian BA, Montgomery SB, Bhatt AS. 2020. A Bioinformatic Analysis of Integrative Mobile Genetic Elements Highlights Their Role in Bacterial Adaptation. Cell Host Microbe 27:140-153.e9.

3. Gerstmans H, Criel B, Briers Y. 2018. Synthetic biology of modular endolysins. Biotechnol Adv 36:624–640.

4. Rathore AS, Arora A, Choudhury S, Tijare P, Raghava GPS. 2023. ToxinPred 3.0: An improved method for predicting the toxicity of peptides. bioRxiv 2023.08.11.552911.

5. Clokie MRJ. 2009. Quantification of host and phage mRNA expression during infection using real-time PCR. Methods Mol Biol 502:177–191.

6. Belnap DM. 2021. Detection of Bacteriophages: Electron Microscopy and Visualization, p. 561–620. *In* Harper, DR, Abedon, ST, Burrowes, BH, McConville, ML (eds.), Bacteriophages: Biology, Technology, Therapy. Springer International Publishing, Cham.

7. Pavlin A, Bajc G, Fornelos N, Browning DF, Butala M. 2022. The Small DdrR Protein Directly Interacts with the UmuDAb Regulator of the Mutagenic DNA Damage Response in Acinetobacter baumannii. J Bacteriol 204:e0060121.

8. Candra B, Cook D, Hare J. 2024. Repression of Acinetobacter baumannii DNA damage response requires DdrR-assisted binding of UmuDAb dimers to atypical SOS box. J Bacteriol 206:e0043223.

9. Croucher NJ, Thomson NR. 2010. Studying bacterial transcriptomes using RNA-seq. Curr Opin Microbiol 13:619–624.

10. Ramírez-Sánchez I, Magos-Castro M, Guarneros G. 2023. Transcriptional analysis in bacteriophage Fc02 of Pseudomonas aeruginosa revealed two overlapping genes with exclusion activity. Front Microbiol 14:1027380.

11. Park PJ. 2009. ChIP–seq: advantages and challenges of a maturing technology. Nat Rev Genet 10:669–680.

12. Myers KS, Park DM, Beauchene NA, Kiley PJ. 2015. Defining bacterial regulons using ChIP-seq. Methods 86:80–88.

13. Pawlowski DR, Koudelka GB. 2004. The preferred substrate for RecA-mediated cleavage of bacteriophage 434 repressor is the DNA-bound dimer. J Bacteriol 186:1–7.

14. Sparks RP, Jenkins JL, Fratti R. 2019. Use of Surface Plasmon Resonance (SPR) to Determine Binding Affinities and Kinetic Parameters Between Components Important in Fusion Machinery. Methods Mol Biol 1860:199–210.

15. Sperandeo P, Martorana AM, Polissi A. 2017. The lipopolysaccharide transport (Lpt) machinery: A nonconventional transporter for lipopolysaccharide assembly at the outer membrane of Gram-negative bacteria. J Biol Chem 292:17981–17990.

16. Pahil KS, Gilman MSA, Baidin V, Clairfeuille T, Mattei P, Bieniossek C, Dey F, Muri D, Baettig R, Lobritz M, Bradley K, Kruse AC, Kahne D. 2024. A new antibiotic traps lipopolysaccharide in its intermembrane transporter. Nature 625:572–577.

17. Zampaloni C, Mattei P, Bleicher K, Winther L, Thäte C, Bucher C, Adam J-M, Alanine A, Amrein KE, Baidin V, Bieniossek C, Bissantz C, Boess F, Cantrill C, Clairfeuille T, Dey F, Di Giorgio P, du Castel P, Dylus D, Dzygiel P, Felici A, García-Alcalde F, Haldimann A, Leipner M, Leyn S, Louvel S, Misson P, Osterman A, Pahil K, Rigo S, Schäublin A, Scharf S, Schmitz P, Stoll T, Trauner A, Zoffmann S, Kahne D, Young JAT, Lobritz MA, Bradley KA. 2024. A novel antibiotic class targeting the lipopolysaccharide transporter. Nature 625:566–571.

18. Evans R, O'Neill M, Pritzel A, Antropova N, Senior A, Green T, Žídek A, Bates R, Blackwell S, Yim J, Ronneberger O, Bodenstein S, Zielinski M, Bridgland A, Potapenko A, Cowie A, Tunyasuvunakool K, Jain R, Clancy E, Kohli P, Jumper J, Hassabis D. 2021. Protein complex prediction with AlphaFold-Multimer https://doi.org/10.1101/2021.10.04.463034.

19. Abramson J, Adler J, Dunger J, Evans R, Green T, Pritzel A, Ronneberger O, Willmore L, Ballard AJ, Bambrick J, Bodenstein SW, Evans DA, Hung C-C, O'Neill M, Reiman D, Tunyasuvunakool K, Wu Z, Žemgulytė A, Arvaniti E, Beattie C, Bertolli O, Bridgland A, Cherepanov A, Congreve M, Cowen-Rivers AI, Cowie A, Figurnov M, Fuchs FB, Gladman H, Jain R, Khan YA, Low CMR, Perlin K, Potapenko A, Savy P, Singh S, Stecula A, Thillaisundaram A, Tong C, Yakneen S, Zhong ED, Zielinski M, Žídek A, Bapst V, Kohli P, Jaderberg M, Hassabis D, Jumper JM. 2024. Accurate structure prediction of biomolecular interactions with AlphaFold 3. Nature 630:493–500.

20. Kelman Z, O'Donnell M. 1995. DNA polymerase III holoenzyme: structure and function of a chromosomal replicating machine. Annu Rev Biochem 64:171–200.

21. Stukenberg PT, Studwell-Vaughan PS, O'Donnell M. 1991. Mechanism of the sliding beta-clamp of DNA polymerase III holoenzyme. J Biol Chem 266:11328–11334.

22. 2024. BIONF/fDOG. Python. BIONF.

23. Robinson A, Brzoska AJ, Turner KM, Withers R, Harry EJ, Lewis PJ, Dixon NE. 2010. Essential Biological Processes of an Emerging Pathogen: DNA Replication, Transcription, and Cell Division in Acinetobacter spp. Microbiol Mol Biol Rev 74:273–297.

24. Jumper J, Evans R, Pritzel A, Green T, Figurnov M, Ronneberger O, Tunyasuvunakool K, Bates R, Žídek A, Potapenko A, Bridgland A, Meyer C, Kohl SAA, Ballard AJ, Cowie A, Romera-Paredes B, Nikolov S, Jain R, Adler J, Back T, Petersen S, Reiman D, Clancy E, Zielinski M, Steinegger M, Pacholska M, Berghammer T, Bodenstein S, Silver D, Vinyals O, Senior AW, Kavukcuoglu K, Kohli P, Hassabis D. 2021. Highly accurate protein structure prediction with AlphaFold. Nature 596:583–589.

25. Louche A, Salcedo SP, Bigot S. 2017. Protein-Protein Interactions: Pull-Down Assays. Methods Mol Biol 1615:247–255.

26. Karimova G, Gauliard E, Davi M, Ouellette SP, Ladant D. 2017. Protein-Protein Interaction: Bacterial Two-Hybrid. Methods Mol Biol 1615:159–176.

27. Geisinger E, Mortman NJ, Dai Y, Cokol M, Syal S, Farinha A, Fisher DG, Tang AY, Lazinski DW, Wood S, Anthony J, van Opijnen T, Isberg RR. 2020. Antibiotic susceptibility signatures identify potential antimicrobial targets in the Acinetobacter baumannii cell envelope. 1. Nat Commun 11:4522.

28. Chu X, Wang L, Zhu Y, Feng Z, Guan Q, Song L, Luo Z. 2023. A unique cell division protein critical for the assembly of the bacterial divisome https://doi.org/10.7554/eLife.87922.2.

29. Grinter R, Morris FC, Dunstan RA, Leung PM, Kropp A, Belousoff M, Gunasinghe SD, Scott NE, Beckham S, Peleg AY, Greening C, Li J, Heinz E, Lithgow T. BonA from Acinetobacter baumannii Forms a Divisome-Localized Decamer That Supports Outer Envelope Function. mBio 12:e01480-21.

30. den Blaauwen T, Hamoen LW, Levin PA. 2017. The divisome at 25: the road ahead. Curr Opin Microbiol 36:85–94.

31. De Silva PM, Kumar A. 2018. Effect of Sodium Chloride on Surface-Associated Motility of Acinetobacter baumannii and the Role of AdeRS Two-Component System. J Membrane Biol 251:5–13.

32. Badrinarayanan A, Lesterlin C, Reyes-Lamothe R, Sherratt D. 2012. The Escherichia coli SMC complex, MukBEF, shapes nucleoid organization independently of DNA replication. J Bacteriol 194:4669–4676.

33. Soppa J. 2001. Prokaryotic structural maintenance of chromosomes (SMC) proteins: distribution, phylogeny, and comparison with MukBs and additional prokaryotic and eukaryotic coiled-coil proteins. Gene 278:253–264.

34. Harvey SH, Krien MJE, O'Connell MJ. 2002. Structural maintenance of chromosomes (SMC) proteins, a family of conserved ATPases. Genome Biol 3:REVIEWS3003.

35. Gruber S. 2011. MukBEF on the march: taking over chromosome organization in bacteria? Mol Microbiol 81:855–859.

36. Gallagher LA, Ramage E, Weiss EJ, Radey M, Hayden HS, Held KG, Huse HK, Zurawski DV, Brittnacher MJ, Manoil C. 2015. Resources for Genetic and Genomic Analysis of Emerging Pathogen Acinetobacter baumannii. J Bacteriol 197:2027–2035.

37. Wang N, Ozer EA, Mandel MJ, Hauser AR. 2014. Genome-Wide Identification of Acinetobacter baumannii Genes Necessary for Persistence in the Lung. mBio 5:e01163-14.

38. Kelley LA, Mezulis S, Yates CM, Wass MN, Sternberg MJE. 2015. The Phyre2 web portal for protein modeling, prediction and analysis. Nat Protoc 10:845–858.

39. Gaber A, Pavšič M. 2021. Modeling and Structure Determination of Homo-Oligomeric Proteins: An Overview of Challenges and Current Approaches. Int J Mol Sci 22:9081.

40. Kshirsagar M, Meller A, Humphreys I, Sledzieski S, Xu Y, Dodhia R, Horvitz E, Berger B, Bowman G, Ferres JL, Baker D, Baek M. 2024. Rapid and accurate prediction of protein homo-oligomer symmetry with Seq2Symm. Res Sq rs.3.rs-4215086.

41. Park T, Woo H, Yang J, Kwon S, Won J, Seok C. 2021. Protein oligomer structure prediction using GALAXY in CASP14. Proteins 89:1844–1851.

42. Petrushenko ZM, She W, Rybenkov VV. 2011. A new family of bacterial condensins. Mol Microbiol 81:881–896.

43. Gerding MA, Liu B, Bendezú FO, Hale CA, Bernhardt TG, de Boer PAJ. 2009. Self-enhanced accumulation of FtsN at Division Sites and Roles for Other Proteins with a SPOR domain (DamX, DedD, and RlpA) in Escherichia coli cell constriction. J Bacteriol 191:7383–7401.

44. Holden SJ, Pengo T, Meibom KL, Fernandez Fernandez C, Collier J, Manley S. 2014. High throughput 3D super-resolution microscopy reveals *Caulobacter crescentus* in vivo Z-ring organization. Proc Natl Acad Sci USA 111:4566–4571.

45. Lyu Z, Yahashiri A, Yang X, McCausland JW, Kaus GM, McQuillen R, Weiss DS, Xiao J. 2022. FtsN maintains active septal cell wall synthesis by forming a processive complex with the septum-specific peptidoglycan synthases in E. coli. Nat Commun 13:5751.

46. Grossman TH. 2016. Tetracycline Antibiotics and Resistance. Cold Spring Harb Perspect Med 6:a025387.

47. Abdi SN, Ghotaslou R, Ganbarov K, Mobed A, Tanomand A, Yousefi M, Asgharzadeh M, Kafil HS. 2020. Acinetobacter baumannii Efflux Pumps and Antibiotic Resistance. Infect Drug Resist 13:423–434.

48. Verma P, Tiwari M, Tiwari V. 2021. Efflux pumps in multidrug-resistant *Acinetobacter baumannii*: Current status and challenges in the discovery of efflux pumps inhibitors. Microbial Pathogenesis 152:104766.

49. Sharma S, Kaushik V, Kulshrestha M, Tiwari V. 2023. Different Efflux Pump Systems in Acinetobacter baumannii and Their Role in Multidrug Resistance. Adv Exp Med Biol 1370:155–168.

50. Kuang S-F, Xiang J, Zeng Y-Y, Peng X-X, Li H. 2024. Elevated Membrane Potential as a Tetracycline Resistance Mechanism in Escherichia coli. ACS Infect Dis 10:2196–2211.

51. Benarroch JM, Asally M. 2020. The Microbiologist's Guide to Membrane Potential Dynamics. Trends Microbiol 28:304–314.

52. Damper PD, Epstein W. 1981. Role of the membrane potential in bacterial resistance to aminoglycoside antibiotics. Antimicrob Agents Chemother 20:803–808.

53. Zhou Y, Joubran C, Miller-Vedam L, Isabella V, Nayar A, Tentarelli S, Miller A. 2015. Thinking Outside the "Bug": A Unique Assay To Measure Intracellular Drug Penetration in Gram-Negative Bacteria. Anal Chem 87:3579–3584.

54. Stewart-Tull DE, Armstrong AV. 1972. The effect of 1-hydroxyphenazine and pyocyanin from Pseudomonas aeruginosa on mammalian cell respiration. J Med Microbiol 5:67–73.

55. Bisschop A, Bergsma J, Konings WN. 1979. Site of interaction between phenazine methosulphate and the respiratory chain of Bacillus subtilis. Eur J Biochem 93:369–374.

56. Donadio G, Mensitieri F, Santoro V, Parisi V, Bellone ML, De Tommasi N, Izzo V, Dal Piaz F. 2021. Interactions with Microbial Proteins Driving the Antibacterial Activity of Flavonoids. Pharmaceutics 13:660.

57. Taheri Y, Suleria HAR, Martins N, Sytar O, Beyatli A, Yeskaliyeva B, Seitimova G, Salehi B, Semwal P, Painuli S, Kumar A, Azzini E, Martorell M, Setzer WN, Maroyi A, Sharifi-Rad J. 2020. Myricetin bioactive effects: moving from preclinical evidence to potential clinical applications. BMC Complement Med Ther 20:241.

58. Reichart O, Szakmár K, Jozwiak A, Felföldi J, Baranyai L. 2007. Redox potential measurement as a rapid method for microbiological testing and its validation for coliform determination. Int J Food Microbiol 114:143–148.

59. Murphy MP, Bayir H, Belousov V, Chang CJ, Davies KJA, Davies MJ, Dick TP, Finkel T, Forman HJ, Janssen-Heininger Y, Gems D, Kagan VE, Kalyanaraman B, Larsson N-G, Milne GL, Nyström T, Poulsen HE, Radi R, Van Remmen H, Schumacker PT, Thornalley PJ, Toyokuni S, Winterbourn CC, Yin H, Halliwell B. 2022. Guidelines for measuring reactive oxygen species and oxidative damage in cells and in vivo. Nat Metab 4:651–662.

60. King LR, Palmer HJ. 1989. Measurement of bacterial oxygen uptake kinetics by a modified respirometric technique. Biotechnol Bioeng 33:932–937.

61. Fuoco D. 2012. Classification Framework and Chemical Biology of Tetracycline-Structure-Based Drugs. Antibiotics (Basel) 1:1–13.

62. Banta AB, Myers KS, Ward RD, Cuellar RA, Place M, Freeh CC, Bacon EE, Peters JM. 2024. A Targeted Genome-scale Overexpression Platform for Proteobacteria. bioRxiv 2024.03.01.582922.

63. Sims D, Sudbery I, Ilott NE, Heger A, Ponting CP. 2014. Sequencing depth and coverage: key considerations in genomic analyses. Nat Rev Genet 15:121–132.

APPENDIX A

Heterogeneity in *A. baumannii* lab strains and implications for molecular studies

I performed transposition and microscopy experiments and wrote this appendix. Ryan Ward assisted with conjugation experiments with Tn*5* donor strains.

Introduction

Acinetobacter baumannii exhibits extensive genomic and phenotypic heterogeneity between strains (1), with a relatively small core genome (an estimated 16.5%, while 25% of the genome is unique to each strain) and an open-pan genome—the capacity to acquire new genes is so great that predicting the size of the entire set of genes within the species is not possible (2). This heterogeneity underlies the divergence between the non-multidrug-resistant laboratory strains of *A. baumannii*, ATCC17978 (17978) and ATCC19606 (19606), and contemporary clinical isolates (3). In fact, American Type Culture Collection (ATCC)-derived laboratory stocks of 17978 are mixed populations of two variants, one with an acquired 44-kb accessory locus (4).

The extensive heterogeneity between strains of *A. baumannii* can present considerable difficulties for genetic and molecular biology studies. For example, transposon mutagenesis is a crucial tool for studying gene function and essentiality; however, the variations between strain makes identifying a core 'essentialome' challenging. Indeed, essentiality calls from high-coverage transposon mutant sequencing (Tn-seq) in AB5075 (5) —the model *A. baumannii* strain for multidrug resistance and pathogenesis—differ from those in similar 17978 Tn-seq experiments (6–8). 17978 and AB5075 each contain 200-300 genes for which there are no orthologs in the other strain, and of the ~3500 orthologous genes, ~5% of calls differ (7). One transposon mutagenesis screen was performed in 19606 but did not establish the extent of coverage or gene essentiality as high-throughput sequencing was not utilized (9). Strain-to-strain variation can also impact the functionality and efficiency of genetic tools across different strains. *A. baumannii* strains can vary significantly in antibiotic resistance profiles (affecting selection markers) (10), natural competence levels, and DNA methylation in conjunction with restriction-modification systems that impact transformation (11).

Furthermore, phenotypic heterogeneity has been observed not only between distinct strains but also within a single clonal strain. For instance, multidrug-resistant strain AB5075 produces two phenotypic variants that form either opaque or translucent colonies that interconvert at high frequency (12, 13). These variants produce multiple significant phenotypic differences, including cell morphology, surface motility, biofilm formation, antibiotic resistance and virulence (12, 14). Strikingly, translucent variants produce larger cells during log-phase growth and are significantly elongated compared to opaque variants at early stationary phase (12). Opaque variants are also highly virulent and can cause disease in mice models (15), while translucent variants are avirulent and more readily form pronounced biofilms and release outer membrane vesicles (13). While exact mechanisms behind this phase-variable switch are unknown, the two types have distinct genomic expression profiles and switching is stimulated by high cell density and quorum sensing signals (12), driven in part by multiple transcriptional regulators (15–17), a two-component system (18), an efflux pump (19), and a predicted small RNA (20). While this phase variation has been well-characterized in AB5075, the model *A. baumannii* strain for multidrug resistance and pathogenesis, 17978 does not appear to produce colony variants (12), and little is known about phase variation in 19606.

In this appendix, I highlight major differences between the lab strains 17978 and 19606 that impact genetic studies. I demonstrate that transposon mutagenesis systems and methods used in 17978 are inefficient in 19606, and that 19606 exhibits cell morphology heterogeneity dependent on growth conditions, likely due to phase variation switching. These findings underscore the importance of considering strain-specific characteristics in the design and interpretation of genetic experiments in *A. baumannii*.

Results

Random transposon mutagenesis is less efficient in 19606 than in 17978

We first tested transposon mutagenesis efficiency in 19606 through conjugation with DAP- *E. coli* donor cells (*E. coli* K-12 WM6026) carrying Tn*5* (21) or *mariner* (6, 22) systems. We additionally tested transposon efficiencies in 17978—though the *mariner* system was developed for Tn-seq in this strain—and two common *E. coli* K-12 strains, DH10B and BW25113, as model organism controls. We found that neither Tn*5* nor *mariner* produced transconjugants in 19606, but that we recovered transconjugants in 17978 and *E. coli* strains at rates of ~10^-6 and ~10^-3, respectively (Fig A.1). Because 17978 reaches a higher cell density at stationary phase than 19606 (23), increasing the amount of donor or allowing a longer incubation time for conjugation could resolve the differences in efficiencies between 17978 and 19606. I tested higher ratios of recipient to donor and different incubation times with the *mariner* transposon donor in 17978 and 19606 and calculated efficiency of transposition. While transposon mutants were recovered in 19606, efficiencies remained 2-3 orders of magnitude lower than in 17978 (Fig A.2). Donor-recipient ratios and incubation time did not appear to make a substantial difference in transposition efficiency, but more robust experimental setups are required to validate this observation.

19606, but not 17978, shows growth phase-dependent variation in cell morphology

To further characterize differences between 19606 and 17978, I looked for heterogeneity in cell shape and size that could point to phase variation of 19606. I grew the strains to stationary phase (~17 hours) either by incubating cells on agar plates or in liquid culture (17 hours). Microscopy of these cells at stationary phase showed distinct morphological differences, with considerable elongation of ATCC19606 after growth in liquid (Fig A.3). This elongated cell phenotype in 19606 was strikingly similar to that of AB5075 translucent variants in early stationary phase (12). However,

Figure A.1. Efficiency of mariner or Tn5 in *A. baumannii* and *E. coli* lab strains. Dot plot illustrating efficiency of *mariner* or Tn*5* transposition (log-scale) in *A. baumannii* 17978 and 19606 and *E. coli* BW25113 and DH10B. Ten-fold serial dilutions were spotted onto plates and transposition efficiency was measured as the ratio of colony-forming units (CFUs) with selection to CFUs without selection. For all samples, the number of CFUs without selection was ~10^7. 19606 had no colonies with either transposon system, so transposition efficiency was zero.

Figure A.1

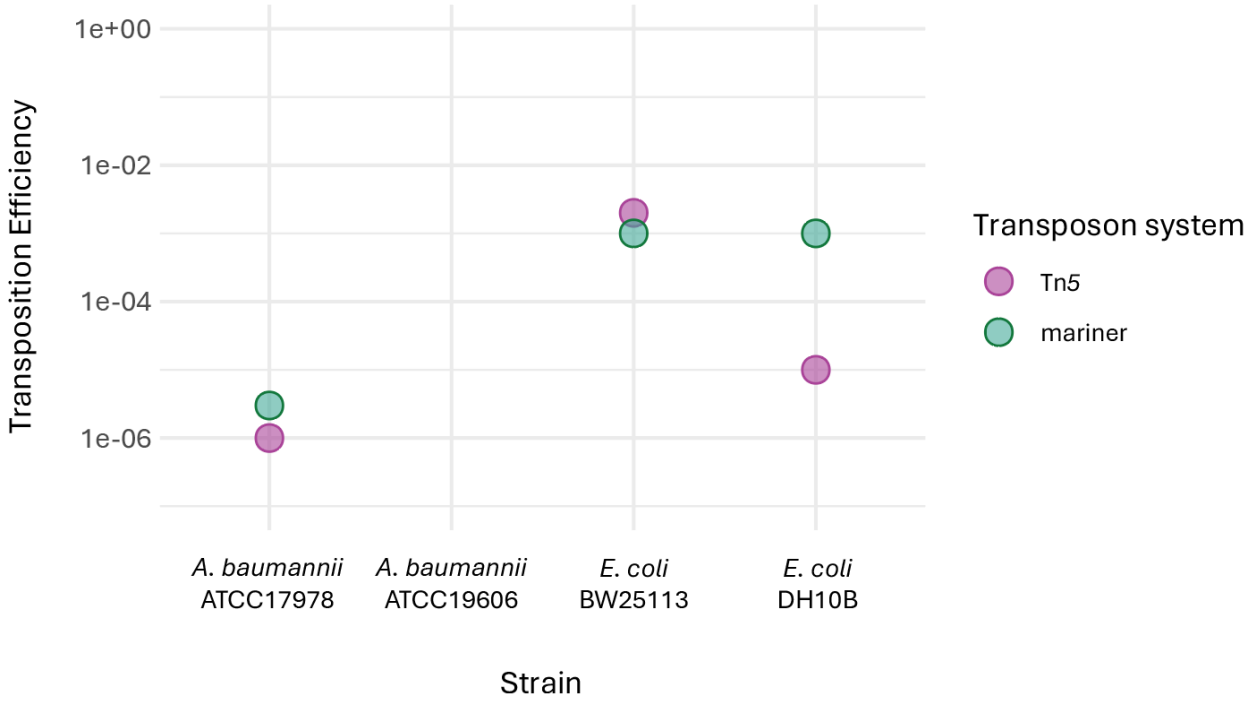
1e+00
1e-02
1e-04
1e-06
Transposition Efficiency
A. baumannii ATCC17978
A. baumannii ATCC19606
E. coli BW25113
E. coli DH10B
Strain
Transposon system
Tn5
mariner

Figure A.2. Efficiency of mariner transposition under varying conjugation conditions in 17978 and 19606. Dot plot illustrating efficiency of *mariner* transposition (log-scale) in 17978 (left) and 19606 (right) with 1:1, 1:3, and 1:5 donor to recipient ratios and 2-hour vs overnight incubation for conjugation (n=1). Ten-fold serial dilutions were spotted onto plates and transposition efficiency was measured as the ratio of colony-forming units (CFUs) with selection to CFUs without selection. For all samples, the number of CFUs without selection was ~10^7.

Figure A.2

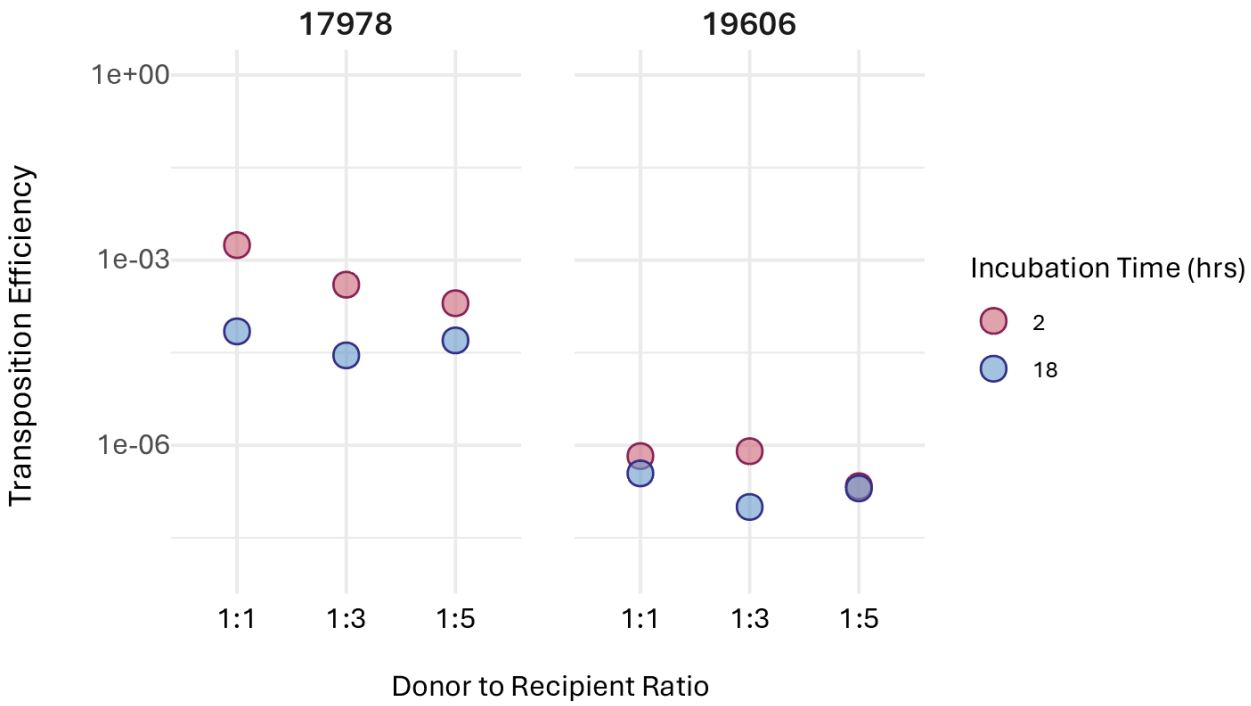
17978
19606
1e+00
1e-03
1e-06
Transposition Efficiency
1:1
1:3
1:5
1:1
1:3
1:5
Donor to Recipient Ratio
Incubation Time (hrs)
2
18

Figure A.3. Microscopy of 19606 and 17978 cells at stationary phase Cell morphology of ATCC19606 or ATCC17978 cells after 17 hours of growth on LB agar plates (left) or in 4 mL LB liquid culture (right). All images were captured with a Nikon Ti-E inverted microscope with an Orca Fusion BT digital CMOS camera (Hamamatsu) using NIS-elements. The ruler at the bottom right in all images is 10 microns.

Figure A.3

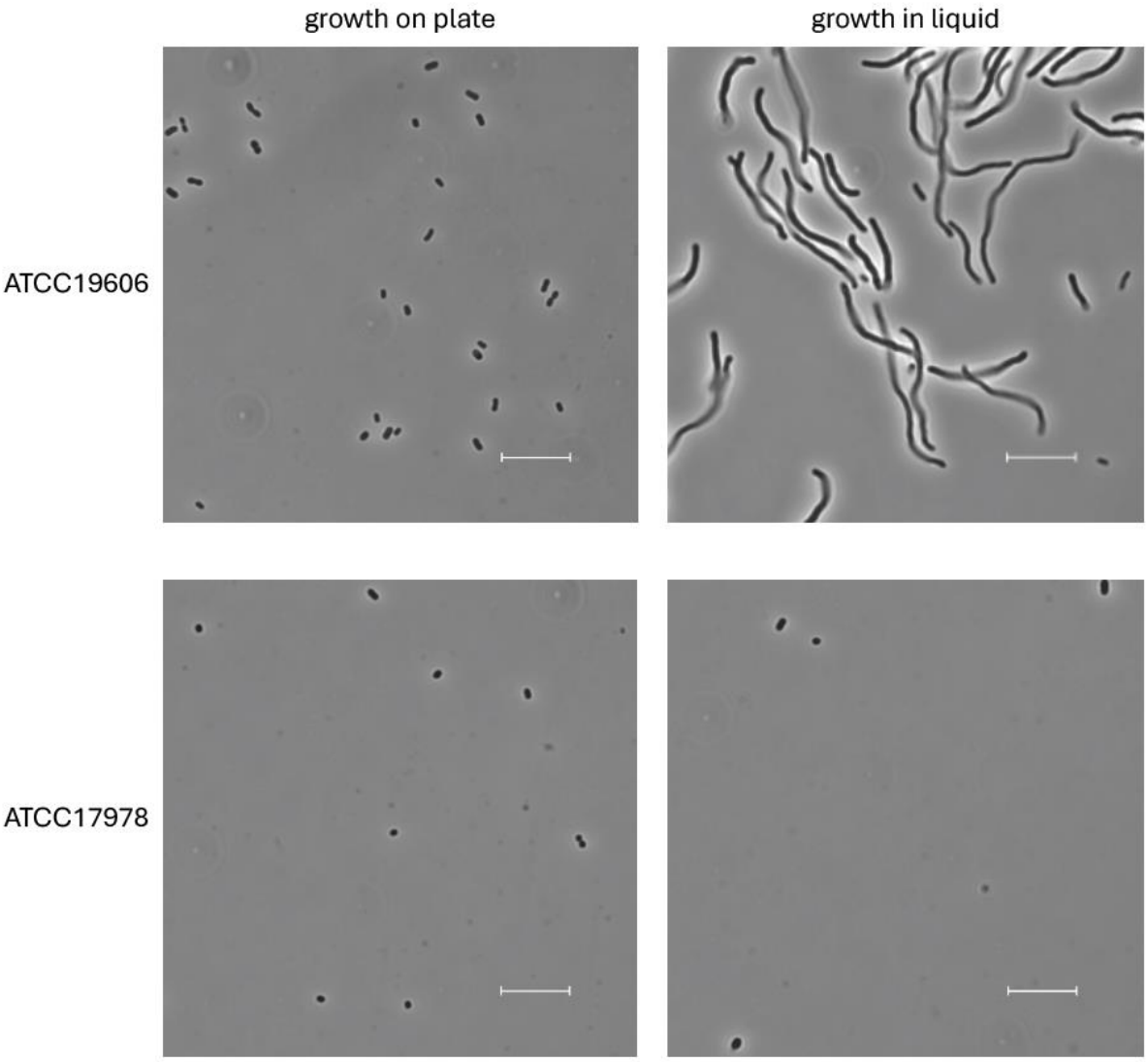

growth to stationary phase on plates did not show this phenotype, possibly pointing to growth conditions as a trigger for specific phase variation switches in this strain. Colony variants are not seen in 17978 (12), and the strain did not display the differences in colony morphology seen in 19606 at stationary phase.

Discussion

These experiments highlight the differences between *A. baumannii* strains 19606 and 17978, particularly in terms of transposon mutagenesis and phenotypic variation. Compared to 17978, the transposition efficiency in 19606 using standard conjugation methods makes high-coverage transposon library generation challenging (22). Although protocol modifications could potentially improve transposition efficiency in 19606, intrinsic differences in DNA methylation and restriction systems between the strains (11) may be limiting transposon plasmid uptake or transposition. Electroporation is an alternative method of delivering the transposon system to diverse bacteria and has been successfully utilized in other studies (5, 7), including in 19606 (9). Electroporation and plasmid optimization could potentially circumvent some limitations, and further work identifying if restriction systems are playing a role in this inefficiency would be informative.

Microscopy analysis revealed additional phenotypic differences in 19606, particularly at stationary phase. The observed heterogeneity mirrors strain variant morphological differences seen in AB5075 (12); however, experiments to determine 19606 macrocolony phenotypes are needed to confirm opaque or translucent phase variants. This heterogeneity poses challenges for the study of cell membrane phenotypes beyond the mid-log growth phase and likely results in changes in global gene expression (17, 24) that could affect expression of constructs *in trans*. Thus, microscopy studies are likely more robust in 17978, and microscopy experiments in 19606 should be limited to early mid-log or growth on solid media to maintain more homogeneity in cell size and shape.

Specific growth condition factors known to influence phase variant switching in AB5075, like cell density and nutrient availability (12), may underlie the phenotypic differences observed, as these factors are vastly different between plates and liquid culture. The cell elongation seen in 19606 and AB5075 also suggests a role of cell wall synthesis and cell division in the production of the elongated variant. Expression of some cell wall components in 19606 are distinct from 17978, and it is known that these differences are directly related to the ability to lose lipooligosaccharides (LOS) in the outer membrane—19606 can survive without LOS, whereas 17978 cannot (25). This potential connection between phase variant morphology and strain heterogeneity warrants further investigation.

Overall, the experiments in this appendix identified crucial differences in the genetic manipulation and phenotypic expression between 17978 and 19606. These findings are informative for selecting appropriate type strains for specific experiments and raise important considerations regarding the generalizability of research findings from either of these lab strains to the rest of the species.

Materials and Methods

Strains are listed in Table A.1 and were grown in LB or LB +1.5% agar at 37°C. 30 μg/mL kanamycin (kan) was used for selection. Diaminopimelic acid (DAP) was added at 300 μM to support growth of E. coli dap- donor strains. Plasmids used are listed in Table A.2.

Transposon mutagenesis

100 μL of saturated overnight culture of donor and recipient strains were added to LB to a final volume of 1 mL, pelleted at ~8,000 × g, washed twice with LB prior to depositing cells on a nitrocellulose filter (Millipore HAWP02500) on an LB plate and incubating at 37°C, ~2 hours unless otherwise specified. Recipient culture volumes were adjusted accordingly for ratio modifications. Cells were removed from the filter by vortexing in 1 mL LB. Ten-fold serial dilutions were spotted onto LB or LB-kan selection plates and grown at 37°C.

Microscopy at stationary phase

Overnight cultures of 19606 and 17978 and cell scrapes from plates resuspended in 1 mL LB were normalized to OD~0.3. Cells were fixed and microscopy images were taken following methods described in Chapter 3.

Table A.1. Strains used in this study.

Strain	Description[1]	Source
19606	*Acinetobacter baumannii* ATCC19606	ATCC
17978	*Acinetobacter baumannii* ATCC17978	ATCC
sJMP624	*E. coli* mating strain (derived from WM6026) with FRT inserted between *mltB* and *srlA*, *recA1*	Ward et al. (26)
sJMP5039	sJMP624 with p5039 (Tn*5* plasmid), kanR, dap-	This study
sJMP4057	sJMP624 with p4017 (*mariner* transposon plasmid), kanR, dap-	This study

[1] kanR = kanamycin-resistant; dap- = requires diaminopimelic acid

Table A.2. Plasmids used in this study.

Plasmid	Description	Source
p5039 (pKMW7)	Tn*5* transposon vector library with >10 million unique 20mer DNA barcodes, flanked by common PCR priming sites	Wetmore et al. (21)
p4017 (pJNW684)	Vector carrying *Himar1 mariner* transposon and transposition machinery	Wang et al. (6); Kazi et al. (22)

Acknowledgements

I thank Adam Deutschbauer and Adam Arkin for the Tn*5* transposon systems and Mark Mandel for the *mariner* system and protocol advice.

References

1. Valcek A, Philippe C, Whiteway C, Robino E, Nesporova K, Bové M, Coenye T, De Pooter T, De Coster W, Strazisar M, Van der Henst C. 2023. Phenotypic Characterization and Heterogeneity among Modern Clinical Isolates of Acinetobacter baumannii. Microbiol Spectr 11:e0306122.

2. Imperi F, Antunes LCS, Blom J, Villa L, Iacono M, Visca P, Carattoli A. 2011. The genomics of Acinetobacter baumannii: insights into genome plasticity, antimicrobial resistance and pathogenicity. IUBMB Life 63:1068–1074.

3. Maure A, Robino E, Van der Henst C. 2023. The intracellular life of Acinetobacter baumannii. Trends Microbiol 31:1238–1250.

4. Wijers CDM, Pham L, Menon S, Boyd KL, Noel HR, Skaar EP, Gaddy JA, Palmer LD, Noto MJ. 2021. Identification of Two Variants of Acinetobacter baumannii Strain ATCC 17978 with Distinct Genotypes and Phenotypes. Infect Immun 89:e0045421.

5. Gallagher LA, Ramage E, Weiss EJ, Radey M, Hayden HS, Held KG, Huse HK, Zurawski DV, Brittnacher MJ, Manoil C. 2015. Resources for Genetic and Genomic Analysis of Emerging Pathogen Acinetobacter baumannii. J Bacteriol 197:2027–2035.

6. Wang N, Ozer EA, Mandel MJ, Hauser AR. 2014. Genome-Wide Identification of Acinetobacter baumannii Genes Necessary for Persistence in the Lung. mBio 5:e01163-14.

7. Geisinger E, Mortman NJ, Dai Y, Cokol M, Syal S, Farinha A, Fisher DG, Tang AY, Lazinski DW, Wood S, Anthony J, van Opijnen T, Isberg RR. 2020. Antibiotic susceptibility signatures identify potential antimicrobial targets in the Acinetobacter baumannii cell envelope. 1. Nat Commun 11:4522.

8. Bai J, Dai Y, Farinha A, Tang AY, Syal S, Vargas-Cuebas G, van Opijnen T, Isberg RR, Geisinger E. Essential Gene Analysis in Acinetobacter baumannii by High-Density Transposon Mutagenesis and CRISPR Interference. J Bacteriol 203:e00565-20.

9. Sun B, Liu H, Jiang Y, Shao L, Yang S, Chen D. 2020. New Mutations Involved in Colistin Resistance in Acinetobacter baumannii. mSphere 5:e00895-19.

10. Valcek A, Collier J, Botzki A, Van Der Henst C. 2022. Acinetobase: the comprehensive database and repository of *Acinetobacter* strains. Database 2022:baac099.

11. Vesel N, Iseli C, Guex N, Lemopoulos A, Blokesch M. 2023. DNA modifications impact natural transformation of Acinetobacter baumannii. Nucleic Acids Res 51:5661–5677.

12. Tipton KA, Dimitrova D, Rather PN. 2015. Phase-Variable Control of Multiple Phenotypes in Acinetobacter baumannii Strain AB5075. J Bacteriol 197:2593–2599.

13. Ahmad I, Karah N, Nadeem A, Wai SN, Uhlin BE. 2019. Analysis of colony phase variation switch in Acinetobacter baumannii clinical isolates. PLoS One 14:e0210082.

14. Mushtaq F, Nadeem A, Yabrag A, Bala A, Karah N, Zlatkov N, Nyunt Wai S, Uhlin BE, Ahmad I. 2024. Colony phase variation switch modulates antimicrobial tolerance and biofilm formation in Acinetobacter baumannii. Microbiol Spectr 12:e0295623.

15. Chin CY, Tipton KA, Farokhyfar M, Burd EM, Weiss DS, Rather PN. 2018. A high-frequency phenotypic switch links bacterial virulence and environmental survival in Acinetobacter baumannii. Nat Microbiol 3:563–569.

16. Tierney ARP, Chin CY, Weiss DS, Rather PN. 2021. A LysR-Type Transcriptional Regulator Controls Multiple Phenotypes in Acinetobacter baumannii. Front Cell Infect Microbiol 11:778331.

17. Pérez-Varela M, Tierney ARP, Kim J-S, Vázquez-Torres A, Rather P. 2020. Characterization of RelA in Acinetobacter baumannii. J Bacteriol 202:e00045-20.

18. Tipton KA, Rather PN. 2017. An ompR-envZ Two-Component System Ortholog Regulates Phase Variation, Osmotic Tolerance, Motility, and Virulence in Acinetobacter baumannii Strain AB5075. J Bacteriol 199:e00705-16.

19. Tipton KA, Farokhyfar M, Rather PN. 2017. Multiple roles for a novel RND-type efflux system in Acinetobacter baumannii AB5075. Microbiologyopen 6:e00418.

20. Anderson SE, Chin CY, Weiss DS, Rather PN. 2020. Copy Number of an Integron-Encoded Antibiotic Resistance Locus Regulates a Virulence and Opacity Switch in Acinetobacter baumannii AB5075. mBio 11:e02338-20.

21. Wetmore KM, Price MN, Waters RJ, Lamson JS, He J, Hoover CA, Blow MJ, Bristow J, Butland G, Arkin AP, Deutschbauer A. 2015. Rapid Quantification of Mutant Fitness in Diverse Bacteria by Sequencing Randomly Bar-Coded Transposons. mBio 6:e00306-15.

22. Kazi MI, Schargel RD, Boll JM. 2020. Generating Transposon Insertion Libraries in Gram-Negative Bacteria for High-Throughput Sequencing. J Vis Exp https://doi.org/10.3791/61612.

23. Grier JT, Arivett BA, Ramírez MS, Chosed RJ, Bigner JA, Ohneck EJ, Metz ML, Wood CR, Arce S, Tartaro A, Relich RF, Actis LA, Fiester SE. 2021. Two Acinetobacter baumannii Isolates Obtained From a Fatal Necrotizing Fasciitis Infection Display Distinct Genomic and Phenotypic Characteristics in Comparison to Type Strains. Front Cell Infect Microbiol 11:635673.

24. Pérez-Varela M, Singh R, Colquhoun JM, Starich OG, Tierney ARP, Tipton KA, Rather PN. 2024. Evidence for Rho-dependent control of a virulence switch in *Acinetobacter baumannii*. mBio 15:e02708-23.

25. Boll JM, Crofts AA, Peters K, Cattoir V, Vollmer W, Davies BW, Trent MS. 2016. A penicillin-binding protein inhibits selection of colistin-resistant, lipooligosaccharide-deficient Acinetobacter baumannii. Proceedings of the National Academy of Sciences 113:E6228–E6237.

26. Ward RD, Tran JS, Banta AB, Bacon EE, Rose WE, Peters JM. Essential gene knockdowns reveal genetic vulnerabilities and antibiotic sensitivities in Acinetobacter baumannii. mBio 15:e02051-23.

APPENDIX B

Effects of media and chemical concentrations on *A. baumannii* growth

I performed all the experiments shown here and wrote this appendix.

Introduction

Bacteria often prefer distinct environmental conditions and vary in their requirements for growth. Thus, the choice of culture media in laboratory experiments is crucial for laboratory study and can affect experimental outcomes (1). Use of defined media, with known quantities of all ingredients, is beneficial in large-scale experiments that take place over many days or weeks because it reduces batch-to-batch variation and increases reproducibility (2). As a non-fermenter, *A. baumannii* cannot utilize glucose (3). Therefore, rich defined media often contain succinate as a carbon source, especially as *Pseudomonas* species—in the same order as the *Acinetobacter* genus—use succinate as a preferred carbon source (4). However, specific carbon utilization varies considerably for *Acinetobacter* species and strains (5), and no standard rich defined media has been established in the field.

For chemical genomics, which involves systematically screening chemical compounds against genetic libraries to study bacterial chemical and gene interactions (6), it is important to have a rich, defined medium to maintain consistency across large experiments and to avoid additional stressors that could confound fitness data. In chemical genomics screens, libraries are probed with chemicals or antibiotics at subinhibitory concentrations, which enable study of more subtle physiological responses to perturbations of essential cell processes (7). In this appendix, I present growth data from *A. baumannii* in a rich defined media, establishing an optimal concentration of added succinate as a carbon source for downstream experiments. Additionally, I tested the growth of *A. baumannii* ATCC19606 in this medium with multiple chemicals at various concentrations, utilizing area under the curve as a metric to define inhibition, establishing concentration ranges for chemical genomics screens in this strain.

Results

Effects of different media on A. baumannii growth in rich defined media

To establish an optimum defined media for growth of *A. baumannii* ATCC19606, I tested growth in a common rich defined media (MOPS-based Rich Defined Medium or EZ RDM, Teknova) (8). EZ RDM is typically supplemented with 0.2% (w/v) glucose, but as *A. baumannii* cannot utilize glucose (3), I additionally tested with 0.2% (w/v) succinic acid. To contrast, I included a defined minimal medium (8), also supplemented with 0.2% succinic acid, and complex media—Lysogeny Broth (LB), made from either premixed dehydrated media or from individual components (Fig B.1A). As expected, the minimal media exhibited the slowest growth. Surprisingly, EZ RDM with 0.2% succinic acid supported faster growth and reached a higher cell density compared to LB, and even EZ RDM with 0.2% glucose showed comparable growth. In the glucose medium, it is possible that *A. baumannii* is utilizing other components of EZ RDM, such as amino acids, as a carbon source, or that residual nutrients from initial growth in rich media prior to the experimental setup supported growth.

With the improved growth of EZ RDM with 0.2% succinic acid (~17mM), I then sought to find an optimal concentration of supplemented succinate. To better match standards from *Pseudomonas* succinate media, which utilize 10mM or 20mM succinate, I then tested a range of succinic acid concentrations from 0mM to 100mM, utilizing LB with added succinic acid as a control (Fig B.1B). In EZ RDM with 20 mM succinic acid, the strain showed a similar growth phenotype, and without an added carbon source, showed a growth defect. Yet succinic acid at a higher concentration caused growth to lag (25 mM) or be entirely inhibited, including adding succinic acid to LB.

I hypothesized that the succinic acid lowered the pH of the EZ RDM, despite the presence of MOPS buffer in the media. Indeed, when made with sodium succinate, the pH of the media was ~7.5, but with only 20 mM succinic acid, the pH dropped to ~5.2. *A. baumannii* is known to grow well in a pH

Figure B.1. 19606 growth curves in various media. (A) Growth over 15 hours in EZ RDM with glucose or succinic acid at 0.2% w/v, LB mixed from components or purchased premixed, and MOPS minimal media with 0.2% w/v succinic acid. (B) Growth over 15 hours in EZ RDM with different concentrations of succinic acid or LB supplemented with 20 mM succinic acid. Lines represent the mean biological replicates (N=3); ribbons are standard deviation.

Figure B.1

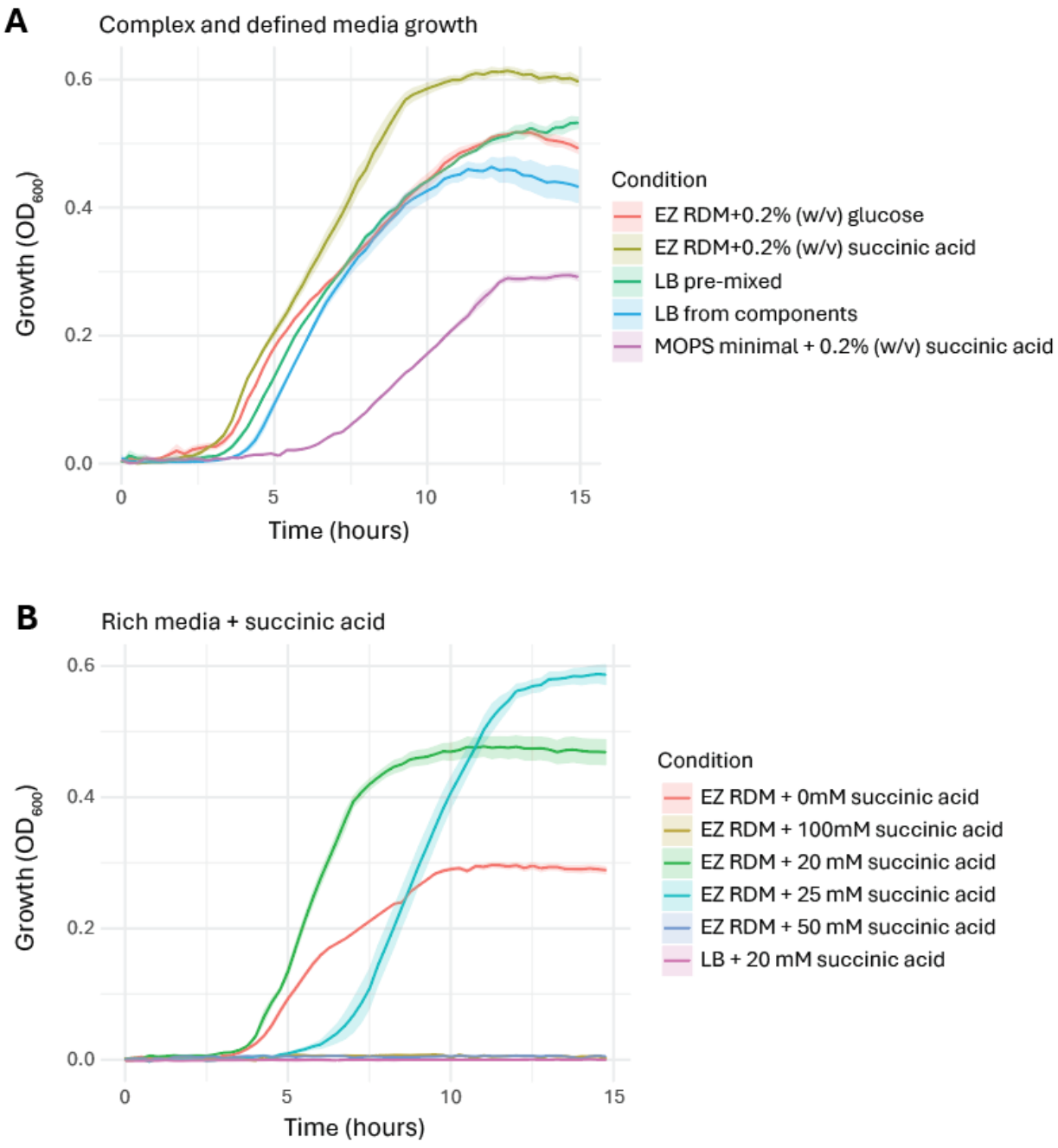
A
Complex and defined media growth
Growth (OD600)
0.6
0.4
0.2
0.0
0
5
10
15
Time (hours)
Condition
EZ RDM+0.2% (w/v) glucose
EZ RDM+0.2% (w/v) succinic acid
LB pre-mixed
LB from components
MOPS minimal + 0.2% (w/v) succinic acid
B
Rich media + succinic acid
Growth (OD600)
0.6
0.4
0.2
0.0
0
5
10
15
Time (hours)
Condition
EZ RDM + 0mM succinic acid
EZ RDM + 100mM succinic acid
EZ RDM + 20 mM succinic acid
EZ RDM + 25 mM succinic acid
EZ RDM + 50 mM succinic acid
LB + 20 mM succinic acid

range of 5-8 (9), suggesting that higher concentrations of succinic acid were inhibitory due to overly acidic conditions. I next tried sodium succinate as a medium additive to increase succinate concentration without a concomitant decrease in pH (Fig B.2A). All concentrations of sodium succinate showed growth comparable to—or better than—LB. Interestingly, 20mM of succinic acid showed a possible slight increase in growth but remained a nonoptimal choice due to overwhelming the buffer solution in EZ RDM.

We then sought to test the application of EZ RDM with sodium succinate in an experimental setup. By growing larger volumes of cell culture with an uninduced essential gene CRISPRi library (10) rather than WT, we better represented actual experimental conditions. I found that cultures of the library with 40 mM of sodium succinate achieved maximal cell density at stationary phase (Fig B.2B). We defined EZ RDM supplemented with 40mM sodium succinate as AbRDM, using this media in subsequent experiments.

Quantification of subinhibitory chemical concentrations

I then tested growth of 19606 in AbRDM with added chemicals at various concentrations to define a range of subinhibitory concentrations for downstream chemical genomics. To achieve this, I sought to determine a method of quantification for inhibition; previous studies of bacterial growth have used metrics like lag time, carrying capacity (asymptote), growth rate (slope of the curve), average doubling time, or more complex mathematical modeling (11–15) (Fig B.3A). However, initial growth curves with antibiotics revealed varying phenotypes for growth inhibition where comparisons including only slope, carrying capacity, or lag time across conditions would be inconsistent. For example, nalidixic acid showed a substantial change in slope and carrying capacity but not lag time with higher concentration (Fig B.3B). In contrast, increasing concentrations of tetracycline caused longer lag times, but slopes remained similar and changes in carrying capacity were inconsistent

Figure B.2. Growth in EZ RDM with sodium succinate. (A) Growth curves over 15 hours in EZ RDM supplemented with sodium succinate, with LB and EZ RDM with 20 mM succinic acid. Lines represent the mean of biological replicates (N=3); ribbons are standard deviation. (B) Boxplot depicting approximate cell density (OD_{600}) of uninduced *A. baumannii* essential gene knockdown library cultures (N=3 biological replicates) after 20 hours of growth. To calculate values, cultures were diluted 1:10 and resulting measurements were multiplied by ten.

Figure B.2

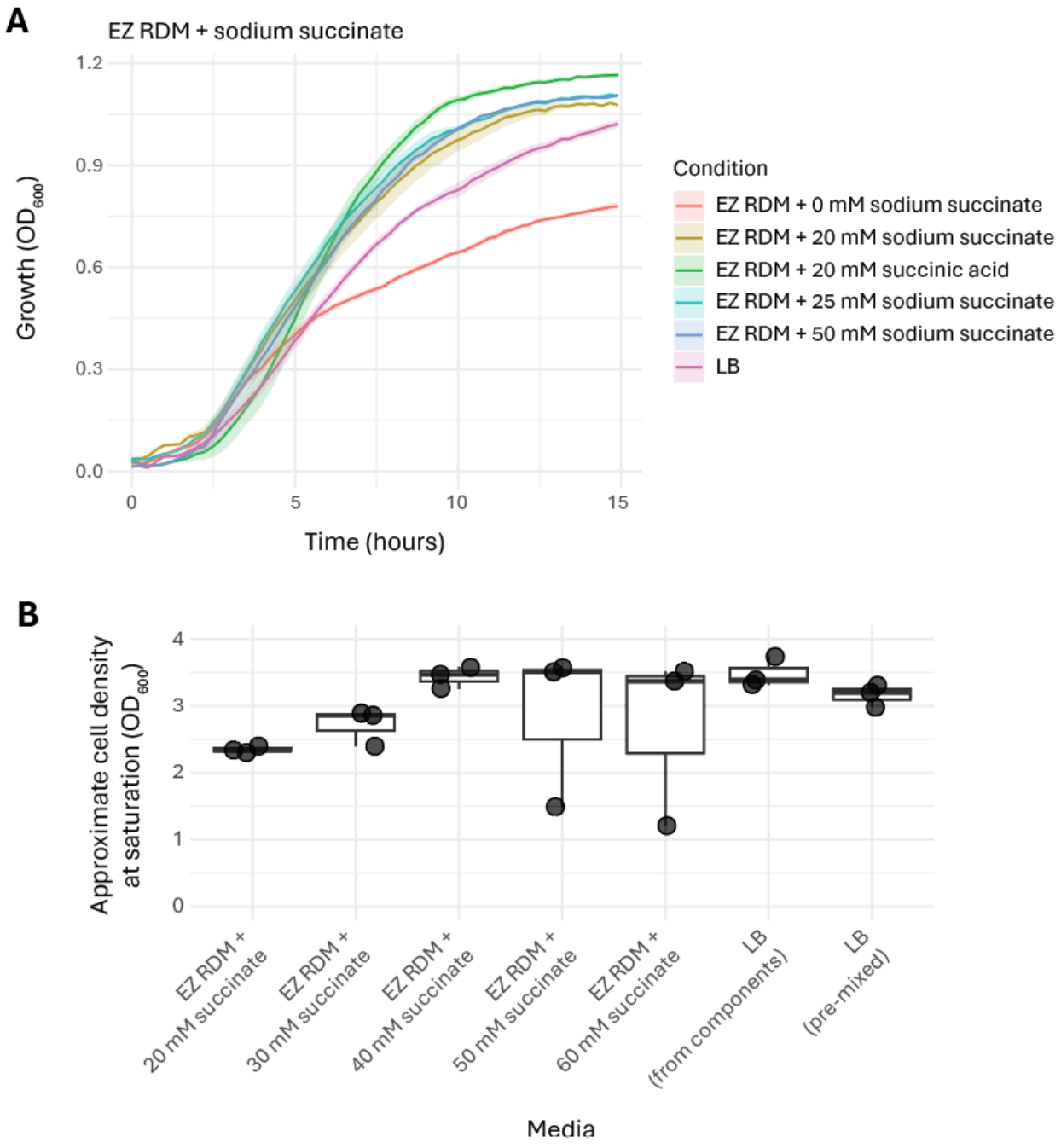
A
EZ RDM + sodium succinate
Growth (OD600)
1.2
0.9
0.6
0.3
0.0
0
5
10
15
Time (hours)
Condition
EZ RDM + 0 mM sodium succinate
EZ RDM + 20 mM sodium succinate
EZ RDM + 20 mM succinic acid
EZ RDM + 25 mM sodium succinate
EZ RDM + 50 mM sodium succinate
LB
B
Approximate cell density at saturation (OD600)
4
3
2
1
0
EZ RDM + 20 mM succinate
EZ RDM + 30 mM succinate
EZ RDM + 40 mM succinate
EZ RDM + 50 mM succinate
EZ RDM + 60 mM succinate
LB (from components)
LB (pre-mixed)
Media

Figure B.3. Effect of subinhibitory chemicals on growth. (A) Graphic depicting a bacterial growth curve with common parameters. Growth data averages are shown for 19606 grown in varying concentrations of (B) nalidixic acid, (C) tetracycline, or (D) fosfomycin to depict growth curve variations. Lag time, slope, and asymptote values are not consistently representative of growth defects from different antibiotics.

Figure B.3

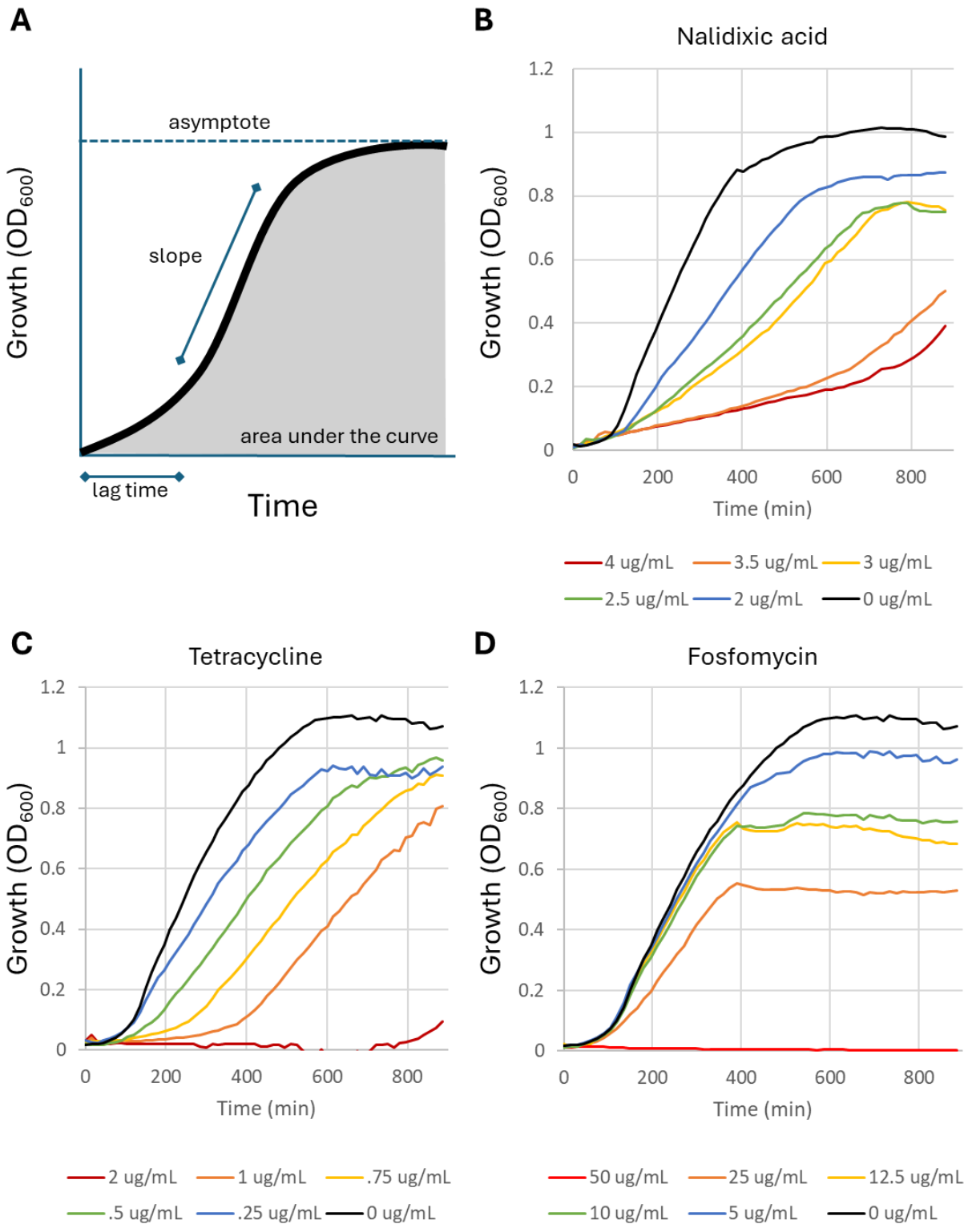
A
asymptote
slope
area under the curve
lag time
Growth (OD600)
Time
B
Nalidixic acid
Growth (OD600)
Time (min)
4 ug/mL
3.5 ug/mL
3 ug/mL
2.5 ug/mL
2 ug/mL
0 ug/mL
C
Tetracycline
Growth (OD600)
Time (min)
2 ug/mL
1 ug/mL
.75 ug/mL
.5 ug/mL
.25 ug/mL
0 ug/mL
D
Fosfomycin
Growth (OD600)
Time (min)
50 ug/mL
25 ug/mL
12.5 ug/mL
10 ug/mL
5 ug/mL
0 ug/mL

(Fig B.3C). Additionally, standard sigmoidal curve modeling may falter with sharp, rather than gradual, changes in growth rate, as observed with fosfomycin (Fig B.3D). Because of these variations between antibiotics, we decided to use an empirical area under the curve (AUC) to define growth and inhibition. The AUC method offers a robust alternative by integrating the entire growth curve, and use of the trapezoidal method to estimate AUC avoids modeling to a mathematical function that may differ in fit across samples. Comparison of the AUC to a control without inhibition allows us to estimate a percent inhibition, and values for numerous chemicals and concentrations are presented in Table B.1. Some chemicals tested were not reported here—with some used in later experiments—due to a complete lack of inhibition at high concentrations (e.g., sodium tungstate, PC190723) or lack of replicability of growth across days and/or concentrations. A single concentration of colistin, a last-resort antibiotic used for clinical treatment, could display both total inhibition and complete lack of inhibition across replicates, corroborating observed *A. baumannii* heteroresistance to this drug at even low concentrations (16).

Table B.1. Antibiotic concentrations and growth inhibition of *A. baumannii* ATCC19606.

Antibiotic	Solvent[1]	Concentration[2] (ug/mL unless otherwise specified)	Average inhibition[3] (%)	Standard deviation of inhibition
A22	DMSO	2.5	10.82	0.63
		4	20.17	0.62
		5	24.18	1.82
		10	36.16	1.30
		20	75.05	3.06
acriflavine	DMSO	1	5.76	0.63
		2	11.07	0.89
		3	14.37	0.77
		4	16.17	0.39
		8	20.27	0.96
		16	48.59	3.15
		24	68.47	6.76
		32	96.30	2.52
		48	98.19	0.35
actinomycin D	DMSO	8	15.39	1.77
		10	25.43	2.04
		12	27.72	1.29
		14	31.35	0.33
		16	34.14	0.79
amikacin	water	1	7.81	0.89
		1.25	13.43	0.95
		1.5	26.21	1.64
		1.75	35.35	1.46
		2	43.23	1.08
		4	94.63	1.78
		8	98.37	0.06
		16	97.71	0.26
amoxicillin	DMSO	10	1.31	0.89
		20	2.04	0.40
		40	0.97	1.36
		80	60.24	1.94
		160	90.85	0.29
apramycin	water	10	38.09	2.55
		20	103.25	5.16
		30	127.00	0.80

		40	127.02	0.85
		50	128.98	0.77
azithromycin	DMSO	0.2	16.24	0.52
		0.4	25.50	0.33
		0.6	30.56	0.92
		0.8	36.14	0.57
		1	29.58	0.99
		1.125	33.50	0.45
		1.25	36.82	0.54
		1.375	40.11	0.10
		1.5	41.52	0.24
aztreonam	water	2	-8.85	1.02
		4	-1.49	2.52
		6	26.62	2.14
		8	47.58	3.44
		10	55.17	5.77
carvacrol	DMSO	40	12.38	0.72
		42.5	16.00	1.46
		45	19.13	1.40
		47.5	19.89	1.53
		50	21.41	1.07
CCCP	DMSO	12.5	30.17	0.21
		25	78.64	1.93
		50	97.45	0.14
		100	97.58	0.05
		200	97.40	0.17
cefaclor	water	48	1.60	0.30
		56	5.16	0.09
		64	7.15	0.23
		72	17.83	0.56
		80	27.10	0.85
cerulenin	DMSO	5	4.67	0.62
		7.5	39.90	1.41
		10	65.13	0.83
		12.5	72.60	2.43
		15	75.19	4.99
chlorhexidine	DMSO	1	-9.80	2.27
		2	-4.41	1.91
		3	-0.78	1.54
		4	11.13	1.66
		5	25.07	2.21

chlorpromazine	DMSO	5	8.38	0.49
		10	23.74	1.41
		12.5	26.13	1.17
		25	46.90	0.75
		50	98.88	0.20
ciprofloxacin	water	0.1	10.79	0.90
		0.2	17.40	0.35
		0.3	25.91	0.22
		0.4	48.36	0.25
		0.5	66.07	0.34
copper (II) sulfate	water	6.25	7.33	0.45
		12.5	7.03	0.62
		25	-0.49	0.18
		50	13.61	0.48
		100	16.65	0.91
d-cycloserine	water	60	13.59	0.56
		70	18.88	1.06
		80	29.60	1.50
		90	32.76	0.68
		100	37.87	1.57
daptomycin	water	6.25	-0.35	0.22
		12.5	0.45	0.59
		25	5.16	0.51
		50	9.04	0.29
		100	10.80	1.84
doripenem	water	0.063	23.10	0.43
		0.125	51.56	0.74
		0.25	75.51	0.93
		0.5	80.29	0.26
		1	88.93	0.65
EDTA	water	31.25 mM	12.87	0.31
		62.5 mM	16.25	2.13
		125 mM	20.33	1.18
		250 mM	27.91	0.18
		500 mM	40.63	0.41
ethidium bromide	water	10	20.97	1.52
		20	25.92	0.53
		30	32.10	0.50
		35	35.51	1.04
		40	37.50	0.75
		45	42.10	0.57

		50	42.15	1.54
fosfomycin	water	16	6.03	1.19
		32	10.35	1.50
		64	41.28	1.68
		128	84.08	2.99
		256	93.46	1.94
imipenem	DMSO	0.025	15.75	0.03
		0.05	30.61	1.15
		0.075	45.23	1.10
		0.1	53.13	1.15
		0.125	59.88	2.36
indole	DMSO	50	3.22	0.75
		75	10.42	3.95
		100	21.81	7.66
		150	47.37	27.49
		200	75.05	17.10
isoniazid	water	100	13.77	0.87
		200	35.17	0.44
		250	70.83	0.91
		300	64.05	19.44
		400	63.50	0.49
levofloxacin	DMSO	0.016	7.26	1.95
		0.031	10.34	2.20
		0.063	12.51	2.66
		0.125	18.61	3.30
		0.25	29.00	3.25
lysozyme	0.02 M sodium acetate buffer; pH=4.6	20	1.97	2.71
		30	9.10	2.79
		40	11.70	4.13
		50	18.66	1.68
		60	17.45	2.39
mecillinam	DMSO	6.25	21.85	1.42
		12.5	25.52	0.35
		25	32.57	0.85
		50	44.07	0.89
		100	63.02	1.00
meropenem	DMSO	0.05	4.31	0.61
		0.1	9.92	1.10
		0.15	16.43	0.77
		0.2	26.67	1.43
		0.25	37.80	0.64

mupirocin	DMSO	62.5	29.24	1.58
		125	35.31	0.47
		250	40.98	0.21
		500	41.00	1.28
		1000	37.02	0.20
myricetin	DMSO	5	-3.07	2.49
		7.5	2.46	0.99
		10	6.07	0.98
		15	9.22	0.22
		20	16.73	0.81
		25	25.12	3.71
		30	27.53	6.14
nalidixic acid	water	2	24.94	1.46
		2.5	41.84	0.80
		3	45.49	1.07
		3.5	73.67	4.47
		4	78.95	4.74
novobiocin	water	0.625	4.60	1.07
		1.25	8.79	0.54
		2.5	14.12	0.10
		5	34.46	0.42
		10	81.54	0.76
polymyxin B	water	1	16.57	0.86
		1.25	62.58	21.71
		1.5	96.87	0.85
		1.75	97.70	0.86
		2	97.59	0.99
phenazine	water	2.5	10.40	0.77
		5	18.16	0.93
		6	23.75	1.52
		7.5	34.35	3.21
		10	56.05	4.04
paraquat	water	5	5.64	0.47
		10	9.97	0.30
		15	14.56	0.28
		20	18.27	0.71
		25	19.20	1.07
pyocyanin	DMSO	6.25	20.10	0.36
		12.5	39.23	0.92
		25	77.74	2.94
		50	68.77	0.19

		100	44.63	0.23
rifampicin	DMSO	0.2	3.50	1.19
		0.4	8.04	1.00
		0.6	14.37	0.51
		0.8	20.02	0.43
		1	31.01	0.62
SDS	water	50	21.69	1.41
		62.5	31.47	0.75
		75	34.18	1.06
		87.5	34.34	1.24
		100	35.62	0.20
sulbactam	DMSO	0.625	75.93	0.96
		1.25	76.38	0.97
		2.5	79.06	0.66
		5	85.21	1.13
		10	82.42	0.52
tazobactam-piperacillin	DMSO	0.125; 1	4.23	0.96
		0.25; 2	2.63	0.26
		0.5; 4	20.27	1.68
		1; 8	62.32	2.49
		2; 16	73.88	1.41
triclosan	DMSO	0.125	20.15	5.15
		0.25	48.84	9.26
		0.5	86.23	4.12
		1	88.93	1.65
		2	94.51	0.09
tetracycline	water	0.25	18.35	1.85
		0.5	30.14	1.67
		0.75	46.13	2.21
		1	62.54	3.08
		2	96.88	0.57
thymol	DMSO	7.5	-0.87	1.18
		15	2.99	0.74
		30	9.41	1.49
		50	13.52	2.03
		60	26.79	2.88
		70	54.86	10.14
		80	78.23	11.06
		90	81.82	14.54
		120	80.10	11.48
tigecycline	DMSO	0.016	11.10	3.03

		0.03	19.52	1.55
		0.06	31.19	2.25
		0.125	62.70	2.29
		0.25	94.72	2.02
trimethoprim	DMSO	2	18.72	2.10
		4	36.28	2.32
		8	61.41	6.18
		16	90.88	1.15
		32	94.55	2.65
trimethoprim-sulfamethoxazole	DMSO	1; 5	10.47	0.33
		2; 10	12.45	0.71
		3; 15	16.31	0.34
		4; 20	19.88	0.80
		5; 25	22.29	0.47
tannic acid	DMSO	12.5	56.86	0.53
		25	72.81	0.67
		50	71.87	2.58
		100	65.82	0.65
		200	59.30	0.52
tobramycin	water	0.2	6.11	0.13
		0.4	17.06	1.04
		0.6	35.38	0.64
		0.8	51.48	2.34
		1	71.16	0.58
		1.25	88.54	1.78
		1.5	93.34	1.88
		1.75	97.33	0.61
		2	97.92	2.69
TPEN	DMSO	1	17.22	0.82
		2	20.65	0.69
		3	21.94	0.85
		4	22.26	0.70
		5	42.87	0.48
		10	48.07	0.55
		15	51.25	0.28
		20	54.07	0.27
		25	57.11	0.10
vancomycin	water	0.625	2.94	0.85
		1.25	2.42	1.79
		2.5	4.58	0.75
		5	17.02	3.72

10	35.00	5.24
30	50.25	0.71
40	58.30	1.22
50	63.53	0.97
60	67.67	0.64
70	71.57	1.04

[1]Solvents used to dissolve initial antibiotic stock and make dilutions. Working stocks added at ~1% of final cultures.

[2]Final concentration of the antibiotic in culture, in ug/mL unless otherwise specified. Concentrations for each component of combination antibiotics are listed in order, separated by a semicolon.

[3]Percent inhibition is calculated as $100*(1-(AUC_{Sample}/AUC_0)$, where AUC_{Sample} is the area under the curve for the sample and AUC_0 is that of the corresponding no antibiotic control. N=3 biological replicates per condition.

Discussion

This appendix reports growth data for *A. baumannii* in EZ RDM, a nutrient-rich and defined medium, compared to LB, and describes concentrations of succinate to use as a carbon source in this medium. While sodium succinate is the preferred source for succinate, *A. baumannii* carbon utilization is still not fully understood. The observations of growth in EZ RDM without a carbon source supplement supports studies showing that *A. baumannii* can utilize amino acids as a carbon source more efficiently than other bacterial species (17, 18). Moreover, although succinate is a known preferred carbon source in *Pseudomonas* (4), *A. baumannii* may be able to incorporate carbon from other untested sources more efficiently. In addition, we observed a possible growth improvement in EZ RDM with 20 mM succinic acid, which has a more acidic pH. While early studies on *Acinetobacter* species suggest an enrichment of growth in lower pH conditions (~5.5) (19), more study is needed to validate our observations and understand effects of pH changes *A. baumannii* growth.

The subinhibitory chemical concentrations reported here serve as a valuable resource, providing a concentration range for future experiments requiring mild perturbations. However, it is important to acknowledge the limitations inherent in this approach. These concentrations were tested in 96-well plates and may change in experimental setups with larger volumes or different conditions. With more potent antibiotics, concentration ranges were often very narrow, and biological and technical variation could significantly impact the observed level of inhibition. Additionally, as noted with colistin, the inherent variability and adaptability of *A. baumannii* can lead to inconsistencies in growth and inhibition patterns. Therefore, we recommend multiple concentrations of each chemical with several technical and biological replicates under test conditions, especially for high-throughput experiments, to ensure robust and reproducible results. Nevertheless, from these

experiments, we established and quantified several subinhibitory chemical concentrations and confirmed AbRDM as a medium for future experiments.

Materials and Methods

Strain *A. baumannii* ATCC19606 (sJMP4001) was used for all growth curve experiments. An essential gene library of ATCC19606 (sJMP2949) from Ward et al. (10) and reported on in Chapters 2 and 3 was used for measuring cell density at saturation in EZ RDM across sodium succinate concentrations. Cells were grown in EZ RDM (Teknova) with supplemented succinate or in LB, either purchased premixed (BD 240230) or mixed from components (10 g tryptone, 5 g yeast extract, 5 g NaCl per liter).

Media growth assays

Growth of *A. baumannii* 19606 WT (sJMP4001) was assessed for growth in different media. Briefly, overnight cultures of three individual isolates in LB was spun down, washed in PBS, and diluted 1:1000 into appropriate media in a 96-well plate to a final volume of 200µL and incubated in a plate reader (Tecan Infinite 200 Pro Mplex) for 15 hours at 37°C with shaking. Growth was monitored by measuring OD_{600} every 15 minutes.

For growth to saturation, sJMP2949 was revived by dilution of 25µL frozen stock (OD_{600} = 15) in 25 mL prepared media (starting OD_{600} = 0.015) and incubated in a 125 mL flask with shaking at 37°C until OD_{600} = 0.2, about 3.5 hours. sJMP2949 culture was then split for triplicate growth and diluted 1:10 into media in 14 mL snap cap culture tubes. Tubes were grown for 20 hours with shaking at 37°C. At saturation, cultures were diluted 1:10 and OD_{600} was measured.

Antibiotic growth assay

Three individual isolates of 19606 WT were resuspended from LB plates and used to inoculate 300µL AbRDM (starting OD_{600} = 0.01) in a deep well microtiter plate. Cultures were grown with shaking at 900 rpm for 3.5 hours or to early mid-log (OD_{600} ~0.2). Cultures were then diluted 1:100

into a 96-well plate at a final volume of 200µL media with antibiotics, diluted in appropriate solvent and added to media at 1% of final volume. Final concentrations are reported in Table B.1.

Quantification of inhibition

Background (media-only) absorbance values were first subtracted from sample absorbance values. Then, the empirical area under the curve (AUC) was calculated for each sample in R using the AUC function (trapezoidal rule for integration) from the DescTools package. Alternate functions, such as trapz from the pracma package or SummarizeGrowthByPlate from the Growthcurver package, will return similar values. Percent inhibition of bacterial growth was calculated using the following formula:

$$Percent\ inhibition = 100 \times (1 - \frac{AUC_{sample}}{AUC_0})$$

where AUC_{Sample} represents the AUC for each unique condition and biological replicate and AUC_0 is the corresponding biological replicate with no added antibiotic within the same plate.
The average percent inhibition for each antibiotic concentration is reported with standard deviations. Code can be found at https://github.com/jentranxd/PhD_Thesis_2024.

References

1. Basu S, Bose C, Ojha N, Das N, Das J, Pal M, Khurana S. 2015. Evolution of bacterial and fungal growth media. Bioinformation 11:182–184.
2. Sezonov G, Joseleau-Petit D, D'Ari R. 2007. Escherichia coli physiology in Luria-Bertani broth. J Bacteriol 189:8746–8749.
3. Baumann P, Doudoroff M, Stanier RY. 1968. A study of the Moraxella group. II. Oxidative-negative species (genus Acinetobacter). J Bacteriol 95:1520–1541.
4. Sonnleitner E, Abdou L, Haas D. 2009. Small RNA as global regulator of carbon catabolite repression in Pseudomonas aeruginosa. Proc Natl Acad Sci U S A 106:21866–21871.
5. Ren X, Palmer LD. 2023. Acinetobacter Metabolism in Infection and Antimicrobial Resistance. Infection and Immunity 91:e00433-22.

6. Zheng XFS, Chan T-F. 2002. Chemical genomics: a systematic approach in biological research and drug discovery. Curr Issues Mol Biol 4:33–43.

7. Nichols RJ, Sen S, Choo YJ, Beltrao P, Zietek M, Chaba R, Lee S, Kazmierczak KM, Lee KJ, Wong A, Shales M, Lovett S, Winkler ME, Krogan NJ, Typas A, Gross CA. 2011. Phenotypic landscape of a bacterial cell. Cell 144:143–156.

8. Neidhardt FC, Bloch PL, Smith DF. 1974. Culture medium for enterobacteria. J Bacteriol 119:736–747.

9. Dekic S, Hrenovic J, Ivankovic T, Van Wilpe E. 2018. Survival of ESKAPE pathogen Acinetobacter baumannii in water of different temperatures and pH. Water Science and Technology 78:1370–1376.

10. Ward RD, Tran JS, Banta AB, Bacon EE, Rose WE, Peters JM. Essential gene knockdowns reveal genetic vulnerabilities and antibiotic sensitivities in Acinetobacter baumannii. mBio 15:e02051-23.

11. Sterniša M, Sabotič J, Klančnik A. 2022. A novel approach using growth curve analysis to distinguish between antimicrobial and anti-biofilm activities against Salmonella. International Journal of Food Microbiology 364:109520.

12. Greulich P, Doležal J, Scott M, Evans MR, Allen RJ. 2017. Predicting the dynamics of bacterial growth inhibition by ribosome-targeting antibiotics. Phys Biol 14:065005.

13. Marques-da-Silva D, Mal SS, Aureliano M, Lagoa R. 2022. The Growth Curve Method to Rapidly Derive the Antibacterial Potential of Polyoxovanadates, p. 2. *In* BiTaP 2022. MDPI.

14. Zwietering MH, Jongenburger I, Rombouts FM, van 't Riet K. 1990. Modeling of the bacterial growth curve. Appl Environ Microbiol 56:1875–1881.

15. Pruitt KM, Kamau DN. 1993. Mathematical models of bacterial growth, inhibition and death under combined stress conditions. Journal of Industrial Microbiology 12:221–231.

16. Novović K, Jovčić B. 2023. Colistin Resistance in Acinetobacter baumannii: Molecular Mechanisms and Epidemiology. Antibiotics (Basel) 12:516.

17. Nairn BL, Lonergan ZR, Wang J, Braymer JJ, Zhang Y, Calcutt MW, Lisher JP, Gilston BA, Chazin WJ, de Crécy-Lagard V, Giedroc DP, Skaar EP. 2016. The Response of Acinetobacter baumannii to Zinc Starvation. Cell Host & Microbe 19:826–836.

18. Semenec L, Cain AK, Dawson CJ, Liu Q, Dinh H, Lott H, Penesyan A, Maharjan R, Short FL, Hassan KA, Paulsen IT. 2023. Cross-protection and cross-feeding between Klebsiella pneumoniae and Acinetobacter baumannii promotes their co-existence. Nat Commun 14:702.

19. Baumann P. 1968. Isolation of Acinetobacter from soil and water. J Bacteriol 96:39–42.

APPENDIX C

Effects of aerobic respiration complex knockdowns in *A. baumannii*

I performed all the experiments shown here and wrote this appendix.

Introduction

Acinetobacter baumannii is an obligate aerobe, relying entirely on oxygen for its energy production. Central to this is oxidative phosphorylation, which harnesses the transfer of electrons to oxygen through a series of oxidation-reduction reactions to generate ATP (1). This electron transport chain (ETC) consists of several major complexes that work together to transfer electrons and pump protons across the bacterial inner membrane, creating the electrochemical gradient necessary for ATP synthase to function (2). Despite its importance, the detailed mechanisms and flux through this pathway in *A. baumannii* are not fully understood. However, Tn-seq experiments have identified four of these complexes as essential for bacterial survival: NADH dehydrogenase (NDH-1), succinate dehydrogenase (Sdh), cytochrome bo_3 oxidase (Cyo), and ATP synthase (Fig C.1) (3, 4).

In this study, we utilized CRISPRi to perturb these essential respiratory complexes in *A. baumannii* ATCC19606 (5). By selectively knocking down genes encoding components of these complexes, we were able to measure subsequent impacts on energy output and membrane potential.

Results

Knockdowns of respiratory complexes reduce cellular levels of ATP

Using the previously described CRISPRi system and guides (5), I created individual knockdown strains, each targeting a single gene that encoded part of an essential respiratory complex. The targeted genes are located upstream of genes encoding other components of the respective complexes within predicted operons (6), and these complexes likely cannot function or assemble without all subunits (7–10) these knockdowns likely affect the entire complex. To test the effect of knockdown of the essential complexes on overall energy production, we measured ATP levels of *nuoB*, *sdhB*, *cyoA*, and *atpB* knockdowns relative to a control containing a non-targeting sgRNA

Figure C.1. Predicted aerobic respiration complexes in *A. baumannii*. Apart from ATP synthase (10, 11), complex function in *A. baumannii* is based heavily on work done in other Gammaproteobacteria (12, 13). Complexes known to be essential are labeled.

Figure C.1

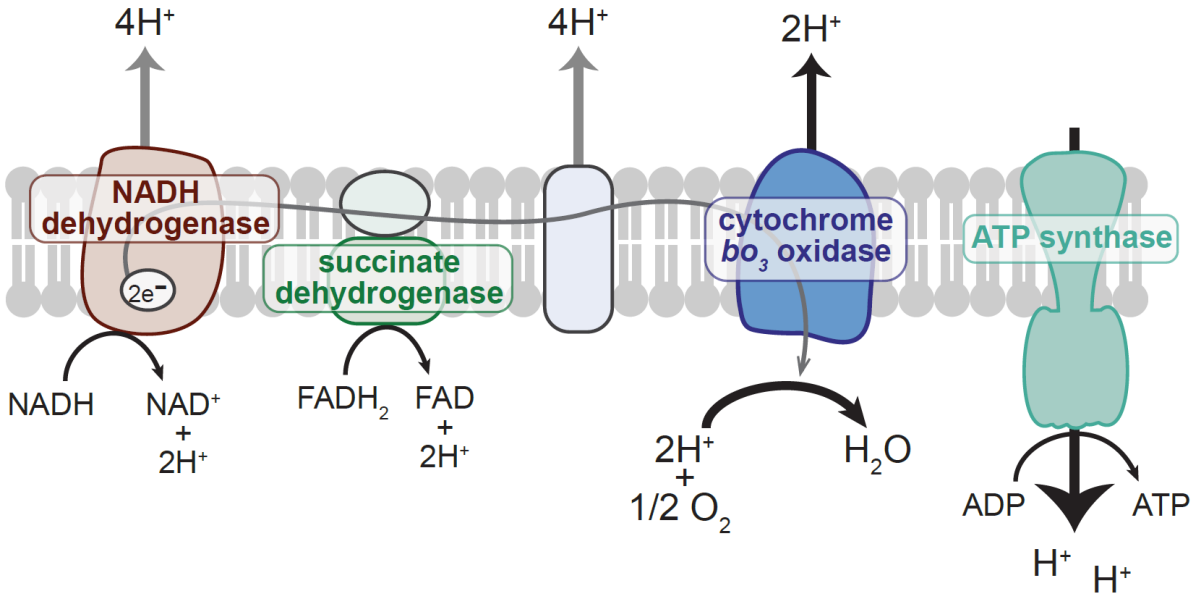
4H+
4H+
2H+
NADH dehydrogenase
2e−
succinate dehydrogenase
cytochrome bo3 oxidase
ATP synthase
NADH
NAD+ + 2H+
FADH2
FAD + 2H+
2H+ + 1/2 O2
H2O
ADP
ATP
H+
H+

using the Promega CellTiter-Glo 2.0 Assay. We found lower levels of ATP for all knockdowns tested; however, knockdown of NDH-1 and Sdh had a greater impact than Cyo or ATP synthase itself (Fig C.2), suggesting that the cell may have compensatory mechanisms that partially mitigate respiratory impacts or that NDH-1 and Sdh acted as bottlenecks in electron transfer. While metabolic compensatory mechanisms for impaired respiration have been documented in both mitochondria (14–17) and in other Gammaproteobacteria (18–21), further study is necessary to understand how *A. baumannii* responds to various respiratory stressors.

Varying effects on membrane potential

Given that ETC complexes significantly contribute to proton motive force (PMF) and ATP synthase utilizes this PMF to function, we hypothesized that knockdowns of these complexes would affect membrane permeability, which is linked to PMF through transporter function (22, 23). To test this hypothesis, we conducted a permeability assay using ethidium bromide (EtBr), which fluoresces upon entering the cell and binding to DNA. Higher fluorescence readings indicate increased membrane permeability. I found that the *sdh* knockdown strain had much lower permeability compared to the non-targeting control, whereas knockdowns of ATP synthase and Cyo had increased permeability (Fig C.3). Despite having opposing effects on PMF, Cyo and ATP synthase displayed similar phenotypes, which may result from compensatory mechanisms or other downstream cellular effects. For example, the synthesis of ATP is crucial to numerous processes, including efflux (24), and Cyo—as the terminal oxidase—may contribute to ROS defense mechanisms (25). Surprisingly, the knockdown of NDH-1 exhibited only a minor defect, if any (Fig C.3) despite previous work demonstrating that NDH-1 knockdown significantly decreased permeability (5). Furthermore, NAD+/NADH assays performed with these knockdowns (Fig C.4) also varied from NDH-1 knockdown data (5), suggesting variations between experiments could significantly affect flux through this pathway or assay measurements.

Figure C.2. Relative ATP levels in aerobic respiration complex knockdowns. Boxplot depicts cellular ATP—measured as luminescence with a CellTiter-Glo 2.0 Assay (Promega)—normalized to the non-targeting control mean (dotted line). Points represent N=4 biological replicates.

Figure C.2

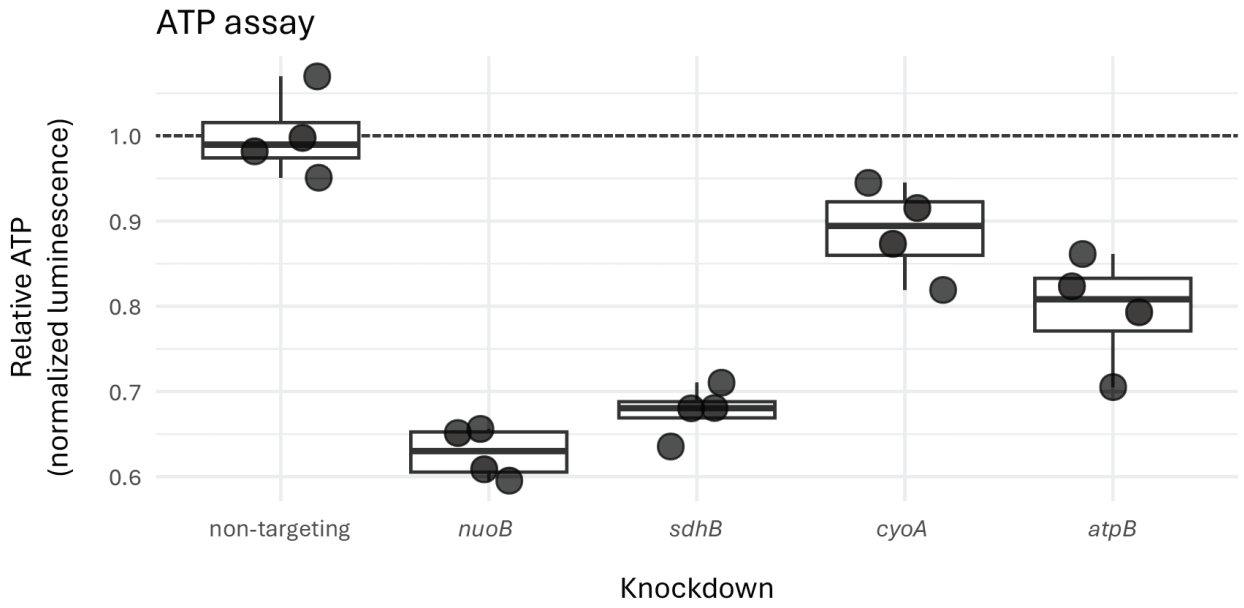
ATP assay
Relative ATP
(normalized luminescence)
1.0
0.9
0.8
0.7
0.6
non-targeting
nuoB
sdhB
cyoA
atpB
Knockdown

Figure C.3. Membrane permeability in knockdowns of aerobic respiration complexes. Ethidium bromide permeability assay of knockdown or non-targeting strains. Lines depict sample means, and ribbons represent standard deviation for N=4 biological replicates.

Figure C.3

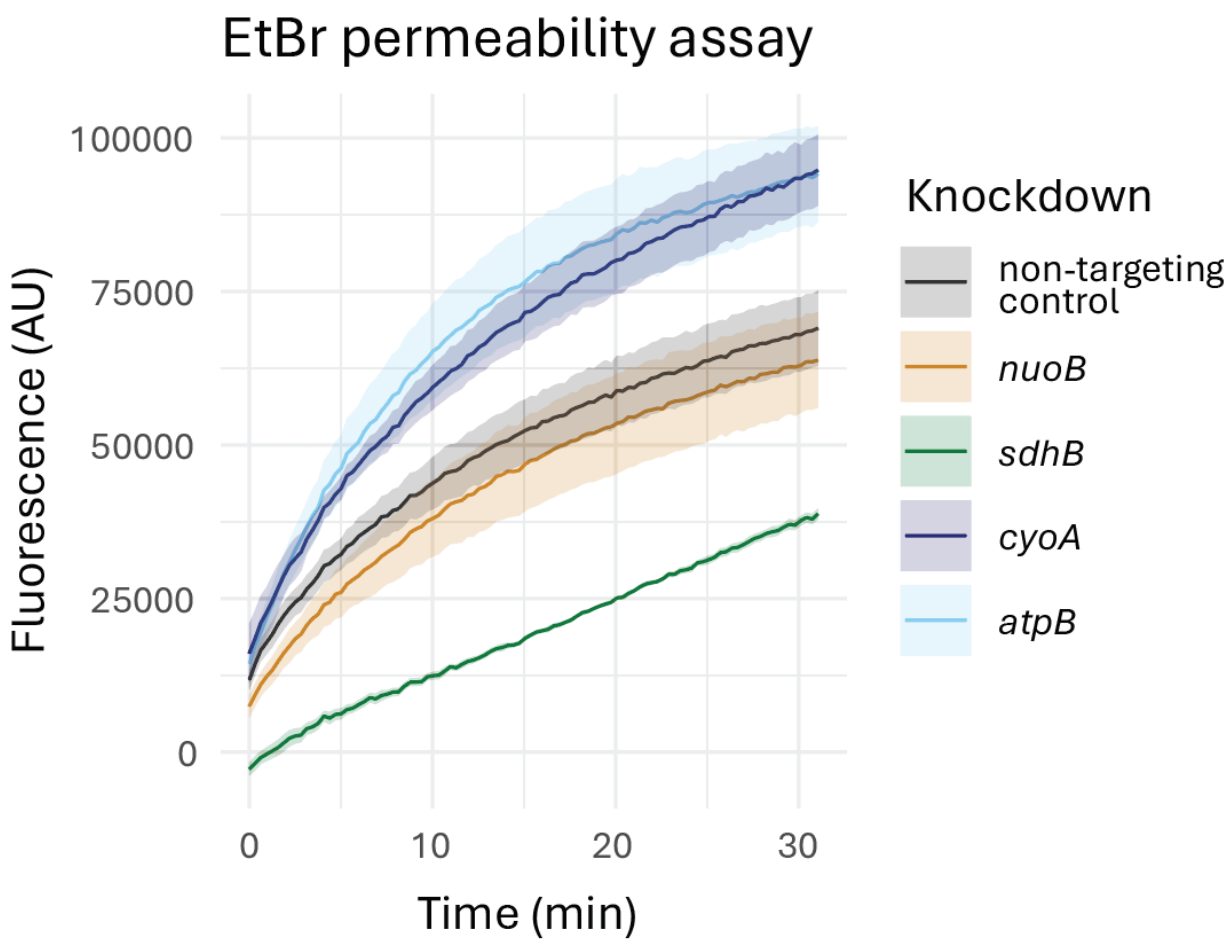
EtBr permeability assay
Fluorescence (AU)
100000
75000
50000
25000
0
0
10
20
30
Time (min)
Knockdown
non-targeting control
nuoB
sdhB
cyoA
atpB

Figure C.4. NAD+/NADH ratios in aerobic respiration complex knockdowns. Boxplot depicts cellular NAD+/NADH ratios, measured as luminescence with a NAD/NADH-Glo™ Assay (Promega). N=3 biological replicates.

Figure C.4

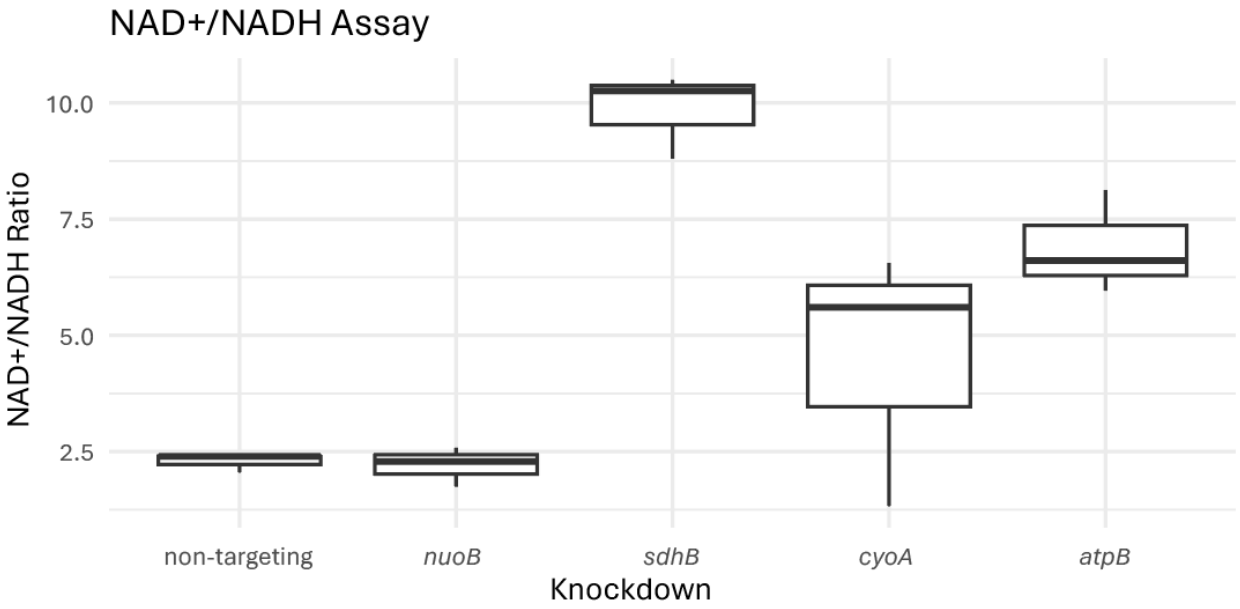
NAD+/NADH Assay
NAD+/NADH Ratio
10.0
7.5
5.0
2.5
non-targeting
nuoB
sdhB
cyoA
atpB
Knockdown

Discussion

My findings indicate that knockdowns of aerobic respiration complexes reduce ATP levels, with NDH-1 and Sdh knockdowns having a more pronounced impact than ATP synthase and Cyo knockdowns. Additionally, ATP synthase and Cyo knockdowns displayed increased permeability, despite predicted opposing effects on proton motive force, whereas Sdh knockdowns were less permeable. Importantly, experimental variations can affect measurements and replicability; only single experiments for permeability and NAD+/NADH data are shown here as experiments were difficult to replicate, and the data differ from previous studies using the same protocols but different media (5). As CRISPRi guide efficacy can vary and these knockdowns likely had transcriptional polarity effects, the actual reduction in complex activity needs to be determined to link the magnitude of phenotypes observed to the underlying mechanisms. Moreover, biological variability and potential compensatory mechanisms complicate connections between phenotypes and knockdown effect, especially as many complexes contribute to other pathways. Most notably, Sdh oxidizes succinate in the TCA cycle, and cells in these experiments were grown in media with succinate as a carbon source. Additional work is required to determine the mechanistic and regulatory impacts of these knockdowns, including effects on metabolic flux (26), but fitness data from Chapter 3 indicate that these knockdowns impact antibiotic resistance and susceptibility in *A. baumannii*. This underscores the complexity of respiratory stress responses and highlights the importance of further investigation, potentially employing techniques such as membrane potential measurements or metabolomics to gain a more comprehensive understanding of the underlying mechanisms.

Materials and Methods

Strains, plasmids, and oligos used are listed in Table C.1-3, respectively. All experiments were conducted in EZ RDM + 40mM sodium succinate (AbRDM, see Appendix B). Selective antibiotics were used when necessary; 100 µg/mL ampicillin or 30 ug/mL kanamycin for *E. coli* donor strains and 150 ug/mL gentamicin for *A. baumannii*. Diaminopimelic acid (DAP) was added at 300 µM to support growth of *E. coli* dap- donor strains.

Knockdown construction

Knockdown strains were constructed as previously described (5, 27).

ATP assay

Overnight cultures were diluted 1:50 into a deep-well 96-well plate with 1mM IPTG (isopropyl b-D-1-thiogalactopyranoside) and grown at 37°C with shaking at 900 rpm. After 3.5 hours, or early log-phase (OD~0.2), 100uL of each sample were collected for use in the CellTiter Glo 2.0 Assay (Promega) according to manufacturer protocol.

NAD+/NADH assay

Overnight cultures were diluted 1:50 into a deep-well 96-well plate with 1mM IPTG (isopropyl b-D-1-thiogalactopyranoside) and grown at 37°C with shaking at 900 rpm. After 3.5 hours, or early log-phase (OD~0.2), 100uL of each sample were collected for use in the NAD/NADH-Glo™ kit (Promega) according to manufacturer protocol.

Ethidium bromide assay

Ethidium bromide assay was performed as previously described by Ward et al. (5) and in Chapters 2 and 3.

Table C.1. Strains used in this study.

Strain	Description[1]	Source
sJMP4001 (19606)	*A. baumannii* ATCC19606	ATCC
sJMP3053	*E. coli* cloning strain (derived from BW25141) (pir+, recAI with anti-CRISPR)	Ward et al. (5)
sJMP3049	*E. coli* mating strain (derived from WM6026) (pir+, recAI with anti-CRISPR)	Ward et al. (5)
sJMP4061	*E. coli* mating strain sJMP3049 with pEVS104 (R6K *ori* helper plasmid for conjugation); kanR, dap-	Ward et al. (5)
sJMP4324	*A. baumannii* 19606 (sJMP4001) with MCi system inserted into the Tn*7 att* site, gmR (non-targeting control sgRNA)	Ward et al. (5)
sJMP10074	*A. baumannii* 19606 (sJMP4001) with MCi system from pJMP10054 inserted into the Tn*7 att* site, gmR (*nuoB* sgRNA)	Ward et al. (5)
sJMP4433	*A. baumannii* 19606 (sJMP4001) with MCi system from pJMP4419 inserted into the Tn*7 att* site, gmR (*sdhB* sgRNA)	This study
sJMP4410	*A. baumannii* 19606 (sJMP4001) with MCi system from pJMP4400 inserted into the Tn*7 att* site, gmR (*cyoA* guide)	This study
sJMP4412	*A. baumannii* 19606 (sJMP4001) with MCi system from pJMP4404 inserted into the Tn*7 att* site, gmR (*atpB* guide)	This study

[1] gmR = gentamicin-resistant; kanR = kanamycin-resistant; ampR = ampicillin-resistant; dap- = requires diaminopimelic acid; MCi = Mobile-CRISPRi

Table C.2. Plasmids used in this study.

Plasmid	Description[1]	Source
pJMP2776	MCi plasmid for A. baumannii; for cloning new guides (BsaI sites), ampR (backbone), gmR (transposon)	Ward et al. (5)
pJMP4419	MCi plasmid for A. baumannii; sdhB guide	This study
pJMP4400	MCi plasmid for A. baumannii; cyoA guide	This study
pJMP4404	MCi plasmid for A. baumannii; atpB guide	This study

[1] gmR = gentamicin-resistant; ampR = ampicillin-resistant; MCi = Mobile-CRISPRi

Table C.3. Oligos used in this study.

Oligo	Sequence (5' to 3')	Description[1]
oJMP1887	TAGTAATAGATCGCAGTCATCATA	*cyoA* top; anneal oligos to clone guides into BsaI sites in MCi vector
oJMP1888	AAACTATGATGACTGCGATCTATT	*cyoA* bottom; anneal oligos to clone guides into BsaI sites in MCi vector
oJMP1891	TAGTGCCAATTTCCATGTACCATC	*atpB* top; anneal oligos to clone guides into BsaI sites in MCi vector
oJMP1892	AAACGATGGTACATGGAAATTGGC	*atpB* bottom; anneal oligos to clone guides into BsaI sites in MCi vector
oJMP1963	TAGTTACCTTCACGGCAAGAACGA	*sdhB* top; anneal oligos to clone guides into BsaI sites in MCi vector
oJMP1964	AAACTCGTTCTTGCCGTGAAGGTA	*sdhB* bottom; anneal oligos to clone guides into BsaI sites in MCi vector

[1] MCi = Mobile-CRISPRi

References

1. Deshpande OA, Mohiuddin SS. 2024. Biochemistry, Oxidative PhosphorylationStatPearls. StatPearls Publishing, Treasure Island (FL).

2. Gel'man NS, Lukoyanova MA, Ostrovskii DN. 1967. Oxidative Phosphorylation in Bacteria, p. 161–192. In Respiration and Phosphorylation of Bacteria. Springer US, Boston, MA.

3. Geisinger E, Mortman NJ, Dai Y, Cokol M, Syal S, Farinha A, Fisher DG, Tang AY, Lazinski DW, Wood S, Anthony J, van Opijnen T, Isberg RR. 2020. Antibiotic susceptibility signatures identify potential antimicrobial targets in the Acinetobacter baumannii cell envelope. 1. Nat Commun 11:4522.

4. Gallagher LA, Ramage E, Weiss EJ, Radey M, Hayden HS, Held KG, Huse HK, Zurawski DV, Brittnacher MJ, Manoil C. 2015. Resources for Genetic and Genomic Analysis of Emerging Pathogen Acinetobacter baumannii. J Bacteriol 197:2027–2035.

5. Ward RD, Tran JS, Banta AB, Bacon EE, Rose WE, Peters JM. Essential gene knockdowns reveal genetic vulnerabilities and antibiotic sensitivities in Acinetobacter baumannii. mBio 15:e02051-23.

6. Romero PR, Karp PD. 2004. Using functional and organizational information to improve genome-wide computational prediction of transcription units on pathway-genome databases. Bioinformatics 20:709–717.

7. Berrisford JM, Baradaran R, Sazanov LA. 2016. Structure of bacterial respiratory complex I. Biochimica et Biophysica Acta (BBA) - Bioenergetics 1857:892–901.

8. Hederstedt L, Rutberg L. 1981. Succinate dehydrogenase--a comparative review. Microbiol Rev 45:542–555.

9. Guo Y, Karimullina E, Emde T, Otwinowski Z, Borek D, Savchenko A. 2023. Monomer and dimer structures of cytochrome bo3 ubiquinol oxidase from Escherichia coli. Protein Sci 32:e4616.

10. Saw W, Le KCM, Shin J, Kwek JHM, Wong CF, Ragunathan P, Fong TC, Müller V, Grüber G. 2023. Atomic insights of an up and down conformation of the Acinetobacter baumannii F 1 -ATPase subunit ε and deciphering the residues critical for ATP hydrolysis inhibition and ATP synthesis. The FASEB Journal 37:e23040.

11. Demmer JK, Phillips BP, Uhrig OL, Filloux A, Allsopp LP, Bublitz M, Meier T. 2022. Structure of ATP synthase from ESKAPE pathogen Acinetobacter baumannii. Science Advances 8:eabl5966.

12. Anraku Y, Gennis RB. 1987. The aerobic respiratory chain of Escherichia coli. Trends in Biochemical Sciences 12:262–266.

13. Arai H. 2011. Regulation and Function of Versatile Aerobic and Anaerobic Respiratory Metabolism in Pseudomonas aeruginosa. Front Microbiol 2:103.

14. Zieliński ŁP, Smith AC, Smith AG, Robinson AJ. 2016. Metabolic flexibility of mitochondrial respiratory chain disorders predicted by computer modelling. Mitochondrion 31:45–55.

15. Celotto AM, Chiu WK, Van Voorhies W, Palladino MJ. 2011. Modes of metabolic compensation during mitochondrial disease using the Drosophila model of ATP6 dysfunction. PLoS One 6:e25823.

16. Van Bergen NJ, Crowston JG, Kearns LS, Staffieri SE, Hewitt AW, Cohn AC, Mackey DA, Trounce IA. 2011. Mitochondrial oxidative phosphorylation compensation may preserve vision in patients with OPA1-linked autosomal dominant optic atrophy. PLoS One 6:e21347.

17. Xu Y, Xue D, Bankhead A, Neamati N. 2020. Why All the Fuss about Oxidative Phosphorylation (OXPHOS)? J Med Chem 63:14276–14307.

18. Lobritz MA, Belenky P, Porter CBM, Gutierrez A, Yang JH, Schwarz EG, Dwyer DJ, Khalil AS, Collins JJ. 2015. Antibiotic efficacy is linked to bacterial cellular respiration. Proceedings of the National Academy of Sciences 112:8173–8180.

19. Händel N, Schuurmans JM, Brul S, ter Kuile BH. 2013. Compensation of the metabolic costs of antibiotic resistance by physiological adaptation in Escherichia coli. Antimicrob Agents Chemother 57:3752–3762.

20. Olivares Pacheco J, Alvarez-Ortega C, Alcalde Rico M, Martínez JL. 2017. Metabolic Compensation of Fitness Costs Is a General Outcome for Antibiotic-Resistant Pseudomonas aeruginosa Mutants Overexpressing Efflux Pumps. mBio 8:e00500-17.

21. Price EE, Román-Rodríguez F, Boyd JM. 2021. Bacterial approaches to sensing and responding to respiration and respiration metabolites. Mol Microbiol 116:1009–1021.

22. Sun R, Han Y, Swanson JMJ, Tan JS, Rose JP, Voth GA. 2018. Molecular transport through membranes: Accurate permeability coefficients from multidimensional potentials of mean force and local diffusion constants. J Chem Phys 149:072310.

23. Benarroch JM, Asally M. 2020. The Microbiologist's Guide to Membrane Potential Dynamics. Trends Microbiol 28:304–314.

24. Abdi SN, Ghotaslou R, Ganbarov K, Mobed A, Tanomand A, Yousefi M, Asgharzadeh M, Kafil HS. 2020. Acinetobacter baumannii Efflux Pumps and Antibiotic Resistance. Infect Drug Resist 13:423–434.

25. Borisov VB, Siletsky SA, Nastasi MR, Forte E. 2021. ROS Defense Systems and Terminal Oxidases in Bacteria. Antioxidants (Basel) 10:839.

26. Zhao J, Zhu Y, Han J, Lin Y-W, Aichem M, Wang J, Chen K, Velkov T, Schreiber F, Li J. 2020. Genome-Scale Metabolic Modeling Reveals Metabolic Alterations of Multidrug-Resistant Acinetobacter baumannii in a Murine Bloodstream Infection Model. Microorganisms 8:1793.

27. Banta AB, Ward RD, Tran JS, Bacon EE, Peters JM. 2020. Programmable Gene Knockdown in Diverse Bacteria Using Mobile-CRISPRi. CP Microbiology 59:e130.